A Multi-modal Parcellation of Human Cerebral Cortex

Matthew F. Glasser[1], Timothy S. Coalson[1]*, Emma C. Robinson[2,3]*, Carl D. Hacker[4]*, John Harwell[1], Essa Yacoub[5], Kamil Ugurbil[5], Jesper Andersson[2], Christian F. Beckmann[6], Mark Jenkinson[2], Stephen M. Smith[2], David C. Van Essen[1]

[1]Department of Neuroscience, Washington University Medical School, Saint Louis, MO, USA; [2]FMRIB centre, Nuffield Department of Clinical Neurosciences, John Radcliffe Hospital, University of Oxford, Oxford, UK; [3]Department of Computing, Imperial College London, UK; [4]Department of Biomedical Engineering, Washington University, Saint Louis, MO, USA; [5]Center for Magnetic Resonance Research (CMRR), University of Minnesota, Minneapolis, MN, USA; [6]Donders Institute for Brain, Cognition and Behavior, Radboud University, Nijmegen, The Netherlands & MIRA Institute for Biomedical Technology and Technical Medicine, University of Twente, Enschede, The Netherlands

*Co-second Authors

Summary

Understanding the amazingly complex human cerebral cortex requires a map (parcellation) of its major subdivisions (cortical areas). Making an accurate areal map has been a century-old objective in neuroscience. Using cutting edge multi-modal magnetic resonance images from the Human Connectome Project (HCP) and an objective semi-automated neuroanatomical approach, we delineated 180 areas per hemisphere bounded by sharp changes in cortical architecture, function, connectivity, and/or topography in a precisely aligned group average of 210 healthy young adults. We characterized 97 new areas and 83 areas previously reported using post-mortem microscopy or other specialized study-specific approaches. To enable automated delineation and identification of these areas in new HCP subjects and in future studies, we trained a machine learning classifier to recognize the multi-modal "fingerprint" of each cortical area. This classifier detected the presence of 96.6% of the cortical areas in new subjects, replicated the group parcellation, and could correctly locate areas in individuals with atypical parcellations. Altogether, the freely available parcellation and classifier will enable unprecedented neuroanatomical precision for studies of the structural and functional organization of human cerebral cortex and its variation across individuals and in development, aging, and disease.

Introduction

Neuroscientists have long sought to subdivide the human brain into a mosaic of anatomically and functionally distinct, spatially contiguous areas (cortical areas and subcortical nuclei), as a prerequisite for understanding how the brain works. Areas differ from their neighbors in microstructural architecture, functional specialization, connectivity with other areas, and/or orderly intra-area topographic organization (e.g. the map of visual space in visual cortical areas)[1-4]. Accurate parcellation is vital: (i) to provide a map of where we are in the brain, enabling efficient comparison of results across studies and communication among investigators; (ii) as a foundation for illuminating the functional and structural organization of the brain; and (iii) as a means to reduce data complexity while improving statistical sensitivity and power for many neuroimaging studies.

The human cerebral cortex has been estimated to contain anywhere from ~50[1,2] to ~200[4,5] areas per hemisphere. However, attaining a consensus whole cortex parcellation has been difficult because of practical and technical challenges that we address here:

(i) Most previous parcellations were based on only one neuroantomical property (e.g. architecture, function, connectivity, or topography), and many cover only part of the cortex. Combining multiple properties provides complementary as well as confirmatory information, as different properties distinguish different sets of areal boundaries, and more confidence can be placed in boundaries that are consistent across multiple independent properties. We analyzed all four properties across all of neocortex in both hemispheres, using new or refined methods applied to the uniquely rich repository of exceptionally high quality magnetic resonance imaging (MRI) data provided by the Human Connectome Project (HCP), which benefited from major advances in image acquisition and preprocessing[6-9]. Architectural measures of relative cortical myelin content and cortical thickness were derived from T1-weighted (T1w) and T2-weighted (T2w) structural images[6,10,11]. Cortical function was measured using task fMRI (tfMRI) contrasts from seven tasks[12]. Resting-state fMRI (rfMRI) revealed functional connectivity (FC) of entire cortical areas plus topographic organization within some areas.

(ii) Previous parcellations typically used either fully automated algorithmic approaches or else manual or partly automated neuroanatomical approaches where

neuroanatomists delineated areal borders, documented areal properties, and identified areas after consulting prior literature. Here, we combined both approaches. For the initial parcellation, we adapted a successful observer-independent semi-automated neuroanatomical approach for generating post-mortem architectonic parcellations[13,14] to non-invasive neuroimaging. We used an algorithm to delineate potential areal borders (transitions in two or more of the cortical properties described above), which two neuroanatomists (MG and DVE) then interpreted, documenting areal properties and identifying areas relative to the extant neuroanatomical literature. We then used a fully automated algorithmic approach, training a machine learning classifier to delineate and identify cortical areas in individual subjects based on multi-modal areal fingerprints, allowing the parcellation to be replicated in new subjects and studies.

(iii) Prior parcellations have either used small numbers of individuals or group averages that are 'blurry' from inaccurate alignment of brain areas across subjects. We aligned cortical data using "areal features," including maps of relative myelin content and resting state networks that are more closely tied to cortical areas than are the folding patterns typically used for alignment[15]. The markedly improved intersubject cortical alignment using cortical folding, myelin and resting state fMRI enabled us to generate the "typical subject's" parcellation from a highly detailed 210-subject group average dataset. In addition to the following main text, this publication contains an Online Methods Summary (OMS), Supplementary Results and Discussion (SRD), Extended Supplementary Methods (ESM), and Neuroanatomical Supplementary Results (NSR), each with numbered sections.

Group map reproducibility of fine details

We analyzed two independent groups of HCP subjects - 210P ('Parcellation') and 210V ('Validation') - aligned using areal-feature-based registration (called 'MSMAll', see OMS #1.2). Figure 1 illustrates the consistency of fine spatial patterns for maps reflecting relative myelin content (left panels) and a task-fMRI language-related activation (right panels). The maps are strikingly similar across the 210P and 210V groups, including variations in relative myelin content within the primary somatosensory cortex related to somatotopic organization (white and black arrows in left panels, see legend) and small features in the task fMRI maps (white ellipses in right panels). The SRD (#1.1) includes

more examples of such cross-group consistency for architecture (myelin and cortical thickness), function (tfMRI contrast maps), and two resting state connectivity measures; see Supplementary Figures 1-5.

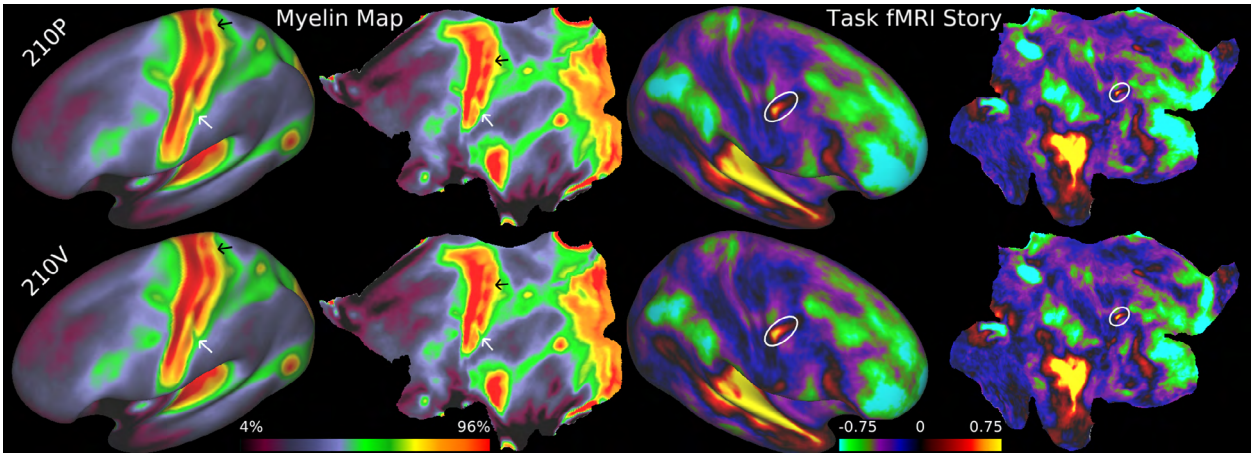

Figure 1 | **Consistency of fine spatial details in independent group averages**. Relative myelin content maps (left hemisphere) and task fMRI contrast beta maps from the LANGUAGE Story contrast (right hemisphere) on inflated (Columns 1 and 3) and flattened surfaces (Columns 2 and 4). Rows 1 and 2 are the group averages of the 210P and 210V datasets respectively. White and black arrows indicate consistent variations in myelin content within primary somatosensory cortex that are correlated with somatotopy (see NSR #6, Figure 8). The white oval indicates a small, sharp, and reproducible feature in the right hemisphere of the LANGUAGE Story contrast. "Relative myelin content" will hereafter be referred to as myelin (See legend of Supplementary Figure 1). Data at http://balsa.wustl.edu/WDpX.

Because of areal-feature-based alignment, maps of average cortical folding in this study are much blurrier than are maps of areal properties because folding patterns and area locations are imperfectly correlated[15] (e.g. compare Supplementary Figure 7e and 7j (group average and individual subject folding)). Group average folding patterns mainly remain sharp in early sensory areas, where areal locations and folds are tightly correlated (e.g. central and calcarine sulci, see Supplementary Figure 1, Rows 3 and 4). The regional difference in sharpness between maps of areal properties and folding highlights the importance of alignment based on areal features, rather than folding patterns, as a prerequisite for accurately parcellating group average data. The high spatial resolution of the HCP's MRI images and lack of aggressive spatial smoothing[11] prior to group averaging also contribute to making our maps substantially sharper than those from traditional neuroimaging studies.

Quantitatively, the 210P and 210V group average datasets were highly correlated across the cortical surface (r=0.998/r=0.994 for myelin/cortical thickness, r=0.996 and

r=0.979 for two cortical folding measures, r=0.995/0.984/0.944 for max/median/min of the task fMRI contrasts, and a median reproducibility of r=0.989 for two measure of resting state connectivity). These excellent map reproducibilities provide confidence that the parcellation will reflect the areal pattern of typical subjects in the healthy young adult population. See OMS #1.3 and ESM #1.3-3.4 for the methods used to generate these maps.

A 180-area Group Average Parcellation

To identify transitions representing candidate areal boundaries, we designed and implemented a semi-automated, quantitative approach adapted for multi-modal neuroimaging data represented on 2D cortical surface models (see OMS #1.4, ESM #4.1-5.3). The approach is similar in spirit to the semi-automated observer-independent approach pioneered by Zilles and Amunts[14,16]. However, instead of objectively identifying potential areal borders in postmortem histological sections, we identified them algorithmically on the cortical surface by computing the first derivitive of each areal feature map (i.e. its spatial gradient magnitude)[17]. Candidate borders were then interpreted by the neuroanatomists to exclude artifacts. Each area's properties were documented (in the NSR), and putative areas were related to the extant neuroanatomical literature.

These semi-automated approaches contrast with classical observer-dependent parcellation approaches[1,2,4] that relied on visual inspection to locate often subtle transitions in cortical architecture and with some modern observer-dependent retinotopic parcellation methods[18,19]. They also differ from fully automated, unsupervised methods[20-22] in which the outcomes depend heavily on algorithmic input parameters (e.g., thresholds or number of requested clusters) and are not validated by a neuroanatomist.

Area 55b illustrates our multi-modal gradient-based parcellation approach using gradients of three areal feature maps (see Figure 2). Area 55b is a small, elongated, and notably distinct area (outlined in black or white) bounded by the frontal and premotor eye fields (FEF & PEF), primary motor cortex (4), ventral premotor cortex (6v), and prefrontal areas 8Av and 8C. In the myelin map (Fig. 2a), area 55b is lightly myelinated and lies between moderately myelinated areas FEF (above) and PEF (below), just anterior to heavily myelinated primary motor cortex (area 4). Thus, area 55b is surrounded on three

sides by myelin gradients (Fig. 2e). Area 55b is strongly activated in the LANGUAGE Story vs Baseline contrast (Fig. 2b) and is entirely surrounded by a strong gradient for this task contrast (Fig. 2f). It also has distinctive functional connectivity, as revealed by a seed location (lightly myelinated area PSL) selectively connected with 55b (Fig. 2c) and a different seed location (heavily myelinated area LIPv) strongly connected with FEF and PEF (Fig. 2d) but not with 55b. The result is strong mean gradients in dense functional connectivity surrounding 55b (Fig. 2g). Hopf[23] illustrated area 55b on a schematic surface map (Fig. 2h) as a lightly myelinated area bounded on three sides by more heavily myelinated areas. Because of the similarity to the dorsal portion of Hopf's 55b we use the same name.

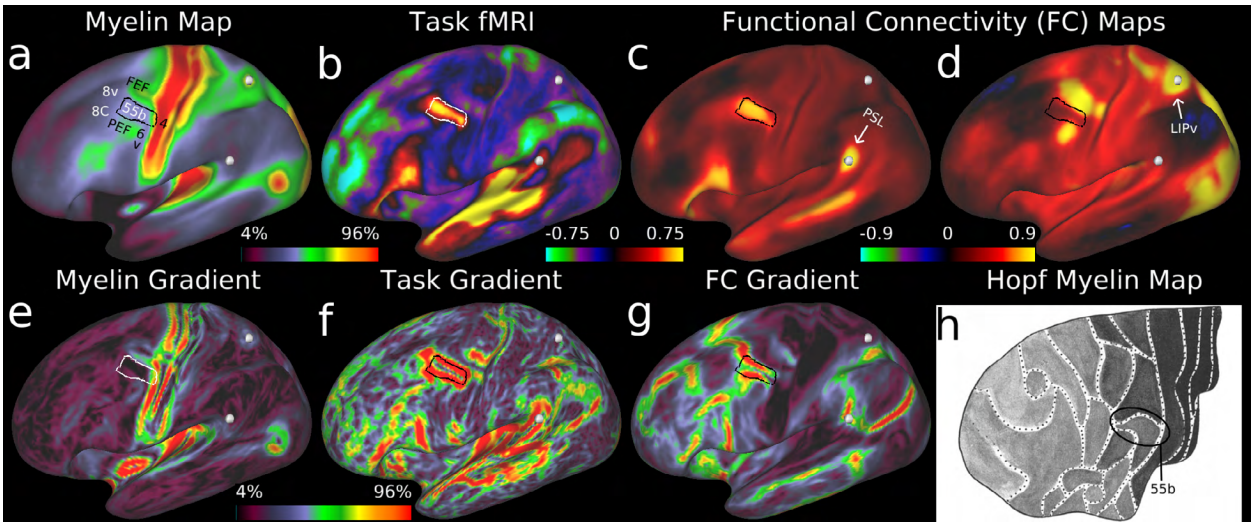

Figure 2 | **Parcellation of exemplar area 55b using multi-modal information**. The border of 55b is indicated by a white or black outline. **a,** myelin map. **e,** myelin map gradients. **b,** group average beta map from the LANGUAGE Story vs Baseline task contrast and, **f**, gradient map. **c,** functional connectivity correlation maps from a seed in area PSL (white sphere, arrow) and **d,** a seed in area LIPv (white sphere, arrow). **g,** mean gradient of the functional connectivity dense connectome (see OMS #1.3 for methods). **h,** a dorsal schematic view of the prefrontal cortex as parcellated by Hopf[23] where shading indicates the amount of myelin found using histological stains of cortical gray matter. Data at http://balsa.wustl.edu/Qv4P.

To generate the complete parcellation of 180 areas and area complexes in each hemisphere, we adopted a systematic, objective, and quantitative approach (see OMS #1.4 and ESM #5.1 - 5.3). Our major criteria, met in nearly all cases, included: (i) spatially overlapping gradient 'ridges' between each pair of areas for at least two independent areal feature maps; (ii) similar gradient ridges present in roughly corresponding locations in both hemispheres; (iii) gradients that were not correlated with artifacts; and (iv) robust

and statistically significant cross-border differences in the feature maps. Another consideration (but not a requirement) was whether published evidence exists for a boundary in an approximately corresponding location. Studies with publicly available parcellations registered onto atlas surfaces were directly compared with our data[5]; however, most regions required indirect comparisons with published figures (e.g., Fig. 1h). Initial areal boundaries meeting these criteria were delineated by two neuroanatomists (MG and DVE).

In a second computational stage, the path of each manually drawn border was optimized algorithmically using gradients of the most informative feature maps selected by the neuroanatomists (i.e. those with visually obvious gradients and differences across the border). These feature maps were confirmed to have robust and statistically significant differences across the final border. The semi-automated gradient-based parcellation approach is further described in ESM (#5.1-5.3), and the entire semi-automated process is illustrated for area V1 in NSR (#1), which contains descriptions and illustrations of the information used to delineate and the literature used to name all 180 cortical areas.

Figure 3 shows the multi-modal cortical parcellation in the left and right hemispheres on inflated and flattened surfaces, with areal boundaries delineated by black contours. 180 areas and areal complexes per hemisphere is near the higher end of earlier estimates noted above[4,5]. We consider 180 a likely lower bound, as some parcels are probably complexes of multiple areas (e.g. based on finer-grained published parcellations, and other regions suffer from reduced sensitivity due to fMRI signal loss). Some areas (83/180) were assigned names based on published parcellations from dozens of separate studies that used a variety of invasive or specialized methods (see NSR Table 2), reflecting how far the field has been from a consensus neuroanatomical parcellation. Some of the newly described 97 areas have de novo names (e.g., DVT for the Dorsal Visual Transitional area), while others represent finer-grained parcellations of previously reported areas (e.g., area 31 into areas 31a, 31pd, and 31pv). A few represent complexes in which a published finer grained parcellation was not visible in our data (e.g. areas 29 and 30 combined into area RSC – the RetroSplenial Complex), but these may be again subdivided once higher resolution data is available. The 180 areas differ widely in their shapes, sizes, and the positions of their borders relative to cortical folds.

The parcellation in Figure 3 is colored to reflect each area's degree of association in the resting state (determined using multiple regression – see ESM #5.4) with five functionally specialized groups of areas: early auditory (red), early somatosensory/motor (green), and early visual areas (blue). These represent the three dominant input streams to the brain. Also used were two core groups of cognitive areas that are strongly anti-correlated in our data, the task positive network (towards white) and task negative (also called the default mode) network (towards black). Hence, the strongly bluish, greenish, and reddish regions are predominantly but not exclusively associated with visual, somatosensory-motor, and auditory processing, respectively. Qualitatively, the predominantly unimodal regions appear to collectively occupy less than half of the neocortical sheet. Areas likely to be more strongly biomodal include blue-green areas such as LIPv and MT (visual and somatosensory-motor) and purple areas such as POS2 and RSC (visual and auditory). The remaining regions form a complex mosaic, with some intermixing of lighter (task-positive) and darker (task-negative) areas along with many light or dark pastel hues suggestive of 'cognitive' areas that may be preferentially associated with one or another sensory modality. The bilateral symmetry of functional organization is striking, insofar as nearly all areas have qualitatively very similar hues in the left and right hemispheres. However, interesting color asymmetries occur in a few areas, especially language-related areas 55b, PSL, SFL, and 44 and their right hemisphere homologues, which also have asymmetric task-fMRI functional profiles (see NSR #8, #15, #21, #22).

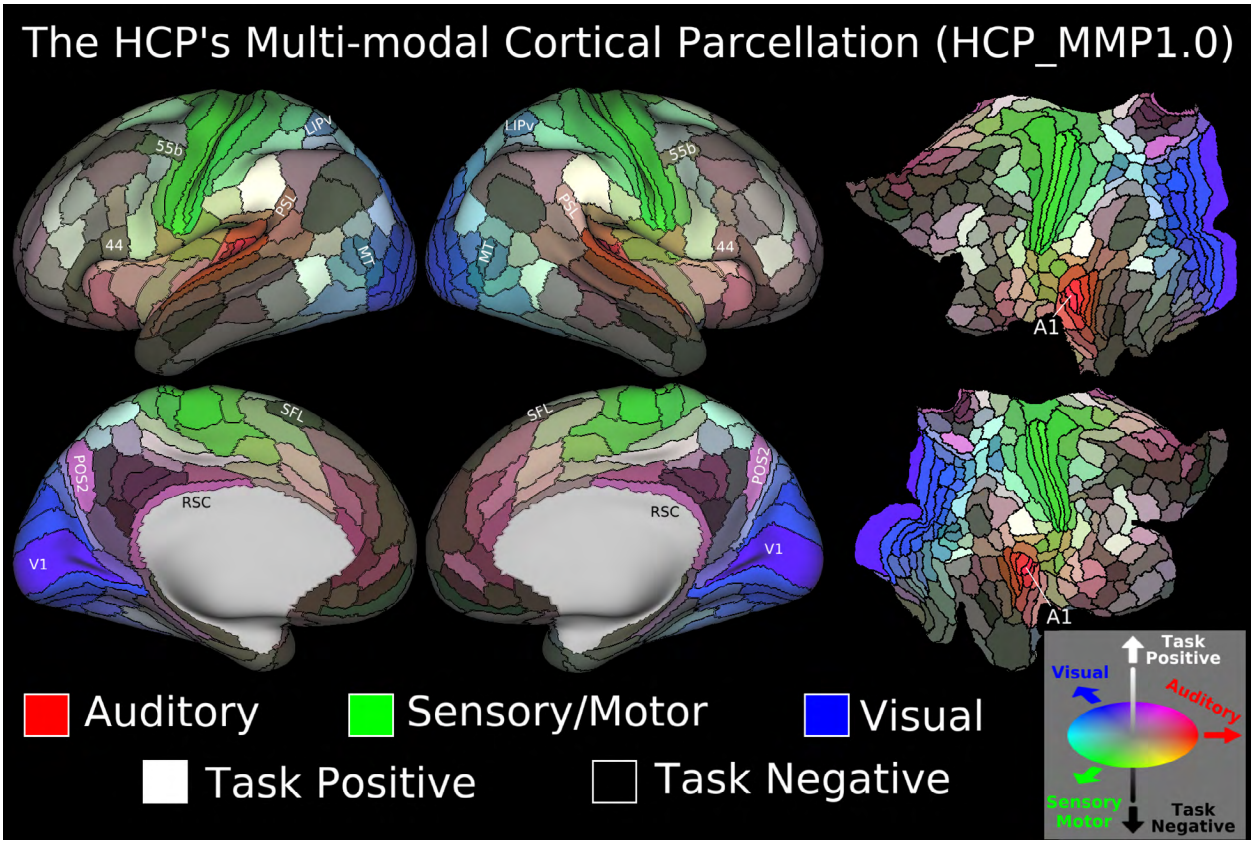

Figure 3 | **The HCP's Multi-Modal Parcellation, v 1.0 (HCP_MMP1.0).** 180 areas delineated and identified in both left and right hemispheres are displayed on inflated and flattened cortical surfaces. Black outlines indicate areal borders. Colors indicate the extent to which the areas are associated in the resting state with auditory (red), somatosensory (green), visual (blue), task positive (towards white), or task negative (towards black) groups of areas (see ESM #5.4). The legend on the bottom right illustrates the 3D color space used in the figure. Data at http://balsa.wustl.edu/WN56.

Internal heterogeneity is evident in some cortical areas, particularly those with topographically organized representations. In the somatosensory-motor strip (largely architecturally defined somatosensory and motor areas 3a, 3b, 1, 2, and 4), we identified five clearly defined topographic subareas in resting state and task fMRI data (see NSR #6 and Figure 8). In this parcellation we treat topographic subdivisions as "subareas" rather than calling them full "areas." For visual cortex, its visuotopic organization revealed a set of hemifield representations in each hemisphere, something not achieved in previous unsupervised resting state functional connectivity-based parcellations[20-22,24]. Also, ultrahigh-field MRI reveals sub-areal cortical organization along both laminar[25,26], and columnar[27,28] axes, so our parcellation represents one of many important levels of granularity in brain organization.

Cross-validation of the parcellation

The initial statistical analysis used in the semi-automated parcellation was circular, insofar as the 210P dataset was used for both creating and testing the parcellation. Hence, we carried out an additional statistical cross-validation using the 210V dataset and a comprehensive set of feature maps (See OMS #1.5; SRD #1.2). This analysis also reveals which areal properties were most useful in defining areal boundaries (a condensed representation of the detailed information provided in the NSR). Supplementary Figure 6 shows four independent categories of features: cortical thickness, myelin maps, task fMRI, and resting state fMRI and how many of these categories showed robust and statistically significant differences across each areal border. Fully 96% of areal borders had robust effect sizes (Cohen's $d > 1$) in two or more feature categories and all were statistically significant after correcting for multiple comparisons in two or more feature categories in cross-border, across-subject t-tests. Resting state fMRI was the most useful category, followed by task fMRI, myelin maps, and lastly cortical thickness, which was consistent with the neuroanatomists' observations and documentation in the NSR.

Exemplar parcellation-based analyses

Spatial smoothing is often used to increase the signal-to-noise ratio (SNR) in neuroimaging analyses, to try to compensate for inaccurate registration of brain areas, and/or to satisfy statistical assumptions. However, smoothing blurs data across boundaries between areas (on the surface) and tissue compartments (in the volume). An areal parcellation enables area-wise analyses (averaging data within each area), thereby improving SNR and statistical power without the deleterious effects of spatial smoothing (to the extent that properties within an area are uniform). Parcellation dramatically reduces data dimensionality, illustrated here using the HCP's myelin, thickness, task, and resting state data (Figure 4).

The 'dense' (vertex-wise) myelin map shown in Fig. 4a has ~30,000 surface gray matter vertices per hemisphere, whereas a 'parcellated' myelin map (Fig. 4f) shows the same overall pattern with 180 cortical areas (vertices within an area have the same value, see also Fig. 4g for parcellated cortical thickness). Example dense and parcellated task

fMRI analysis contrast maps (Figs. 4b and 4c, LANGAUGE Story vs Baseline) can be represented as a single column (white) in a 180-area by 86-task-contrast matrix (Fig. 4d). Parcellated analyses hold great promise for task fMRI studies, as they improve the signal to noise ratio (SNR) by averaging fMRI timeseries within parcels prior to fitting the task design, increasing Z statistics (Fig. 4e). Parcellation is effectively a neurobiologically constrained smoothing approach that also increases statistical power by efficiently consolidating otherwise non-independent statistical tests. This approach will benefit studies aimed at understanding the functional and structural organization of the brain in health or disease at an area-wise level (i.e. studies that currently summarize results using 3D coordinates in a standardized stereotaxic space). Parcellated analyses also aid in the clarity and efficiency of communicating results (e.g. "area 55b in the left hemisphere showed a statistically significant +1% BOLD activation in my language task").

Parcellated analyses are comparably useful when characterizing structural or functional connectivity, as previously recognized[24,29]. Preprocessing of HCP data results in fMRI data represented as 'grayordinates' (cortical grey matter surface vertices and subcortical grey matter voxels[6]). A dense connectome, containing connectivity between all pairs of 91,282 grayordinates is $\sim 3.3*10^5$-fold larger than an area-wise parcellated connectome for ~500 areas (connectivity between all pairs of areas), yet the parcellated connectome captures the neurobiologically relevant variance at the areal level. Parcellated connectomes are illustrated using a seed location in area PGi (black dot) for full correlation (Fig. 4h) and partial correlation (Fig. 4i) FC brain maps together with their associated parcellated connectome matrices (Fig 4j, full correlation below and partial correlation above the diagonal). In both cases, the task negative (default mode) network is evident, though the partial correlation connectome is substantially sparser than the full correlation connectome.

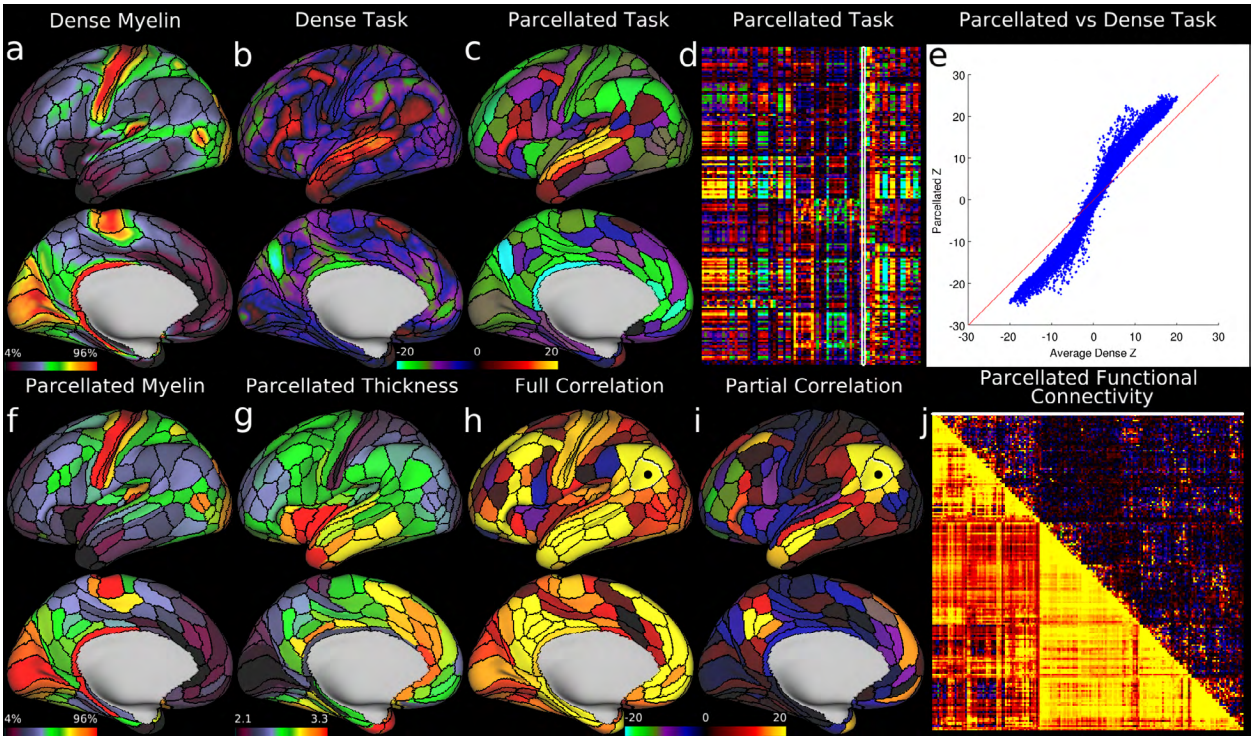

Figure 4 | **Example parcellated analyses using the HCP's multi-modal cortical parcellation**. **a,** dense and **f,** parcellated myelin maps. **g,** a parcellated folding-corrected cortical thickness map (in mm). **b,** example dense and **c,** parcellated task fMRI analysis (LANGUAGE Story vs Baseline). **d,** the entire HCP task fMRI battery's Z statistics for 86 contrasts (47 unique, see OSM #1.3) analyzed in parcellated form and displayed as a matrix (rows are parcels, columns are contrasts, white outline indicates the map in **c**). **e,** a major improvement in Z statistics from fitting task designs on parcellated timeseries instead of fitting them on dense timeseries and then parcellating afterwards (blue points are 360 parcels x 86 task contrasts; note the upward tilting deviation from the red line). **h, i,** parcellated FC maps on the brain (seeded from area PGi, black dot). These parcellated connectomes are computed using either full or partial correlation (see ESM #7.1). In both cases, the task negative (default mode) network is apparent. **j,** a parcellated connectome matrix view with the full correlation connectome below and the partial correlation connectome above the diagonal (white line shows the displayed partial correlation brain map). Data at http://balsa.wustl.edu/RG0x.

Individuals with atypical areal patterns

The precisely aligned group average multi-modal cortical parcellation represents the overall spatial arrangement of cortical areas in the 'typical' individual from a healthy young adult population. However, we found atypical topological arrangements of some areas in some individuals that are discernible across multiple modalities, including resting-state networks, task-fMRI activations, and myelin maps. Distinguishing genuinely atypical areal topologies from inadequately aligned typical patterns depended on the MSMAll areal-feature-based registration to align cortical areas precisely. We summarize key findings here and extensively characterize this important phenomenon in the SRD (#1.3).

Previously described area 55b and neighboring areas FEF and PEF showed particularly notable individual differences in topological arrangements. For the 210P subjects, 89% showed the typical configuration (area 55b bordered by area PEF inferiorly and area FEF superiorly, as in Figure 2), which was well aligned with group average area 55b after MSMAll registration. However, in one subgroup (4%, n=9), a patch having the multi-modal characteristics of area 55b is shifted superiorly relative to the upper limb subregion of sensori-motor cortex (Supplementary Figure 7). In another subgroup (6%, n=12), area 55b is split into two pieces by a merger of areas FEF and PEF, rather than the typical splitting of FEF and PEF by 55b (Supplementary Figure 8). Such topological deviations in individual subjects' areal maps raise intriguing questions for future exploration. They also cannot be corrected by a topology-preserving registration aimed at aligning individual subjects' areas with the group average "atlas" parcellation. Thus, we introduce an alternative fully automated cortical parcellation approach that can identify and delineate both typical and atypical areas in individual subjects that were not a part of the original 210P group.

Automated individual-subject parcellation

The semi-automated neuroanatomical approach described above is impractical for de novo individual subject parcellation of all ~1100 HCP subjects having complete MRI datasets so as to identify the atypical areal topologies mentioned above. Instead, we developed an automated method for generating individual subject parcellations based on a supervised machine learning classifier previously used to identify resting state functional networks in individual subjects[30]. In our case, the areal classifier learns the multi-modal 'areal fingerprint' of each cortical area that distinguishes it from surrounding cortex. Based on multi-modal feature maps that represent the areal properties of architecture, function, connectivity, and topography, the areal classifier returns a prediction (0% to 100%) that each area exists at a given cortical surface vertex. The highest prediction value across areas at each vertex is used to generate the individual subject parcellation (see OMS #1.6 and ESM #6.1-6.8). Once trained using the 210P subjects (and a separate '29T' group of test subjects, see OSM #1.1), the areal classifier should be able to use only the multi-modal

areal fingerprints that it has learned to reproduce the parcellation in an independent group of validation subjects (210V).

A critical early test of the areal classifier was whether it could accurately and reliably map areas that are not aligned with the population-based atlas parcellation after MSMAll areal-feature-based alignment (SRD #1.4). Examples of successful classification of areas 55b, FEF, and PEF are shown in the SRD (Supplementary Figure 9) for typical subjects, shifted 55b subjects, and split 55b subjects. In each illustrated case, the classifier correctly identified 55b and its neighbors (as assessed by the neuroanatomist's inspection of the multi-modal areal features shown in the figure). Supplementary Figure 10 in the SRD shows that these atypical 55b topologies and classifications are stable across widely spaced repeat scanning sessions in a 'test-retest' group of 27 subjects (see OSM #1.1).

Areal Detection and Parcellation Consistency

Another critical test of both the parcellation and the areal classifier is the classifier's performance in detecting the 180 cortical areas in individual subjects, particularly in independent validation subjects that were not used to generate the parcellation or train the classifier. The top two rows of Figure 5 show the performance of the classifier in detecting each area (See OMS #1.6). Importantly, the classifier aims to detect whole areas based on their multi-modal fingerprints, rather than detecting differences in areal features across paired areal boundaries as was done in the cross-validation analysis (Supplementary Figure 6). The overall areal detection rate was 98.0% of all areas across all subjects for the 210P parcellation and training dataset (row 1) and 96.6% for the independent 210V validation dataset (row 2), indicating excellent overall performance of the areal classifier.

The areal classifier was used to generate probabilistic maps of each cortical area (illustrating residual variability in spatial location after MSMAll areal feature-based registration), and to assess the reproducibility of the parcellation in the independent 210V dataset. Rows 3 and 4 of Figure 5 show strikingly similar probabilistic maps of 8 non-overlapping areas with differing degrees of spatial variability (V1, M1, RSC, MT, LIPv, TE1a, 46, and 10r) from the 210P and 210V groups. All probability maps were combined to produce a group maximum probability map (MPM), where the area with the highest probability at each vertex was found. Row 5 shows the original semi-automated

parcellation borders, and row 6 compares the group MPM maps from 210P (blue) and 210V (red), with purple representing overlapping vertices. The borders in Row 6 are almost entirely purple, indicating very high reproducibility of the group MPM maps (r=0.965, Dice=0.960, see OMS #1.6). This reproducibility is similar to that of the original group average feature maps discussed above. The correlation of the original semi-automated parcellation (Row 5) with the 210P group MPM (Row 6) was r=0.913, Dice=0.902, indicating that the classifier made modest adjustments to better fit the data. We predict there will be very high reproducibility of the parcellation across the rest of the ~1100 subject HCP dataset. Example individual subject parcellations and their reproducibility based on repeated scan sessions are shown in Supplementary Figure 11. The individual parcellations are reasonably reproducible (median r=0.77, Dice=0.72) but, unsurprisingly, not as reproducible as the group parcellations, which benefit from averaging across many subjects. Other analyses yield interesting information about the sizes of cortical areas in the group average and variability in areal size across individuals (SRD #1.5).

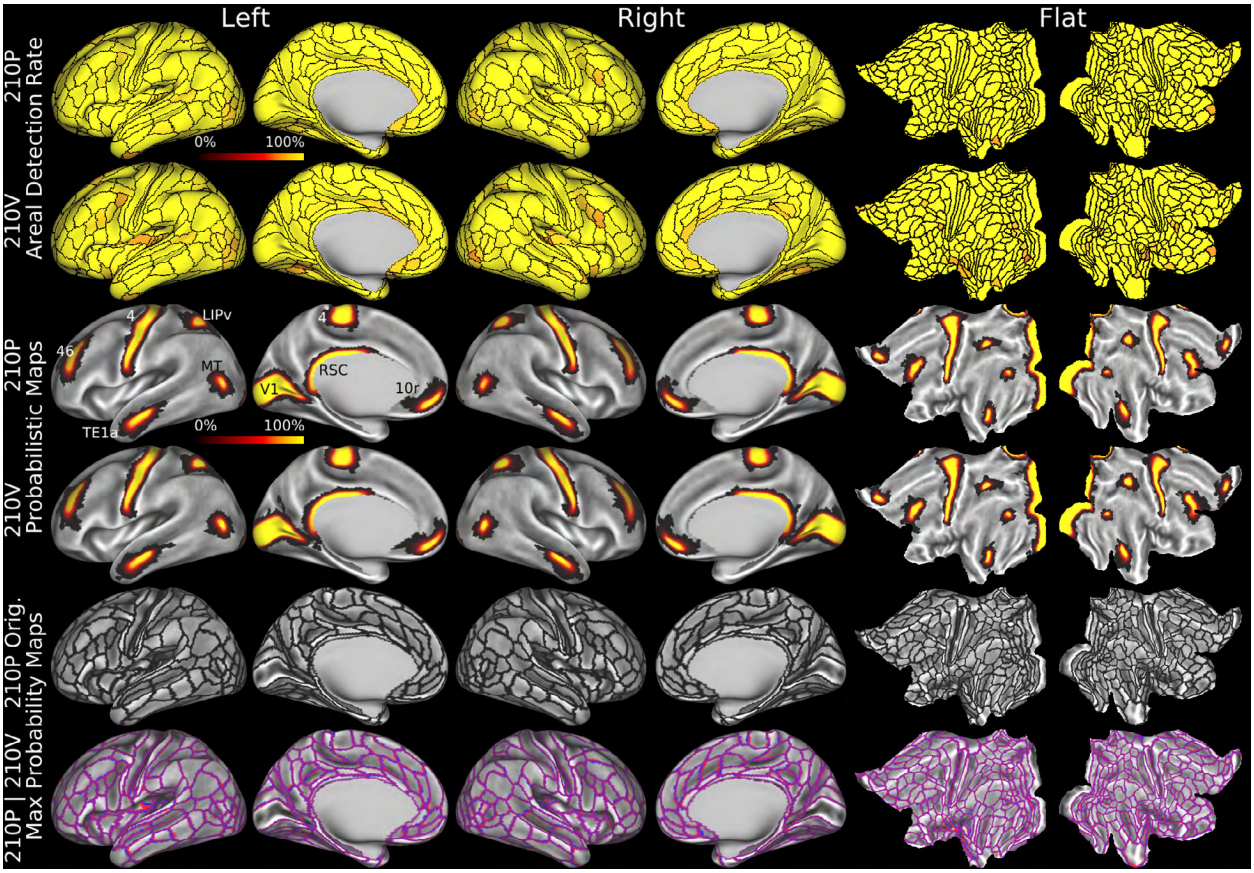

Figure 5 | **Areal detection rates, probabilistic areas, and parcellation reproducibility**. Rows 1 (210P) and 2 (210V) show the individual subject areal detection rates (see OMS #1.6) as parcellated maps. Most areas are yellow (100%), and the minimum detection rate across both rows was 73%. Rows 3 and 4 illustrate probabilistic maps of areas V1, M1, RSC, MT, LIPv, TE1a, 46, and 10r for the 210P (Row 3) and 210V (Row 4) groups. Row 5 shows the original parcellation derived from the semi-automated neuroanatomical approach. Row 6 shows the group MPM maps from 210P (blue), 210V (red), and their overlap (purple). Data at http://balsa.wustl.edu/WL8m.

Generalizing the Classifier for Future Studies

In contrast to the semi-automated approach (above) where neuroanatomists chose the information to delineate and identify the 180 cortical areas in group-average data (see NSR), the areal classifier automatically determines (without human intervention) what information is most useful for delineating and identifying these cortical areas in individual subjects (SRD #1.6). As illustrated in Supplementary Figure 12, the areal classifier uses the task fMRI data least, perhaps because task fMRI feature maps are noisier in individual subjects than other feature maps and its information content is largely redundant with resting state[31]. This finding is important for generalizability of the areal classifier to other studies because replicating the customized, hour-long HCP task fMRI battery is unlikely to

be feasible for most neuroimaging studies. Ideally, the areal classifier would be able to perform nearly as well relying only on architecture, connectivity, and topography. Accordingly, we trained the classifier again on the 210P dataset, but omitted the task fMRI-based feature maps. When trained this way, the classifier indeed performed nearly as well as when all features were used, detecting 97.6% of areas in 210P (vs 98.0% using all features) and 96.4% of areas in 210V (vs 96.6% using all features). Hence, we anticipate that the areal classifier will generalize to other studies that acquire the following core set of MRI images: high-resolution T1w and T2w; spin echo-based b0 field map; and extensive fMRI data acquired using 'multiband' pulse sequences to improve spatial and temporal resolution[8] (see SRD #2.9). These are the same image acquisition requirements as the HCP's minimal preprocessing pipelines[6] and the MSMAll areal feature-based registration pipeline[15] (ESM). Future studies adhering to these image acquisition guidelines will be able to use the unified framework of the HCP's analysis pipelines to automatically generate individualized parcellated analyses from raw MR images, a major advance over traditional neuroimaging methods that have often relied on comparisons with Brodmann's hand drawn parcellation published in 1909[1,2].

Discussion

We have produced a population-based 180-area per hemisphere human cortical parcellation using exceptionally high quality multimodal data from hundreds of Human Connectome Project subjects aligned using an improved areal feature-based cross-subject alignment method (MSMAll). Inspired by an observer-independent post-mortem architectural parcellation approach[14], we developed a semi-automated neuroanatomical approach adapted to non-invasively acquired multi-modal MRI data. Though algorithms determined the final areal borders, the multi-modal data were carefully interpreted by neuroanatomists, the properties of each cortical area were documented, and each area was named in relation to the extant neuroanatomical literature (in the NSR). A cross-validation showed that the areas forming the parcellation were robustly and statistically significantly different from their neighbors across multiple modalities. We identify this parcellation as

HCP-MMP1.0 (Human Connectome Project Multi-Modal Parcellation v1.0), with version 1.0 anticipating future refinements as better data become available (see SRD #2.1).

Unexpectedly, we discovered that despite improved intersubject alignment, some areas have atypical topological arrangements in some subjects, which we demonstrated for areas 55b, FEF, and PEF. We developed a fully automated method for parcellating individual subjects based on a machine learning classifier that can cope with this kind of individual variability. The areal classifier detected 96.6% of individual subject cortical areas in new subjects, including atypical areas, and replicated the group parcellation in an independent sample. Though we made extensive use of the HCP's specialized task fMRI battery when generating the parcellation, we showed that task fMRI data is not essential for future studies aiming to use the areal classifier to automatically define the cortical areas in their subjects. Instead, it suffices to acquire the same core set of MRI images needed for the rest of the HCP's software pipelines.

By generating a robust neuroanatomical map of human neocortical areas - a century-old aim of neuroscience – and providing methods for mapping these areas in any individual undergoing study with non-invasive neuroimaging, the present work stands apart from previous human cortical parcellations. The overall approach described here shows that we can produce sharp, reproducible brain images across multiple non-invasive neuroimaging modalities. We can generate a highly reproducible and generalizable cortical parcellation through state-of-the-art methods of data acquisition, preprocessing, and analysis designed to compensate for individual variability and thereby minimize blurring of images. These improvements, together with the new parcellation, make it desirable to use spatial localization methods that move beyond the traditional use of stereotaxic coordinates combined with Brodmann areal assignments to characterize centers of cortical activation in fMRI studies. From a neuroanatomical perspective, there has often been substantial uncertainty whether any two neuroimaging studies have found results in the same cortical areas or not. The situation is analogous to astronomy where ground-based telescopes produced relatively blurry images of the sky before the advent of adaptive optics and space telescopes.

Many topics are discussed further in the SRD #2.1-2.10 (e.g. avenues for improving the parcellation and other issues left for future work, further discussion of the

neuroscientific implications of our results, and additional datasets that could profitably be linked to our parcellation). As the topographic organization of higher cognitive areas becomes better understood, some parcels currently considered to be full areas may later be considered to be subareas of larger topographically organized cortical areas (analogous to somatotopic subregions of topographically organized sensory and motor areas illustrated in NSR #6). Though our use of multiple modalities likely mitigates this issue relative to traditional uni-modal parcellations, the extent to which the human multi-modal cortical parcellation may be revised along such lines remains a question for future work using the state of the art methods mentioned above (see SRD #2.8).

The MSMAll registration and the areal classifier are or will soon be freely available on GitHub, the visualization tool Connectome Workbench is on humanconnectome.org and the parcellation, data, and scenes for reproducing each of the figures are in the BALSA database[32]. These tools can be used to address fundamental questions of "which cortical area," when reporting results or thinking about and discussing brain organization in relation to studies of human cognition, lifespan, and disease. Several additional interesting avenues of investigation are now open. The ability to discriminate individual differences in the location, size, and topology of cortical areas from differences in their activity or connectivity should facilitate the dissection of how each property is related to behavior and genetic underpinnings, for example, in learning disabilities or those with distinctive cognitive traits. The ability to non-invasively and automatically delineate cortical areas in living subjects may have clinical implications, for example by providing neurosurgeons with detailed, individualized maps of the brains on which they operate. There are also important implications for our understanding of human cortical evolution. The dramatic expansion in neocortex along the human lineage occurred mainly in higher cognitive regions of lateral prefrontal, parietal, and temporal cortices[10,14,33,34]. Comparisons with nonhuman primates, including marmosets and macaques (both widely used in invasive studies), and great apes, may yield new insights regarding the emergence of new cortical areas and the divergences in areal functions, which collectively led to the amazing cognitive capabilities that make us uniquely human as a species and as individuals.

End Notes

Supplementary Information is linked to the online version of the paper at www.nature.com/nature.

*Acknowledgements***.** We thank the members of the WU-Minn-Ox HCP Consortium for invaluable contributions to data acquisition, analysis, and sharing and Erin Reid and Susan Danker for assistance with preparing the manuscript. Supported by NIH F30 MH097312 (MG), ROIMH-60974 (DVE), NIH F30 MH099877 (CH), the Human Connectome Project grant (1U54MH091657) from the 16 NIH Institutes and Centers that support the NIH Blueprint for Neuroscience Research, and the Wellcome Trust Strategic Award 098369/Z/12/Z (SS, JA, CB, MJ).

Author Contributions: MG and DVE designed the study and carried out the analyses. MG, TC, ER, CH, JH, EY, KU, JA, CB, MJ, and SS contributed novel methods. MG, TC, ER, CH, EY, JA, CB, MJ, SS, and DVE wrote the paper.

The authors have no competing financial interests as defined by Nature Publishing Group, or other interests that might be perceived to influence the results and/or discussion reported in this article.

Correspondence and requests for materials should be addressed to glasserm@wustl.edu or vanessen@wustl.edu.

1. Online Methods Summary

1.1 Subjects and Acquisition

449 young adult twins and non-twin siblings (ages 22-35) from the Human Connectome Project (HCP) were scanned according to the HCP's acquisition protocol[6-8]. The MRI acquisition included collecting T1w and T2w structural images, task-based and resting state-based fMRI images, diffusion weighted images, and b0 field maps. Images were acquired at high spatial and temporal resolution on a customized Siemens 3 tesla (3T) scanner and with customized slice accelerated sequences for fMRI (see ESM #1.1-1.2). All subjects from the HCP 500-subject data release (July, 2014) having complete fMRI sessions were included. They were divided into two independent groups of 210 subjects that shared no family members between them, together with a remaining group of 29 test (29T)

subjects that shared family members with 210P but not 210V. The first group of subjects (210P) was used for creating the parcellation and training the areal classifier, which also made use of the 29T group to avoid overfitting. The second group of subjects (210V) was used only for statistical cross-validation of the parcellation, areal classifier detection rates in independent subjects, and group parcellation reproducibility measures. A test-retest group of 27 subjects scanned twice through the entire MRI protocol and independently processed through the HCP pipelines was used for individual subject reproducibility measures. Subject recruitment procedures and informed consent forms, including consent to share de-identified data, were approved by the Washington University institutional review board. Datasets were de-identified and are publicly shared on the ConnectomeDB database (https://db.humanconnectome.org).

1.2 Image Preprocessing

Spatial image preprocessing (i.e. distortion correction and image alignment) was carried out using the HCP's spatial minimal preprocessing pipelines[6]. This included steps to maximize alignment across image modalities, to minimize distortions relative to the subject's anatomical space, and to minimize spatial smoothing (blurring) of the data. The data were projected into the 2 mm standard CIFTI grayordinates space, which includes cortical grey matter surface vertices and subcortical grey matter voxels[6]. This offers substantial improvements in spatial localization over traditional volume-based analyses, enabling more accurate cross-subject and cross-study registrations and avoiding smoothing that mixes signals across differing tissue types or between nearby cortical folds. Additionally, we did minimal smoothing within the CIFTI grayordinates space to avoid mixing across areal borders prior to parcellation.

For cross-subject registration of the cerebral cortex, we used a two-stage process based on the Multimodal Surface Matching (MSM) algorithm[15] (see ESM #2.1-2.5). An initial 'gentle' stage, constrained only by cortical folding patterns (FreeSurfer's 'sulc' measure), was used to obtain approximate geographic alignment without overfitting the registration to folding patterns, which are not strongly correlated with cortical areas in many regions. Previously, we found that more aggressive folding-based registration (either MSM-based or FreeSurfer-based) slightly decreased cross-subject task-fMRI

statistics, suggesting that aligning cortical folds too tightly actually reduces alignment of cortical areas[15]. A second, more aggressive stage used cortical areal features to bring areas into better alignment across subjects while avoiding neurobiologically implausible distortions or overfitting to noise in the data. The areal features used were myelin maps, resting state network maps computed with weighed regression (an improvement over dual regression[35] described in the ESM #2.3) and resting state visuotopic maps (see ESM #4.4). Areal distortion was measured by taking the log base-2 of the ratio of the registered spherical surface tile areas to the original spherical surface tile areas. The mean (across space) of the absolute value of the areal distortion averaged across subjects from both registration stages was 30% less than the standard FreeSurfer folding-based registration and the maximum (across space) of this measure was 54% less. Despite less overall distortion, the areal-feature-based registration delivers substantially more accurate registration of cortical areas than does FreeSurfer folding-based registration as judged by cross-subject task fMRI statistics, an areal feature that was not used to drive the registration[15]. Because MSM registration preserves topology and is relatively gentle (i.e. it does not tear or distort the cortical surface in neurobiologically implausible ways), it is unable to align some cortical areas in some subjects where the areal arrangement differs from the group average (see SRD #1.3-1.4 for more details on atypical areas). Group average registration drift away from the gentle folding-based geographic alignment was removed from the surface registration[36] (see ESM #2.5) to enable comparisons of this dataset with datasets registered using different areal features (e.g. post-mortem cytoarchitecture). Group average registration drift is any consistent effect of the registration during template generation on the mean size, shape, or position of areas on the sphere (as opposed to the desired reductions in cross-subject variation). An obvious example is the 37% increase in average brain volume produced by registration to MNI space[5]. Uncorrected drifts during surface template generation can cause apparent changes in cortical areal size, shape, and position when comparing across studies.

Resting state fMRI data were denoised for spatially specific temporal artifacts (e.g. subject movement, cardiac pulsation, and scanner artifacts) using the ICA+FIX approach, which includes detrending the data and aggressively regressing out 24 movement parameters[37,38]. We avoided regressing out the 'global signal' (mean gray-matter

timecourse) from our data because preliminary analyses showed that this step shifted putative connectivity-based areal boundaries so that they lined up less well with other modalities, likely because of the strong areal specificity of the residual global signal after ICA+FIX clean up. Task fMRI data were temporally filtered using a high pass filter. More details on resting state and task fMRI temporal preprocessing are described in the ESM (#1.6-1.8). Substantial spatial smoothing was avoided for both datasets, and all images were intensity normalized to account for the receive coil sensitivity field. Artifact maps of large vein effects, fMRI gradient echo signal loss, and surface curvature were computed as described in ESM #1.9.

1.3 Modalities for Parcellation

The multi-modal cortical parcellation used information related to the four areal properties of architecture, function, connectivity, and topography[3]. Architecture was measured using T1w/T2w myelin content maps plus cortical thickness maps with surface curvature regressed out[6,10,11] (ESM #1.5). Function was measured using task-fMRI responses to 7 tasks in 86 task contrasts (47 unique; 39 were sign-reversed contrasts). Effect size maps (i.e. beta maps) after correction for the receive field were used instead of Z statistic maps because we are interested in regional differences in the magnitude of BOLD signal change induced by the tasks, rather than differences in the significance of the BOLD signal change. Functional connectivity was measured using pairwise Pearson correlation of the denoised resting state timeseries of each pair of grayordinates. Topographic organization was explored using resting state timeseries in visual cortex, with spatial regressors representing polar angle and eccentricity patterns in area V1 combined with a modified "dual regression-like" approach that weights each surface vertex according to the cortical surface area that it represents (see ESM #4.4). The semi-automated multi-modal parcellation was generated using group average data for all of these modalities from the 210P group of subjects (see ESM #3.1-3.3 for details on how the group averages were created for each modality). The reproducibility of these group average maps was assessed by correlating the spatial maps for the 210P and 210V groups (see SRD #1.1).

1.4 The Gradient-based Parcellation Approach

Classically, cortical areas have been defined based on sharp changes in one or more of the areal properties of architecture, function, connectivity, and topography. Traditionally, this relied heavily on visual inspection, until more objective and quantitative approaches became available[13,14]. One highly successful approach to post-mortem architectural parcellation involves computing a dissimilarity metric, (the Mahalanobis distance) between neighboring feature profiles generated from segmented histological images and testing for statistically significant and large spikes in dissimilarity that indicate putative areal boundaries. For in vivo data, a similarly powerful approach involves taking the first derivative (i.e. the spatial gradient) of a measure of interest along cortical surface and using the gradient magnitude to objectively identify locations where the measure is changing rapidly. One can then draw putative areal boundaries along the resulting gradient ridges[11,17,20]. Here we combined elements of both approaches in a multi-modal context to generate semi-automatically drawn areal borders that were then evaluated statistically. Gradients were computed for architectural, functional, connectivity, and topographic modalities (See ESM #4.1-4.4).

To incorporate expert knowledge and priors from the neuroanatomical literature into the parcellation process, the neuroanatomists (MG and DVE) evaluated the multi-modal neuroimaging data and its gradients to define initial areal borders based on the following criteria: 1) Presence of a colocalized gradient ridge in at least two independent modalities was taken as strong evidence of an areal border, and the vast majority of areal borders satisfied this criterion. 2) Presence of corresponding gradients in the left and right hemispheres provided further evidence for a genuine areal border. For the vast majority of borders, the same modalities yielded robust gradients in both hemispheres. We did not find strong evidence for an area present in one hemisphere that was absent in the other (though a few areas show hemispheric asymmetries in their functional 'signature' and/or in their spatial relationships with neighboring areas). 3) We ignored gradients clearly attributable to imaging artifacts (see NSR for details). 4) Cortex on opposite sides of the border needed to differ robustly and significantly in the areal features used to delineate the border. 5) Confidence was increased if prior literature described a corresponding areal border. 6) Early runs of a supervised machine learning algorithm (areal classifier, see #1.6 below)

needed to be able to learn to distinguish each cortical area from its neighbors in a large majority of individual subjects based on individual subject multi-modal features (the early runs were only done using 210P and 29T, keeping 210V independent for later analyses). After the neuroanatomists delineated the initial areal borders and chose the important areal features that defined them, an automated algorithm then optimized the border placement so that it followed the most probable path based on the chosen areal features (see ESM #5.1-5.3). The NSR documents the information that was used to distinguish each of the 180 areas from its neighbors.

The neuroanatomists named areas based on previous parcellations whenever a reasonable match to the literature could be made. In some cases, areal identification was based on the similarity of the area's properties relative to previously reported areas (e.g. area 4, primary motor cortex, is known to be heavily myelinated and thick; area V2 has a mirror-image visuotopic map relative to neighboring area V1). In most cases, however, the information used to describe previous cortical areas (e.g. cytoarchitecture) was not available in the HCP data, and areal identification mainly reflected spatial correspondences relative to cortical folding patterns (if reliable for that region of cortex) or spatial relationships between neighboring cortical areas. The strongest evidence for areal identification came from studies that provided surface-based probabilistic or maximum probability maps, ideally also registered using areal features and dedrifting of templates[36]. In these cases, we directly compared these data with our data and show the degree of overlap in the NSR. When such data were unavailable, we used published information to the degree feasible (see ESM #5.3 for limitations of non-surface-based/not publically available data) to make areal identifications or to describe new areas that had not previously been identified. The information used to name each cortical area is described in the NSR.

1.5 Statistical Cross Validation of the Multi-modal Parcellation

Once the parcellation has been created, parcellated representations of data from each modality can be generated using either the group parcellation or the individual subject parcellations. For the statistical cross-validation, we created parcellated myelin, cortical thickness, task fMRI, and resting state functional connectivity datasets using the

semi-automated multimodal group parcellation (see ESM #7.1). For myelin and cortical thickness, we simply averaged the values of the dense individual subject maps within each area. For task fMRI, we averaged the timeseries within each area prior to computing task statistics (to benefit from the CNR improvements of parcellation demonstrated in Main Text Figure 4e). For the same reason, we averaged resting state timeseries within each parcel prior to computing functional connectivity to form a parcellated functional connectome.

For each pair of areas that shared a border in the parcellation, we computed a paired samples 2-tailed t-test across subjects on these parcellated data for each feature (ignoring tests that involved the diagonal in the resting state parcellated functional connectome). We thresholded these tests at the Bonferroni-corrected significance level of $p<9*10^{-8}$ (# of area pairs across both hemispheres (1050) X number of features (266) X number of tails (2) * 0.05) and an effect size threshold of Cohen's d>1. We grouped the features into 4 independent categories (myelin, cortical thickness, task fMRI, and resting state fMRI) to determine for each area pair whether it showed robust and statistically significant differences across multiple modalities. For more details, see ESM #7.2.

1.6 The Cortical Areal Classifier

We used a supervised machine learning classifier to automatically delineate and identify each cortical area from its neighbors across a large majority of individual subjects based on multi-modal information. Besides validating the robustness of the parcellation, this provides useful information about each individual subject's parcellation, along with an approach to generalizing the parcellation to other datasets. To automatically parcellate individual subjects, we adapted the multi-layer perceptron used by Hacker et al[30] to delineate and identify seven resting state networks more accurately than simpler linear methods including dual regression. We used the multi-layer perceptron to classify all 180 areas in our parcellation using multi-modal feature maps and relied on two neuroanatomically sensible assumptions to simplify the problem: 1) After areal feature-based registration (MSMAll), we assumed that each cortical area was approximately in the same general location across subjects (e.g. we don't expect to find V1 outside the occipital lobe). This also means that we consider widely separated regions having similar multi-

modal areal fingerprints to be distinct cortical areas even if they have similar architecture, coactivation in functional tasks, and belong to the same resting state network. These assumptions allowed us to reduce the overall classification problem to a set of 180 classification problems per hemisphere, each involving discrimination of one area from the areas around it. 2) Also, instead of classifying each area from all of its neighbors specifically (i.e. one class for the area plus one class for each neighboring area), we set up the problem as a binary classification (the most robust kind of classification problem), classifying each area from all of the surrounding cortex as a single alternate class. This surrounding cortex represents a "searchlight" for the area, and this searchlight was the group parcel location plus a 30 mm radius surrounding the group parcel in all directions across the surface (meaning that for a 10 mm circular area, the searchlight would be a circle of 70 mm in diameter, still a quite large region of cortex). The 30 mm radius (geodesic distance computed on the group average midthickness surface corrected for vertex area loss due to averaging) was chosen because it easily encompassed the individual variation in area 55b in the 210P group (55b approaches a worst case because it is a relatively small and highly variable cortical area). The training labels were the group area from the semi-automated parcellation (class 1), and the remaining cortex in the searchlight (class 2).

The features used by the classifier covered the same set of modalities used for the original parcellation, including architectural measures of myelin and cortical thickness with curvature regressed out; task fMRI maps (redundant information was reduced and SNR increased with a d=20 ICA-based approach run on the task contrast beta maps, see ESM #6.4); the 77 surface-related resting state fMRI network maps computed on individual subjects using weighted regression from an overall d=137 group ICA; five visuotopic topographic maps transformed into a format interpretable by the classifier; and maps of artifacts that the classifier used to interpret differences in areal features due to artifactual effects (see ESM #6.3-6.5 for further description of each modality's classifier features). These 112 multi-modal feature maps were generated for each vertex in each of the 449 subjects and the 27 repeated subjects, with each hemisphere processed separately. Other than the 30 mm radius searchlight ROI, the classifier has no spatial concept of where the area should be (it operates independently on each vertex and only knows what the area's

fingerprint looks like in the feature space). Consequently, special consideration was given to the spatial visuotopic patterns, which were transformed into maps whose values reflected the alternating mirror symmetric organization of visual areas (i.e. maps whose values reflect the orientation of the visuotopic gradient vector relative to the vector that points "geodesically" towards V1, see ESM #6.5).

The classifier analyses were conducted using a standard machine learning train/test/validation approach. The classifier was trained using the 210P subjects and tested against overfitting using the extra 29T subjects. The 210V subjects were used as the validation sample, and thus were not involved in the classifier training, testing, or the parcellation itself, and also shared no family relationships with the 210P or the 29T groups. A short initial run of the classifier was used to identify features that the classifier was particularly sensitive to for each area (see below and ESM #6.6). These features were compared in each individual subject with the group average pattern to exclude subjects that were potentially misaligned with the typical subject in this region (and hence for which the group defined training labels were likely inaccurate). This area-specific set of subjects in the 210P and 29T groups were excluded from the final classifier training of each area. The classifier's output (ranging from 0 to 1) represents the likelihood that a given vertex in a subject is part of the area being classified or part of the surrounding cortex of the searchlight. Once the classifier training weights have been generated, it is possible to classify any subject who has the 112 multi-modal maps computed, including those whose areas are misaligned with the group (see SRD #1.4).

The trained classifier was applied to the 449 subjects and 27 repeat subjects to generate individual subject likelihood maps for each of the 180 areas in each hemisphere. These probability maps were combined by finding the largest probability for each vertex and then regularized within local neighborhoods (see ESM #6.7) to make an individual subject 'winner take all' parcellation. An area was considered to have been detected in a subject for the purposes of the areal detection measures (the overall classifier areal detection rate and the maps of areal detection rate for each area) if its size was between 1/3 and 3 times the size of the original population-based parcel (a pragmatic threshold chosen prior to performing the analysis that tolerates modestly greater neuroanatomical variability across subjects than the empirical range reported in cytoarchitectonic

studies[39,40]). Probabilistic maps of each area were then created by separately averaging the individual subject winner-take-all parcellation areas for the 210P and 210V subject groups. A group maximum probability map (MPM) parcellation was then created by assigning the identity of the maximum areal probability to each vertex. The reproducibility of the parcellation was assessed by correlating these two MPM maps and by computing a Dice coefficient. In both cases the parcellation was first turned into 180 concatenated binary ROIs per hemisphere (each area was represented by a separate map, ~30,000 vertices per hemisphere, with ones for all vertices inside the area and zeros for all vertices outside). The reproducibility of the individual subject hard parcellation maps was assessed similarly. For more details, see ESM #7.2.

Multi-modal areal fingerprints learned by the classifier were visualized using a classifier sensitivity metric. This metric was the partial derivative with respect to each feature of each area multiplied by the gradient magnitude of the feature (see ESM #6.8). The measure indicates which areal features the classifier finds most informative when classifying a given area and whether increases or decreases in the value of the feature make the area more likely to be present. The sensitivity metric can be visualized both at the dense (vertex-wise) level for each feature and each area, or summarized at a parcel level. For each feature, the sensitivity metric was summarized at the parcel level by taking the maximum absolute value of the metric (i.e. finding the border where the feature was most influential) and using this maximum to represent the area in a parcellated or a matrix view, as shown in Supplementary Figure 12.

References

1 Brodmann, K. Vergleichende Lokalisationslehre der Grosshirnrinde in ihren Prinzipien dargestellt auf Grund des Zellenbaues. *Leipzig, J.A. Barth; English translation available in Garey, L.J. Brodmann's Localization in the Cerebral Cortex (Smith Gordon, London, 1994).* (1909).

2 Brodmann, K. *Brodmann's: Localisation in the Cerebral Cortex*. (Springer Science & Business Media, 2007).

3 Felleman, D. J. & Van Essen, D. C. Distributed hierarchical processing in the primate cerebral cortex. *Cereb Cortex* **1**, 1-47 (1991).

4 Nieuwenhuys, R. The myeloarchitectonic studies on the human cerebral cortex of the Vogt-Vogt school, and their significance for the interpretation of functional neuroimaging data. *Brain structure & function* **218**, 303-352, doi:10.1007/s00429-012-0460-z (2013).

5 Van Essen, D. C., Glasser, M. F., Dierker, D. L., Harwell, J. & Coalson, T. Parcellations and hemispheric asymmetries of human cerebral cortex analyzed on surface-based atlases. *Cereb Cortex* **22**, 2241-2262, doi:10.1093/cercor/bhr291 (2012).
6 Glasser, M. F. *et al.* The minimal preprocessing pipelines for the Human Connectome Project. *NeuroImage* **80**, 105-124, doi:10.1016/j.neuroimage.2013.04.127 (2013).
7 Smith, S. M. *et al.* Resting-state fMRI in the Human Connectome Project. *NeuroImage* **80**, 144-168, doi:10.1016/j.neuroimage.2013.05.039 (2013).
8 Ugurbil, K. *et al.* Pushing spatial and temporal resolution for functional and diffusuion MRI in the Human Connectome Project. *NeuroImage* (2013).
9 Van Essen, D. C. *et al.* The WU-Minn Human Connectome Project: an overview. *NeuroImage* **80**, 62-79, doi:10.1016/j.neuroimage.2013.05.041 (2013).
10 Glasser, M. F., Goyal, M. S., Preuss, T. M., Raichle, M. E. & Van Essen, D. C. Trends and properties of human cerebral cortex: correlations with cortical myelin content. *NeuroImage* **93 Pt 2**, 165-175, doi:10.1016/j.neuroimage.2013.03.060 (2014).
11 Glasser, M. F. & Van Essen, D. C. Mapping human cortical areas in vivo based on myelin content as revealed by T1- and T2-weighted MRI. *The Journal of neuroscience : the official journal of the Society for Neuroscience* **31**, 11597-11616, doi:10.1523/JNEUROSCI.2180-11.2011 (2011).
12 Barch, D. M. *et al.* Function in the human connectome: task-fMRI and individual differences in behavior. *NeuroImage* **80**, 169-189, doi:10.1016/j.neuroimage.2013.05.033 (2013).
13 Caspers, S., Eickhoff, S. B., Zilles, K. & Amunts, K. Microstructural grey matter parcellation and its relevance for connectome analyses. *NeuroImage* **80**, 18-26, doi:10.1016/j.neuroimage.2013.04.003 (2013).
14 Schleicher, A., Amunts, K., Geyer, S., Morosan, P. & Zilles, K. Observer-independent method for microstructural parcellation of cerebral cortex: a quantitative approach to cytoarchitectonics. *NeuroImage* **9**, 165-177 (1999).
15 Robinson, E. C. *et al.* MSM: a new flexible framework for Multimodal Surface Matching. *NeuroImage* **100**, 414-426, doi:10.1016/j.neuroimage.2014.05.069 (2014).
16 Zilles, K. & Amunts, K. Centenary of Brodmann's map--conception and fate. *Nat Rev Neurosci* **11**, 139-145, doi:10.1038/nrn2776 (2010).
17 Cohen, A. L. *et al.* Defining functional areas in individual human brains using resting functional connectivity MRI. *NeuroImage* **41**, 45-57, doi:10.1016/j.neuroimage.2008.01.066 (2008).
18 Kolster, H., Peeters, R. & Orban, G. A. The retinotopic organization of the human middle temporal area MT/V5 and its cortical neighbors. *The Journal of neuroscience : the official journal of the Society for Neuroscience* **30**, 9801-9820, doi:10.1523/JNEUROSCI.2069-10.2010 (2010).
19 Wang, L., Mruczek, R. E., Arcaro, M. J. & Kastner, S. Probabilistic Maps of Visual Topography in Human Cortex. *Cereb Cortex* **25**, 3911-3931, doi:10.1093/cercor/bhu277 (2015).
20 Gordon, E. M. *et al.* Generation and Evaluation of a Cortical Area Parcellation from Resting-State Correlations. *Cereb Cortex*, doi:10.1093/cercor/bhu239 (2014).

21 Shen, X., Tokoglu, F., Papademetris, X. & Constable, R. T. Groupwise whole-brain parcellation from resting-state fMRI data for network node identification. *NeuroImage* **82**, 403-415 (2013).
22 Yeo, B. T. *et al.* The organization of the human cerebral cortex estimated by intrinsic functional connectivity. *J Neurophysiol* **106**, 1125-1165, doi:10.1152/jn.00338.2011 (2011).
23 Hopf, A. Über die Verteilung myeloarchitektonischer Merkmale in der Stirnhirnrinde beim Menschen. *J Hirnforsch* **2**, 311-333 (1956).
24 Van Essen, D. C. & Glasser, M. F. In vivo architectonics: a cortico-centric perspective. *NeuroImage* **93 Pt 2**, 157-164, doi:10.1016/j.neuroimage.2013.04.095 (2014).
25 Olman, C. A. *et al.* Layer-specific fMRI reflects different neuronal computations at different depths in human V1. *PloS one* **7**, e32536 (2012).
26 Polimeni, J. R., Fischl, B., Greve, D. N. & Wald, L. L. Laminar analysis of 7T BOLD using an imposed spatial activation pattern in human V1. *NeuroImage* **52**, 1334-1346 (2010).
27 Yacoub, E., Harel, N. & Ugurbil, K. High-field fMRI unveils orientation columns in humans. *Proceedings of the National Academy of Sciences of the United States of America* **105**, 10607-10612 (2008).
28 Zimmermann, J. *et al.* Mapping the organization of axis of motion selective features in human area MT using high-field fMRI. *PLoS One* **6**, e28716 (2011).
29 Smith, S. M. *et al.* Functional connectomics from resting-state fMRI. *Trends Cogn Sci* **17**, 666-682, doi:Doi 10.1016/J.Tics.2013.09.016 (2013).
30 Hacker, C. D. *et al.* Resting state network estimation in individual subjects. *NeuroImage* **82**, 616-633, doi:10.1016/j.neuroimage.2013.05.108 (2013).
31 Tavor, I. *et al.* Task-free MRI predicts individual differences in brain activity during task performance. *Science* **352**, 216-220 (2016).
32 Van Essen, D. C. *et al.* The Brain Analysis Library of Spatial maps and Atlases (BALSA) Database. *NeuroImage*, doi:doi: 10.1016/j.neuroimage.2016.04.002 (2016).
33 Hill, J. *et al.* A surface-based analysis of hemispheric asymmetries and folding of cerebral cortex in term-born human infants. *The Journal of neuroscience : the official journal of the Society for Neuroscience* **30**, 2268-2276, doi:10.1523/JNEUROSCI.4682-09.2010 (2010).
34 Van Essen, D. C. & Dierker, D. L. Surface-based and probabilistic atlases of primate cerebral cortex. *Neuron* **56**, 209-225, doi:10.1016/j.neuron.2007.10.015 (2007).
35 Filippini, N. *et al.* Distinct patterns of brain activity in young carriers of the APOE-epsilon4 allele. *Proceedings of the National Academy of Sciences of the United States of America* **106**, 7209-7214, doi:10.1073/pnas.0811879106 (2009).
36 Abdollahi, R. O. *et al.* Correspondences between retinotopic areas and myelin maps in human visual cortex. *NeuroImage* **99**, 509-524, doi:10.1016/j.neuroimage.2014.06.042 (2014).
37 Griffanti, L. *et al.* ICA-based artefact removal and accelerated fMRI acquisition for improved resting state network imaging. *NeuroImage* **95**, 232-247 (2014).
38 Salimi-Khorshidi, G. *et al.* Automatic denoising of functional MRI data: combining independent component analysis and hierarchical fusion of classifiers. *NeuroImage* **90**, 449-468 (2014).

39 Caspers, S. *et al.* The human inferior parietal lobule in stereotaxic space. *Brain structure & function* **212**, 481-495, doi:10.1007/s00429-008-0195-z (2008).
40 Malikovic, A. *et al.* Cytoarchitectonic analysis of the human extrastriate cortex in the region of V5/MT+: a probabilistic, stereotaxic map of area hOc5. *Cereb Cortex* **17**, 562-574, doi:10.1093/cercor/bhj181 (2007).

Supplementary Methods For
A Multi-modal Parcellation of Human Cerebral Cortex

Matthew F. Glasser[1], Timothy S. Coalson[1]*, Emma C. Robinson[2,3]*, Carl D. Hacker[4]*, John Harwell[1], Essa Yacoub[5], Kamil Ugurbil[5], Jesper Andersson[2], Christian F. Beckmann[6], Mark Jenkinson[2], Stephen M. Smith[2], David C. Van Essen[1]

[1]Department of Neuroscience, Washington University Medical School, Saint Louis, Missouri 63110, USA. [2]FMRIB Centre, Nuffield Department of Clinical Neurosciences, John Radcliffe Hospital, University of Oxford, Oxford OX3 9DU, UK. [3]Department of Computing, Imperial College, London SW7 2AZ, UK. [4]Department of Biomedical Engineering, Washington University, Saint Louis, Missouri 63110, USA. [5]Center for Magnetic Resonance Research (CMRR), University of Minnesota, Minneapolis, Minnesota 55455, USA. [6]Donders Institute for Brain, Cognition and Behavior, Radboud University, Nijmegen 6525 EN, The Netherlands. [7]Department of Cognitive Neuroscience, Radboud University Medical Centre Nijmegen, Postbus 9101, Nijmegen 6500 HB, The Netherlands.

**These authors contributed equally to this work.*

1. Subjects, Image Acquisition, and Initial Image Preprocessing

1.1 Subjects

We used the "HCP500" dataset (June, 2014 data release) of adults aged 22-35 drawn from a pool of twins and their non-twin siblings ((Van Essen et al., 2013); http://www.humanconnectome.org/documentation/S500/). All 449 subjects that had complete structural (at least one T1w and one T2w scan), rfMRI (4 runs X 15 minutes), and tfMRI (7 tasks, 60 minutes total) datasets were included. The subjects were divided into two main analysis groups: 210 parcellation subjects (the '210P' group) and 210 validation subjects (the '210V' group). Group independence was preserved by ensuring that no families were split between the 210P and 210V groups (210 subjects per group was the maximum number for evenly sized complete datasets from this release where all members of each family were assigned to either one group or the other). A third auxiliary group of 29 subjects (the 29T group, including some family relationships shared with the 210P group) was used only in training the cortical areal classifier as the initial 'test' dataset to prevent overfitting of random noise (see #6.6). Additionally, 27 of the 449 subjects were scanned using the entire HCP MRI acquisition protocol a second time, reanalyzed, and used to check the reproducibility of the individual subject parcellations. The HCP data were acquired using protocols approved by the Washington University institutional review board, deidentified, and publicly shared on the ConnectomeDB database (https://db.humanconnectome.org; (Hodge et al., 2015)).

1.2 Image Acquisition

The HCP MRI data acquisition has previously been described in detail ((Glasser et al., 2013; Smith et al., 2013a; Ugurbil et al., 2013);

http://www.humanconnectome.org/documentation/S500/HCP_S500+MEG2_Release_Appendix_I.pdf). Images were acquired using a customized 3T Siemens 'Connectom' Skyra having a 100mT/m SC72 gradient insert and using a standard Siemens 32-channel RF-receive head coil. At least one good quality 3D T1w MPRAGE image (as assessed by a trained rater, (Marcus et al., 2013)) was acquired at 0.7 mm isotropic resolution. At least one good quality 3D T2w SPACE image was also acquired at 0.7 mm isotropic resolution in the same session as the T1w image. Whole brain rfMRI and tfMRI data were acquired using identical multi-band EPI sequence parameters of 2 mm isotropic resolution with a TR=720 ms. Field maps were acquired during both the structural and fMRI scanning sessions to enable accurate cross-modal registrations of the T2w and fMRI images to the T1w image in each subject. Additionally, the spin echo phase reversed images acquired during the fMRI session (with matched geometry and echo spacing to the gradient echo fMRI data) were used to compute a more accurate fMRI bias field correction and to segment regions of gradient echo signal loss.

1.3 Data analysis software

Data were analyzed using the publicly released HCP pipelines (Glasser et al., 2013), plus additional pipelines for cross-subject registration and individual subject parcellation that have been or will soon be released. The software packages used for analysis included Connectome Workbench commandline tools, FSL, and FreeSurfer (Fischl, 2012; Jenkinson et al., 2012). Pipelines were written in Bash shell scripts and Matlab (https://github.com/Washington-University/Pipelines). Connectome Workbench 'wb_view' GUI (http://www.humanconnectome.org/software/connectome-workbench.html) was used for all visualization and for some interactive data analysis. All neuroanatomical (brain-related) figures for this study were generated in Connectome Workbench using the Tile Tabs (to make multiple figure panels) and Annotations (to label panels, areas, and features) capabilities and were directly exported as PNG image files, bypassing the need for image editing software (these tools are available in Connectome Workbench version 1.2.0 or higher). More importantly, these figures were also saved as Connectome Workbench "scene" files, to allow anyone who downloads the scene and associated data files to reproduce an interactive version of each figure in Connectome Workbench for further exploration of the data and comparison to their own data. The scene files and associated data files are available in the BALSA database (Brain Analysis Library of Spatial maps and Atlases) ((Van Essen et al., 2016); http://balsa.wustl.edu) to facilitate comparisons across studies and with future data, and they are directly accessible via URLs in the relevant figure legends.

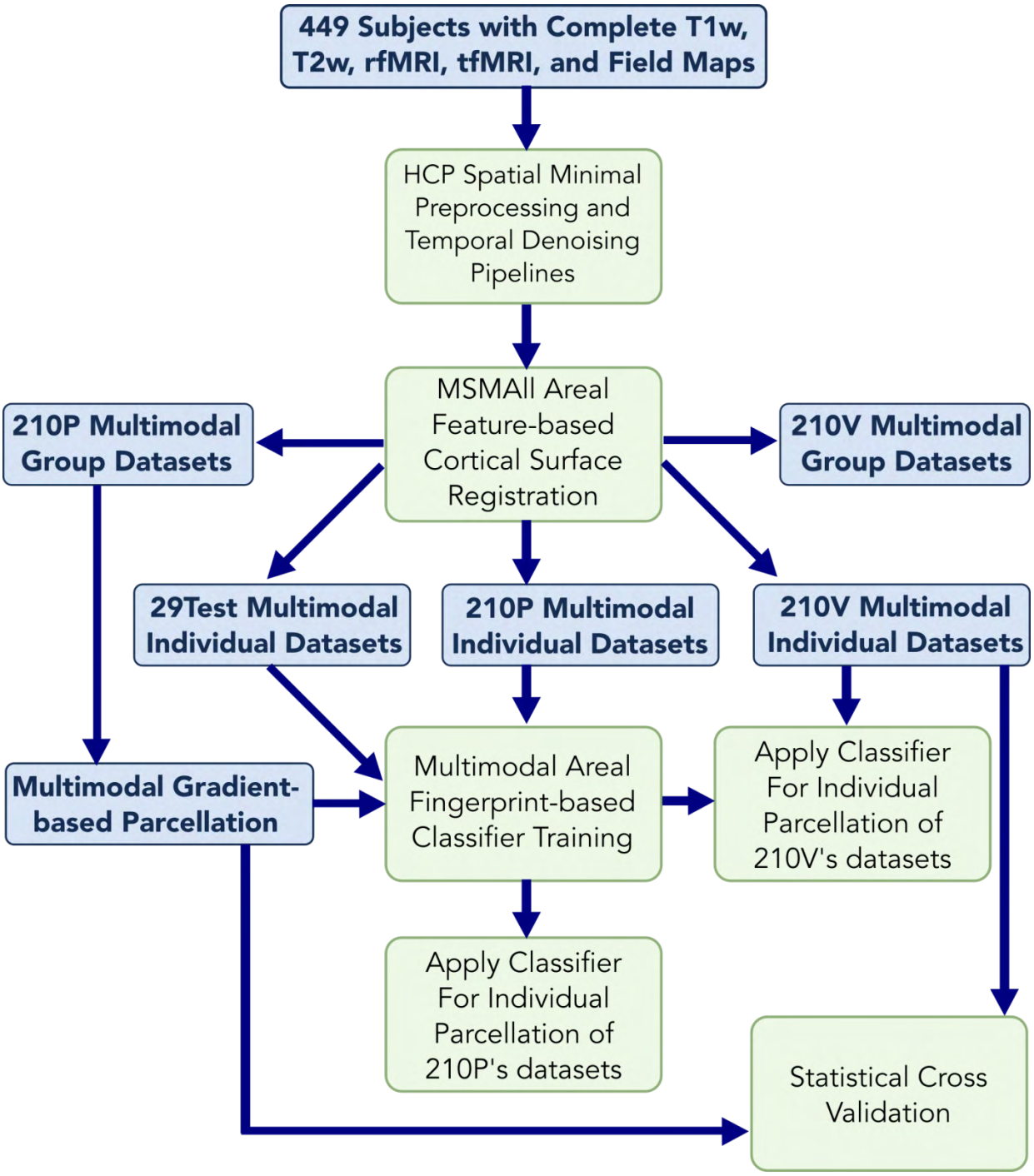

Figure 1 shows the overall workflow of the paper. After initial spatial and temporal preprocessing and areal-feature-based registration, the data were divided into groups, and group average datasets were produced. The 210P group dataset was used for semi-automated multi-modal gradient-based parcellation. This parcellation was cross-validated using the 210V individual subject datasets. The 210P individual datasets were used for training of the multi-modal areal fingerprint-based individual subject areal classifier, along with the 29T test dataset. The 210P and 210V datasets were parcellated by applying the trained classifier to their individual subject data, and group maximum probability parcellations were generated. In this and analogous figures, datasets are light blue and processes are light green.

1.4 Overview of data analysis methods

Many methods were developed *de novo* or were improved upon to produce a high quality multi-modal parcellation at the group level and to use this parcellation to identify individual subject cortical areas. Methods described in previous HCP-related publications are only summarized briefly here, whereas new or substantially improved methods are described in more detail. Figure 1 provides an overview of the major processing steps/stages that are described in subsequent sections. The minimally preprocessed (Glasser et al., 2013) data were downloaded from ConnectomeDB, and MSMAll areal-feature-based surface registration was performed on 449 subjects. The multi-modal data were then split into parcellation and validation groups of 210 subjects each, and group averages were created. The 210P subjects' group average data were used to generate a multi-modal gradient-based parcellation, and their individual data were used together with 29 additional test subjects to train a machine learning classifier to delineate and identify cortical areas in individual subjects using their multi-modal areal fingerprints. This trained classifier was applied to the 210P and 210V datasets to generate individual subject parcellations and group maximum probability maps. The 210V dataset was used for statistical cross-validation of the 210P-based original parcellation.

1.5 Initial Preprocessing: Structural

The HCP structural preprocessing pipelines (Glasser et al., 2013) include PreFreeSurfer, FreeSurfer, and PostFreeSurfer components and were run inside ConnectomeDB for the 500-subject HCP release. The PreFreeSurfer pipeline includes: (i) aligning and averaging repeated T1w and T2w scans of good or excellent quality when they exist; (ii) removing gradient nonlinearity and readout distortion (b0 distortion in 3D images) to create an unbiased "native" volume space for each subject that is rigidly aligned to the MNI template; (iii) cross-modal alignment between the T1w and T2w images with FreeSurfer's boundary based registration (BBR) method (Greve and Fischl, 2009); (iv) bias field correction using sqrt(T1w X T2w); and (v) nonlinear volume-based registration to the MNI template using FSL's FNIRT algorithm. A customized version of Freesurfer version 5.3's recon-all was used to generate white and pial cortical surfaces (using both T1w and T2w volumes at 0.7 mm resolution) plus a subcortical segmentation, all carried out in the subjects' native volume space. PostFreeSurfer converted the FreeSurfer data into standard NIFTI, GIFTI, and CIFTI file formats and also brought the data into MNI space.

The Multimodal Surface Matching (MSM) surface registration algorithm (Robinson et al., 2014) was used to perform an initial gentle non-rigid surface registration based on folding patterns (MSMSulc). This supplanted the FreeSurfer folding-based registration previously used (Glasser et al., 2013), because it achieved slightly better initial alignment of functionally corresponding regions (e.g., task fMRI) than Freesurfer's algorithm while inducing much lower local distortions (Robinson et al., 2014). This registration, together with the FNIRT nonlinear registration, was used to bring an initial version of the data into standard grayordinates space (32k standard mesh for each hemisphere's cortical surface at 2 mm average vertex spacing and 2 mm isotropic MNI-space voxels for the subcortical volume data). Myelin maps were computed using the ratio of T1w/T2w images and normalized for residual transmit field inhomogeneity (Glasser et al., 2014a; Glasser et al.,

2013; Glasser and Van Essen, 2011; Robinson et al., 2014). Because gyral crowns tend to be thicker than sulcal fundi, the FreeSurfer-generated measure of cortical thickness was corrected for folding-related biases by regressing out the FreeSurfer mean curvature measure from each subjects' thickness data (Glasser and Van Essen, 2011).

1.6 Initial Preprocessing: Functional

The HCP functional preprocessing pipelines include volumetric (fMRIVolume) and surface-based (fMRISurface) components (Glasser et al., 2013; Smith et al., 2013a) applied to both rfMRI and tfMRI data. The fMRIVolume pipeline includes removing image distortions due to gradient nonlinearity and b0 inhomogeneity; motion correction; cross modal alignment to the T1w image with BBR (Greve and Fischl, 2009); concatenation of all transforms, including the nonlinear volume registration to MNI space; and resampling the original timeseries into MNI space using a single spline interpolation. Several intensity normalization steps occur, including a crude fMRI bias field correction based on the structural data from a separate imaging session (this bias field correction is replaced with a better one in later processing as described below, which has also been incorporated into the latest version of the pipelines), and grand 4D mean normalization to 10,000. The fMRISurface pipeline was then used to map grey matter timeseries data into the 91282-grayordinate standard space (2 mm average cortical vertex spacing and 2 mm subcortical voxels) using a 2 mm FWHM smoothing kernel (constrained to the cortical surface and subcortical grey matter segmentation). These steps produce a CIFTI "dense timeseries" file for each rfMRI and tfMRI run. The crude bias field correction map was also mapped into standard CIFTI space so that it could be replaced with the better one (by dividing it back out and multiplying by the new correction).

1.7 Initial Preprocessing: Resting State fMRI Temporal Denoising

For rfMRI runs, the ICA+FIX pipeline (Beckmann et al., 2005; Griffanti et al., 2014; Salimi-Khorshidi et al., 2014; Smith et al., 2013a) was used to remove spatially specific temporally structured artifacts. ICA+FIX includes several steps: 1) highpass temporal filtering with a sigma of 1,000 s (run length = 864 s) to remove linear trends in the data; 2) MELODIC independent component analysis (ICA) with auto dimensionality selection up to 250 components, producing component spatial maps and timeseries; 3) classification of these components into signal and noise categories by the FMRIB's ICA-based Xnoiseifier (FIX) trained ICA component classifier; 4) regression out of the data and all ICA components of 24 motion parameters (which were also temporal highpass filtered with sigma of 1,000 s). Regression coefficients were computed using all ICA component timeseries, and the noise component timeseries were then weighted by the regression coefficients and subtracted from the data (a "non-aggressive" regression approach). The ICA+FIX algorithms were run on the volumetric timeseries data, then the highpass filter and the nuisance regression steps were also applied to the grayordinates timeseries data. The ICA+FIX cleanup was reapplied to the rfMRI dense timeseries data after the original uncleaned native mesh data had been resampled into the standard grayordinates space according the areal-feature-based MSM surface registration (see below #2.5). Regression of the mean gray signal (aka 'global signal') was used in early analyses, but it was

discontinued because it shifted some rfMRI functional connectivity (FC) gradient locations in ways that reduced cross-modal alignment. No additional spatial smoothing or temporal lowpass filtering was performed, as these types of "lossy" preprocessing steps would reduce the accuracy of the parcellations and proved unnecessary for the purposes of the current study.

1.8 Initial Preprocessing: Task fMRI Analysis

For task fMRI runs, the HCP's task analysis pipeline was run to generate grayordinate-based task analyses (Barch et al., 2013). This pipeline is an adaption of FSL's FEAT analysis pipeline (Smith et al., 2004) to CIFTI grayordinate space. A temporal highpass filter with a sigma of 100 s was run on the data to remove low frequency fluctuations presumably unrelated to the task design. These fluctuations likely include both temporal artifacts and the spontaneous intrinsic BOLD fluctuations that are the focus of rfMRI analyses. As with the rfMRI preprocessing, no additional spatial smoothing or temporal lowpass filtering was performed. FSL's FILM algorithm was used to compute the first level (single run) task fMRI statistics (including temporal autocorrelation smoothing constrained to the cortical surface and subcortical parcels), and FSL's FLAME algorithm was used in a fixed effects analysis to combine across runs within subjects. The tfMRI analysis pipeline was run after the tfMRI timeseries data had been resampled into the standard grayordinates space using areal-feature-based MSM surface registration (as explained in the MSMAll section below, see also Figure 10 and sections #3.2 and #6.4 below for a full description of the task fMRI processing used in this paper).

1.9 Initial Preprocessing: Artifact Map Generation

Three maps were generated for use as artifact indicators: a large vessel effect map, a gradient echo fMRI dropout map, and a curvature map. In addition to generating the myelin maps, the T1w/T2w ratio images were also used to estimate the effect of large blood vessels on the fMRI data. Blood vessels have a much higher T1w/T2w ratio than brain tissue and were segmented via thresholding normalized to the mean and standard deviation of the T1w/T2w image. This segmentation was regularized (dilated and eroded equal amounts, and above threshold values not near the boundary of the brain parenchyma were removed), slightly dilated, and smoothed using a 2 mm FWHM volume smoothing kernel to account for proximity effects of blood vessels. The gradient echo fMRI dropout map was created by identifying voxels having a ratio of less than 50% signal intensity in the single band reference (SBRef) gradient echo image relative to the spin echo image after using a spatial highpass filter of sigma=5 mm (smooth, then subtract from the unsmoothed data) to reduce residual low spatial frequency variation in the ratio image (related to the differences in the transmit field between the two images). This dropout segmentation was dilated one 0.7 mm voxel and smoothed at 2 mm FWHM in the volume. After removing transmit field effects and excluding dropout regions, the low spatial frequency intensity variations (sigma=5 mm) within grey matter were used to compute a more accurate, smoother receive bias field for the fMRI data. This field was also scaled to a volume mean of 10,000, just like the fMRI timeseries data were scaled by the HCP minimal preprocessing pipelines. The scaled field was used as a reference BOLD intensity image when computing

bias free beta effect size maps (after having reverted the previous bias field correction). The vascular effect maps, dropout maps, and the reference images were mapped into the standard CIFTI grayordinates space. The curvature maps were taken directly from FreeSurfer and mapped into the standard CIFTI grayordinates surface space.

2. Multi-modal Areal-feature-based Surface Registration ("MSMAll")

Achieving good intersubject cortical alignment was critical to our group average gradient-based parcellation efforts. This entailed major refinements to the recently published MSM approach (Robinson et al., 2014). The following sections describe (i) the motivation for areal feature-based cortical surface registration; (ii) a novel method of weighted regression to generate more individualized and refined RSN maps in individual subjects by upweighting the most aligned regions; (iii) details on the implementation of the MSMAll method; (iv) "de-drifting" used to minimize registration-induced biases in group-average datasets; and (v) the final one-step resampling of the data from the subjects' native meshes to their standard 32k meshes. Our overall approach to surface registration is illustrated in Figure 2.

2.1 Motivation

The boundaries of cortical areas are correlated with cortical folding patterns, but the strength of this correlation is variable across the cerebral cortex. Early areas such as V1 in the calcarine sulcus and areas 4, 3a, and 3b in the central sulcus have particularly high correlations with folding patterns (Fischl et al., 2008). Association areas implicated in 'higher' levels of processing, e.g. areas 44 and 45 in the inferior frontal gyrus, often have substantially lower correlations with folding patterns (Fischl et al., 2008). Moreover, the folding patterns themselves do not necessarily have one-to-one correspondence across subjects in these higher association regions (Van Essen, 2005; Van Essen et al., 2012). To improve the alignment of cortical areas across subjects and thus the validity of our group average analyses, we used MSM (Robinson et al., 2014) to perform registration based on areal features. Registration using myelin and Resting State Network (RSN) maps can improve the cross-subject alignment of independent tfMRI datasets (Robinson et al., 2014), while at the same time decreasing the cross-subject alignment of cortical folding patterns that do not correlate with cortical areal locations.

2.2 General approach to MSMAll

The MSMSulc folding-based surface registration from the HCP minimal preprocessing pipelines (in PostFreeSurfer, see above #1.5) was used to initialize the areal feature-based registration (MSMAll). MSMAll used myelin maps, RSN maps, and rfMRI visuotopic maps (see below #4.4) in a joint multi-modal registration to drive cross-subject alignment. Because there is no temporal correspondence across subjects in the rfMRI timeseries, the only corresponding rfMRI subject-wise dataset (i.e. without reference to group data) is the rfMRI FC "dense connectome" (91,282 X 91,282 X 4 bytes = 32.5GB). This dense connectome is not suitable for driving the registration process, however, because of its sheer size and the fact that it contains an enormous amount of redundant

information plus unstructured noise, neither of which are useful for registration[1]. What is needed instead is a dimensionality reduction of the dense connectome across individual subjects in which the data remains matched across subjects. We used Group ICA along with spatial multiple regression to produce RSN template maps and their corresponding individual subject maps for this purpose.

To generate the RSN template maps needed to initiate the process, melodic group ICA (Beckmann et al., 2005; Beckmann and Smith, 2004; Smith et al., 2014) was performed in CIFTI grayordinates space (Smith et al., 2013a; Smith et al., 2013b) using resting state data from the 210P group that had previously been registered with MSMRSN (Robinson et al., 2014) across a range of ICA dimensionalities (d = 22 to 100, sparsely sampled, and then searched using binary search to identify the optimal dimensionality). Thus the RSN templates that served as the input to this process were generated from the data presented in (Robinson et al., 2014) after removing the group average registration drift (see below #2.5 and (Abdollahi et al., 2014). We used two metrics to estimate the optimal group ICA dimensionality in a 28-subject "registration optimization" subset of the 210P+29T subject groups. (i) An analysis of tfMRI z-statistic cluster mass (thresholded at +/-z=2.32) using a group mixed effects analysis (Robinson et al., 2014) yielded a broad peak of similar tfMRI cluster mass values over the range of 33-42 components. (ii) An analysis of average cortical surface vertex-associated areal distortion showed a monotonic decrease in surface areal distortion (averaged across the hemisphere) when registering using higher numbers of components. Consequently, a group ICA dimensionality of 41 was used for the MSMAll registration, as this dimensionality was the local maximum in cluster mass that had the least areal distortion.[2] This included three artifactual components and four predominantly subcortical components, which were excluded from the cortical surface registration but were included in the multiple regression model that was used to generate the individual subject RSN component maps (see below #2.4).

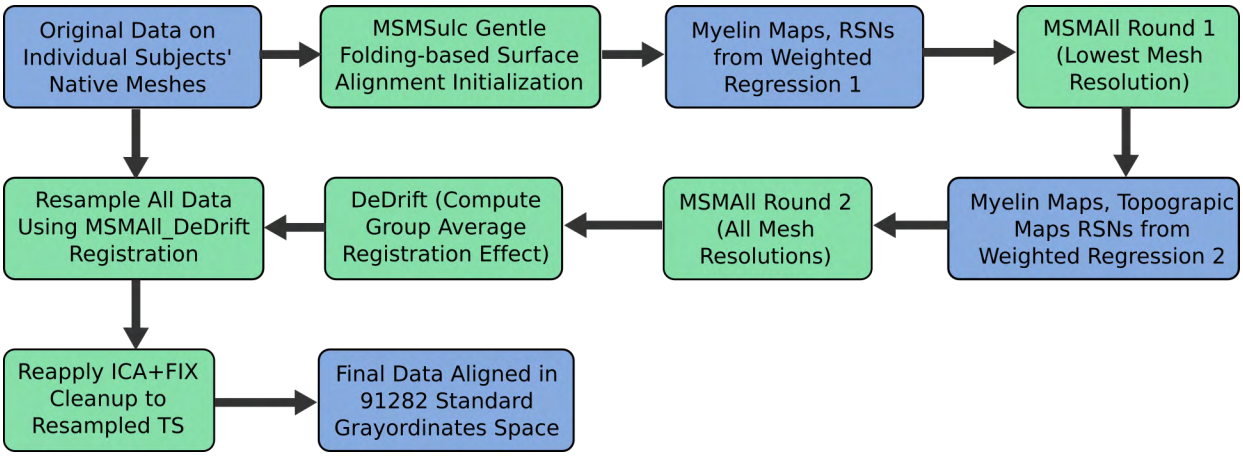

[1]Though see below (#3.3-3.4) for a method that downweights the effects of unstructured noise in dense connectomes without spatial or temporal smoothing

[2]In the ConnectomeDB version of the MSMAll Pipeline that was used for the 900 subject HCP data release, this process was reapplied using the registration templates generated from this study's data, and a dimensionality of 40 was found to be optimal.

Figure 2, above, shows the overall approach to surface registration used in this study. First, MSMSulc was used to perform an initial gentle non-rigid folding-based registration of the native mesh data. Then myelin maps and resting state network maps (using weighted regression, see below #2.3) were generated. The first round of MSMAll used these maps in a joint multi-modal registration for only the lowest mesh resolution in order to get both hemispheres roughly aligned based on areal features. Then myelin maps, resting state network maps (using weighted regression based on the rough alignment) and topographic maps were generated based on this alignment. The second round of MSMAll uses these maps in a joint multi-modal registration for all three mesh resolutions (see below #2.4) to get each hemisphere finely aligned by areal features. Registration drift is computed by averaging all of the individual subject registrations relative to MSMSulc—any group average registration effect is considered drift. The combined registration, MSMAll_DeDrift, is used to resample all datasets from the native mesh into the standard grayordinates space with a single interpolation step, and then the ICA+FIX cleanup is reapplied to the resampled dense timeseries (TS).

Figure 3, below, shows the steps of the Weighted Regression method used in this study and compares it to the standard dual regression steps (shown in **BOLD**). In the weighted regression method, the vertex area weighting maps are always used to weight the spatial multiple regressions. An alignment weighting map is derived from low dimensional ICA maps (d=7-21) by correlating the individual subject maps with the group maps, averaging across dimensionalities, and spatial highpass filtering (medium grey box). The first round of weighted regression uses both the vertex area map and the alignment map together to weight the spatial multiple regression of the high dimensional group ICA spatial maps to produce initial subject specific spatial maps (lightest grey box). The second round uses only the vertex area map to weight the first round initial individual subject spatial maps to produce the refined individual subject spatial maps (darkest grey box). These spatial maps can then be used for registration or areal classification. Note that to produce the visuotopic maps (not shown in diagram), a single round of weighted regression equivalent to the second round is used (where the subject specific V1-only spatial regressors take the place of the subject specific ICA spatial maps from the first round).

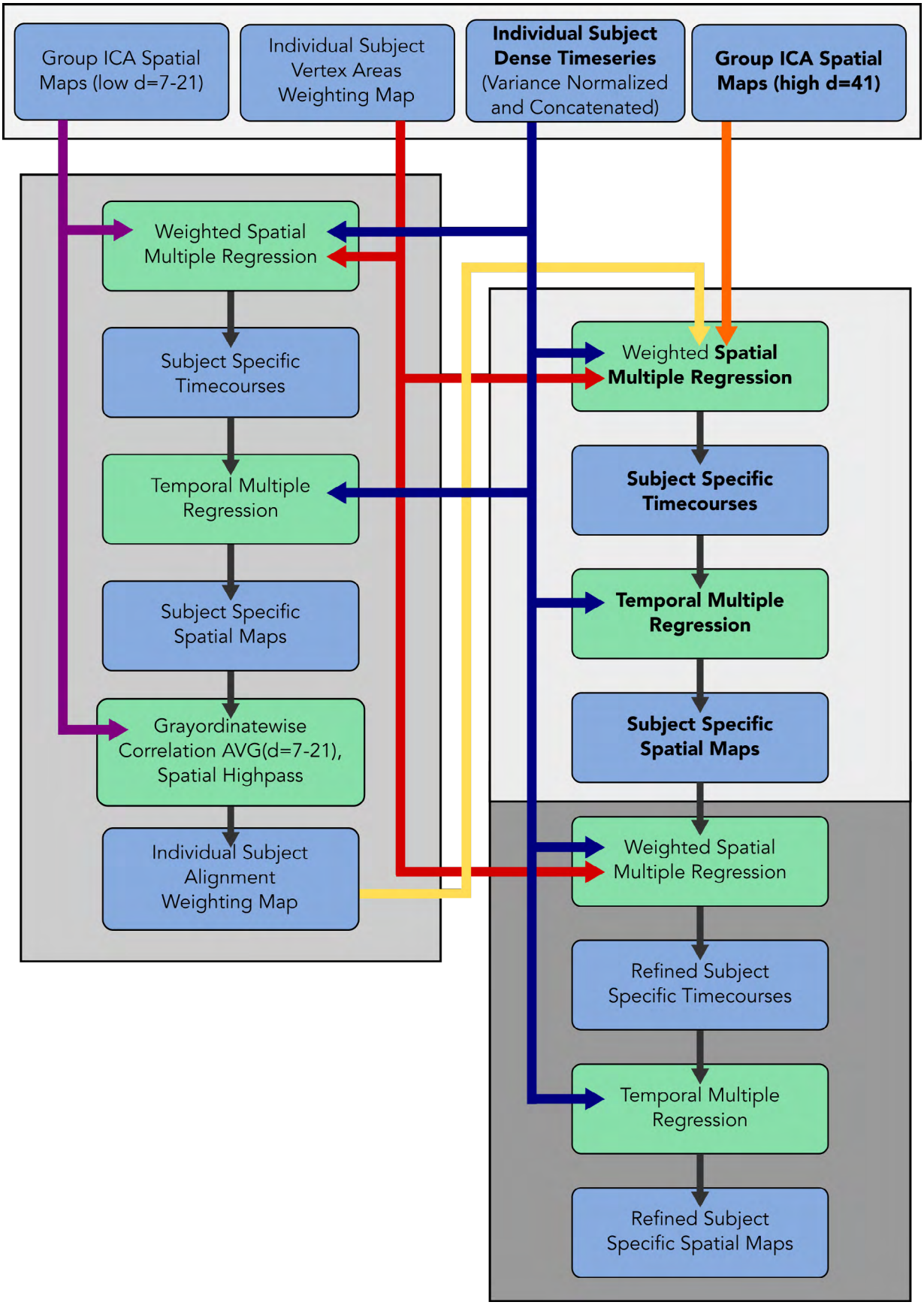
Group ICA Spatial Maps (low d=7-21)
Individual Subject Vertex Areas Weighting Map
Individual Subject Dense Timeseries (Variance Normalized and Concatenated)
Group ICA Spatial Maps (high d=41)
Weighted Spatial Multiple Regression
Subject Specific Timecourses
Temporal Multiple Regression
Subject Specific Spatial Maps
Grayordinatewise Correlation AVG(d=7-21), Spatial Highpass
Individual Subject Alignment Weighting Map
Weighted Spatial Multiple Regression
Subject Specific Timecourses
Temporal Multiple Regression
Subject Specific Spatial Maps
Weighted Spatial Multiple Regression
Refined Subject Specific Timecourses
Temporal Multiple Regression
Refined Subject Specific Spatial Maps

2.3 Weighted Regression for Generating Refined Individual Subject RSN Maps from Group Maps

To generate refined individual subject RSN component maps for registration and areal classification, we implemented a Weighted spatial multiple Regression (WR) technique, see Figure 3. The technique is adapted from standard dual regression (DR) (Filippini et al., 2009) which seeks to use spatial overlap between the group and individual to find individualized versions of the group maps and has two main stages (see **BOLD** portions of Figure 3): (i) subject-specific component timecourses are generated by spatial regression of the group component spatial maps onto the individual dense timeseries, equation (2) below, then (ii) subject-specific component spatial maps are generated by a temporal regression of these timecourses onto the individual dense timeseries, equation (4). Mathematically, we can consider the variables: Y = data (grayordinates X timepoints), X = group model (grayordinates X maps), T = parameter estimates (maps X timepoints), and x = individual maps (grayordinates X maps). To find the subject specific component timeseries, one can use the following equations:

$$Y = XT \quad (1)$$

$$T=pinv(X)Y \quad (2)$$

Where 'pinv' is the pseudoinverse. To find the subject specific component spatial maps, one can use the following equations:

$$Y' = T' x' \quad (3)$$

$$x' = pinv(T')Y' \quad (4)$$

Where the prime (') represents the transpose.

However, we improved this procedure substantially by incorporating a spatial weighting map in the spatial regression and by running a second round of spatial and temporal regression based on the results of the first round (i.e., 2 spatial and 2 temporal regressions total). The individual subject dense timeseries used for the weighted regression were first demeaned (removing the mean of each grayordinate's timeseries) and variance normalized to equalize unstructured noise variance (see below #3.3 for the method of computing the unstructured noise variance map), and then concatenated across all four runs (4800 timepoints/subject).

The spatial weighting map used in WR is the elementwise product of two separate maps: 1) a "Vertex Area Map" map, and 2) an "Alignment Map." The vertex area map represents the vertex areas of the individual subject's midthickness surface resampled onto the standard 32k mesh in native volume space. It compensates for three sources of distortion in surface vertex area between the native midthickness surface in the subject's physical space and the 32k standard MNI space midthickness surface. These arise from (i) the non-rigid volume registration to MNI space, (ii) projection of the anatomical surface to a sphere, and (iii) registration of the individual spherical surface to the atlas spherical

surface. Correcting for these distortions is important because vertex areas (which are homogeneous on standard spherical surfaces) vary over a two-fold range (~3±1 mm^2) when measured on each subject's 32k standard mesh cortical midthickness.

The "Alignment Map" map upweights regions likely to be already well aligned to the group in the individual subject and downweights misaligned regions. This is important because misalignments contribute adversely to the individual subject component timeseries and spatial maps that are generated by DR, insofar as they cause mixing among different resting state networks (and cortical areas). This can cause the resultant DR individual subject spatial maps to be less "individualized" than the true individual subject spatial maps (i.e. more like the group maps than they should be). The problem gets worse as the dimensionality of the ICA being used in the DR increases because there is less information available to estimate each unique component timeseries and spatial map.

To generate the Alignment Map (Figure 3, left column), we used weighted dual regressions (weighted only by the Vertex Area Map) of low ICA dimensionalities. Grayordinates that are already well aligned between the individual and group will, by definition, have individual subject component spatial map values that are strongly correlated to the group map values, whereas misaligned regions will have weaker correlations. Hence, to measure alignment quality we correlated the values of the group component maps to the values of the individual subject component maps, generating a spatial map of Fisher-transformed group versus individual component correlations for each low ICA dimensionality. Dimensionalities between 7 to 21 components yielded the most consistent results when tested in a pilot analysis, so we averaged the correlation maps across these dimensionalities. Undesirable low spatial frequency SNR differences were removed by applying a spatial highpass filter with sigma=14mm.

After generation of the Alignment Map, the WR algorithm includes two rounds of weighted regression, as follows (Figure 3, right column): Round 1a) individual subject timecourses for each component were generated by *spatial* multiple regression of the group component maps into the individual subject dense timeseries, weighted according to the element-wise product of the Vertex Area Map and the Alignment Map. Round 1b) these individual subject component timecourses were then *temporally* multiple regressed into the individual subject dense timeseries to produce the initial individual subject component spatial maps. Round 2a) these inital individual subject component spatial maps were *spatially* multiple regressed into the individual subject dense timeseries, weighted this time only by the Vertex Area Map, to produce a refined set individual subject component timecourses. Round 2b) these refined individual subject component timecourses were *temporally* multiple regressed into the individual subject dense timeseries to generate a refined set of individual subject component spatial maps. The weighted form of the spatial regression looks like equation (5). (W=spatial weights, grayordinates X 1, .* is the elementwise product repeated to match the dimensions of X and Y, the square root is elementwise).

$$T=\text{pinv}(X.*\sqrt{W})(Y.*\sqrt{W}) \quad (5)$$

This second round of regressions helped to refine the resultant spatial maps so that they more closely reflect the individual spatial variation of the subject's resting state data, and allowed the entire individual subject's dataset (i.e. without the Alignment Map

weighting) to contribute to the spatial regression when producing the final refined individual subject component spatial maps. The resulting individual subject component spatial maps were then used in the MSMAll registration or areal classification. In practice we found that this WR approach substantially improved the ability of our classifier to delineate and identify misaligned cortical areas (see #6.3). It also had the benefit of increasing the optimal MSM ICA dimensionality (41 vs the original 26) and requiring fewer registration iterations to reach convergence (2 iterations of MSM and WR vs the original 6 iterations of MSM and DR (Robinson et al., 2014)).

2.4 Implementation of Multi-modal Areal Feature-based Surface Registration Using MSM

Of the 41 component maps, four were excluded because they were predominantly subcortical, and an additional three were excluded because they were dominated by obvious spatial artifacts, leaving 34 well-defined cortical surface RSN component maps. The following 44 maps were jointly used in the final iteration of MSMAll: 34 RSNs, the subject's myelin map, eight V1-based rfMRI visotopic regressor maps (see below #4.4), and a binary non-cortical medial wall ROI (i.e. the region of the surface mesh that does not contain neocortical grey matter). Group versions of all these maps served as the multi-modal registration target. tfMRI contrast maps were not used because (i) it was useful to preserve an independent dataset with which to evaluate whether the registration was objectively improving areal feature alignment (e.g. to check the aforementioned optimal RSN dimensionality for registration) and (ii) the individual subject task contrast maps have less useful contrast to noise (CNR) per map than the individual subject maps of the other modalities as determined by the classifier (see Supplementary Figure 12 in the Supplementary Results and Discussion)[3].

For surface-based registration of spherical surfaces, we used a modified version of the MSM algorithm reported in (Robinson et al., 2014). This achieves smoother deformations by penalizing the warps of each face of the spherical mesh (rather than pairs of points). As the method uses discrete optimization, it utilizes a method for incorporating higher order terms, called Higher-order Clique reduction (HOCR) (Glocker et al., 2010; Ishikawa, 2009, 2014). An exponent of 3 was also used on the regularizer function to nonlinearly penalize larger distortions. We found that this approach achieved comparable alignment of areal features while significantly reducing distortions of the surface mesh. Registration was performed in a multi-resolution setting in which registration used a series of low-resolution control point meshes. These were placed over the original mesh and constrained the deformations so that coarse (low frequency) features of the data are aligned first, and iteratively improves alignment until the fine details are brought into correspondence. We used three resolution levels with control point spacings of 30.0 mm, 15.1 mm, and 7.6 mm. Correlation was used as a similarity metric to drive alignment of the myelin, resting state network maps, and resting state visuotopic maps in a joint multi-modal registration.

[3]Thus, if a substantial amount of rfMRI data were not available, tfMRI data would likely be better treated as rfMRI data in MSMAll registration or areal classification, because with a similar number of timepoints tfMRI data closely resembles rfMRI data (Cole, M.W., Bassett, D.S., Power, J.D., Braver, T.S., Petersen, S.E., 2014. Intrinsic and task-evoked network architectures of the human brain. Neuron 83, 238-251.).

Two iterations of MSM and weighted regression were used, with the first iteration performing only the lowest control point resolution level to achieve a coarse alignment. The V1-based rfMRI visuotopic regressors (see below #4.4) were included only in the second iteration to align the fine visuotopic patterns. (V1, where the visuotopic pattern is defined, is highly correlated with folding (Fischl et al., 2008) and should be well aligned across subjects at this stage of the registration.) Each map was normalized to have a spatial mean of zero and a spatial standard deviation of 1. Other registration parameters at each resolution level included regularization multiplier lambdas of 0.01, 0.05, 0.1; number of internal MSM iterations of 10, 10, 5; and internal smoothing sigmas of 2, 2, 1 mm. Sampling meshes were 7.6 mm spacing, 3.8 mm spacing, and 1.9 mm spacing. Data meshes were 3.8 mm spacing and 1.9 mm spacing. The final output of the registration was a deformed native mesh sphere—"registered sphere" for each individual hemisphere. This sphere contains the same number of vertices as the original individual subject native sphere produced by FreeSurfer, but its vertices have been moved across the surface nonlinearly to maximize alignment with the multi-modal registration target, so that like areal features are aligned across subjects.

2.5 DeDrifting and Final Resampling

The final registration stage involves removal of the group average registration "drift", which is an undesirable byproduct of repeated registration during a template generation process (Abdollahi et al., 2014). Unless corrected, this drift can cause registration template features to drift away from the typical subject in the group. As a particularly sobering example, while volumetric non-rigid registration to MNI space greatly reduces the variability in individual brain volumes (desirable), it also induces a large expansional drift in brain volume (undesirable) so that the group average brain volume is 37% larger than the typical subject's native space brain volume (Van Essen et al., 2012). For surface registration, the problem is not one of anatomical expansion (because the spherical coordinates used in registration are not tied to anatomical coordinates), but of local drifts in cortical areal size, shape, and position that differ across different registration templates and hence can lead to inaccuracies in cross-study spatial comparisons.

Surface-based atlases are fundamentally linked to standard spheres in which large and consistent brain landmarks (i.e. major cross-subject consistent sulci and gyri) have particular latitudes and longitudes in spherical mesh coordinates (Drury et al., 1998; Fischl et al., 1999a; Fischl et al., 1999b; Van Essen, 2005). We used a coordinate system based on the FreeSurfer 'fsaverage' template (Desikan et al., 2006) after registration to a standard mesh sphere that accurately aligns geographically corresponding features in the left and right hemispheres (Van Essen et al., 2012). The high-resolution version of this mesh has 163,842 vertices and is referred to as the '164k_fs_LR' mesh. For most analyses we used a lower-resolution mesh (32,492 vertices; the '32k_fs_LR' mesh, with a 2 mm average vertex spacing on the midthickness surface) matched to the 2 mm volume resolution of the HCP fMRI data (Glasser et al., 2013). Although there is inherently some arbitrariness in how this geographic coordinate system was initialized, it is important to avoid drifts away from this geographic convention to enable the most precise cross-study spatial localization, even when differing areal feature-based registration modalities and templates are used. We used the following approach to remove drifts from our MSMAll registered data. Spheres

whose coordinate locations represent the MSMAll registration warp relative to the gentle MSMSulc folding-based surface alignment were resampled to the 32k_fs_LR standard mesh for each hemisphere and averaged across subjects. These average registered spheres represent the group average warp from the MSMAll registration across all 449 subjects. The inverse of this average spherical warp was applied to each individual's registered sphere, eliminating the group-average drift while maintaining the subject-specific alignment improvements. Each subjects' registration features were then resampled to the atlas sphere and averaged, creating the dedrifted registration template for use by other studies. Each subject's final registered spheres (one for each hemisphere, on the native mesh) represent the MSMAll_DeDrift surface registration (referred to as the 'MSMAll' registration in this study's other documents and in the HCP 900 subject public release).

Using the MSMAll_DeDrift registration, all data used for the parcellation analysis (myelin maps, thickness maps, artifact localization maps, resting state timeseries, and task fMRI timeseries) from all subjects were resampled from the subjects' original native meshes into the 91,282 standard grayordinates space using a single step of adaptive barycentric resampling (Glasser et al., 2013). This avoids unnecessary blurring that can occur with multiple resampling steps. The adaptive barycentric resampling algorithm insures that all native mesh data contribute when downsampling to a lower mesh resolution (~136k native meshes to 32k standard meshes). Additionally, all individual subject surfaces (e.g., midthickness, white, pial) were resampled using regular barycentric interpolation, and Connectome Workbench specification ('spec') files were generated for the MSMAll_DeDrift resampled datasets. These resampled datasets were used for all further analyses, including the following remaining individual subject preprocessing and analysis steps: (i) the task analysis pipeline described above (#1.8) was run; (ii) reapplication of the ICA+FIX resting state structured noise removal on the MSMAll_DeDrift registered and resampled CIFTI dense timeseries; and (iii) recalculation of the myelin map normalization (see above #1.5), which relies on finding very low spatial frequency differences between the individual and group myelin maps using surface registration (Glasser et al., 2013).

3. Creation of Group Average Multi-modal Datasets for Parcellation

3.1 Group Average Structural

Structural data from the 210-subject parcellation (210P) and validation (210V) groups was processed separately as follows. MSMAll_DeDrift-resampled unsmoothed myelin maps plus thickness maps corrected for curvature were averaged vertex-wise across subjects while excluding outliers greater than 3 standard deviations above or below the group mean. Though not used in the semi-automated multi-modal parcellation, average maps of folding patterns (FreeSurfer sulc and curv) were also produced from individual subject maps resampled according to MSMAll_DeDrift. Group averages of the individual MSMAll_DeDrift-resampled surfaces (i.e., averages of coordinate positions for corresponding vertices) were used to display group results.

For some analyses (e.g. gradient computation, see below #4.2-4.3), it is important to have reliable group average measures of the surface area associated with each vertex derived from the individual midthickness surfaces (via the tiles associated with each

vertex, see also above #2.3). Vertex areas computed directly from group average surfaces are inherently inaccurate owing to the blurring effects caused by averaging folding patterns that differ across individuals (see Supplementary Figure 1 in the Supplementary Results and Discussion). This issue arises for folding-based registration because there is not 1 to 1 correspondence of many folds across subjects, and it is exacerbated when using alignment based on areal features, because areal features are imperfectly related to folding patterns across much of the cerebral cortex. Group average vertex area maps were computed by averaging the vertex area maps of individual subjects' native volume space MSMAll_DeDrift-resampled midthickness surfaces, and were used in group computations that required accurate vertex areas such as gradients (see below #4.2-4.3).

3.2 Group Average Task fMRI

For the 86 task contrasts from the seven HCP tasks (47 unique, 39 sign reversed), cross-subject mixed effects analyses were computed using FSL's FLAME algorithm (FLAME1) applied to the individual subject cross-run results. The excellent intersubject alignment provided by MSMAll and a large number of subjects yields high z-statistic values without the need for conventional spatial smoothing. The cross-subject alignment of areal features and lack of smoothing preserves fine spatial details in the group-average maps (see Supplementary Figure 2 in the Supplementary Results and Discussion) and produces high reproducibility across all non-outlier contrasts (see Supplementary Figure 3 in the Supplementary Results and Discussion). For the parcellation and areal classifier we used the effect size maps (betas, after reverting the minimal preprocessing pipelines' bias field correction and applying the improved correction by dividing the beta map by the aforementioned BOLD reference image). We used effect size maps because they are a measure of the task induced effect itself, rather than the significance/precision of the measured task induced effect. Thus, the effect size maps area more analogous to the other maps used for parcellation (e.g., myelin maps).

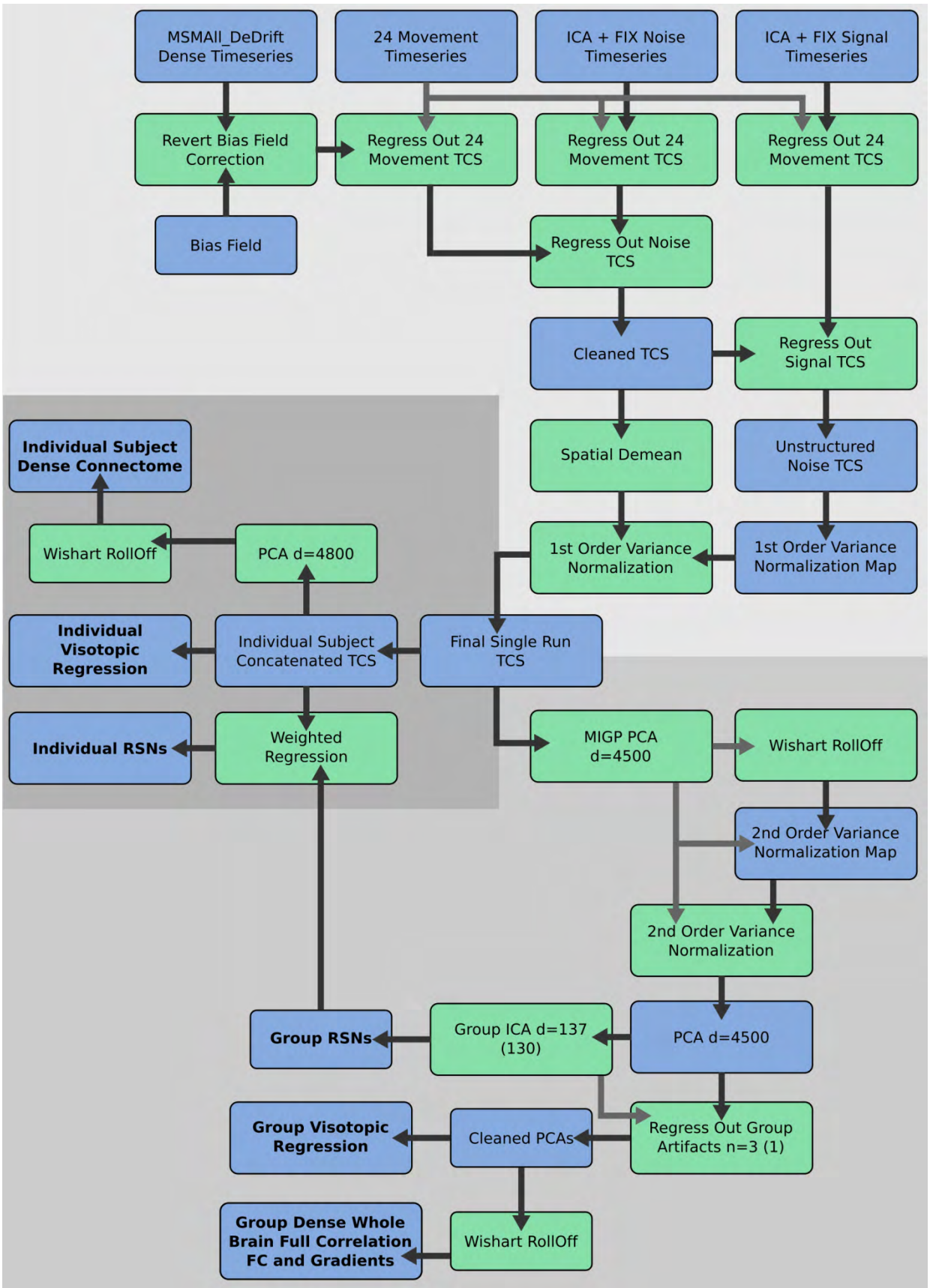
MSMAll_DeDrift Dense Timeseries
24 Movement Timeseries
ICA + FIX Noise Timeseries
ICA + FIX Signal Timeseries
Revert Bias Field Correction
Regress Out 24 Movement TCS
Regress Out 24 Movement TCS
Regress Out 24 Movement TCS
Bias Field
Regress Out Noise TCS
Cleaned TCS
Regress Out Signal TCS
Individual Subject Dense Connectome
Spatial Demean
Unstructured Noise TCS
Wishart RollOff
PCA d=4800
1st Order Variance Normalization
1st Order Variance Normalization Map
Individual Visotopic Regression
Individual Subject Concatenated TCS
Final Single Run TCS
Individual RSNs
Weighted Regression
MIGP PCA d=4500
Wishart RollOff
2nd Order Variance Normalization Map
2nd Order Variance Normalization
Group RSNs
Group ICA d=137 (130)
PCA d=4500
Group Visotopic Regression
Cleaned PCAs
Regress Out Group Artifacts n=3 (1)
Group Dense Whole Brain Full Correlation FC and Gradients
Wishart RollOff

Figure 4, above, shows the resting state processing and analysis stages used in this study separated into 3 main groups. The inputs include: the bias field, the MSMAll_DeDrift resampled dense timeseries (TCS), the 24-parameter motion timeseries, the ICA+FIX noise component timeseries, and the ICA+FIX signal component timeseries (all timeseries have been temporally filtered with a sigma of 1,000 s). The most important outputs are identified by **BOLD** font. Datasets are in light blue boxes and processes are in light green boxes. The first group (lightest gray background) includes reverting the bias field correction, repeating the ICA+FIX cleanup stages (since the MSMAll_DeDrift dense timeseries was resampled from native mesh timeseries that had not yet been cleaned), subtracting the mean of each grayordinate's timecourse, and computation of the first order variance normalization map from the square root of the variance of the unstructured noise timeseries (all cleanup done and all RSNs regressed out) and then division of the dense timeseries by this map, producing the final single run dense timeseries. At this point, the second group (darkest gray background) breaks off to continue individual subject processing. The subject's resting state runs are concatenated, and these data were used to produce the individual subject visuotopic regression maps, the individual subject RSN maps (from the group RSN maps and weighted regression), and, with PCA and Wishart RollOff, a high CNR individual subject dense functional connectome. Also breaking off at this point is the third group (medium gray background), which enables computationally efficient processing of the 210P and 210V group average rfMRI datasets. This module starts with the final single run dense timeseries and uses the MIGP PCA algorithm (d=4500) to combine and dimensionality reduce the resting state data across subjects. The output PCA Series of this algorithm has residual spatial variation unstructured noise variance and requires second order variance normalization (computed from the square root of the difference of the variance before and after a Wishart RollOff, see below). Then PCA is run again without dimensionality reduction to incorporate the spatial reweighting (d=4500). Group ICA (d=137 for 210P; d=130 for 210V) is run on the output PCA series to identify group level RSNs and artifacts (3 for 210P and 1 for 210V). The artifacts are regressed out of the data, and the result can be used for the group visuotopic regression maps. Finally a second Wishart RollOff is performed prior to group dense functional connectivity matrix generation (whole brain full correlation FC and gradients) to improve the CNR of the functional connectivity maps and to eliminate ringing artifacts.

3.3 Group Average Resting State fMRI

A variety of novel and advanced methods were used to maximize the information gained from the resting state fMRI data, while minimizing computational requirements and reducing the impact of structured and unstructured noise. Figure 4 shows an overview of the resting state processing used in this study after resampling from the native mesh dense timeseries into standard grayordinates space according to the MSMAll_DeDrift surface registration. First, the bias field correction is reverted (see below #4.4), the ICA+FIX temporal cleanup is reapplied, and the variance normalization described below is applied to make the cleaned, variance normalized individual run dense rfMRI timeseries (lightest grey box in Figure 4).

In rfMRI studies involving modest numbers of subjects, group analyses are typically carried out by temporally concatenating the individual subject dense timeseries data after subtracting the mean of each grayordinate's timecourse (and perhaps after performing variance normalization). In the present study, a concatenated dense timeseries would be prohibitively large (~342GB, based on 210 subjects X 4800 timepoints = 1,008,000 total timepoints X 91282 grayordinates X 4 floating point bytes). For a computationally tractable group rfMRI dense "timeseries" dataset that closely approximates a full concatenation, we applied the parallelizable and distributable Melodic's Incremental Group PCA (MIGP) algorithm (Smith et al., 2014) to generate a 4500 component group dense PCA series. The dimensionality reduction from 1,008,000 to 4500 removes a large amount of unstructured noise variance while retaining the strongly structured resting state BOLD

signals that are consistent across subjects. The dense PCA series from MIGP, while being much more compact than the full concatenated dense timeseries, is analogous to a timeseries in many respects; however, we will invoke the term PCASeries when a PCA series is being used in an algorithm, reserving the term timeseries for genuine timeseries data.

We found that MIGP performance was improved (i) by reverting the fMRI bias field correction incorporated in the version of the HCP minimal preprocessing pipelines used in the 500 subject HCP data release and (ii) by applying variance normalization based on the amount of unstructured temporal noise in the dense timeseries of each rfMRI run. This normalization ensures that each grayordinate in each run of each subject has a comparable amount of unstructured noise variance prior to MIGP PCA (Beckmann and Smith, 2004). The result is an equal likelihood of detecting false positives across the grayordinates space and improvement in the performance of subsequent algorithms (e.g. ICA, multiple regression). The unstructured noise variance normalization map was computed as the square root of variance remaining after performing all ICA+FIX cleanup steps (high pass filter, 24 movement parameter regression, and structured noise component timeseries regression) and additionally after regressing out the structured RSN signals identified by ICA+FIX (see Figure 4, top & right group).

The large dimensionality reduction by the MIGP algorithm from 1,008,000 to 4500 PCA components results in spatial differences in the residual unstructured noise in the data and can yield undesirable ringing artifacts when visualizing seed-based functional connectivity (http://www.humanconnectome.org/documentation/mound-and-moat-effect.html). A multi-step process was used to avoid this problem (Figure 4, right & bottom module). Emulating an approach introduced by Beckman and Smith (2004), we fit a Wishart eigenspectrum distribution function (Beckmann and Smith, 2004; Wishart, 1928) to the tail of the eigenspectrum of the dense PCA series (whose eigenvectors represent mostly unstructured noise and which have the lowest eigenvalues) to estimate the profile of unstructured noise in the data in PCA space. This distribution was subtracted from the eigenvalues, thereby downweighting ('rolling off') the 'temporal' effects of unstructured noise in the data. The difference in the variances between the original PCA Series and the Wishart rolled off PCA Series represents the residual pattern of spatial variation in unstructured noise in the data. The square root of this map was used as a second order variance normalization map. The spatial variation in this map's values were inversely related (i) to the vertex areas of the surface grayordinates (smaller vertex areas had larger amounts of residual unstructured noise; larger vertex areas had lower amounts) and (ii) to the CNR of the subcortical voxels (lower CNR voxels like those in the iron rich globus pallidus had higher values relative to other voxels). After second order variance normalization, PCA was run again without dimensionality reduction (i.e. PCA d=4500) to incorporate the changes in spatial weighting across the grayordinates space. The resulting PCA series was now appropriate for group ICA.

Group ICA was performed on the 210P data to identify cross-subject consistent RSNs as well as artifactual components that slipped through the ICA+FIX cleanup. An ICA dimensionality of d=137 was chosen because when a find-the-biggest operation across components was performed, it described the data using the smallest number of spatially contiguous pieces (whose size exceeded a surface area of 25 mm^2 or a volume of 125 mm^3) relative to a wide range of dimensionalities (d=95 to 150 in unit steps and 150 to 300 in

5's). Also it was the largest local minimum before the number of subcortical pieces began to increase monotonically (around d=140), suggesting that further splitting was due to the ICA beginning to incorporate more unstructured noise into the subcortical components whose voxels have the lowest CNR and therefore are most vulnerable. Visually, the d=137 decomposition exhibited a striking degree of left/right symmetry, with RSN components either being bilaterally symmetrical or having a symmetrical pair of unilateral components (e.g. see the RSNs shown in the top four rows of Supplementary Figure 4 in the Supplementary Results and Discussion). This strong bilateral symmetry may explain why d=137 was a local minimum in the spatially contiguous pieces measure. Three consistent artifactual components were identified in the d=137 decomposition of the 210P dense PCA series: the tranverse venous sinus; a fronto-polar, orbitofrontal, and anterior temporal component likely attributable to motion and/or motion's interaction with susceptibility artifacts; and an anterior and middle cerebral artery pulsation artifact. These artifactual components were regressed out of the dense PCA Series to produce a cleaned dense PCA Series appropriate for the group visuotopic regression (see below #4.4) and further processing. To produce the cleaned dense connectome for the 210V validation group in Supplementary Figures 4 and 5 in the Supplementary Results and Discussion, group ICA was also performed separately on the 210V data, identifying a d=130 local minimum and only one artifactual component (the tranverse venous sinus).

Although the second order variance normalization reduces spatial inhomogeneities in unstructured noise variance in the MIGP dense PCASeries, it does not address the temporal effects of this noise on dense functional connectivity matrices (CNR reduction and ringing). To address these temporal issues, a Wishart function was fit to the second order variance normalized and cleaned PCA series eigenspectrum. For this stage, the desired output was the Wishart rolled off PCA series and dense connectome (the eigenvalues were reduced by the fitted Wishart null-eigenvalue distribution, remultiplied by the eigenvectors, and the dense connectome formed via the outer-product of the weighted eigenvectors). The Wishart roll off has several benefits: 1) It eliminates ringing induced by the hard cutoff of the PCA series at 4500 components and 2) it addresses the same goal of CNR improvement by unstructured noise reduction as do spatial and temporal smoothing. However, instead of smoothing all signals equally (whether they are of interest or not), the Wishart roll off procedure downweights less structured signals while preserving the sharpness of the structured resting state signals of interest. Highly structured RSN signals (represented by PCA components with high eigenvalues above the Wishart noise eigenvalue distribution) are not downweighted, whereas less structured signals (represented by PCA components with low eigenvalues along the Wishart noise eigenvalue distribution) are downweighted. Thus, the Wishart roll off acts as an edge-preserving spatial and temporal filter.

Empirically, the Wishart roll off improved the CNR of grayordinatewise rfMRI FC dense connectivity matrices, which otherwise have low CNR because there is no averaging across space, as in a parcellated connectivity analysis, an ICA analysis, or a multiple regression analysis, without blurring the signals of interest. Grayordinatewise rfMRI FC was performed using Pearson correlation (when computed on the PCA Series, the data are not spatially demeaned), generating a dense functional connectivity matrix. Also, the Fisher Z transform was not used because it shifted connectivity gradient peaks slightly. The decision not to use the Fisher Z transform was empirically based (not using it resulted

in better alignment of resting state gradients with those of other modalities) and there is not a principled reason for doing it one way or the other. In practice, the difference in gradient peak location was relatively small, however. Despite being processed completely separately through the process shown in Figure 4, the 210P and 210V dense functional connectivity datasets show remarkable reproducibility (see Supplementary Figures 4 and 5 in the Supplementary Results and Discussion). Thus, the approach used here for computationally efficient processing of group resting state data objectively shows good performance. An additional benefit of this approach is that the use of a Wishart rolloff reduces the non-specific "seed bloom" of high correlation near the seeded grayordinate, which arises from spatial autocorrelation in the noise induced by various image reconstruction (e.g. multi-band) and preprocessing steps (e.g. resampling or smoothing). The remaining local connectivity around the seed tends to follow the same areal feature boundaries as more distant functional connectivity does, along with boundaries found in other modalities, making it useful to the neuroanatomist.

3.4 Individual Resting State fMRI

The left-middle group of Figure 4 (darkest gray background) shows the processing steps after temporal concatenation of the final dense timeseries across rfMRI runs in each subject. Visuotopic regression was done using this concatenated dense timeseries (see below #4.4). Also, the individual subject RSN maps were computed using the concatenated dense timeseries and the group RSN map with the weighted regression algorithm (see above #2.3). The PCA decomposition (d=4800) and Wishart roll off technique can additionally be used for generating high CNR individual-subject rfMRI FC dense connectivity matrices without the need for spatial or temporal smoothing. The process is similar to that for the group analyses, except that no dimensionality reduction is performed and therefore there is no need for second variance normalization and a second PCA. These dense functional connectivity matrices, which do not make use of any group information, could provide a useful reference to compare with the individual subject RSN maps generated using group ICA components and weighted regression.

4. Objective, Observer Independent Assessment of Multi-modal Differences Across the Cerebral Cortex: The Gradient-based Approach

4.1 Motivation

Classical neuroanatomists used visual inspection to delineate areal boundaries based on regional differences in cytoarchitecture or myeloarchitecture, often resulting in divergent opinions and controversies as to where boundaries were located. A major advance was the advent of observer independent, objective approaches that could be applied to postmortem histological sections (Caspers et al., 2013; Schleicher et al., 1999; Schleicher et al., 2009; Zilles and Amunts, 2010). The Zilles and Amunts group used cytoarchitectonic feature vectors to characterize each location along a histological section contour and focused on peaks in a vector difference measure (the Mahalanobis distance) to identify abrupt changes that represent candidate areal boundaries. These transitions could then be tested statistically for significance and interpreted by neuroanatomists to ensure

that they were not artifactual (e.g. from folding, veins, etc.). Here we apply a spatial-gradient-based approach that is similar in spirit to the histological Mahalanobis distance approach but is customized for multi-modal MRI data on 2D cortical midthickness surfaces rather than histological sections. We compute the magnitude of the first spatial derivative (gradient) of each modality, which indicates the rate of change in the modality at each spatial location. Locations of sharp change in a modality represent candidate areal borders. These spatial gradients also provide a common medium in which to compare changes across multiple modalities. As discussed below (#5), locations with transitions (gradients) in multiple modalities make particularly strong candidates for areal boundaries.

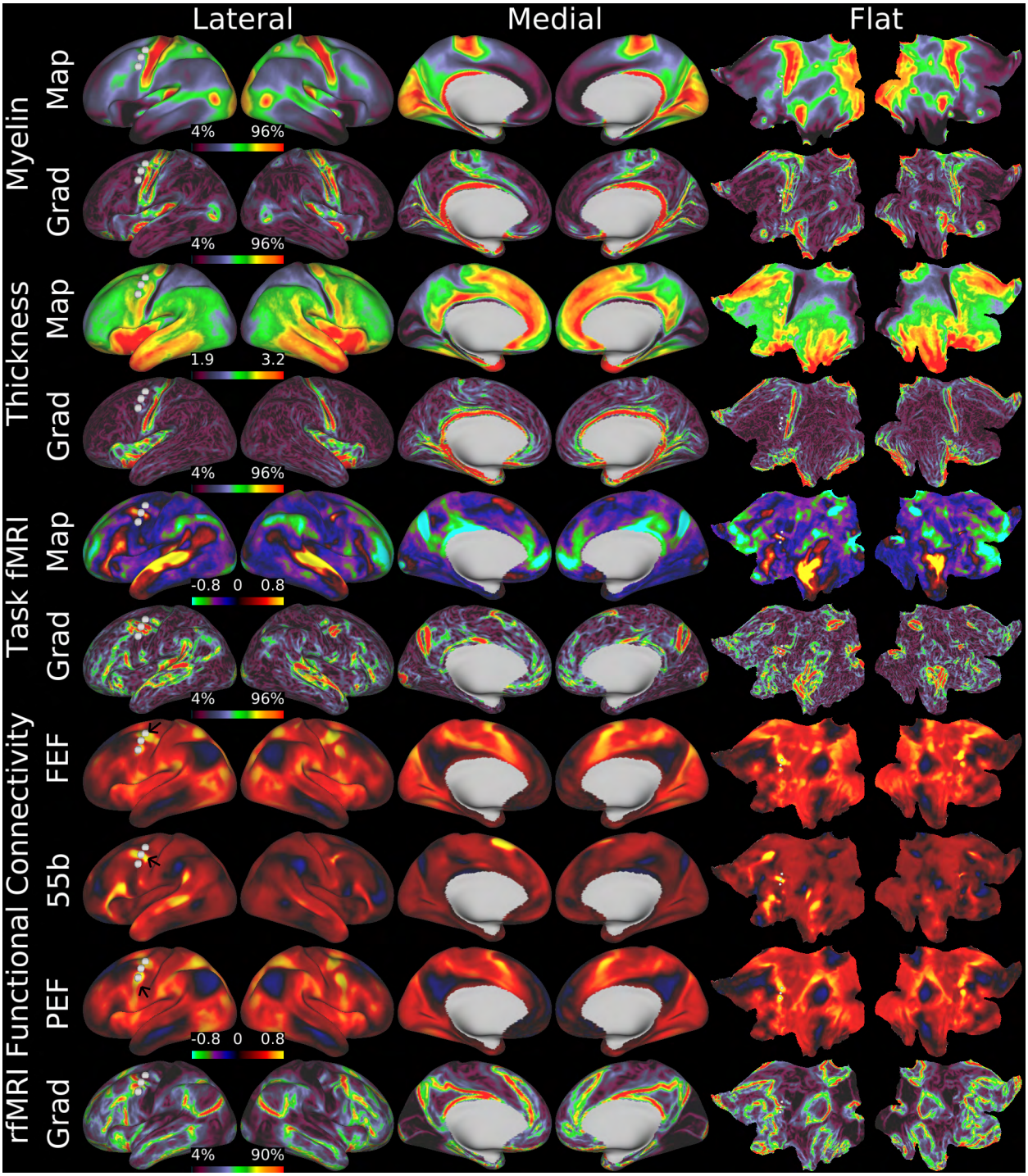

Figure 5, above, shows the four feature categories and their gradients. Rows 1 and 2 show inflated and flat map views of cortical myelin maps and gradients. Rows 3 and 4 show cortical thickness maps with curvature regressed out and their gradients. Rows 5 and 6 show an example task contrast effect size map (scaled to beta = +/-0.8) and its gradient from the LANGUAGE Story vs Baseline contrast. Task fMRI effect size maps can be treated similarly to the architectural myelin and thickness measures as far as gradient computation is concerned. Rows 7, 8, and 9 show three functional connectivity maps from the white spheres representing seed locations in FEF, 55b, and PEF (Row 7 is the most dorsal, Row 8 is the middle, and Row 9 is the most ventral). Row 10 shows the mean functional connectivity gradient map. Note that as one crosses the strong gradients surrounding area 55b from FEF to 55b to PEF, the functional connectivity pattern changes

dramatically. This is correlated with smaller changes in myelin density (moderate to light to moderate, See Main Results). Also, note that the functional connectivity map from the 55b seed (Row 8) strongly resembles the LANGUAGE Story task activation map (Row 5). Data at http://balsa.wustl.edu/W1GV.

4.2 Calculation of Surface Gradients on Modality Spatial Maps

Gradients of myelin, thickness, tfMRI contrast effect size maps, and visuotopic regression maps were computed using the following approach (see Figures 5 and 8 for example modality gradients): For each vertex of the cortical midthickness surface on the 32k standard mesh, average the normals of the vertex's associated mesh triangles to obtain the vertex normal vector. Then, "unroll" the vertex and its neighbors (within the cerebral cortex ROI) onto a plane orthogonal to the vertex normal that passes through the vertex as follows (see Figure 6): (i) between the center vertex and a neighboring vertex, draw a circular arc that is tangent to the plane at the center vertex; (ii) compute the length (L_{unroll}) of this arc using the formula $L_{unroll} = L_{Euclid} * \sin^{-1}(L_{opposite} / L_{Euclid}) * L_{Euclid} / L_{opposite}$, where $L_{opposite}$ is the dot product of the vector representing the edge and the normal vector of the vertex, noting that for small angles this calculation may be unstable due to the large radius, and should be skipped for such cases as the correction is negligible; (iii) project the neighboring vertex onto the plane, then modify the projected position to keep the projected direction from the center vertex, but maintain a distance from the center vertex equal to the circular arc length. Fit a linear function within the plane ($f(t, u) = at + bu + c$, where t and u are distances along orthogonal axes within the plane) to the values and positions of the center vertex and the unrolled neighboring vertices neighbors, via regression. The gradient vector is the spatial coefficients, projected into 3D space by the unit vectors of the plane's coordinate system. If the regression is undefined, for instance if there is only one neighbor because the vertex is along the medial wall, instead average the gradient vectors obtained by taking each within-roi unrolled neighbor and using the relative position and difference in value.

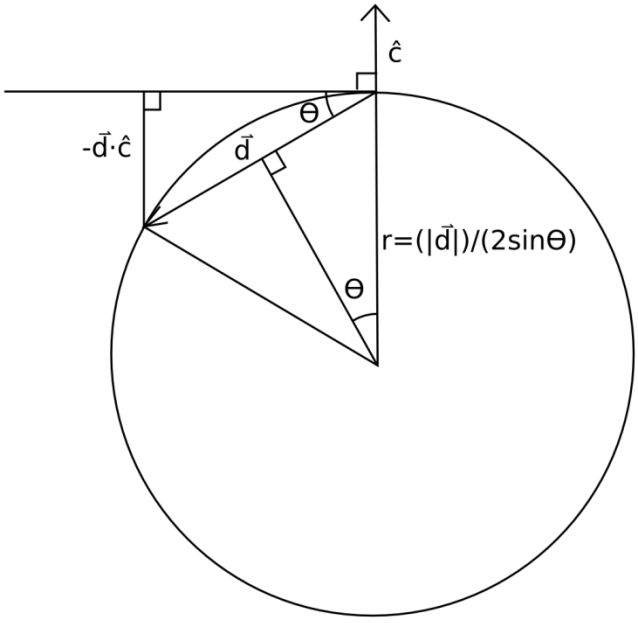

Figure 6 schematizes the geometry associated with the 'unrolling' process involved in computing gradients along the surface. $\vec{d}$ is the vector from the center vertex to the neighboring vertex being unrolled. The circle defining the arc that gets unrolled is drawn, and radii are drawn to both ends of $\vec{d}$. θ is defined as half the angle of the arc, so that the identical right triangles formed from cutting the triangle of $\vec{d}$ and the two radii in half, each have the angle θ at the center of the circle. Hence, the radius of the circle is half the length of $\vec{d}$, divided by the sine of θ. To determine the angle θ, consider the right triangle formed from a line drawn perpendicular to the tangent placed at the center vertex, connecting to the neighbor vertex being unrolled (the head of $\vec{d}$). The length of this segment is (for situations where the circle curves away from the normal vector, as in the figure) the negative of the dot product of $\vec{d}$ and the unit normal vector at the center vertex, denoted as $\hat{c}$. θ is therefore the inverse sine of this negative dot product divided by the length of $\vec{d}$. The length of an arc is the angle of the arc in radians times the radius of the circle, and we now have both, giving the final value as $|\vec{d}| * \sin^{-1}((-\vec{d} \bullet \hat{c})/|\vec{d}|) * (|\vec{d}|/(-\vec{d} \bullet \hat{c}))$, simplifying the sine θ expression as θ is defined by an inverse sine. Due to the properties of sine, the negatives can be dropped from both dot products, giving the simplified formula $|\vec{d}| * \sin^{-1}((\vec{d} \bullet \hat{c})/|\vec{d}|) * (|\vec{d}|/(\vec{d} \bullet \hat{c}))$. Whether the curvature is towards or away from the normal vector, both dot products have the same sign, and therefore the result is positive, meaning that this formula generalizes to both directions of curvature.

When taking the gradient of group-averaged data, a group-average surface is used, along with a group average of the surface areas associated with each surface vertex (referred to as the "corrected vertex areas"). These surface areas enable an approximate correction for the reduction in distance caused by the increased smoothness of the group-average surface. The length of each edge on the group average surface is assumed to be split into two parts, each part residing entirely within the area associated with the vertex at its end. Furthermore, the ratio between the lengths of these parts is assumed to be equal to the ratio of the square roots of the surface areas of the vertices, as given by just the group average surface, without using the corrected vertex areas. To find the corrected length of this edge, scale each of these parts by the ratio between the square roots of the vertex areas from the group-average surface and the corrected vertex areas. This works out to the formula: $L_{corrected} = L_{surface} * (\sqrt{Area}_{corrected}(A) + \sqrt{Area}_{corrected}(B)) / (\sqrt{Area}_{surface}(A) + \sqrt{Area}_{surface}(B))$, where A and B are the vertices that the edge being corrected joins, and the subscript "surface" denotes lengths and vertex areas derived only from the group surface without correction. The result of the gradient algorithm that is used for parcellation is the magnitude of the gradient vector at each vertex for each map.

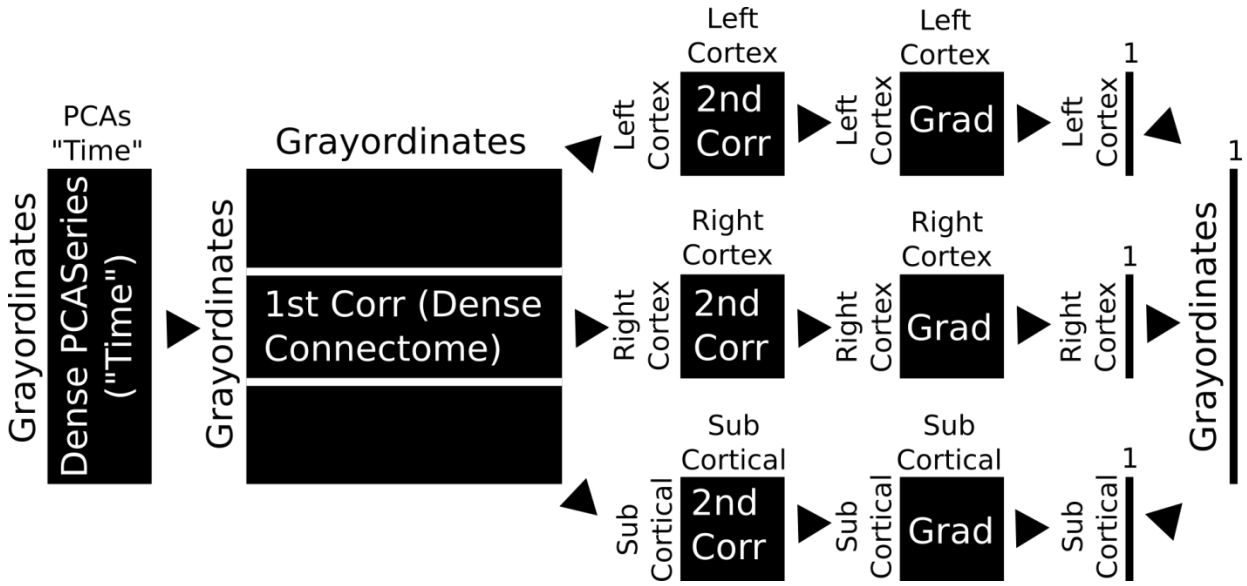

Figure 7 shows the steps used for computation of whole brain full correlation gradients. The process begins with the cleaned, Wishart rolled off dense PCA series (or individual subject timeseries), and includes generation of the dense connectome, a second correlation of functional connectivity patterns between grayordinates of each major structure (e.g. Left Cerebral Cortex or Right Thalamus), computation of the gradient map on each column of the second order correlation matrix, averaging along the rows the resultant gradient matrix, and spatially concatenating the mean gradients of all of the major structures back into an all grayordinates X 1 mean gradient map.

4.3 Calculation of Whole Brain Full Correlation rfMRI Functional Connectivity Gradients

For resting state fMRI, the 2D matrix-based nature of functional connectivity data required a more complicated approach to computing a final gradient map (see Figure 7). For all vertices in either the left or right hemisphere, the grayordinatewise FC maps were correlated to determine the similarity between each vertex's FC map and all others from the same structure. This produced a vertices X vertices 2nd order correlation matrix (as we want gradients in the similarity of functional connectivity maps—integrating information across the whole brain—rather than gradients in the similarity of rfMRI timecourses). Then the spatial gradient was taken of each of these 2nd order correlation maps, forming a vertices X vertices gradient magnitude matrix. The mean was then taken across this matrix to produce a mean gradient map, referred to as an rfMRI FC gradient map. This gradient map represents the average rate of change in functional connectivity pattern as one moves across the surface. Subcortical gradients were computed similarly, except the voxels of each subcortical structure were used instead. This method is similar in spirit to that proposed in (Cohen et al., 2008), except that here gradients were computed on the group average midthickness surface instead of resampling to a Cartesian grid overlaid on a flattened surface, edge detection was not used, and the second similarity matrix is correlation instead of eta^2.

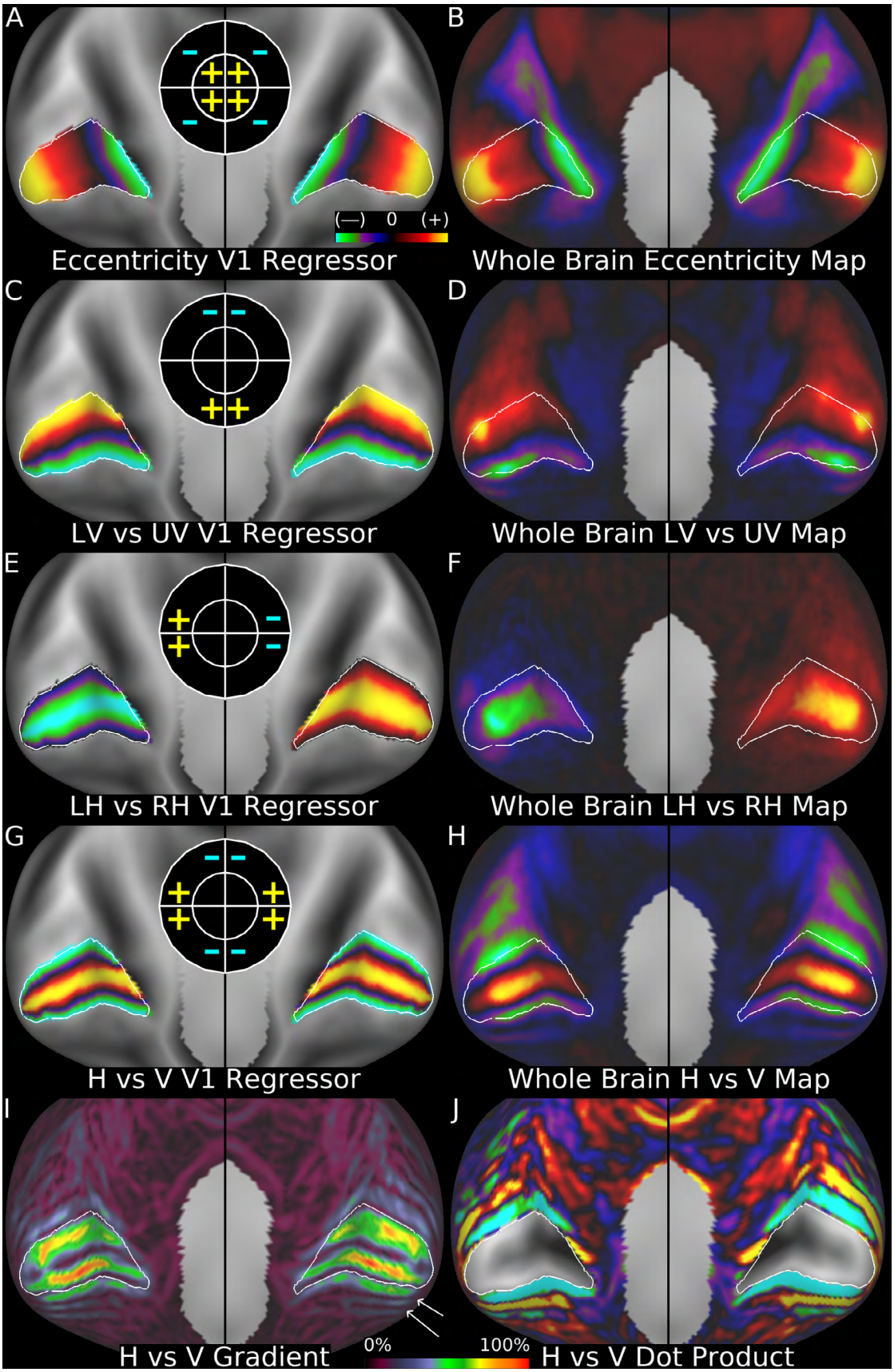
A
B
(—) 0 (+)
Eccentricity V1 Regressor
Whole Brain Eccentricity Map
C
D
LV vs UV V1 Regressor
Whole Brain LV vs UV Map
E
F
LH vs RH V1 Regressor
Whole Brain LH vs RH Map
G
H
H vs V V1 Regressor
Whole Brain H vs V Map
I
J
H vs V Gradient
0%
100%
H vs V Dot Product

Figure 8, above, shows the V1-constrained spatial regressors and their corresponding whole brain spatial maps (along with icons representing the portions of the visual field being contrasted). Panels A and B show the foveal vs peripheral contrast. Panels C and D show the upper vs lower vertical meridian contrast. Panels E and F show the left vs right horizontal meridian contrast. Panels G and H show the horizontal vs vertical meridian contrast, which is the most useful for visual area parcellation. Panel I shows the gradient magnitude of Panel H, where local gradient minima represent the locations of polar angle reversal. Panel J shows the dot product of the gradient vector of Panel H with a reference vector that points towards V1. The early visual areas alternate between positive and negative with the zero point lying on their borders (this measure is undefined inside of V1, see #6.5). Data at http://balsa.wustl.edu/J5k3.

4.4 Extraction of Topographic Information from Resting State fMRI Data

The above gradient-based methods enable objective delineation of areal boundaries based on rapid changes in spatial maps for one or more of four feature categories. Information useful for parcellation also came from continuous, topographically organized gradients in rfMRI FC within cortical areas. For example, antero-posterior gradients related to eccentricity in the visual field have previously been reported for the functional connectivity of early visual cortex (Yeo et al., 2011). Similarly, we previously described continuous topographic gradients associated with polar angle in the early visual cortex (Glasser et al., 2014b). Here, we analyzed continuous visuotopic rfMRI FC gradients using an improved, multiple regression-based method applicable to both group data (high CNR) and individual subjects (low CNR):

We first defined the full extent of area V1 using a combination of Lateral Geniculate Nucleus (LGN) rfMRI FC maps, myelin gradients, and thickness gradients (see Supplementary Neuroanatomical Results #1). Then, based on published maps (e.g. (Sereno et al., 1995)) of eccentricity and polar angle in V1, a set of nine spatial regressors based on continuous linear gradients were defined across V1 (see Figure 8), including 1) a spatial contrast between upper and lower vertical meridians (Panel C, varying from 1 to -1); 2) a spatial contrast between left and right horizontal meridians (Panel E, varying from 1 to -1); 3) a spatial contrast between the full (upper + lower) vertical meridian and the full (left + right) horizontal meridian (Panel G, varying from 1 to -1); 4) the third contrast shifted by 45 degrees (to complete the harmonic); 5) Foveal vs peripheral (Panel A, varying from 1 to -1); 6) the foveal vs peripheral gradient squared; 7) the foveal vs peripheral gradient cubed; 8) bilateral entire V1 (all ones); and 9) All grayordinates as ones. Outside of V1 the first 8 spatial regressors were all zeros. These regressors were defined using linear intensity gradients, which were computed algorithmically from a standard set of surface borders by dilation, using either the group average midthickness surface for the group maps or the individual subject midthickness surface for the individual maps (i.e., borders representing the horizontal meridian known to run down the center of V1 in the fundus of the calcarine sulcus, the vertical meridians known to run along the superior and inferior borders of V1, and the eccentricity arrangement known to run from foveal posteriorly to peripheral anteriorly). More specifically, generation of linear gradients involved a customized form of dilation on the surface, starting with a spatial map having a set of desired values along isoeccentricity or isopolar lines within V1 or along its border. For each V1 vertex that did not already have a value, the vertices within a specified distance whose straightest surface-based path to the chosen V1 vertex did not cross another vertex that already had a value were selected. From this set, the pair of vertices that had the

largest value for the difference in their input values divided by the sum of their distances from the chosen vertex was selected. This was used to linearly interpolate the output value based on the pair's distances and input values.

These nine V1 regressors were multiple-regressed into the group average dense PCASeries (or individual subject dense timeseries) using a variant of the WR process described above (#2.3, see Figure 9). Specifically, the V1 regressors were first spatially regressed into the group dense PCASeries (or individual subject dense timeseries) using only the Vertex Area spatial weighting map to generate V1 regressor-specific PCACourses (or timecourses). These PCACourses (or timecourses) were then temporally regressed into the group dense PCASeries (or individual subject dense timeseries) to generate a set of whole brain spatial maps (Panels B, D, F, H), one associated with each of the originally V1 restricted spatial regressors. For the MSMAll registration, the resulting individual subject whole brain maps were registered to the group whole brain maps (an earlier version of the visuotopic maps was used for the MSMAll registration that spanned the eccentricity space as bands rather than continuous linear gradients).

The spatial maps generated using the vertical vs horizontal meridian contrast (Panel H) and the upper vs lower hemifield contrast (Panel D) were particularly useful in delineating extrastriate visual areas, as they identify the polar angle reversals that occur at areal borders. Visuotopic areal borders generally occur at representations of the vertical or horizontal meridian (Sereno et al., 1995), corresponding to local maxima or minima in these spatial maps and to local minima in the spatial gradients computed from these maps. For example, Panel I shows the spatial gradient magnitude of the map in Panel H and has multiple spatial minima (e.g. arrows) that we later show correspond to areal boundaries (see Supplementary Neuroanatomical Results #2). The topographic information revealed by rfMRI FC was particularly useful for defining early visual cortical areas, including V2, V3, V4, V3A, and parts of some higher visual areas including V6, V7, V8, VVC, LO1, ProS, V3B, V3CD, VMV1, VMV2, VMV3 (see Supplementary Neuroanatomical Results #2-4).

Additional useful characterization of visuotopic organization was obtained by computing the dot product at each vertex between the gradient vector and a vector pointing towards V1 along the surface. This map is shown in Panel J for the gradient vector associated with the vertical vs horizontal meridian contrast gradient magnitude in Panel I. This reveals where the visuotopic gradient vector changes direction at visuotopic areal borders and is analogous to the field sign measure of (Sereno et al., 1994). Because the resulting dot products are all positive or all negative in a given area, this information is directly interpretable by the areal classifier (see below #6.5), which otherwise does not have access to explicit information about intra-areal spatial patterns. This dot product can also be compared statistically across the areal boundary.

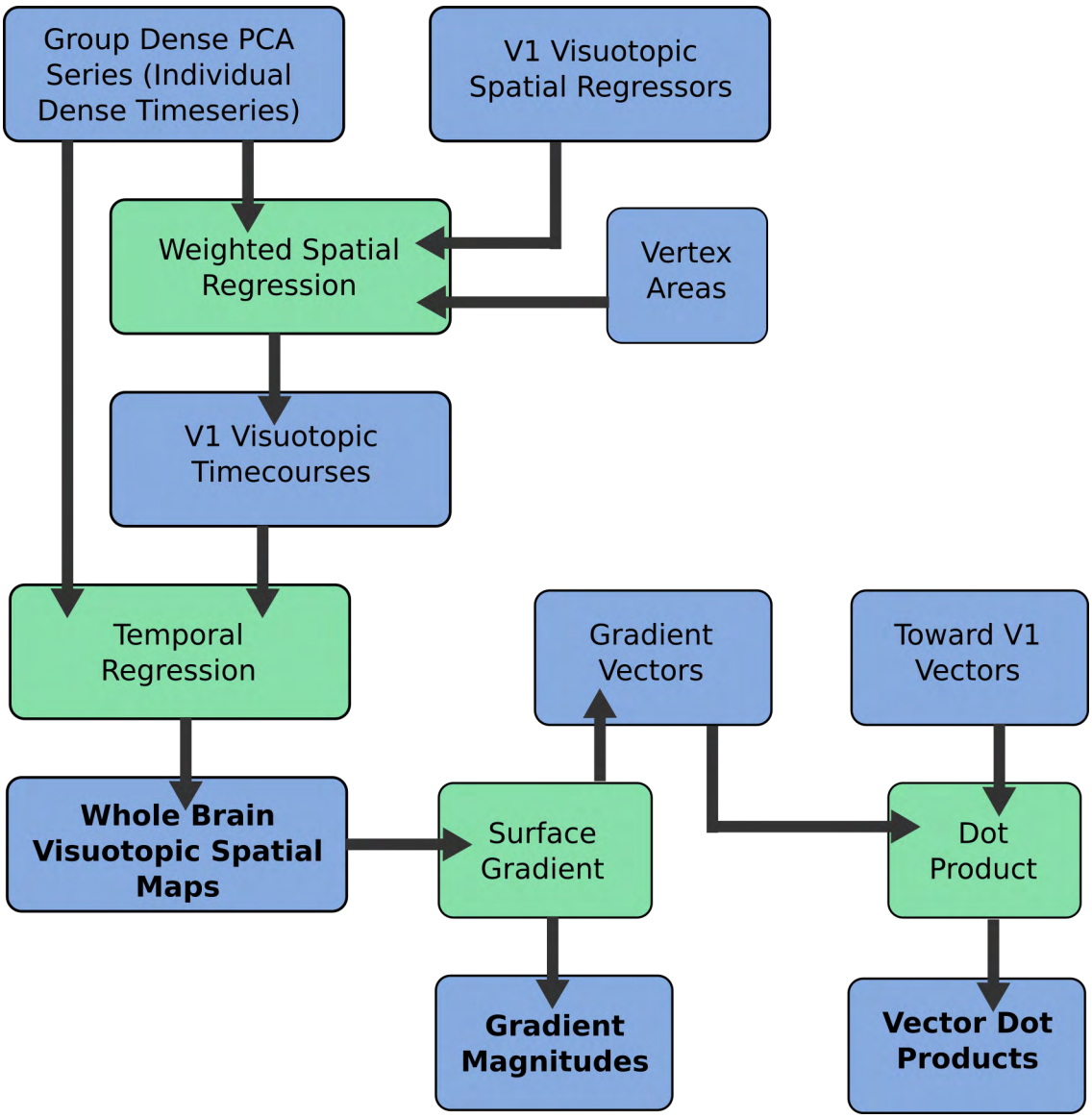

Figure 9 shows how V1-specific spatial regressors are used to produce corresponding whole brain spatial maps of various visuotopic spatial contrasts. The useful outputs are marked in **BOLD** font. The procedure can be used on either group dense PCA series or individual subject dense timeseries. It first makes use of the vertex areas in a weighted spatial regression, and the resulting V1-specific timecourses are used in a temporal regression together with the dense series to produce whole brain spatial maps. Gradient magnitudes can be computed on these maps, the local minima of which are useful for positioning areal borders (minima instead of maxima because the topographic maps themselves are gradients, and we are interested in local maxima or minima in these gradient maps where the second derivative is close to zero, as these locations delineate areal borders). Additionally, the gradient vectors can be multiplied in a dot product with the vectors that point towards V1 along the surface to determine where the visuotopic vectors switch direction (which occurs at the areal border, similar to the field sign measure of (Sereno et al., 1994)). This dot product yielded maps in which the values within a given visual area are all one sign (and different from neighboring areas), which were interpreted by the areal classifier (see below #6.5) and were also used to measure initial cross-border statistics.

5. Multi-modal Cortical Parcellation Using Gradients

5.1 Neuroanatomical Criteria for Multimodal Delineation of Cortical Areas

The preceding sections have described algorithmic methods for extracting information useful for parcellation from multiple independent modalities in a common grayordinates space (i.e. allowing visualization of modalities and their gradients on the same surfaces in Connectome Workbench). Gradient maxima from myelin maps, thickness maps, tfMRI contrast maps, rfMRI FC maps, plus gradient minima in continuous, topographically organized rfMRI FC within cortical areas together provide objective evidence for cortical areal boundaries. These non-invasive measures of architecture, function, connectivity, and topography are analogous to measures acquired invasively in non-human primates and in post-mortem human brains. To integrate this information across modalities and facilitate comparisons with published cortical parcellations, we combined a semi-automated boundary-delineation algorithm described below with neurobiologically informed interpretations based on five general criteria.

(1) To accept a putative areal boundary, we placed a strong reliance on consistent boundary location across independent modalities (for this analysis, the various ways of processing rfMRI were not considered "independent" in a full statistical sense, but agreement between them was still considered helpful).

(2) Presence of a putative boundary at corresponding locations in the left and right hemispheres increased our confidence in it. In this study we did not identify any areas that were present in one hemisphere but not the other because we did not find strong enough evidence to support such a parcellation, though some homologous areas assigned the same names show substantial lateralization of function and/or connectivity (see Supplementary Neuroanatomical Results and Main Text). A small number of areas have differing topological relationships across hemispheres or use different features for delineation in the two hemispheres. More focused future studies that find strong multi-modal evidence for hemispheric differences in cortical areal parcellation might choose to revise this criterion, however.

(3) Candidate boundaries were rejected if they were attributable to known imaging artifacts, which include: (i) fMRI signal loss from magnetic susceptibility in orbitofrontal and inferior temporal cortical regions[4]; (ii) folding-related artifacts in myelin maps that occur in thin, heavily myelinated early visual cortex (attenuated in 0.7 mm isotropic T1w and T2w images, but not eliminated); (iii) susceptibility-related artifacts in cortical thickness (in the same regions as fMRI, but less extensive, and caused by signal loss in the gradient echo T1w image); (iv) limitations related to task design in the tfMRI contrast data, including left hemisphere activation of right hand regions from button box pressing in cognitive tasks and preferential activation of the central visual fields because of the limited region of the visual field able to be stimulated by the task in the scanner; and (v) differential activation of foveal visual cortex from the visual fixation crosshair in rfMRI scans. Each of these artifacts can give rise to spatial gradients that are irrelevant to cortical

[4]Susceptibility-loss regions were smaller in the high resolution HCP data than in conventional fMRI scans, but were nonetheless present.

parcellation. Reliable automated detection of such artifacts is currently impractical, requiring interpretation of the data by a neuroanatomist with expertise in neuroimaging.

(4) Cortex on opposite sides of a putative areal boundary should differ robustly and statistically significantly in areal features, in order to exclude gradient ridges that are simply local noise-related fluctuations.

(5) Confidence in a putative areal boundary is increased by correspondence with a published areal boundary. Many areas that we identified correspond to previously reported areas but can now be delineated in a large number of living subjects based on the high-quality HCP data and analyses.

(6) Initial runs of the areal classifier (see below #6.1-6.8) on only the 210P and 29T subject groups were invaluable for finding putative areas in the initial draft parcellation that were not consistently identifiable in individual subjects. Also, the initial areal classifier results revealed "area holes" in which no area tended to reach at least 50% probability across subjects yet were not otherwise explainable by poor multi-modal CNR (e.g. susceptibility artifacts). Some of these regions were more finely parcellated, thereby improving classifier performance (see Section #6.7). Thus, the automated individual subject areal classifier served as one objective check on the neuroanatomists' interpretation of the gradient data.

5.2 A Semi-automated Algorithm for Objective Gradient-based Delineation of Areal Borders and Initial Internal Statistical Validation

We implemented a semi-automated algorithm for objective gradient-based delineation of areal borders. When a putative areal border was identified in a given region (based on visual inspection of multiple areal features and gradients), it was manually drawn in approximately the correct location using the border-drawing tool in Connectome Workbench. An optimization region of interest that included a substantial portion of the two cortical areas on opposite sides of the border was also drawn manually. Using the border optimization function in Connectome Workbench, the modalities used by the neuroanatomists to recognize the border were selected, and the modality gradients were combined inside this ROI by a method that uses a tunable tradeoff between averaging and multiplying. Each gradient is individually rescaled, mapping its minimum and maximum value within the ROI to 0 and 1, respectively, then put through the formula "precombine = rescaled * strength + 1 – strength", where strength is a tunable parameter between 0 and 1 (default of 0.7). The resulting "precombine" values are multiplied together across modalities at each vertex, and the result is again rescaled to the range of 0 to 1 and then inverted, so that where the gradients are maximum, the value is 0. We used these values to assign a cost to each edge (line segment between adjacent surface vertices) within the entire ROI by multiplying the length of the edge by the expression "1 + followstrength * (data(i) + data(j))", where "i" and "j" are the vertices at each end of the edge being evaluated, "data" is the combined gradient data, as described above, and "followstrength" is a tunable parameter that controls how much the gradient data can influence the cost of an edge (which indirectly controls how much the optimal path can deviate from the shortest geodesic path between the endpoints, and has a default value of 5). The initial border was then revised by taking the first and last points of the border segment inside the optimization ROI and using an "A*" search (a standard graph search algorithm (Hart et al.,

1968)), to construct a new path having the minimal sum of the costs of the edges in the path.

For the vast majority of the borders we kept the strength and followstrength parameters at their defaults (which were considered to be reasonable values by TSC, the algorithm designer and indeed worked well in initial testing). The approximate reasoning behind the initial choice of followstrength was that a value of 5 allows the path to be up to 5 times longer than the shortest path, as long as there is an undisputable gradient ridge to follow, which seemed sufficiently loose for the search to choose reasonable paths given realistic gradients. For the strength parameter used during the combination of gradients, a value of 0 means to ignore the map (and 0.01 for all inputs would result in something very close to pure addition of the gradient maps), 1 means pure multiplication, and 0.7 was considered a reasonable balance to achieve a more forgiving multiplication-like effect, given what the extremes represent. In some cases, the strength parameter was set to zero for the feature maps where we wished to compute cross-border statistics (so that we could report the difference between the areas in the Supplementary Neuroanatomical Results) but did not want the map to contribute to the final effective gradient. For example, if myelin, resting state, and 5 task contrasts were all significant, but we did not want the task modality to dominate the effective gradient, we would set some task contrast maps to zero. Otherwise, we kept the followstrength parameter set to its default, except in two explicity noted instances where a border passed through a susceptibility artifact and we did not want it to take a highly circuitous route (here we reduced the followstrength value, which weights the border more towards the shortest path).

Each automatically defined border segment was used to assess the effect size (Cohen's d value) and significance of the differences between feature map values on opposite sides of the border within the optimization ROI. For most modalities the p value was based on a t-test for the feature map values on either side of the border. For functional connectivity, a different approach was used. For each "seed" vertex within the optimization ROI, an average functional connectivity map was made for each side of the border within the optimization ROI; a unique average was made for each vertex to exclude vertices within 2 mm geodesic distance of the seed vertex (mainly to exclude the seed vertex itself). The seed vertex's connectivity map was then correlated with each of these average connectivity maps (average for side "A" and average for side "B"). The resulting correlation values were Fisher z-transformed and grouped according to which side the seed vertex is on, and which side the average connectivity map is from. Two t-tests were then performed on these Fisher z-transformed correlation values: one was between the group of values from seed vertices from side A to average connectivity maps on side A versus the group of values from seed vertices from side B to average connectivity maps on side A. The other was between the group of vertices from side A to side B vs side B to side B. The test having the higher p value and lower Cohen's d was used for checking if the border indeed had a robust and statistically significant effect. Two tests were used because there are inherently four groups, but two pairings are not meaningfully comparable for our purposes (A to A average with B to B average, A to B average with B to A average).

For each modality, p values were generated, and boundaries that did not have significant p values ($p<0.05$) in at least one modality were not retained. In practice, if the neuroanatomist recognized a border, the p value tended to be very low and the Cohen's d standard effect size measure was large (maximum $p<0.001$ and minimum Cohen's $d>0.5$),

because the group average data for our large subject groups has relatively low noise. We used both p values and Cohen's d values in order to identify differences that were both robust and statistically significant. In initial testing, we found that the exact location of the initial border estimate and the optimization ROI had little impact on the final automatically delineated border location or the statistical test values, as long as the initial estimate was within a few mm of the combined gradient and the border optimization ROI covered a substantial portion of the cortical areas on either side of the boundary.

This initial statistical test served mainly as an additional check for the neurobiological plausibility of the boundaries being defined (i.e. criterion #4 above; see section #7.2 below for more rigorous statistical cross validation of the parcellation reproducibility and multi-modal cross-border differences using the independent 210V dataset). The end result of the semi-automated process was a set of objectively defined boundaries dividing the neocortex of both hemispheres into a mosaic of areas differing in architecture, function, connectivity, and/or topography. The primary representation of these boundaries was in the form of surface borders (strings of points projected to a surface tessellation but not constrained to discrete surface vertices). These borders were used to generate ROIs (collections of vertices) and labels for each area.

5.3 Neuroanatomical Criteria for Identifying Cortical Areas Based on Spatial Neighborhood Relationships

The final stage of the group-average parcellation process involves identification and naming of cortical areas. For purposes of continuity with prior studies, we retained cortical areal names if they were well matched to a published parcellation, whereas new names were assigned to areas that lacked such a match. When a previously identified cortical area could be subdivided in our multi-modal analysis, we used a similar area name with appropriate modifiers (See Supplementary Neuroanatomical Results). Similarly, if previous studies reported multiple subdivisions of a region identified as a single cortical area in our analysis, we incorporated both names into the area name and called it a "complex."

For some areas, we were able to use specific areal features (such as heavy myelination or visuotopic organization) as part of the evidence for matching our areas to published parcellations based on in vivo or postmortem analyses. However, in most cases spatial location and topological relationships with adjoining areas were the primary basis for matching with published parcellations. If a published parcellation and the multi-modal parcellation show a similar set of areas with similar spatial relationships, the most parsimonious explanation is that they represent corresponding cortical areas.

A major challenge in using spatial relationships to compare across parcellation studies is the diversity of methods used for intersubject alignment, of which six categories warrant brief mention. (i) We placed highest confidence in group average areal definitions that are based on cortical areal feature-based surface registration (which will produce maximally sharp group maps) and include dedrifting during template generation, so that an overlay of data from different studies has minimal bias and highest fidelity (Abdollahi et al., 2014). (ii) Next best are probabilistic maps based on folding-constrained surface registration (e.g. (Fischl et al., 2008)) that are overlaid together with the multi-modal parcellation. Comparisons with the present data should be reasonably accurate, though

they may be blurrier in regions of high folding variability or high variability between areas and folds. Additionally, unless dedrifting has been done (see above #2.5), there may be spatial drift between the group average patterns of different studies (this may explain some discrepancies between our area V1 and that of (Fischl et al., 2008), see Supplementary Neuroanatomical Results #1). (iii) Surface-based figures and drawings from published studies were often useful for matching with our parcellation even when direct comparison on the same surface mesh in Connectome Workbench was not feasible. (iv) Volume-registered probabilistic maps of cortical areas (e.g. (Eickhoff et al., 2005)) were more challenging to use because of inaccuracies in mapping from group average volume to group average surface spaces, as well as inaccuracies in intersubject alignment contributing to a group-average volumetric map ((Anticevic et al., 2008; Fischl et al., 2008; Fischl et al., 1999b; Frost and Goebel, 2012; Smith et al., 2013a; Tucholka et al., 2012; Van Essen et al., 2012)). Volume-based registration can also have group average drifting issues (for instance, if using the MNI template). However we did use the JuBrain online resource ((Caspers et al., 2013); https://www.jubrain.fz-juelich.de) to help with identifying some areas. (v) Volume-based group average figures in published studies typically lack the detail required to distinguish cortical areal boundaries and their spatial relationships, so these were used sparingly. (vi) Stereotactic coordinates (e.g. MNI or Talairach), based typically on centers of volumetrically analyzed group-average task activation foci, generally lack information about cortical areal borders and are thus of limited utility for making definitive areal identifications, even though a major fraction of the neuroimaging literature uses this approach as a primary means of expressing spatial localization (see examples of this difficulty in (Glasser and Van Essen, 2011) myelin mapping Figure 11).

5.4 Coloration of the Multi-modal Parcellation

A parcellation can be colored in many ways, e.g. solving the map-coloring problem (Ringel and Youngs, 1968) with random colors, using only a single color, or coloration based on some data driven metric. For our parcellation, we wanted a color scheme that (i) utilizes a large portion of the printable and computer-displayable 3D color space (hue, saturation, and luminance) and (ii) is neurobiologicaly informative, for example by conveying how the major sensory inputs and two major anti-correlated cognitive networks are organized and how they are mixed in different cortical areas. We used rfMRI relationships between each area and five core groups of areas for this purpose. The group MIGP PCASeries was parcellated (i.e., the average PCASeries was computed inside each area) according to the multi-modal parcellation separately for each hemisphere. Core groups of areas (with each group covering similar amounts of cortical territory) were selected that are associated with auditory (A1+MBelt+LBelt+PBelt+RI), somatosensory (4+3a+3b+1), visual (V1+V2+V3), task positive (PF+PHT+23c+46), and task negative (a.k.a default mode) networks (PGi+PGs+TE1a+7m+v23ab+10r+10v). Auditory, somatosensory, and visual groups were selected because these represent the main input modalities to the brain. Task positive and task negative cognitive networks were selected because they are the strongest anticorrelated resting state networks in the brain (Fox et al., 2005). In calling these networks "task positive" and "task negative" we do not mean to suggest that tasks never activate the task negative network or always activate the task positive network (e.g. the LANGUAGE Story vs baseline task contrast in the HCP dataset activates the task

negative network but not the task positive network), but rather to highlight the anti-correlated relationship between these networks and avoid making assertions about what the brain's "default mode" is. Nodes of the task positive and task negative networks were selected in parietal, temporal, cingulate, and frontal lobes.

Five area groups were chosen because that is the maximum number whose colors can be blended uniquely. The mean PCASeries of the 5 groups of areas were computed and these were temporally multiple regressed into the parcellated PCASeries, producing a 180 X 5 partial beta matrix. This matrix was then scaled to range from 0 to 1. The scaled matrix was then matrix multiplied with a primary colors matrix [255 0 0 ; 0 255 0 ; 0 0 255 ; 255 255 255 ; 0 0 0] (pure red, green, blue, white, black) to produce an 180 X 3 color components matrix. This matrix was rescaled from 0 to 255 and used as the label colors for each area (e.g. in Main Text Figure 3, see associated text for discussion of the neurobiological interpretations of the color patterns).

6. Automatically Defining and Identifying Cortical Areas in Individual Subjects Using Multi-modal Areal Fingerprints

6.1 Motivation

The group average parcellation described in the preceding methods sections and in the Supplementary Neuroanatomical Results is very useful in its own right for various purposes. However, it is also desirable to generate parcellations of individual subjects (including those who were not part of the original group-average parcellation) that are as accurate as possible at capturing individual variability. Despite the improvements in areal feature-based surface registration reported here and elsewhere (Robinson et al., 2014), there remain residual misalignments between particular individuals in particular areas and the typical subject's areas found in the population-based parcellation. We found that a major source of these residual misalignments involved topologically incompatible differences in the spatial neighborhood relationships between some areas in some individuals and the typical pattern of areal spatial neighborhood relationships in the group. For example, this includes areas that are a single contiguous region in most individuals, but with strong evidence for multiple nearby but discrete patches in some individuals (see Supplementary Results and Discussion #1.3-1.4). Topology-preserving spatial registration, such as MSM, is inherently unable to compensate for such topological differences (and if regularization was relaxed in an attempt to align such areas, the resulting estimated warps would contain excessive, neurobiologically implausible amounts of areal distortion).

One approach to individual-subject parcellation is to rely on the alignment achieved by the registration process to map the group-average parcel boundaries back to each individual. However, this does not take into account the residual misalignments after the registration process, such as the topological mismatches noted above. To enable accurate analyses of individual variability in areal size, functional activity, or connectivity, we sought a way to generate multi-modal parcellations in the individual subjects that account for the residual spatial variability in areal locations. The semi-automated methods used to generate the group parcellation above would be far too tedious, especially when dealing with a large number of subjects (e.g., the full ~1100 subjects having MRI scans for the HCP or future studies that may wish to take advantage of the multi-modal parcellation).

Fortunately, we were able to capitalize on machine learning methods capable of addressing this problem once the typical subject's parcellation has been generated at the group level.

6.2 Machine Learning Classifier Design

We started with a multi-layer perceptron machine learning classifier used to classify 7 resting state networks from functional connectivity maps (Hacker et al., 2013) and adapted it to the problem of classifying cortical areas based on their multi-modal areal fingerprints. Classifying 180 areas in a single classifier run across the whole brain is an extremely hard problem, made even harder by the fact that spatially distant areas (e.g., in different lobes) may have similar areal fingerprints. Fortunately, the problem becomes much simpler by making two neurobiologically reasonable assumptions: (1). We assume that after the areal feature-based surface registration, individual cortical areas are in reasonably close proximity to the group areal definition. (2) It is sufficient to distinguish each cortical area from all of its spatially adjacent neighbors combined into a single class. Binary classification (class one=area, class two=neighbors) is the simplest and most robust kind of classification problem. Thus, the classification problem setup and classifier architecture were as follows: For each of 180 areas in each hemisphere, a multi-layer perceptron was trained to classify whether or not each vertex in an ROI containing the group areal definition plus a 30 mm surface geodesic distance surrounding it is a part of the area or not—the neuroanatomical "searchlight" for the area. The multi-layer perceptron had 3 layers (1 input, 1 hidden, 1 output) and the same nonlinear functions as in (Hacker et al., 2013) and used 9 hidden nodes (a reasonable compromise between accuracy and training speed for this problem). The training labels were the group average areal definition and the 30 mm radius spatial neighborhood surrounding it (see below #6.6 for detecting and excluding residually misaligned areas in specific subjects from classifier training).

6.3 Multi-modal Features for Areal Classification: Myelin, Thickness, and Resting State Functional Connectivity

The features used by the classifier were based on the various modalities used in the semi-automated parcellation, but they were optimized for single subject analyses, classifier training speed, and accuracy. Simplest were the individual subject myelin and cortical thickness maps corrected for folding effects, for which we used the unsmoothed left and right cortical surface maps of each measure.

Because there is no temporal correspondence across subjects in the rfMRI timeseries, the only corresponding rfMRI subject-wise (i.e. without reference to group data) dataset is the rfMRI FC "dense connectome" (91,282 X 91,282 X 4 bytes = 32.5GB). As mentioned above in the section on areal feature registration, each dense connectome contains a large amount of redundant information and (unless adequately processed) a large amount of unstructured noise (see above #2.2). Such data is impractical as input to a classifier, and, as with the MSMAll registration, a dimensionality reduction with consistency across subjects is required. As with MSMAll registration, this was done using group ICA (d=137) of the MIGP PCASeries, followed by weighted regression into the

individual subjects' final dense timeseries (see above #2.3) to obtain individual subject versions of the component spatial maps with the same splitting and component numbers.

The choice of RSN dimensionality for the classifier rfMRI modality entails a balance between classifier accuracy (measured by detection rate of the area—was an area found with between 0.33x and 3x the group area size) and the classifier's ability to detect misaligned areas (assessed by visual inspection in the 210P dataset for a few cortical areas determined to have substantial cross-subject variability in spatial position of areal features easily discernible for multiple modalities). Because a central objective of the classifier is to detect these misaligned areas, the classifier step is not useful if it only finds the area in the typical group location in every subject, if in fact some subjects actually have it in an atypical location.

Preliminary classifier runs using dual regression (DR), large numbers of components (e.g. 200), and with the original MSMRSN registration that tolerated substantial distortion (Robinson et al., 2014) tended to have this negative property of failing to identify misaligned areas. Better misaligned area performance was achieved with classifier runs using much lower RSN dimensionalities (e.g. 27), despite having overall lower areal detection rates. Although larger numbers of group ICA components tap deeper into the partial correlation relationships between areas, it is problematic if they begin to cause overfitting of the classifier. The effort to address this tradeoff between overall detection rate and ability to identify misaligned cortical areas for low vs high RSN dimensionalities led to a number of the methodological improvements described in this study. This includes the use of the less distorting MSMAll registration; the use of weighted regression instead of DR; the use of only the predominantly surface RSNs in the classifier (i.e. only maps with useful contrast); and the use of an RSN dimensionality that describes the data by a local minimum in the number of spatially contiguous regions, prior to the point at which the ICA starts adding substantial amounts of unstructured noise to the subcortical components (as mentioned above, at around d=140). All of these changes empirically improved classifier performance (at detecting misaligned areas at higher RSN dimensionalities) and helped avoid overfitting. Some of them also improved the speed of training the classifier by reducing the number of features used. Thus, an RSN dimensionality of d=137 was chosen because it offered high areal detection rates while still being able to detect misaligned areas well, perhaps because it contains most of the available useful rfMRI information in the HCP dataset.

Figure 10, below, shows the task processing used in this study. Starting from the task design and the MSMAll_DeDrift resampled tfMRI dense timeseries for each run, the important outputs in **BOLD** font are produced. The task GLM is fit and fixed effects cross-run within subject analyses are performed to produce 86 individual subject task contrast maps. Cross-subject mixed effects analyses are also performed to produce 86 group task contrast maps (beta maps) and their associated gradients. Because there is a lot of duplicate information in the task fMRI contrast map datasets, group ICA can then be performed on these maps at d=20 (>99% of the variance across contrasts retained), to find the unique information in the tfMRI dataset and produce spatial maps and contrast series. These contrast series can be multiple regressed into the individual subject task contrast maps using a single "temporal" regression stage to produce 20 individual subject tfMRI component maps that can be used in the areal classifier. These 20 maps contain higher CNR than the original 86 maps because of cross-contrast averaging and reduction of the redundant information across contrasts. Additionally, the mean task fMRI image is included as a feature but not shown above (because the ICA decomposition does not include the mean image).

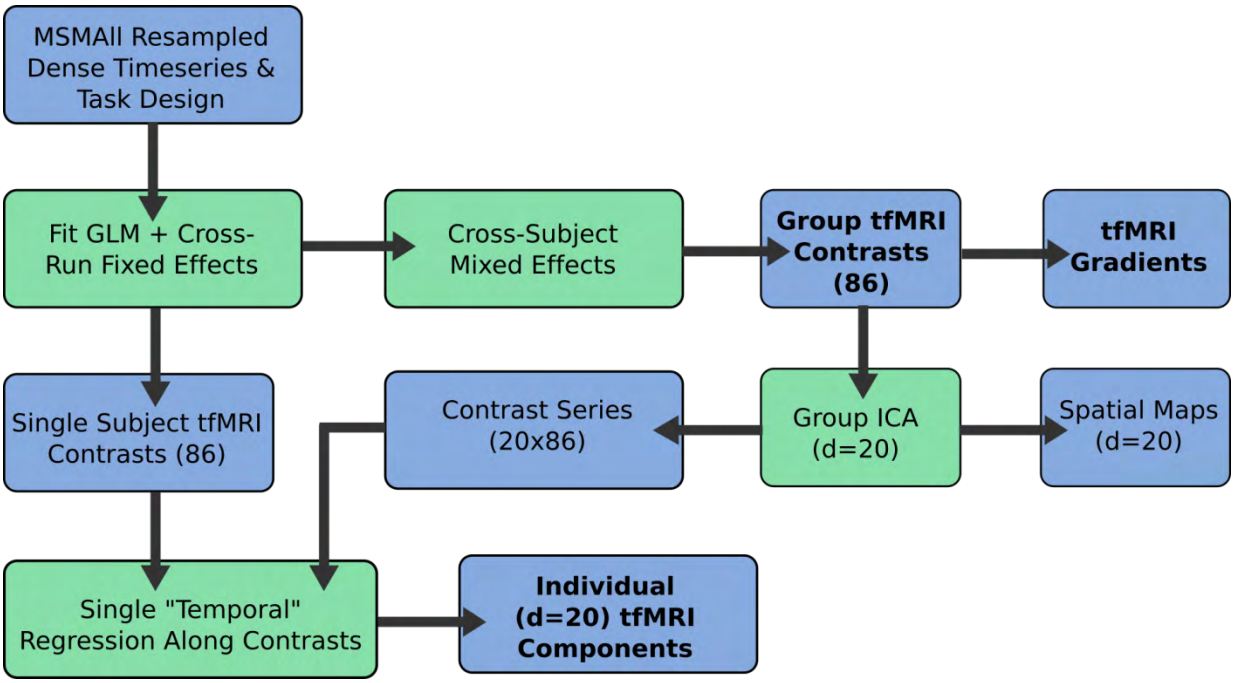

6.4 Multi-modal Features for Areal Classification: Task fMRI

Figure 10 provides an overview of the tfMRI processing used in this paper. The HCP task analysis pipeline generates 86 task contrasts, so the tfMRI contrast information is a 91,282 X 86 contrast beta matrix for each subject (and each whole group). By both visual inspection and preliminary classifier performance, the individual subject tfMRI contrast maps had substantially lower CNR per map than the other features used in the classification (thickness may contain less overall useful information, but the information it does contain has high CNR). Additionally there is extensive redundancy of information in the group and individual tfMRI contrast maps. At the group level, this redundancy was assessed by performing group ICA on the 86 group mixed effects tfMRI contrast beta maps. Twenty ICA components sufficed to represent >99% of the variance in these 86 group contrast maps. Interestingly, by visual inspection many of these ICA components closely resemble rfMRI group ICA components, though the dimensionality at which they emerge may be higher than a d=20 rfMRI group ICA. Also some components found in the d=20 rfMRI group ICA are absent from the d=20 tfMRI contrast map group ICA. This suggests that the HCP task battery was imperfect in covering all possible cognitive brain states measurable by BOLD fMRI, even though efforts were made to provide broad spatial coverage of the brain (Barch et al., 2013). The finding of similarities between rfMRI group ICA components and tfMRI contrast map group ICA components is reminiscent of (Smith et al., 2009) and is consistent with (Cole et al., 2014)'s finding of very similar patterns when all of the HCP tfMRI data are processed like rfMRI data and compared with rfMRI data.

Because the d=20 dimensionality reduction of the group ICA components reduces redundancies, it reduced classifier computational time and also improved individual subject tfMRI contrast map CNR. Group ICA produces both component spatial maps and component "contrast series" (the equivalent of a component timeseries when using rfMRI

data). Because each of the 86 tfMRI contrasts means the same thing across subjects (as opposed to resting state timeseries that do not correspond across subjects), a simple single "temporal" multiple linear regression stage was sufficient to produce individual subject dimensionality-reduced tfMRI contrast maps. The 20 group component tfMRI contrast series were "temporally" regressed into the 86 individual subject tfMRI contrast maps. This produced 20 tfMRI component contrast maps with the redundant information removed and CNR improved because of averaging across multiple contrast maps. Additionally the mean contrast map was included because the ICA decomposition does not represent the mean map, only the variance across maps. These 21 maps were used in the areal classifier to represent the tfMRI modality. Preliminary classifier runs indicated that this data was used more efficiently than using 86 contrast maps, as evidenced by higher feature weights for tfMRI. Also, in a separate analysis (see Main Text) the classifier was run without including any tfMRI data at all to see how it would perform in studies where the HCP's task fMRI battery was not available.

6.5 Multi-modal Features for Areal Classification: Within-area Smooth Gradients in Visuotopic Maps Derived from Resting State Functional Connectivity

A final source of information fed into the areal classifier was the visotopically-organized rfMRI FC used for defining early extrastriate visual areas (see above #4.4, and Supplementary Neuroanatomical Results #2-4). The multi-layer perceptron classifier cannot directly interpret smoothly varying intra-area topographic gradients within the whole-brain visuotopic spatial regression maps. This is because the classifier treats each value of each feature independently, and has no way of assessing spatial patterns in the values (it only knows if they are distinctly higher or lower in a given cortical area vs the 30 mm surrounding it). As mentioned above (see Figures 8 and 9), it was necessary to transform the topographic data into a form that the areal classifier could use. We achieved this by taking the dot product of the gradient vector of the visuotopic whole brain regression map and a reference vector whose direction is based on the start of the shortest geodesic path towards the V1 ROI.

The resulting dot product maps contain positive values when the gradient vector points towards V1 and negative values when it points away from V1. The change from positive to negative should occur at visuotopic areal boundaries, converting the within-area spatially varying pattern into a map that is consistent across the entire area and can be used by the classifier in the same way that it handles other modalities. For example, we used the gradient of the spatial contrast between horizontal and vertical meridians to define cortical areas V2 and V3 in extrastriate cortex (Supplementary Neuroanatomical Results #2). To the extent that visuotopy within areas V2 and V3 is perfectly orderly, the gradient vector of this spatial contrast should always point away from V1 within V2 (dot product of the gradient vector with the V1 ROI reference vector producing negative values), and point towards V1 within V3 (with the dot product of the vectors producing positive values). Thus, the transition between negative and positive values occurs at the V2/V3 border (in an analogous way to how the field sign changes at the areal border (Sereno et al., 1995). The classifier made use of this transformed information, just as it does for the other modalities, to define areas V2 and V3 in individual subjects. This type of transformation was computed for all four polar-angle related spatial contrasts and the first eccentricity

related contrast, producing useful information for the classifier to delineate and identify visuotopically organized areas in individual subjects. The transformation was also computed on the upper vs lower vertical meridian contrast after the absolute value is taken so that areas V2, V3, and V4 have the same sign throughout their extents (otherwise for this contrast in V2 for example, the superior portion would have a positive sign and the inferior portion would have a negative sign). This is because the gradient vectors always point towards the higher number (e.g. they will point away from a local minimum).

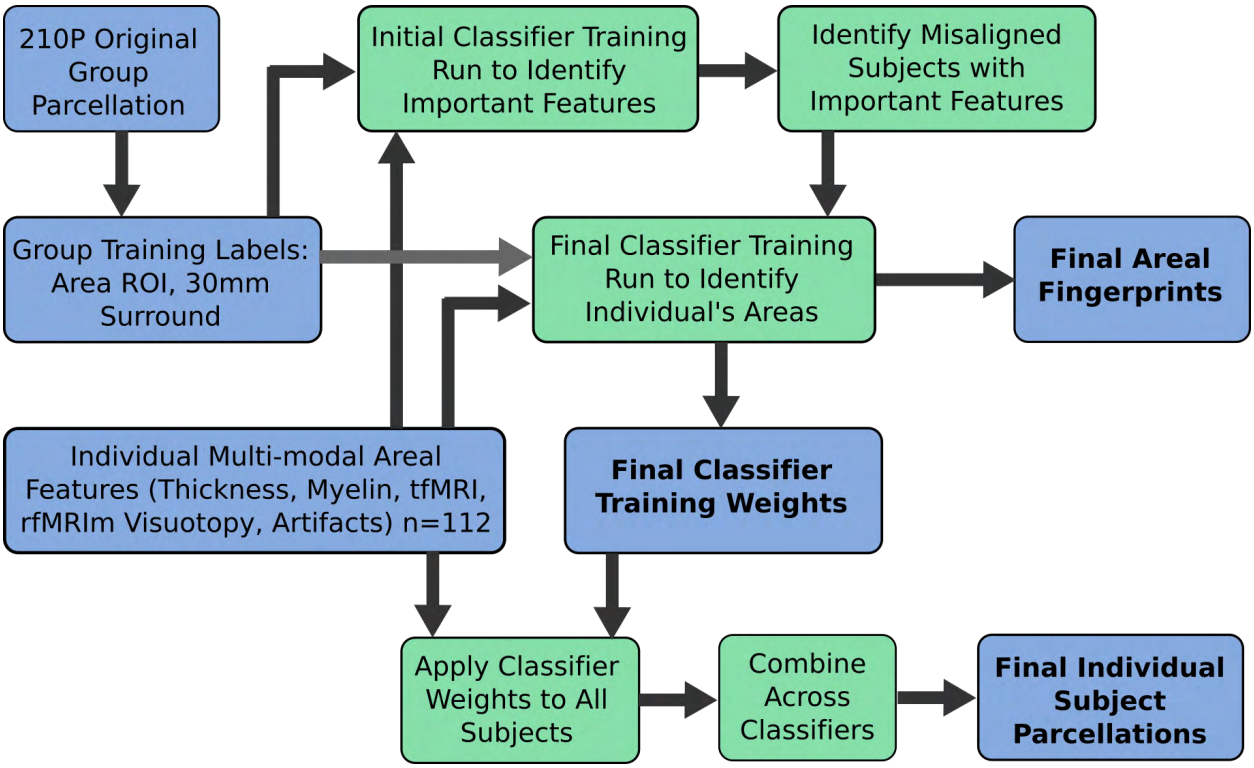

Figure 11 shows the procedure used to go from the group parcellation and individual subject multi-modal areal features to the important outputs produced by the areal classifier and listed in **BOLD** font. The individual subject multi-modal areal features are concatenated (n=112) and used together with the group area ROI and 30 mm surround as training labels for the initial classifier training. This abbreviated training is used to identify the important areal features, which are then used to detect the subjects that are likely to have a misaligned cortical area. These subjects are excluded from the final classifier training (which also uses the group training labels) so that they do not confuse the classifier (as they will be outliers for which the group training labels will not be valid). This final training produces the final classifier training weights, which can be used in the 210V group or another study. These weights are used to simply apply the classifier to the individual subject multi-modal features, producing the final areal fingerprints (what the classifier has determined are the distinctive features of each cortical area relative to it neighbors). Then the classifiers are combined across areas to produce the final individual subject parcellations.

6.6 Implementation of the Machine Learning Classifier

Figure 11 shows an overview of the implementation of the areal classifier. 112 feature maps representing all of the parcellation modalities in each individual were provided to the classifier for training (1 thickness map corrected for curvature, 1 myelin

map, 1 surface curvature map, 1 mean tfMRI activation map, 20 tfMRI component contrast maps, 77 surface rfMRI RSN maps from a d=137 ICA, 1 map of vein effects, 1 fMRI dropout map, 1 map of insular surface artifacts, 1 map of the resting state timeseries standard deviation, 1 map of the mean grey timecourse beta, and 5 topographic regression dot product maps). Classifier training used these maps from the 210P (training set) and 29T (test set) subject groups together with areal distortion maps for each subject. The areal features were demeaned and normalized so that each modality had a similar spatial standard deviation (to initially give each modality equal weight in proportion to the number of features it contains). An initial "quick" 1,000-iteration classifier training was done after excluding areal distortion outliers, by using all subjects that had a mean areal distortion within the area being classified of less than 2-fold expansion or contraction (in practice few subjects in few areas were excluded by this criterion because of the improvements in the MSMAll registration used in this study).

After the initial quick classifier training, the output weight matrices were algorithmically examined to determine which features drove the areal classification of each area. Specifically, for each area class, its partial derivatives with respect to the input data values were computed and evaluated using the feature data. This measure was then multiplied by the features' gradient magnitudes to generate a classifier 'sensitivity' metric. Spatially, these sensitivities were highest in absolute value along the parcel boundaries. Features whose sensitivities were higher in absolute value contribute more to the areal classification than those whose sensitivities had lower absolute value. We used this sensitivity information to automatically select features that were particularly predictive of areal misalignment in individual subjects for a given area (because the features most strongly used in classification should also be most likely to differ if an individual cortical area is misaligned with the group average cortical areal definition—the training label). If in a particular individual for the region near a particular area deviated substantially from the group values in the region, the subject was excluded from training.

After potentially misaligned subjects were excluded from the training and test sets, the classifier was trained using a full 4,000 iterations (the learning rate nonlinearly increased with iteration number). The classifier learning rate was automatically adjusted down if the classifier was stopping too early (i.e. it detected it was overfitting itself to the 210P training dataset, insofar as performance on the 29T test dataset began to drop) and the number of iterations was extended (since the training would take longer with a lower learning rate). The overall loop (that was able to adjust the learning rate) was terminated when the most recent training run was the best and the classifier had finished the requested number of iterations, or the classifier AUC (Area Under Curve) was greater than 0.98. If the most recent run did worse than a previous run with a higher learning rate, the process was also stopped and the previous run was used. The goal was to either get an AUC of >0.98 or to complete the full number of training iterations without prematurely stopping. Classifier performance was evaluated using AUC and MSE (Mean Squared Error) as standard metrics. Once satisfactory classification had been achieved, the trained classifier was applied to every subjects' data (including the misaligned subjects). Classifier performance was also evaluated by confirming that in subjects with known misaligned areas the classifier was correctly classifying these areas (visually based on multi-modal information, see for example Supplementary Figures 9 and 10 in the Supplementary Results and Discussion).

6.7 Combination Across Areal Classifiers

Classifier output values ranged from 0 to 1 for each class (class one=area, class two=neighborhood), indicating the likelihood that a given vertex in a given individual is part of either the cortical area or the neighborhood. The areal probability maps (class one) for each area in a subject were combined using a find the biggest approach. Regions where no areal probability exceeded 50% were also marked as areal "holes" (when present consistently across subjects, these represented candidates for draft parcellation revision, see above #5.1). There were several instances (e.g. among the VMV1-3 areas, particularly VMV1) where this occurred. We think the hole arises when the classifier encounters two distinct areal fingerprints within a larger draft parcel. It likely only learns the larger of these, so the smaller one is neglected. Because it is not represented by a high areal probability for any classifier, the smaller region becomes an "area hole." The issue is resolved if an appropriate subparcellation is done, as each areal classifier learns the areal fingerprint of its subparcellated area, and both will now be detected with high probability.

This initial combined parcellation was regularized (i) to remove very small patches (less than 25 mm^2); (ii) to join pieces of areas that were broken by only a few vertices of another area (as long as the piece being joined was proportionally larger than any piece being split off from another area as a result of the joining operation); and (iii) to make sure that if any multiple pieces remained, they were at least 0.33x the size of the largest piece and within 30 mm of its nearest edge. Any remaining holes in the parcellation were filled by nearest neighbor dilation. After careful consideration of the multi-modal evidence, we did not enforce a strict spatial contiguity constraint on the parcels in individual subjects. We found strong multi-modal evidence of parcels that were split into multiple pieces in some atypical individuals, although in the typical subject (i.e. group average) they were joined (see Supplementary Results and Discussion #1.3-1.4). The resulting initial individual subject parcellations were checked relative to the group parcellations to see if the areas found were within 0.33x to 3x the size of the group area. If this was the case, the area was considered to have been detected in the individual subject.

6.8 Classification of Individual Subject Cortical Areas Based on Their Multi-modal Areal Fingerprints

The final classifier training weights were applied to the 210P and 210V subject groups to make final individual subject cortical parcellations. Additionally, the partial derivatives were tracked through the classifier application and multiplied by the feature map gradient magnitudes to produce the final areal fingerprints of each cortical area—that is, the information the classifier learned that uniquely distinguishes the cortical area from surrounding cortex (see above #6.1, Supplementary Figure 12 in the Supplementary Results and Discussion).

7. Parcellating Data and Validating the Parcellation

7.1 Creation of Parcellated Datasets of Multiple Modalities

Parcellated datasets offer a tremendous reduction in data size and complexity, together with performing a neurobiologically valid form of spatial integration that does not blur across tissue types or areal boundaries as happens with conventional smoothing. They increase statistical sensitivity and power both by reducing unstructured noise and multiple comparisons. For most whole brain analyses, parcellated datasets should be easier to work with and more likely to show interesting effects (e.g. correlations with behavior, genetics, etc.). Also, they provide a level of coarseness appropriate for integration with non-MRI modalities such as magnetoencephalography (MEG; (Larson-Prior et al., 2013). Thus, we created parcellated datasets of each modality used in this study, except for the within area topographic gradients, which are an example of a phenomenon that is inherently more appropriate to study using dense, grayordinate-wise data.

Myelin maps and thickness maps were simply averaged across each parcel. For the fMRI modalities, cross-parcel averaging substantially reduces the unstructured noise present in the timeseries data. tfMRI timeseries data were averaged within parcels and then the tfMRI analysis pipeline (described above) was run (with autocorrelation smoothing turned off). This generated parcellated task contrast maps, which are advantageous for assessing the statistical significance of activations without resorting to conventional statistical approaches for dealing with voxelwise multiple comparisons that are likely less sensitive (e.g. Threshold-Free Cluster Enhancement, (Smith and Nichols, 2009)), and, in the case of Gaussian Random Field theory, use geometrical models that are poorly matched to areal shapes in the convoluted cortex. One still needs to do multiple comparison correction; however, because of the reduced number of tests, there is more power. rfMRI timeseries data were averaged within parcels. Parcellated functional connectomes were computed using full and partial correlation (by inverting the covariance matrix) using FSLNets ((Smith et al., 2013b) http://fsl.fmrib.ox.ac.uk/fsl/fslwiki/FSLNets). These connectomes were converted to Z-scores using the Fisher transform and an empirical correction for temporal autocorrelation (see FSLNets).

To produce group average parcellated datasets, myelin and thickness parcellated maps were simply averaged. tfMRI contrast maps were combined across subjects by processing the data through the group tfMRI analysis pipeline using a mixed effects analysis (FSL's FLAME). rfMRI FC parcellated connectomes were also combined across subjects using a mixed effects analysis (a one-sample t-test performed across subjects on each cell to produce group mixed effects Z statistic maps). Thus, both individual subject and group average parcellated datasets were generated for myelin, thickness, tfMRI contrasts, and rfMRI FC full and unregularized partial correlation connectomes.

7.2 Validation of the Multi-modal Parcellation with an Independent HCP Dataset

All parcellation and areal classifier training analyses described in preceding sections were performed on the 210P parcellation subjects (plus 29T classifier test subjects). The 210V validation subjects were set aside as an independent cross-validation dataset. Given

the large number of subjects in each group, we expected that aggregate results would be very similar between the two groups (as was shown in the Supplementary Figures 1-5 in the Supplementary Results and Discussion and #1.1 for the reproducibility of the dense features used for parcellation). To produce individual-subject parcellations in the 210V group, the multi-modal individual subject features were generated and the trained classifiers (i.e. two weight matrices and two nonlinear functions for each cortical area) were applied to each individual subject's multi-modal areal features to define and identify their cortical areas. The classifier outputs were combined as described above. Two approaches were then used to cross-validate the parcellation.

1) Parcellated datasets of 210V individuals were generated using the original semi-automated parcellation from the 210P dataset (applied as an atlas parcellation, rather than using the areal classifier) for myelin maps, cortical thickness maps, tfMRI contrast maps, and an rfMRI full correlation parcellated connectome. These data were concatenated into an areas X features X subjects matrix. t-tests across subjects were done between each pair of areas that shared a border in the original 210P parcellation for each feature to determine whether the feature was robustly and statistically significantly different between the two neighboring areas. A conservative Bonferroni threshold of $p<9*10^{-8}$ was imposed on the data (# of area pairs across both hemispheres (1050) X number of features (266) X number of tails (2) * 0.05). 63% of all possible feature/border combinations were significant, including many features that the classifier regarded as unimportant for defining the relevant area. We therefore opted to additionally threshold based on effect size (Cohen's $d>1$). We grouped features into 4 independent categories: myelin, thickness, tfMRI contrasts (though technically the seven tasks are independent) and the rfMRI full correlation parcellated connectome. We then binned areal pairs according to how many feature categories in which they had a robust and statistically significant difference across their mutual border. The parcellated connectome's diagonal was ignored for this test (else areas would always be different from their neighbors because of a connectivity difference with the diagonal). The vast majority of areal pairs had robust and statistically significant effect sizes in more than one independent feature category in the independent cross-validation dataset (see Main Results, Supplementary Results and Discussion #1.2).

2) Probabilistic maps of each cortical area within each hemisphere were generated by averaging the areal definitions across subjects within the 210P and 210V groups separately, and a maximum probability map MPM map was calculated for each group based on the probabilistic maps. The group MPM maps were converted into binary ROIs (180 of them, one for each area), which were concatenated into a single vector. The 210P MPM vector and the 210V MPM vectors were correlated (also the 210P MPM was correlated with the original semi-automated multimodal parcellation). Because some readers found the Dice coefficient more intuitive than correlation for this application we also computed it for each parcellation reproducibility test. The Dice coefficent is $(2 * A \cap B)/(A + B)$.

3) The individual subject parcellations of the 27 individuals who were scanned and analyzed with the whole protocol on two separate occasions were also correlated and Diced as in 2) above.

References

Abdollahi, R.O., Kolster, H., Glasser, M.F., Robinson, E.C., Coalson, T.S., Dierker, D., Jenkinson, M., Van Essen, D.C., Orban, G.A., 2014. Correspondences between retinotopic areas and myelin maps in human visual cortex. Neuroimage 99, 509-524.

Anticevic, A., Dierker, D.L., Gillespie, S.K., Repovs, G., Csernansky, J.G., Van Essen, D.C., Barch, D.M., 2008. Comparing surface-based and volume-based analyses of functional neuroimaging data in patients with schizophrenia. Neuroimage 41, 835-848.

Barch, D.M., Burgess, G.C., Harms, M.P., Petersen, S.E., Schlaggar, B.L., Corbetta, M., Glasser, M.F., Curtiss, S., Dixit, S., Feldt, C., Nolan, D., Bryant, E., Hartley, T., Footer, O., Bjork, J.M., Poldrack, R., Smith, S., Johansen-Berg, H., Snyder, A.Z., Van Essen, D.C., Consortium, W.U.-M.H., 2013. Function in the human connectome: task-fMRI and individual differences in behavior. Neuroimage 80, 169-189.

Beckmann, C.F., DeLuca, M., Devlin, J.T., Smith, S.M., 2005. Investigations into resting-state connectivity using independent component analysis. Philosophical Transactions of the Royal Society of London B: Biological Sciences 360, 1001-1013.

Beckmann, C.F., Smith, S.M., 2004. Probabilistic independent component analysis for functional magnetic resonance imaging. Medical Imaging, IEEE Transactions on 23, 137-152.

Caspers, S., Eickhoff, S.B., Zilles, K., Amunts, K., 2013. Microstructural grey matter parcellation and its relevance for connectome analyses. Neuroimage 80, 18-26.

Cohen, A.L., Fair, D.A., Dosenbach, N.U., Miezin, F.M., Dierker, D., Van Essen, D.C., Schlaggar, B.L., Petersen, S.E., 2008. Defining functional areas in individual human brains using resting functional connectivity MRI. Neuroimage 41, 45-57.

Cole, M.W., Bassett, D.S., Power, J.D., Braver, T.S., Petersen, S.E., 2014. Intrinsic and task-evoked network architectures of the human brain. Neuron 83, 238-251.

Desikan, R.S., Ségonne, F., Fischl, B., Quinn, B.T., Dickerson, B.C., Blacker, D., Buckner, R.L., Dale, A.M., Maguire, R.P., Hyman, B.T., 2006. An automated labeling system for subdividing the human cerebral cortex on MRI scans into gyral based regions of interest. Neuroimage 31, 968-980.

Drury, H.A., Essen, D., Corbetta, M., Snyder, A., 1998. Surface based analyses of the human cerebral cortex. Brain Warping, 337.

Eickhoff, S.B., Stephan, K.E., Mohlberg, H., Grefkes, C., Fink, G.R., Amunts, K., Zilles, K., 2005. A new SPM toolbox for combining probabilistic cytoarchitectonic maps and functional imaging data. Neuroimage 25, 1325-1335.

Filippini, N., MacIntosh, B.J., Hough, M.G., Goodwin, G.M., Frisoni, G.B., Smith, S.M., Matthews, P.M., Beckmann, C.F., Mackay, C.E., 2009. Distinct patterns of brain activity in young carriers of the APOE-epsilon4 allele. Proc Natl Acad Sci U S A 106, 7209-7214.

Fischl, B., 2012. FreeSurfer. Neuroimage 62, 774-781.

Fischl, B., Rajendran, N., Busa, E., Augustinack, J., Hinds, O., Yeo, B.T., Mohlberg, H., Amunts, K., Zilles, K., 2008. Cortical folding patterns and predicting cytoarchitecture. Cereb Cortex 18, 1973-1980.

Fischl, B., Sereno, M.I., Dale, A.M., 1999a. Cortical surface-based analysis: II: inflation, flattening, and a surface-based coordinate system. Neuroimage 9, 195-207.

Fischl, B., Sereno, M.I., Tootell, R.B., Dale, A.M., 1999b. High-resolution intersubject averaging and a coordinate system for the cortical surface. Human brain mapping 8, 272-284.
Fox, M.D., Snyder, A.Z., Vincent, J.L., Corbetta, M., Van Essen, D.C., Raichle, M.E., 2005. The human brain is intrinsically organized into dynamic, anticorrelated functional networks. Proc Natl Acad Sci U S A 102, 9673-9678.
Frost, M.A., Goebel, R., 2012. Measuring structural-functional correspondence: spatial variability of specialised brain regions after macro-anatomical alignment. Neuroimage 59, 1369-1381.
Glasser, M.F., Goyal, M.S., Preuss, T.M., Raichle, M.E., Van Essen, D.C., 2014a. Trends and properties of human cerebral cortex: correlations with cortical myelin content. Neuroimage 93 Pt 2, 165-175.
Glasser, M.F., Robinson, E.C.C., T.S. Smith, S.M. , Jenkinson, M. Van Essen, D.C. , 2014b. Retinotopic Organization of Visual Cortex Revealed by Resting State Functional Connectivity. Organization for Human Brain Mapping, Hamburg, Germany.
Glasser, M.F., Sotiropoulos, S.N., Wilson, J.A., Coalson, T.S., Fischl, B., Andersson, J.L., Xu, J., Jbabdi, S., Webster, M., Polimeni, J.R., Van Essen, D.C., Jenkinson, M., Consortium, W.U.-M.H., 2013. The minimal preprocessing pipelines for the Human Connectome Project. Neuroimage 80, 105-124.
Glasser, M.F., Van Essen, D.C., 2011. Mapping human cortical areas in vivo based on myelin content as revealed by T1- and T2-weighted MRI. J Neurosci 31, 11597-11616.
Glocker, B., Heibel, T.H., Navab, N., Kohli, P., Rother, C., 2010. Triangleflow: Optical flow with triangulation-based higher-order likelihoods. Computer Vision–ECCV 2010. Springer, pp. 272-285.
Greve, D.N., Fischl, B., 2009. Accurate and robust brain image alignment using boundary-based registration. Neuroimage 48, 63-72.
Griffanti, L., Salimi-Khorshidi, G., Beckmann, C.F., Auerbach, E.J., Douaud, G., Sexton, C.E., Zsoldos, E., Ebmeier, K.P., Filippini, N., Mackay, C.E., 2014. ICA-based artefact removal and accelerated fMRI acquisition for improved resting state network imaging. Neuroimage 95, 232-247.
Hacker, C.D., Laumann, T.O., Szrama, N.P., Baldassarre, A., Snyder, A.Z., Leuthardt, E.C., Corbetta, M., 2013. Resting state network estimation in individual subjects. Neuroimage 82, 616-633.
Hart, P.E., Nilsson, N.J., Raphael, B., 1968. A formal basis for the heuristic determination of minimum cost paths. Systems Science and Cybernetics, IEEE Transactions on 4, 100-107.
Hodge, M.R., Horton, W., Brown, T., Herrick, R., Olsen, T., Hileman, M.E., McKay, M., Archie, K.A., Cler, E., Harms, M.P., 2015. ConnectomeDB—sharing human brain connectivity data. Neuroimage.
Ishikawa, H., 2009. Higher-order clique reduction in binary graph cut. Computer Vision and Pattern Recognition, 2009. CVPR 2009. IEEE Conference on. IEEE, pp. 2993-3000.
Ishikawa, H., 2014. Higher-order clique reduction without auxiliary variables. Proceedings of the IEEE Conference on Computer Vision and Pattern Recognition, pp. 1362-1369.
Jenkinson, M., Beckmann, C.F., Behrens, T.E., Woolrich, M.W., Smith, S.M., 2012. Fsl. Neuroimage 62, 782-790.

Larson-Prior, L.J., Oostenveld, R., Della Penna, S., Michalareas, G., Prior, F., Babajani-Feremi, A., Schoffelen, J.M., Marzetti, L., de Pasquale, F., Di Pompeo, F., Stout, J., Woolrich, M., Luo, Q., Bucholz, R., Fries, P., Pizzella, V., Romani, G.L., Corbetta, M., Snyder, A.Z., Consortium, W.U.-M.H., 2013. Adding dynamics to the Human Connectome Project with MEG. Neuroimage 80, 190-201.

Marcus, D.S., Harms, M.P., Snyder, A.Z., Jenkinson, M., Wilson, J.A., Glasser, M.F., Barch, D.M., Archie, K.A., Burgess, G.C., Ramaratnam, M., Hodge, M., Horton, W., Herrick, R., Olsen, T., McKay, M., House, M., Hileman, M., Reid, E., Harwell, J., Coalson, T., Schindler, J., Elam, J.S., Curtiss, S.W., Van Essen, D.C., Consortium, W.U.-M.H., 2013. Human Connectome Project informatics: quality control, database services, and data visualization. Neuroimage 80, 202-219.

Ringel, G., Youngs, J., 1968. Solution of the Heawood map-coloring problem. Proc Natl Acad Sci U S A 60, 438.

Robinson, E.C., Jbabdi, S., Glasser, M.F., Andersson, J., Burgess, G.C., Harms, M.P., Smith, S.M., Van Essen, D.C., Jenkinson, M., 2014. MSM: a new flexible framework for Multimodal Surface Matching. Neuroimage 100, 414-426.

Salimi-Khorshidi, G., Douaud, G., Beckmann, C.F., Glasser, M.F., Griffanti, L., Smith, S.M., 2014. Automatic denoising of functional MRI data: combining independent component analysis and hierarchical fusion of classifiers. Neuroimage 90, 449-468.

Schleicher, A., Amunts, K., Geyer, S., Morosan, P., Zilles, K., 1999. Observer-independent method for microstructural parcellation of cerebral cortex: a quantitative approach to cytoarchitectonics. Neuroimage 9, 165-177.

Schleicher, A., Morosan, P., Amunts, K., Zilles, K., 2009. Quantitative architectural analysis: a new approach to cortical mapping. J Autism Dev Disord 39, 1568-1581.

Sereno, M.I., Dale, A.M., Reppas, J.B., Kwong, K.K., Belliveau, J.W., Brady, T.J., Rosen, B.R., Tootell, R.B., 1995. Borders of multiple visual areas in humans revealed by functional magnetic resonance imaging. Science 268, 889-893.

Sereno, M.I., McDonald, C.T., Allman, J.M., 1994. Analysis of retinotopic maps in extrastriate cortex. Cereb Cortex 4, 601-620.

Smith, S.M., Beckmann, C.F., Andersson, J., Auerbach, E.J., Bijsterbosch, J., Douaud, G., Duff, E., Feinberg, D.A., Griffanti, L., Harms, M.P., Kelly, M., Laumann, T., Miller, K.L., Moeller, S., Petersen, S., Power, J., Salimi-Khorshidi, G., Snyder, A.Z., Vu, A.T., Woolrich, M.W., Xu, J., Yacoub, E., Ugurbil, K., Van Essen, D.C., Glasser, M.F., Consortium, W.U.-M.H., 2013a. Resting-state fMRI in the Human Connectome Project. Neuroimage 80, 144-168.

Smith, S.M., Fox, P.T., Miller, K.L., Glahn, D.C., Fox, P.M., Mackay, C.E., Filippini, N., Watkins, K.E., Toro, R., Laird, A.R., Beckmann, C.F., 2009. Correspondence of the brain's functional architecture during activation and rest. Proc Natl Acad Sci U S A 106, 13040-13045.

Smith, S.M., Hyvarinen, A., Varoquaux, G., Miller, K.L., Beckmann, C.F., 2014. Group-PCA for very large fMRI datasets. Neuroimage 101, 738-749.

Smith, S.M., Jenkinson, M., Woolrich, M.W., Beckmann, C.F., Behrens, T.E., Johansen-Berg, H., Bannister, P.R., De Luca, M., Drobnjak, I., Flitney, D.E., Niazy, R.K., Saunders, J., Vickers, J., Zhang, Y., De Stefano, N., Brady, J.M., Matthews, P.M., 2004. Advances in functional and structural MR image analysis and implementation as FSL. Neuroimage 23 Suppl 1, S208-219.

Smith, S.M., Nichols, T.E., 2009. Threshold-free cluster enhancement: addressing problems of smoothing, threshold dependence and localisation in cluster inference. Neuroimage 44, 83-98.
Smith, S.M., Vidaurre, D., Beckmann, C.F., Glasser, M.F., Jenkinson, M., Miller, K.L., Nichols, T.E., Robinson, E.C., Salimi-Khorshidi, G., Woolrich, M.W., Barch, D.M., Ugurbil, K., Van Essen, D.C., 2013b. Functional connectomics from resting-state fMRI. Trends Cogn Sci 17, 666-682.
Tucholka, A., Fritsch, V., Poline, J.B., Thirion, B., 2012. An empirical comparison of surface-based and volume-based group studies in neuroimaging. Neuroimage 63, 1443-1453.
Ugurbil, K., Xu, J., Auerbach, E.J., Moeller, S., Vu, A., Duarte-Carvajalino, J.M., Lenglet, C., Strupp, J., Sapiro, G., De Martino, F., Wang, D., Harel, N., Garwood, M., Chen, L., Feinberg, D.a., Smith, S.M., Miller, K.L., Sotiropoulos, S.N., Jbabdi, S., Andersson, J.L., Behrens, T.E.J., Glasser, M.F., Van Essen, D.C., Yacoub, E., 2013. Pushing spatial and temporal resolution for functional and diffusuion MRI in the Human Connectome Project. Neuroimage.
Van Essen, D.C., 2005. A Population-Average, Landmark- and Surface-based (PALS) atlas of human cerebral cortex. Neuroimage 28, 635-662.
Van Essen, D.C., Glasser, M.F., Dierker, D.L., Harwell, J., Coalson, T., 2012. Parcellations and hemispheric asymmetries of human cerebral cortex analyzed on surface-based atlases. Cereb Cortex 22, 2241-2262.
Van Essen, D.C., Smith, J., Glasser, M.F., Elam, J., Donahue, C.J., Dierker, D.L., Reid, E.K., Coalson, T., Harwell, J., 2016. The Brain Analysis Library of Spatial maps and Atlases (BALSA) Database. Neuroimage.
Van Essen, D.C., Smith, S.M., Barch, D.M., Behrens, T.E., Yacoub, E., Ugurbil, K., Consortium, W.U.-M.H., 2013. The WU-Minn Human Connectome Project: an overview. Neuroimage 80, 62-79.
Wishart, J., 1928. The generalised product moment distribution in samples from a normal multivariate population. Biometrika, 32-52.
Yeo, B.T., Krienen, F.M., Sepulcre, J., Sabuncu, M.R., Lashkari, D., Hollinshead, M., Roffman, J.L., Smoller, J.W., Zollei, L., Polimeni, J.R., Fischl, B., Liu, H., Buckner, R.L., 2011. The organization of the human cerebral cortex estimated by intrinsic functional connectivity. J Neurophysiol 106, 1125-1165.
Zilles, K., Amunts, K., 2010. Centenary of Brodmann's map--conception and fate. Nat Rev Neurosci 11, 139-145.

Supplementary Neuroanatomical Results For A Multi-modal Parcellation of Human Cerebral Cortex

Matthew F. Glasser[1], Timothy S. Coalson[1]*, Emma C. Robinson[2,3]*, Carl D. Hacker[4]*, John Harwell[1], Essa Yacoub[5], Kamil Ugurbil[5], Jesper Andersson[2], Christian F. Beckmann[6], Mark Jenkinson[2], Stephen M. Smith[2], David C. Van Essen[1]

[1]Department of Neuroscience, Washington University Medical School, Saint Louis, Missouri 63110, USA. [2]FMRIB Centre, Nuffield Department of Clinical Neurosciences, John Radcliffe Hospital, University of Oxford, Oxford OX3 9DU, UK. [3]Department of Computing, Imperial College, London SW7 2AZ, UK. [4]Department of Biomedical Engineering, Washington University, Saint Louis, Missouri 63110, USA. [5]Center for Magnetic Resonance Research (CMRR), University of Minnesota, Minneapolis, Minnesota 55455, USA. [6]Donders Institute for Brain, Cognition and Behavior, Radboud University, Nijmegen 6525 EN, The Netherlands. [7]Department of Cognitive Neuroscience, Radboud University Medical Centre Nijmegen, Postbus 9101, Nijmegen 6500 HB, The Netherlands.

**These authors contributed equally to this work.*

Introduction and Overview

The Supplementary Neuroanatomical Results presented below provide extensive documentation describing our identification of 180 human neocortical areas and the evidence used to delineate their boundaries based on the 210P group average multi-modal data. This introductory section gives an overview of the Supplementary Neuroanatomical Results and general comments covering the subsequent 22 region-by-region sections that describe the boundary between each pair of cortical areas. Each boundary is described only once, in the first section where it is encountered.

Grouping by Regions

For organizational purposes, we grouped the 180 cortical areas into 22 regions based on several criteria: Each region includes a set of geographically contiguous areas that can be seen in their entirety from a single viewing perspective on the inflated cortical surface or in some cases on a flatmap. In addition, the areas within a region often share common properties, based on architecture, task-fMRI profiles, and/or functional connectivity. Figure 1 shows each region in a different color, with areal boundaries in black, displayed on lateral and medial views of the left and right hemisphere inflated cortical surfaces and on the corresponding flatmaps. The color choices below were inspired by the predominant colors in each region in Main Text Figure 3.

Area names and terminological styles

Supplemental Table 1 at the end of this document lists each area by parcellation index number, along with the area's brief name, full name, whether it was newly described, the primary (**Bold**) and secondary text section numbers that describe the features used to

distinguish the area from its neighbors, some synonyms for the area in the literature (or 'quasi-synonymns' for areas that are similar but not convincingly identical), and the primary reference(s) used in assigning these names. Supplemental Table 2 lists the studies used to identify the areas in this parcellation together with our area names and how they correspond to those mentioned in each study. In general, we used existing terminology whenever we could identify a reasonable match between an area in an existing parcellation and an area identified in the HCP data. Correspondence was based on similarity in location, using inferred local geographic landmarks (gyri and sulci) together with the spatial relationships with neighboring areas whose correspondence to our parcellation's areas was already established. Because we registered the data based on cortical areal features instead of folding patterns, only those folding features having consistent relationships with cortical areas were preserved in the group average data. Finally, we used specific areal features (e.g., degree of myelination, type of functional specialization, or topographic organization) when available in the prior studies (e.g. the comparison of myelin maps around 55b in Main Text Figure 2). In many instances, alternative names could have reasonably been selected. We strove for names that reflected the 'best fit', and secondarily to use similar terminology when feasible to describe the areas in a given region. However, in several regions we either introduced completely new terminology because we did not find appropriate correspondences in the literature, or we modified existing names to reflect a finer grained parcellation than was found in earlier studies.

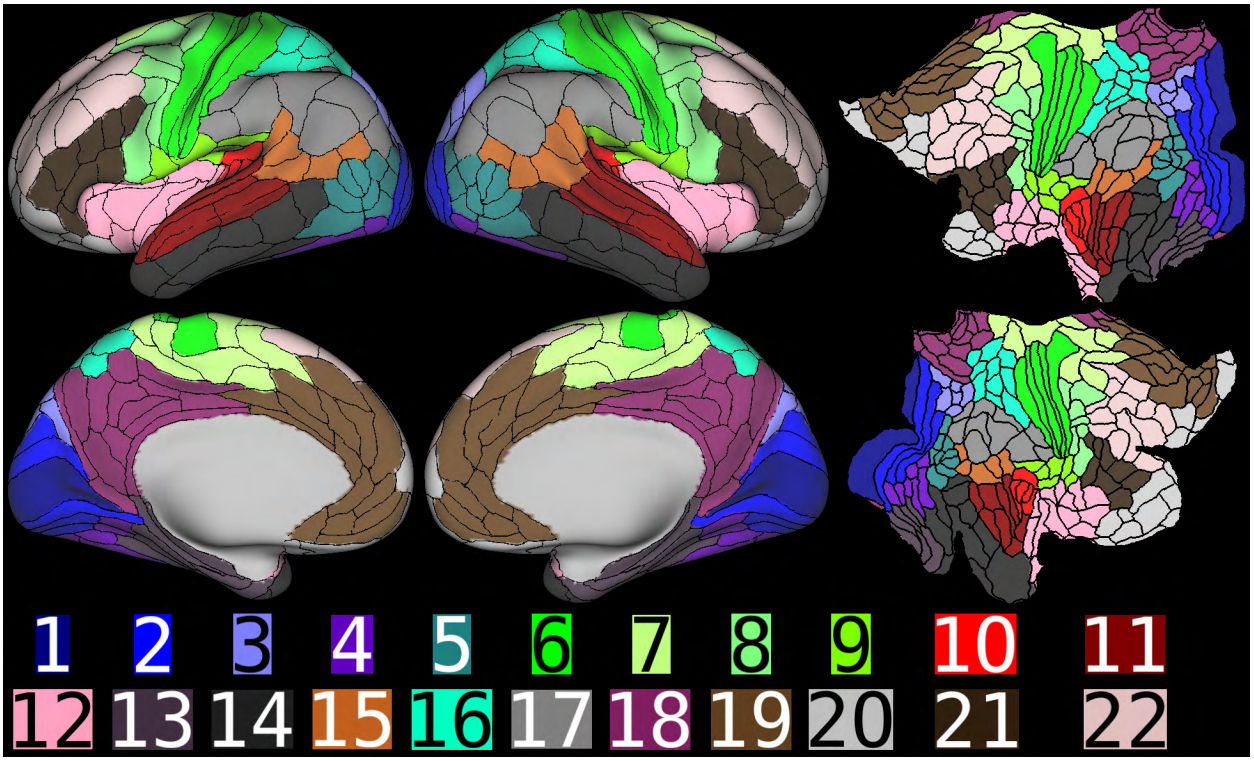

Figure 1 shows the 22 numbered results sections to be covered below. Data at http://balsa.wustl.edu/QnXj.

Given the diverse terminological styles used over the past century of parcellation work, our parcellation contains a mixture of these styles. Some areas are described by numerals (e.g., areas 1, 2, 4), others by all-caps letters (e.g., MT, PF), and others by

combinations of letters and numbers (e.g. V1, V2, OP1). Lower case letters typically represent subdivisions of a once-larger parcel, and they signify relative position within the brain. Some of these use the anterior/posterior convention (e.g., 6mp and 6ma), whereas others use the rostral/caudal convention (e.g., 47r). Some use the dorsal/ventral convention (e.g., LIPd, LIPv) whereas others use the superior/inferior convention (e.g., PGi, PGs). Others use numerals or letters for finer-grained parcellation that is not readily described using cardinal axes (e.g., TPOJ1, TPOJ2, TPOJ3). In some cases we adopted an existing name except for a format change. (i) We used capital 'L' instead of lower-case 'l' to avoid confusion with numeral '1' (e.g., area 7AL instead of 7Al). (ii) We converted the forward-slash '/' to a hyphen '-'(e.g., area 6-8 instead of published area 6/8), because '/' is a reserved character in many programming languages. (iii) We converted ['] to [pr] ('prime') for a similar reason.

Multi-modal Areal Differences

Nearly all areas identified in our parcellation had borders with their neighbors that reflected significant differences by at least two areal feature measures. The semi-automated border delineation tool provided estimates of statistical significance and effect size for each areal feature used to delineate each areal boundary. Most p values were very small (with a substantial fraction having p values too small to represent in float32), with a maximum pvalue of $p<0.001$ for all reported areal features across all boundaries. Additionally, most effect sizes were Cohen's $d>1$, with a minimum Cohen's $d>0.5$ for all reported areal features across all boundaries (0.5 is a 'medium' effect size). These statistical significance and effect size measures were used mainly to screen areal feature gradients to ensure they were likely to be statistically significantly and robustly different and thus strong candidates for true areal boundaries. However, because the tests were performed on the same data as were used to make the parcellation, the parcellation was additionally evaluated with non-circular statistical tests across all areal features using the 210V dataset (see Supplementary Figure 6 and #1.2 in the Supplementary Results and Discussion).

Some parcels are internally heterogeneous in single modalities that might hint at finer grained parcellation. Other parcels may have previously been parcellated more finely in published parcellations. However, we strove to include areal boundaries only when they are strongly supported by multiple modalities in our own data. Hence, our number of 180 cortical areas per hemisphere likely reflects a lower bound. Some areas may be further parcellated using new datasets and/or analysis methods, and some areas are explicitly identified as 'area complexes' (e.g., the Fusiform Face Complex, FFC). Additionally, there are some areas that are impossible to parcellate accurately with the current HCP data due to signal loss in the fMRI modalities from susceptibility artifacts or venous shadows. Higher resolution data with fewer artifacts, different task batteries, or other novel information will likely lead to refinements to this parcellation, which is why it is described as version 1.0.

Organization of subsequent sections

The primary purpose of the 22 sections that follow is to describe and illustrate much of the evidence that was used to delineate borders between each cortical area and each of its neighbors, using the gradient-based semi-automated border optimization method described in the Supplementary Methods. For these border delineations, only a subset of the possible feature contrasts were used. Hence, the descriptions of distinguishing areal features often do not include every feature that was significantly different, but they nonetheless provide a useful tabulation of many of the features that distinguish each area from its neighbors. For many/most area pairs, there are many more statistically significant areal-feature differences than are described in the sections below. The complete multi-modal signatures for each area and their differences relative to neighboring areas can be more systematically and robustly analyzed using the same approach that was used in the statistical cross-validation analysis (Supplementary Figure 6 in the Supplementary Results and Discussion).

In describing the positions of one area relative to its neighbors, we generally use superior/inferior instead of dorsal/ventral, and anterior/posterior instead of rostral/caudal, based on their locations on the HCP group average midthickness surface. To aid in reading the admittedly dense prose, we highlight the 'reference' area name in bold when making a between-area comparison (e.g., "Relative to its dorsal neighbor XX, **area YY** has more myelin, etc."

Most of the figures have a similar format: The first panel shows the borders of the region's constituent areas overlaid on a map showing the group average cortical folding pattern (based on FreeSurfer's mean curvature maps) on inflated or flattened surfaces, along with Connectome Workbench brain annotations naming all of the areas and many of their neighbors. The remaining panels use the same viewing perspective as the first panel together with the areal borders to illustrate much of the information that was used in delineating the areal borders with the semi-automated border optimization method in Connectome Workbench. These are typically ordered as (i) myelin maps, (ii) thickness maps, (iii) functional connectivity gradients, and (iv) various task-fMRI contrasts that are particularly informative about the region being discussed. Aside from the first section, we generally do not show gradients of many of the modalities, thereby reducing by ~half the number of panels in each figure. Each of the figures is available as a Connectome Workbench 'scene' that can be accessed via the BALSA database using the scene-specific URLs in each figure legend (http://balsa.wustl.edu/BALSA_Scene_ID). All scenes in this document are included in a single scene file that can be downloaded along with all associated data files for interactive visualization (with annotations included) in the 'wb_view' software (Connectome Workbench v1.2.0 and higher).

Caveats and comments on specific modalities:

Myelin. We use the expression that an area "has more myelin" or "has less myelin" than a neighbor to refer to cross-border differences in which a statistically significant and robust difference was found when comparing the two areas for the values of T1w/T2w mapped to the cortical surface as described in the Supplementary Methods (e.g., with bias correction). Strictly speaking, the T1w/T2w ratio is not a 'pure' measure of myelin content, as it may be influenced by other characteristics within each voxel (see Supplementary Figure 1 legend

in the Supplementary Results and Discussion, and also (Glasser et al., 2014; Glasser and Van Essen, 2011).

Cortical Thickness. Thickness measures were compensated for systematic folding-related biases (relative to neutral sulcal banks, gyral cortex is thicker and fundal cortex is thinner). Such variation will mask the area-specific differences in cortical thickness that are useful for parcellation. We compensated thickness for folding biases by regressing out FreeSurfer's mean curvature map (see Supplementary Methods #1.5), but refer to the resulting measure simply as 'cortical thickness' below.

Functional Connectivity. Functional connectivity in most cases is described only as demonstrating robust and statistically significant across-border 'connectivity differences', which are also generally evident in the mean functional connectivity gradient map. Some differences are larger than others. For example, there are prominent differences in local connectivity across a boundary, whereas most other brain regions have similar connectivity with the two areas, resulting in a mean gradient that appears weaker (from being "washed out" in the averaging) than the quantitative statistics and the functional connectivity maps would suggest. The functional connectivity maps associated with each area are often very informative with regard to specific spatial patterns (e.g., association with particular modalities or networks), but it was outside the scope of this document to illustrate these routinely. The dense connectomes from 210P and 210V used in this parcellation study can be viewed using this BALSA link (http://balsa.wustl.edu/WrwG).

Task fMRI Contrasts. Task contrasts were very useful for confirming the delineation of many borders, and also for providing some hints at the functional specialization of many areas. From the seven HCP tasks, the pipelines generate 86 task contrasts, 47 of which are unique (the other 39 are sign-reversed versions). In the text descriptions, we generally label task contrasts by the name assigned to each task contrast map in the tfMRI CIFTI files (https://wiki.humanconnectome.org/display/PublicData/Task+fMRI+Contrasts). Some of these map names are self-explanatory, whereas others (e.g., 'TOM – RANDOM' in the SOCIAL task) are less transparent. Supplemental Table 3, based on (Barch et al., 2013) provides brief additional descriptions of each task contrast.

We generally use terms 'more activated', 'less activated', 'more deactivated' and 'less deactivated' to refer to the magnitude of the BOLD signal deviation relative to the baseline across an areal boundary for a specified task contrast (i.e. the difference in beta values across the boundary). This avoids making assumptions about the absolute magnitude of the BOLD signal in one condition or contrast or on the complex relationship between BOLD signals and neural activity (impulses and synaptic activity) in a given grayordinate.

Primary vs secondary (task-specific) contrasts.

Many (31 of 47) of the unique task activations reported are 'primary' contrasts (BOLD responses to a complex task vs a fixation-only baseline condition for all but the Emotion and Language tasks; for the latter two, the baseline was the intercept of the GLM, i.e., the mean across the scan). The activations and deactivations associated with these primary contrasts are often stronger than those for the various differential activations

between two task conditions (e.g., STORY – MATH) and include changes related to the information provided to carry out the task (e.g., auditory for the two categories of LANGUAGE task; visual images for the four stimulus categories of the Working Memory task). There were 16 of the differential or 'secondary' contrasts. For our purposes, we consider any differential activity that distinguishes one area from another as a valid basis for identifying areal boundaries. We also avoid using information related to topographic activations in sensori-motor and visual cortices (e.g. right upper limb cortex in the left hemisphere from right handed button box pressing, or gradients along the eccentricity axis from visual task stimulation). Finally, because the primary task contrasts often show similar information (aside from the MOTOR and LANGAUGE tasks), we sometimes state that a border was present in multiple primary task contrasts without naming them all.

Information on the slopes.

Each task contrast shows a complex spatial profile in which typically only a few regions have BOLD signals approaching the peak magnitude. In contrast to common practice in many task-fMRI studies, we made use of the entire spatial pattern of BOLD responses, including information on the slopes of the profiles, rather than just focusing on the peak responses. This was feasible because of the high quality of the task-fMRI data, the improvements in intersubject alignment, and the large number of subjects included in the group analysis (see Supplementary Figures 2 and 3 in the Supplementary Results and Discussion). In general, we consider a strong spatial gradient in task-fMRI responses that correlates with other measures to be relevant evidence for identifying areal boundaries regardless of whether the underlying values represent a peak, a valley, or lie on the slopes in between. Thus, we presume that differences based on gradients at low activation or deactivation may still be neuroanatomically significant.

Additional Notes on the Strategy Used and Presentation.

In order to define the areal boundaries based on multiple modalities, we first looked at the intrinsic modalities (i.e. those not dependent on a task design) to identify candidate areal borders, i.e. gradients in myelin, thickness, resting state connectivity, and resting state visuotopy, which constituted a relatively minimal set of maps to look at. In many cases this set of putative areal borders already showed cross-modal correspondences as noted below. We then searched through the task fMRI data for boundaries that agreed with one or more of the intrinsic modalities (usually finding several task contrasts that agreed). Boundaries that relied solely on task fMRI gradients were rare (and those boundaries show agreement across many task contrasts). As a result, there are some areas in our parcellation where one or more tasks have gradients that cut across the area. Future studies may choose to subparcellate these areas into additional areas based on more multi-modal evidence not yet available.

Also, though there may be continuous gradual gradients in a modality within an area (e.g. the eccentricity gradient in the visual areas) we chose to focus on sharp transitions that allowed the semi-automated border-drawing tool to follow along a gradient ridge. There were some examples of gradients that cut across known cortical areas for known or strongly hypothesized reasons (e.g. the somatotopic subdivisions of sensory and motor

cortex or a strong gradient across early visual cortex that may reflect foveal stimulation from the eyes open resting state fixation cross). In the case of the somatotopic subdivisions, we characterized these separately (see Figure 8) as subareas of the known cortical areas. In the case of the visual cortex gradient, we ignored it because it is a likely "task-induced" artifact. In brain regions were we do not have such extensive and well-established priors, we did not ignore multi-modally present gradients. For this reason, it is possible that some areas that we describe here may be reclassified as subareas as the topographic organization of higher cognitive areas becomes better understood. We are hopeful that this parcellation, together with the methods that make it possible, will provide a framework for advancing such understanding.

The general parcellation strategy involved MG making an initial manual draft parcellation of parcel boundaries and names for areas within one of the regions shown in Figure 1 using the semi-automated border optimization algorithm, documenting the parcellation, and generating draft scene files similar to those illustrated in this document for visualization in Connectome Workbench. DVE then reviewed the documentation and scene file together with the data, boundaries, area names, and statistical outputs from the semi-automated border optimization algorithm for each areal border and suggested changes as appropriate for that region. These revisions were then discussed by the two neuroanatomists, region-by-region, and the parcellation presented here represents their consensus interpretation, and the borders represent the output of the semi-automated border drawing algorithm.

Finally, to keep the presentation of the data below manageable, we only show the resting state functional connectivity gradients, which represent a summary of the connectivity differences, rather than the functional connectivity maps in most cases. However, we did routinely inspect these maps to confirm that the functional connectivity patterns were indeed different on either side of a gradient. The functional connectivity data are part of the public data release, however, so that others may examine the connectivity differences themselves.

The following 22 sections, covering the multi-modal parcellation of 180 areas and areal complexes spanning the entire cerebral neocortex, are grouped by geographic proximity and functional similarities. As already noted, Figure 1 illustrates the regions to be covered (each in a different color) and numbered by the order in which they are presented. The first five regions cover early and intermediate visual cortex, including sections on V1 (1), early visual cortex (2), the dorsal stream (3), the ventral stream (4), and the MT+ Complex (5) and its neighbors. The next four regions cover the early somatosensory and motor cortex (6), the sensori-motor associated paracentral lobular and mid cingulate cortex (7), the premotor cortex (8), and the posterior opercular cortex (9). Next are three regions covering the early auditory (10) and association auditory cortex (11) and the insular and frontal opercular cortex (12). Then are two regions covering the rest of the temporal cortex including medial (13) and lateral temporal cortex (14). Then there are four regions covering the rest of the posterior cortex including the sensory "bridge" regions of the temporal-parietal-occipital junction (15) and the superior parietal and IPS cortex (16), along with the inferior parietal cortex (17), and the posterior cingulate cortex (18). The final four regions cover the rest of anterior cortex including the anterior cingulate and medial prefrontal cortex (19), orbital and polar frontal cortex (20), inferior frontal cortex (21), and the dorsolateral prefrontal cortex (22).

The Multi-modal Cortical Parcellation Region by Region

1. Primary Visual Cortex (V1)

We begin with area V1, given its importance to the subsequent visuotopic analyses and its status as arguably the most intensively studied cortical area in primates. We also use V1 to demonstrate the semi-automated border definition method and the initial statistical checks and to describe our "neuroanatomist's" approach to interpreting the data in more detail than is feasible for subsequent areas. V1 is the only cortical area that can be recognized in unstained brain slices, without the aid of microscopy, thanks to the heavily myelinated stria of Gennari in layer 4B (Gennari, 1782). In the HCP 0.7mm T1w/T2w myelin maps, the stria is discernible in some parts of the calcarine sulcus in many individuals, but the resolution is inadequate for delineating it reliably throughout V1. Although all modalities used in this study can provide useful information for delineating at least part of V1's borders with neighboring areas V2 and pro-striate cortex (ProS), we focus on myelin maps, LGN functional connectivity, and cortical thickness, as these were the modalities used by the semi-automated border optimizer to define the boundaries of V1. In a pattern to be emulated in subsequent sections, we will mention the areas adjacent to the region being discussed but cover them in more detail in their own region's section. We will also reference the figure panel that illustrates a given areal property if it is shown in the figure, otherwise such a reference will not appear for data that is not shown.

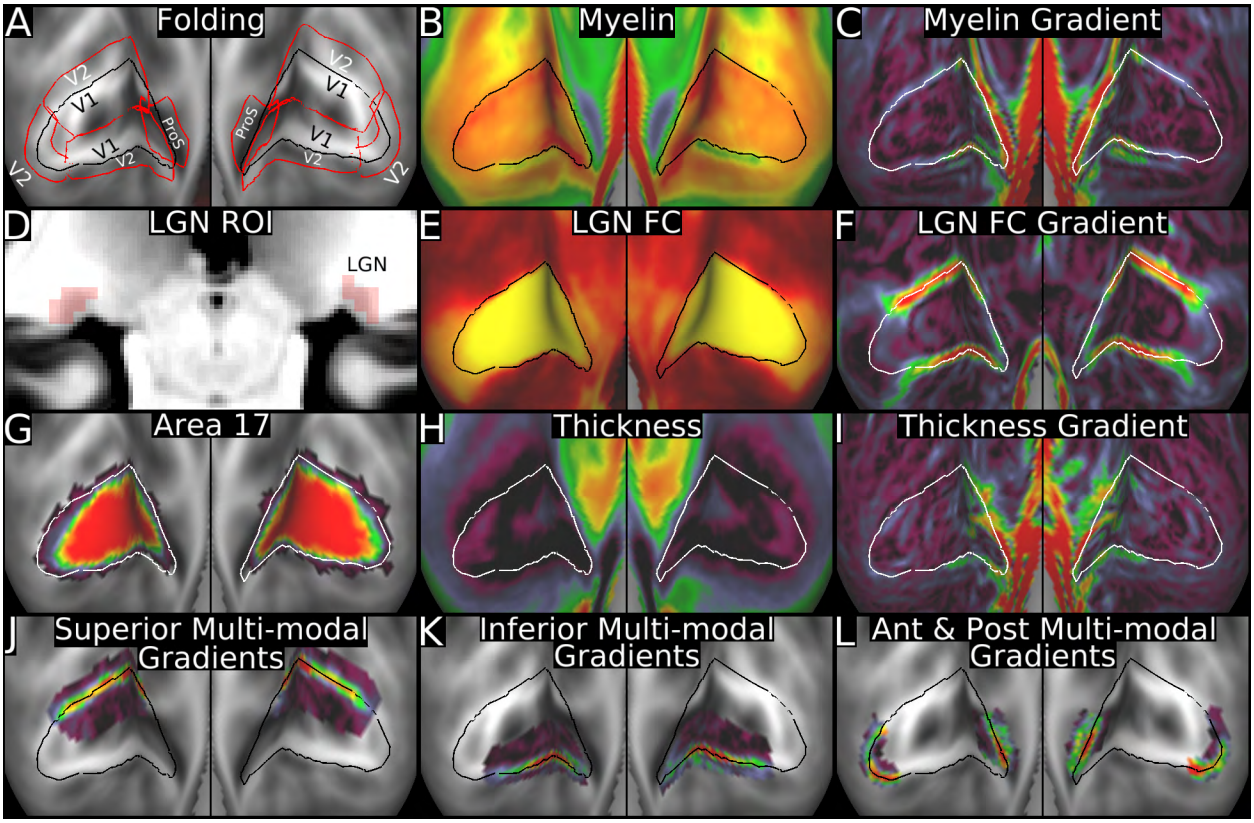

Figure 2, above, shows how the semi-automated border optimizer method was used to define V1, including the modalities used for areal delineation. The black or white outline in all panels is the V1 border. Panel A shows V1 on a group average cortical folding map (FreeSurfer mean curvature) together with the ROIs used for semi automated border drawing and the names of V1's neighbors. Panels B and C show the group average myelin map and gradients. Panels D, E, and F, show the LGN ROI (translucent red) displayed on the group average T1w image, the group average LGN functional connectivity map, and its gradient. Panel G shows the area 17 probabilistic maps (Fischl et al., 2008). Panels H and I show the group average cortical thickness maps and gradients. Panels J, K, and L show the effective combined gradients used by the algorithm for final border placement. Data at http://balsa.wustl.edu/Jg5v.

Figure 2, Panel A shows the borders of area **V1** as a black line on a group average map of the folding pattern (FreeSurfer mean curvature map). V1 occupies the entire calcarine sulcus, which is well defined despite areal feature-based registration, indicating that V1's location is tightly correlated with cortical folding patterns, as previously demonstrated (Fischl et al., 2008). Because there were some regional differences in which modalities best defined the border between V1 and V2 along its extent, the borders were automatically refined and the cross-border statistics were assessed separately for the anterior, superior, inferior, and posterior borders of V1, as indicated by the optimization ROIs (red outlines) in Panel A. Panels B and C respectively illustrate the group-average myelin maps and myelin map gradients. A gradient ridge runs along the margin of **V1**, but its magnitude varies, being strongest anteriorly (including the boundary with the lightly myelinated prostriate area ProS) and weakest posteriorly (in foveal V1). A striking delineation of the full extent of **V1** comes from seed-based functional connectivity (FC), using the left and right LGNs as seed ROIs. The LGNs are identifiable in the high resolution T1w and T2w volumes (Panel D ROI is translucent red, LGN is darker grey). The group-average LGN-seeded functional connectivity is high throughout **V1** (Panel E), and the LGN FC gradients (Panel F) have prominent ridges superiorly and inferiorly in mid-eccentricity ranges. The myelin (Panel C) and FC gradients (Panel F) were precisely colocalized along the superior and inferior borders of **V1**, and the semi-automated border optimizer easily followed their combined gradients. Along the anterior boundary with the prostriate area, the myelin and LGN FC gradient ridges overlap one another, but the myelin gradient ridge is broader and centered more anteriorly. The semi-automated gradient delineator identified a consensus border between the two gradient peaks. Along the superior boundary, the cross-border modality differences were largest for LGN-seeded FC (Cohen's d=7.06 (L) and d=6.46 (R)) and substantial for myelin (d=1.63 (L) and d=2.09 (R)). Differences were comparable along the inferior boundary for LGN-seeded FC (d=5.08 (L) and d=4.35 (R)) and for myelin (d=1.68 (L) and d=1.09 (R)). Panels J and K show the effective gradients used by the algorithm for these boundaries. Along the anterior border (adjoining the prostriate area) the differences were larger in magnitude for myelin (d=4.93 (L) and d=4.54 (R)) and smaller for LGN-seeded FC (d=3.73 (L) and d=2.36 (R)). Panel L shows the effective gradient used by the algorithm for this boundary. For all of the above comparisons, p values were less than $7 * 10^{-17}$ (p<floating point precision for all tests except right inferior myelin). Note that cortical thickness could also have been used to help define the anterior boundary of V1 with the Prostriate cortex (ProS) (Panels H and I).

The posterior (foveal) border of **V1** was more difficult to define because the gradients were less prominent for each modality and were less well aligned (and so more pre-gradient smoothing was used, sigma=2mm). In this region, we used myelin (Panels B

and C), cortical thickness (Panels H and I), and LGN connectivity (Panels E and F). The semi-automated border optimizer identified a trajectory based on all three gradients but closest to the thickness gradient ridge. The cross-border modality differences were substantial (Cohen's d=1.66 (L) and d=0.71 (R) for myelin, d=-0.83 (L) and d=-1.11 (R) for thickness, and d=2.56 (L) and 3.12 (R) for LGN connectivity), and all trans-border p values were less than 0.0003 in this region. Panel L shows the effective gradient used by the algorithm for this boundary.

As is well known (Abdollahi et al., 2014; Amunts et al., 2000; Fischl et al., 2008), the V1 border runs along the margins of the calcarine sulcus, just outside the gyral crown on the superior and inferior banks of the sulcus. This is evident in Panel A, where the V1 border is displayed over maps of folding patterns. Interestingly, in foveal cortex we identified a previously unappreciated correlation with cortical folding around the occipital pole posterior and lateral to the calcarine sulcus, in which the V1 boundary runs along a gyral ridge in the average midthickness surface. To enable direct comparison with a previous surface-based analyses of cytoarchitectonically defined V1/area 17, Panel G shows our V1 border overlaid on probabilistic architectonic maps of area 17 generated from 10 postmortem subjects (Amunts et al., 2000). The cytoarchitectonic definitions were mapped onto individual subject surfaces, registered to the fsaverage surface (Fischl et al., 2008), and then to the fs_LR atlas (Van Essen et al., 2012b), which has vertex correspondence with our HCP average surface. In general there is good agreement between the two studies, insofar as the (Fischl et al., 2008) 50% probability level (green) runs close to our V1 group average boundary, especially along the superior and inferior margins of the calcarine sulcus. There are modest discrepancies in foveal V1, where our border is modestly lateral to that of (Fischl et al., 2008), especially in the left hemisphere. In the far peripheral representation in the anterior calcarine sulcus, our V1 extends slightly farther anterior. These differences may be attributable in part to biases that arise in registering the (Fischl et al., 2008) dataset without the opportunity to incorporate the de-drifting process (see Supplementary Methods #2.5) because the individual postmortem surface reconstructions from that study were not available to us. Another technical consideration that might selectively impact analyses of foveal cortex is that the spacing of standard-mesh surface vertices near the occipital pole is larger than for most other regions, owing to how the elongated hemisphere is mapped to the sphere used for registration and resampling. This reduces the spatial resolution and sensitivity in a region that also contains early visual cortical areas that are notably narrow strips in this region.

2. Early Visual Cortex

Human area V1 is surrounded mainly by areas V2 and V3. Though they are concentrically arranged, V2 and V3 do not encircle V1 completely, as the far anterior extent of V1 is adjoined by an architectonically distinct prostriate area in humans (Sanides, 1970; Sanides and Vitzthum, 1965), similar to that found in the macaque (Morecraft et al., 2000; Van Essen et al., 1982). Many studies have mapped much of V2 and V3 using retinotopic fMRI (Abdollahi et al., 2014; Schira et al., 2009; Wandell and Winawer, 2011; Wang et al., 2015); however, this approach fails to capture the representation of the far periphery because it is difficult to stimulate the peripheral retina within the confines of an MRI scanner. Cytoarchitecture has also been used to map extrastriate occipital cortex, including

area 18 (Amunts et al., 2000), and subdivisions of classical area 19, or area OC, including hOC3v, hOC4v (Rottschy et al., 2007), hOC3d, hOC4d (Kujovic et al., 2013), hOC4lp, hOC4la (Malikovic et al., 2015), hOC5d, and hOC5v (Malikovic et al., 2007). Using functional connectivity to map the borders of early visual areas has proven challenging in previous studies, mainly because the central and peripheral parts of the visual field have very distinct patterns of functional connectivity, (Power et al., 2011; Van Essen et al., 2014; Yeo et al., 2011) and topographically corresponding regions of neighboring visual areas are highly functionally correlated (Heinzle et al., 2011). Here, we used a novel approach to delineate the full extent of areas V2, V3, and V4, based on topographically organized resting state functional connectivity with V1 (see Supplementary Methods #4.4). Figure 3 Panel A shows the arrangement of these areas overlaid on the group-average cortical folding map, along with the approximate locations of their 15 neighboring areas: V3A, V6, the Dorsal Visual Transitional area (DVT), the prostriate area (ProS), the presubiculum (PreS), parahippocampal area 1 (PHA1), the ventromedial visual areas (VMV1-3), V8, the PIT complex, LO1, LO2, V3CD, and V3B. We discuss areas V2 and V3 first, followed by area V4, whose analysis is more complex.

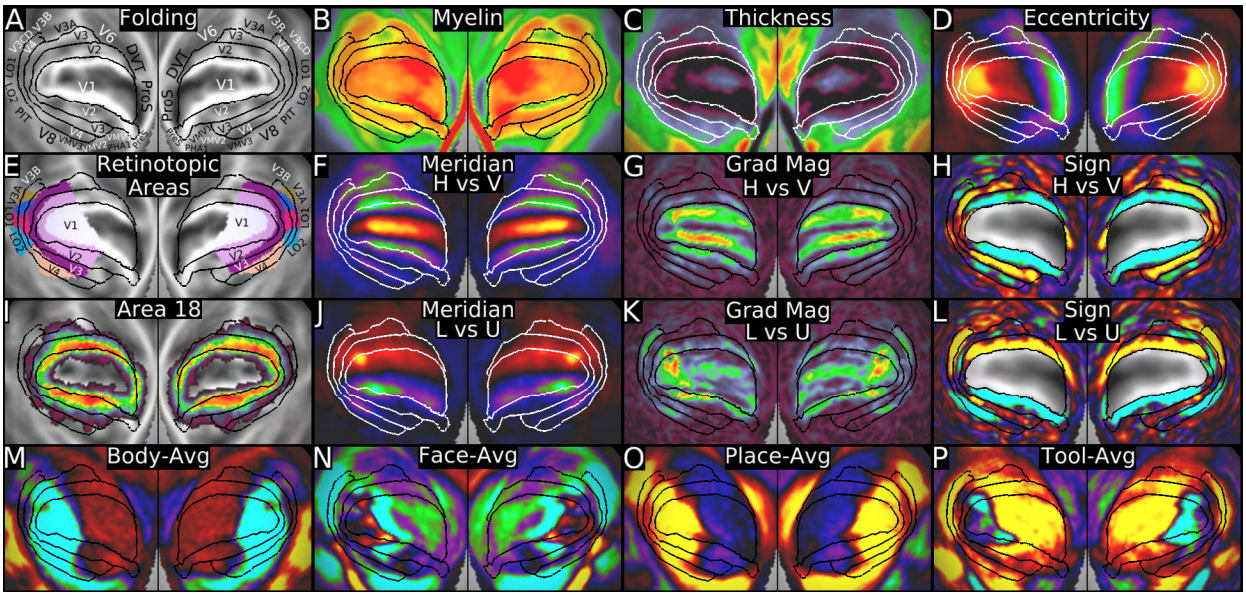

Figure 3 shows the delineation of early visual cortical areas. Panel A shows areas V1, V2, V3, and V4 overlaid on a folding map. Panels B and C show myelin and cortical thickness maps. Panel D shows the foveal vs peripheral eccentricity contrast. Panel E shows retinotopic parcels from (Abdollahi et al., 2014). There is notable agreement between these definitions in mid-eccentricity regions, but better coverage of peripheral regions in the present study and there are some differences in foveal regions and V4. Panels F, G, and H show the horizontal vs vertical meridian contrast, the gradient magnitude of the contrast, and the visuotopic sign produced by taking the dot product of the gradient vector with a vector that points towards V1 (see Supplementary Methods #4.4). Panel I shows area 18 (V2) from post-mortem cytoarchitecture registered across subjects on the surface (Fischl et al., 2008). Panels J, K, and L show the visuotopic maps for the lower vs upper vertical meridian contrast. Note that unlike the horizontal vs vertical meridian contrast, in the lower vs upper field contrast, the visuotopic signs are opposite for superior and inferior portions of each area. Panels M, N, O, and P show the working memory BODY-AVG, FACE-AVG, PLACE-AVG, and TOOL-AVG contrasts. Data at http://balsa.wustl.edu/WM22.

V2 was distinguished from V1 using mainly myelin (Panel B) and LGN connectivity (see section #1 V1 Results and Figure 2). To define the borders between V2 and V3 and between V3 and V4, we used visuotopic connectivity information. As described in the Supplementary Methods (#4.4; see Figure 8), spatial contrasts of horizontal vs vertical meridians and of lower vs upper vertical meridians (both restricted to V1) were used in a multiple regression to derive whole brain maps of the associated resting state functional connectivity, as in Panel F for horizontal meridian (more positive) vs vertical meridian (more negative). Spatial gradients of these maps were used to identify reversals in polar angle, which occur at local *minima* of the gradient magnitude (Panel G). In addition, Panel H shows a map of the dot product between the gradient vector and a reference vector that always points towards V1 (along the cortical surface). This serves as a 'visuotopic sign' that is analogous to the field sign maps developed by (Sereno et al., 1995; Sereno et al., 1994). Panels J, K, and L show analogous maps for the lower field (yellow, red) vs upper field (green, blue, indigo) contrast. Panel D shows the foveal (yellow, red) vs peripheral (green, blue, indigo) eccentricity contrast. The borders between V2 and V3 and between V3 and V4 are represented by both gradient magnitude minima (Panel G) and a horizontal vs vertical meridian visuotopic sign change from negative (V2, cyan/indigo) to positive (V3, yellow-red), and back to negative (V4) (Panel H).

In this parcellation, the inferior half of **V2** adjoins the entire inferior border of V1, extending to the anterior tip of the calcarine sulcus, where the lightly myelinated prostriate area ProS (Panel B) adjoins it as well as V1. **V2** also does not share V1's visuotopic pattern (Panel H). Relative to VMV1 inferiorly, inferior **V2** is substantially thinner (Panel C), has more myelin (Panel B), and has a clear visutopic pattern that VMV1 does not share (Panels H and L). Relative to area PHA1 inferiorly, **V2** has more myelin (Panel B) and is thinner (Panel C). Superior **V2**, in contrast, extends only to the fundus of the parieto-occipital sulcus (POS), where it adjoins a more lightly myelinated dorsal visual transitional area (DVT) (Panel B). Relative to DVT, superior **V2** also has a different task activity profile, being activated vs deactivated in the BODY-AVG (Panel M) and TOOL-AVG (Panel P) contrasts and deactivated vs activated in the PLACE-AVG (Panel O) and TOM-RANDOM contrasts. The large difference in myelin between heavily myelinated **V2** and lightly myelinated DVT was primarily used to define the boundary (Panel B). Superior **V2** also borders V6, where there is a visuotopic sign change in the horizontal vs vertical meridian contrast (Panel H) from negative in **V2** to positive in the inferior portion of V6.

Area **V3** surrounds most of V2, except in the far peripheral representation. Inferiorly, **V3** is bordered by areas VMV1 and VMV2, which do not share its visuotopic map (Panel H, weaker visuotopic signs) and have less myelin (Panel B, VMV2) or are thicker (Panel C, VMV1). The border between superior **V3** and V3A is primarily demarcated by a visuotopic sign change in both the horizontal vs vertical and the lower vs upper vertical meridian contrasts (Panels H and L). Also **V3** locally has less myelin than V3A and V6 (Panel B), and it has a different pattern of functional connectivity with higher visual areas in the MT+ complex.

In our parcellation, area V4 surrounds most of V3 and contains a full hemifield representation, with the upper quadrant represented inferiorly and the lower quadrant superiorly. This is similar to the arrangement reported in the macaque (Felleman and Van Essen, 1991) and to a previous parcellation of human V4 (Hansen et al., 2007) but contrary to several other human retinotopic parcellations (e.g., (Abdollahi et al., 2014; Goddard et

al., 2011; Wade et al., 2002; Winawer et al., 2010). Two lines of evidence suggest that this parcellation is the best fit for our data (though we acknowledge we do not definitively resolve the above controversy): 1) Visuotopic organization is evident in both superior and inferior portions of V4 in both the horizontal vs vertical and lower vs upper vertical meridian contrasts without strong evidence for finer-grained subdivisions (areas) of either region (Panels H and L). 2) In our parcellation the anterior border of V4 coincides with a decrease in myelin content (Panel B, superior V4) and an increase in cortical thickness (Panel C, inferior V4). In contrast, alternative published parcellations that involve multiple areas adjacent to V3 include not only the thin, heavily myelinated portion (part of our superior V4) but also the more lightly myelinated, thicker cortex outside of this area (e.g. areas LO1, LO2, V3A, and V3B (Abdollahi et al., 2014) (Panel E).

The superior boundaries of **V4** with V3B, V3CD, and LO1 were defined using visuotopic sign changes (reduced magnitude and/or sign reversal outside **V4**) in the horizontal vs vertical and lower vs upper vertical meridian contrasts (Panels H and L), decreases in myelin content (higher in **V4**, Panel B), and increases in cortical thickness (thinner in **V4**, Panel C). The boundary of **V4** with LO2 was defined by changes in myelin content (higher in **V4**, Panel B), cortical thickness (thinner in **V4**, Panel C), and activation vs deactivation in the PLACE-AVG task fMRI contrast (Panel O). Relative to the neighboring PIT complex, **V4** has more myelin (Panel B), is thinner (Panel C), is deactivated vs activated in the FACE-AVG task fMRI contrast (Panel N), and activated vs deactivated the PLACE-AVG contrast (Panel O). The boundary of **V4** with both V8 and VMV3 was defined primarily using visuotopic sign changes in the horizontal vs vertical meridian contrast (negative to positive in Panel H), but also **V4** is thinner (Panel C), and in the FACES-SHAPES contrast **V4** was less deactivated/activated vs more deactivated in VMV3. Relative to area VMV2, inferior **V4** has a greater magnitude of the visuotopic sign in the horizontal vs vertical meridian contrast (Panel H), more myelin (Panel B), and is deactivated vs activated in the TOM-RANDOM contrast.

Our maps of areas V1, V2, and V3 overlap extensively with the population-average retinotopic maps reported by (Abdollahi et al., 2014) (Panel E) and with the probabilistic architectonic map of area 18 (Fischl et al., 2008) (Panel I). There is agreement that V2 and V3 are narrower in the foveal region but continuous between superior and inferior portions, an interpretation supported by high-resolution retinotopic mapping of the foveal confluence (Schira et al., 2009). The discrepancies near the center of the foveal representation may reflect methodological limitations in one or both studies, as it is difficult to accurately map very low eccentricities in retinotopic studies (e.g., (Abdollahi et al., 2014)), and there are spatial sampling limitations near the occipital pole in our own analyses (see preceding Section #1 Primary Visual Cortex (V1)). In the visual periphery, retinotopic studies are limited by the range of eccentricities explored (maximum 7.75 degrees (Abdollahi et al., 2014)). Also the architectonic maps of area 18 (Amunts et al., 2000; Fischl et al., 2008) report complete encircling of area V1 (Panel I) despite published evidence for at least one architectonically distinct region (prostriate area ProS) adjoining V1 in anterior calcarine cortex (see above and also Section #1 Primary Visual Cortex (V1)). The inferior portion of our V4 overlaps extensively with that in (Abdollahi et al., 2014), but as noted above the superior portion overlaps with their V3A, V3B, LO1, and LO2 (Panel E). Published surface renderings of volume-based maximum probability postmortem cytoarchitectonic maps suggest that our V3 corresponds to hOC3d (Kujovic et al., 2013)

plus hOC3v (Rottschy et al., 2007). Our inferior V4 may correspond to hOC4v (Rottschy et al., 2007) and superior V4 may correspond to some or all of hOC4lp (Malikovic et al., 2015). More accurate comparisons would be made possible by reconstructing the postmortem individual subject surfaces and registering them to a surface template so that the cytoarchitectonic definitions could be compared directly with our HCP surface data as areas 17 and 18 were above.

3. Dorsal Stream Visual Cortex

The dorsal visual stream includes higher visual areas generally implicated in perceiving where visual stimuli are located and in planning visually guided actions (Goodale and Milner, 1992; Mishkin and Ungerleider, 1982) rather than object identification ('what it is'). In this section we discuss six dorsal stream areas (areas V3A, V3B, V6, V6A, V7, and IPS1) that are well visualized in Figure 4, as shown by the border outlines and labels in Panel A, overlaid on a map of the group-average folding pattern. These areas are bordered by three areas already discussed (V2, V3, V4) plus areas V3CD, IP0, MIP, and DVT. We start with area V3A, the largest area within this region, followed by V3B and V7, V6 and V6A, and IPS1. Figure 4 shows architectural, functional, connectivity, and topographic differences between these areas.

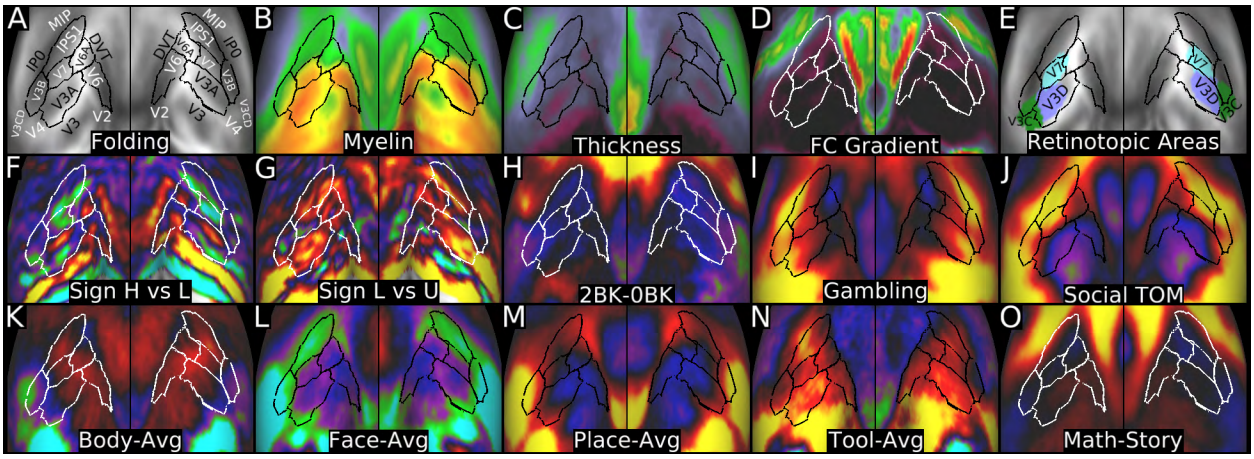

Figure 4 shows some of the architectonic, functional, connectivity, and topographic information that enabled delineation of areas V3A, V3B, V7, V6, V6A, and IPS1 in the dorsal visual stream. Panel A shows the folding pattern together with the areas discussed in this section. Panel B shows the areas together with the myelin map. Panel C shows the areas with the cortical thickness map. Panel D shows the functional connectivity gradient (note how there is a gradient above IPS1). Panel E shows some retinotopic areas (Abdollahi et al., 2014) that correspond to our areas. Panel F shows the horizontal vs vertical meridians' visuotopic sign and Panel G shows the lower vs upper vertical meridians' visuotopic sign. Panels H, I, and J show the working memory 2BK-0BK contrast, a GAMBLING primary contrast, and the SOCIAL TOM contrast. Panels K, L, M, and N show the BODY-AVG, FACE-AVG, PLACE-AVG, and TOOL-AVG category task fMRI contrasts. Panel O shows the MATH-STORY contrast. Data at http://balsa.wustl.edu/RB2m.

The border of **V3A** with V3 is based on a change in the visuotopic sign of the vertical vs horizontal meridian contrast (Panel F) and the lower vs upper vertical meridian contrast (Panel G), as discussed in Section #2 Early Visual Cortex. Unlike earlier visual areas, area **V3A** contains upper fields (red/yellow, superiorly) and lower fields (cyan, inferiorly)

(Larsson and Heeger, 2006; Swisher et al., 2007; Tootell et al., 1997), and thus contains both positive and negative visuotopic signs in the horizontal vs vertical meridian contrast (Panel F). In contrast, the visuotopic sign in the lower vs upper vertical meridian contrast is all positive (yellow/red) in **V3A**, reflecting a continuous gradient from lower to upper visual field from **V3A's** border with V3 to **V3A's** border with V7 (Panel G). **V3A** also has more myelin than many of its neighbors (Panel B, V3B, V6A, and locally more so than V4, V7, and V3). The border of **V3A** with V7 (adjoining antero-superiorly) is based primarily on visuotopic sign changes in the vertical vs horizontal meridian and in the lower vs upper vertical meridian contrasts (Panels F and G). **V3A** also has substantially lower functional connectivity with IPS1 than does V7. Relative to its medial neighbor V6, area **V3A** has a different visuotopic sign pattern (stronger +/- pair) in the horizontal vs vertical meridian contrast (Panel F), a stronger visuotopic sign in the lower vs upper vertical meridian contrast (Panel G), locally less myelin (Panel B), and is more activated in the GAMBLING (Panel I) and EMOTION primary contrasts. Relative to its antero-medial neighbor V6A, area **V3A** has more myelin (Panel B), is activated vs deactivated in the GAMBLING primary contrasts (e.g., Panel I), and is deactivated vs activated in the SOCIAL primary contrasts (e.g., Panel J). Relative to its latero-inferior neighbor V4, area **V3A** differs in having an upper-plus lower-field representation instead of lower-field only (Panel F), and is deactivated vs activated in the working memory and SOCIAL primary contrasts (e.g. panel J). Relative to its lateral neighbor V3B, area **V3A** has more myelin (Panel B), is thinner (Panel C), is more activated in the TOOL-AVG (Panel N) and RANDOM-TOM contrasts, and has stronger visuotopic sign changes in the horizontal vs vertical meridian and the lower vs upper vertical meridian contrasts (Panels F and G). Our V3A overlaps extensively with area V3D of (Abdollahi et al., 2014), but extends further medially, presumably because our multimodal map includes the peripheral representation, whereas their retinotopic map did not. It also likely corresponds to architectonic area hOC4d (Kujovic et al., 2013). We use the more common name of V3A (Larsson and Heeger, 2006; Swisher et al., 2007; Tootell et al., 1997; Wandell and Winawer, 2011; Wang et al., 2015) for broader consistency with the literature.

Areas **V7** (Tootell et al., 1998) and **V3B** (Smith et al., 1998) lie superior to V3A along the superior margin of heavily myelinated visual cortex. They differ from areas V6A, IPS1, IP0, and V3CD in having more myelin (Panel B). Relative to its antero-superior neighbor IPS1, area **V7** also differs in functional connectivity and is also less activated in the working memory primary contrasts and less deactivated in the FACE-AVG contrast (Panel L). The visuotopic patterns in group average data are not as clear in these areas; however, they both have a negative (or less positive) visuotopic sign throughout much of their extents in the lower vs upper vertical meridian contrast (Panel G). **V7** and also IPS1 differ from V6A in several task vs baseline primary contrasts, especially their stronger activation in the SOCIAL TOM task (Panel J) and also the GAMBLING primary contrasts (e.g. Panel I). **V7** and also V6A differ from IPS1 in being less deactivated in the FACE-AVG category task contrast (Panel L). Relative to its lateral neighbor V3B, area **V7** has more myelin (Panel B), is activated vs deactivated in the BODY-AVG contrast (Panel K), less deactivated in the FACE-AVG contrast (Panel L), and less activated in the MOTOR CUE contrast. Relative to its superior neighbor IP0, area **V3B** has more myelin (Panel B), is thinner (Panel C), is locally less activated in the PLACE-AVG contrast (Panel M), locally activated vs deactivated in the TOOL-AVG contrast (Panel N), and less activated in the TOM-RANDOM contrast. Relative to

its lateral neighbor area V3CD, area **V3B** has more myelin and is less deactivated in the FACE-AVG contrast (Panel L) and less activated in the TOOL-AVG contrast (Panel N). Relative to its superior neighbor IPS1, area **V3B** has more myelin (Panel B), is deactivated vs activated in the BODY-AVG contrast (Panel K), and activated vs deactivated in the FACES-SHAPES contrast. Our V7 corresponds closely to that from (Abdollahi et al., 2014) (Panel E), and our V3B shows a similar topological relationship to V3A and V7 as is reported in other studies (Larsson and Heeger, 2006; Swisher et al., 2007; Wang et al., 2015) and some overlap with area V3C from (Abdollahi et al., 2014).

Areas **V6** and **V6A** lie mainly medial and anterior to areas V2, V3, V3A, and V7 along the posterior bank of the partieto-occipital sulcus and have been studied extensively (Pitzalis et al., 2006; Pitzalis et al., 2013). V6 is heavily myelinated relative to most of its neighbors (particularly V6A and DVT, the dorsal transitional visual area, Panel B). Relative to its superior neighbor V6A, area **V6** is weakly activated vs weakly deactivated in the Working Memory contrast (2BK-0BK, Panel H), and less deactivated in the MOTOR AVG contrast. Areas **V6** and **V6A** have more myelin than DVT, are deactivated vs activated in the PLACE-AVG contrast (Panel M), and are activated vs deactivated in the TOOL-AVG contrast (Panel N). Finally, **V6** and **V6A** differ in functional connectivity compared to DVT, as **V6** and **V6A** are more strongly correlated with earlier visual cortex, whereas DVT is more strongly correlated with higher association areas. Areas V6 and V6A may correspond largely to myeloarchitectonic area 112 from the Vogt school (Nieuwenhuys et al., 2015), and V6 has also been recognized via its myelin content signature (Sereno et al., 2013).

We identified **IPS1** (Hagler et al., 2007; Swisher et al., 2007; Wang et al., 2015) on the basis of its strong functional connectivity with other visual areas, its position superior to area V7, and some visuotopic organization (e.g. all positive visuotopic sign in the lower vs upper vertical meridian contrast, Panel G). Like V6A, area **IPS1** has less myelin than V7 and V3B (Panel B). **IPS1** also has notably lower functional connectivity with more posterior visual areas than do its posterior neighbors (e.g. V7, V3B, V3A) and stronger connectivity with more anterior areas along the border between visual and cognitive regions. That being said, it is much more visually connected than its superior neighbor MIP, with a resting state functional connectivity gradient separating these areas (Panel D). **IPS1** differs strongly from adjoining MIP and IP0 in several task fMRI contrasts, including being much less activated in the LANGUAGE MATH-STORY contrast (Panel O), deactivated vs activated in the Working Memory contrast (Panel H), and less activated in the MOTOR CUE and CUE-AVG contrasts. Additionally **IPS1** is thinner than IP0 (Panel C). **IPS1** has more myelin than DVT (Panel B) and differs from DVT and V6A in multiple task fMRI contrasts, including greater activation in the SOCIAL TOM (Panel J) and RELATIONAL vs baseline task contrasts.

4. Ventral Stream Visual Cortex

This section focuses on seven areas and complexes anterior to the early visual areas lying along the ventral aspect of each hemisphere: V8, the Ventral Visual Complex (VVC), the PIT Complex, the Fusiform Face Complex (FFC), and Ventro-Medial Visual areas 1, 2, and 3. They are surrounded by areas V2, V3, V4, LO2, PH, TE2p, TF, parahippocampal areas PHA1, PHA2, and PHA3, which were discussed already or will be discussed later. The ventral visual areas are intermediate in myelination relative to more heavily myelinated

earlier visual areas (posterior/superior) and neighboring lightly myelinated "cognitive" areas (anterior). Consistent with the areas being part of the ventral stream (Goodale and Milner, 1992), the categories task in the task fMRI battery was particularly useful in distinguishing between many of these areas. Some of these areas are dubbed "complexes" because they are likely to contain multiple subdivisions, based on published data and/or evidence in our data that was too weak or inconsistent in individuals to allow the areal classifier to reliably detect a finer-grained parcellation in individual subjects. Figure 5, shows architectural, connectivity, topographic, and functional information used to define the areal boundaries. Panel A shows the areas on a cortical folding map.

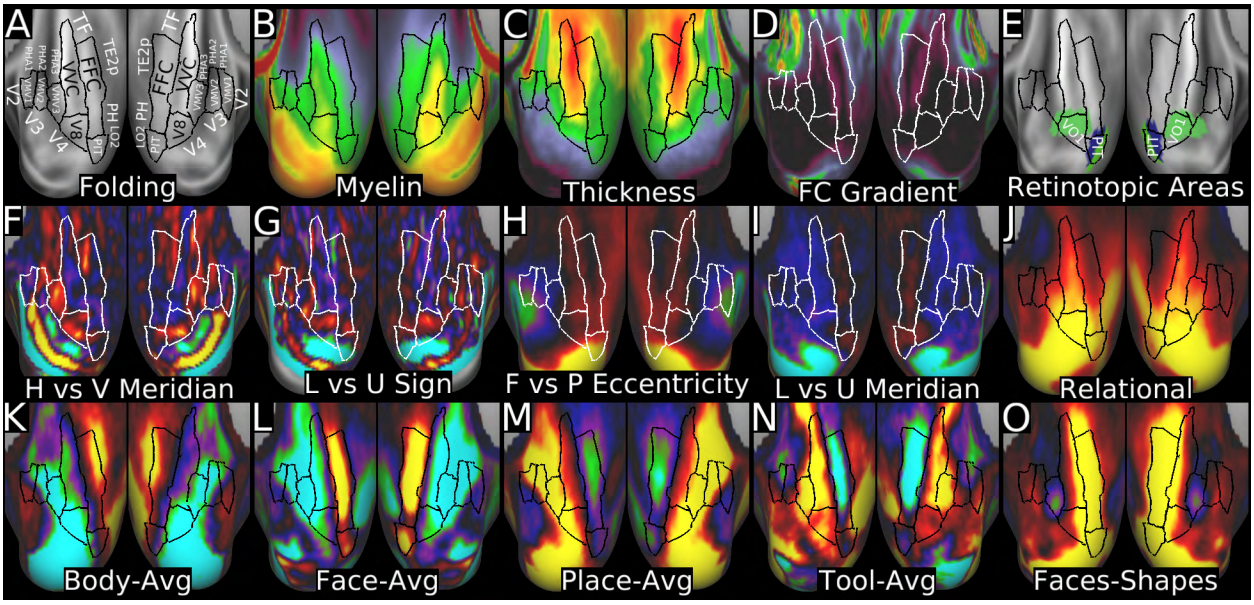

Figure 5 shows architectonic, connectivity, topographic and functional information that was used to parcellate the ventral stream visual cortex. Panel A shows the areas on a cortical folding map. Panels B and C show myelin and cortical thickness maps. Panel D shows the functional connectivity gradients. Panel E shows several retinotopic areas (Abdollahi et al., 2014) (areas PITd and PITv are shown separately but named PIT for space efficiency). Panels F and G show the horizontal vs vertical meridian contrast's visuotopic sign map and the lower vs upper vertical meridian contrast's visutopic sign map. Panels H and I show the foveal vs peripheral and lower vs upper vertical meridian whole brain contrast maps. Panel J shows a RELATIONAL primary contrast. Panels K, L, M, and N show the BODY-AVG, FACE-AVG, PLACE-AVG, and TOOL-AVG contrasts. Panel O shows the FACES-SHAPES contrast. Data at http://balsa.wustl.edu/Jlz0.

V8 and the VVC form a heavily myelinated core of the ventral stream visual region (Panel B). V8 is so named because of multiple similarities with area V8 of (Hadjikhani et al., 1998): It adjoins the horizontal meridian representation of inferior V4 (Panels F and G, the vertical-vs-horizontal and lower-vs-upper field visuotopic sign maps); it includes an upper field representation mainly on the medial side and a lower-field representation mainly on the lateral side (respectively blue and red in Panel I, the whole brain map of lower- vs upper-field contrast); and its eccentricity representation includes central fields mainly anterior and (somewhat) more peripheral fields mainly posterior (respectively red and black/blue in Panel H, the whole brain map of foveal vs peripheral contrast). Its border with the VVC was primarily defined by a transition in visuotopic sign in the lower vs upper vertical meridian contrast (Panel G), but there is also a statistically significant increase in

cortical thickness (Panel C). V8 overlaps substantially with VO1 from (Abdollahi et al., 2014) (Panel E).

Functionally, **V8** and the **VVC** are strongly de-activated in the FACE-AVG contrast (Panel L) and strongly activated in the PLACE-AVG contrast (Panel M, V8 more than VVC) and in the TOOL-AVG contrast (Panel N, VVC more than V8). These contrasts plus the difference in myelin (Panel B) robustly distinguish them from laterally adjoining areas PIT and FFC. Relative to its medial neighbor VMV3, the **VVC** has more myelin (Panel B), is thicker (Panel C), is activated vs deactivated in the FACES-SHAPES task contrast (Panel O), and is less deactivated in the BODY-AVG contrast (Panel K). Thickness and the FACES-SHAPES contrast were primarily used to delineate the border. Relative to its medial neighbor parahippocampal area PHA3, the **VVC** has more myelin (Panel B), is thicker (Panel C), is separated by a resting state functional connectivity gradient (Panel D), and is more activated in primary task contrasts (e.g. Panel J, RELATIONAL). Finally, relative to its anterio-lateral neighbor TF, the **VVC** has more myelin (Panel B), differs in functional connectivity (Panel D), is activated vs deactivated in the TOOLS-AVG contrast (Panel N), and is deactivated vs activated in the FACE-AVG contrast (Panel L). We consider **VVC** an areal complex because other studies (Arcaro et al., 2009; Wandell and Winawer, 2011; Wang et al., 2015) have distinguished multiple visuotopic maps that overlap with this region (VO1, VO2, PHC1, PHC2), and there is weak evidence for multiple visuotopic maps in our data as well.

The Ventro-medial Visual Areas (**VMV1**-**3**) lie medially, between heavily myelinated inferior portions of V2, V3, and V4 and the more lightly myelinated parahippocampal areas PHA1, PHA2, and PHA3 (Panel B). The VMV areas show strong functional connectivity with early visual areas (in contrast to a very different pattern for PHA1-3) but they lack a clear visuotopic organization (Panel F and G). **VMV1** (the most medial) is much thinner and more heavily myelinated that PHA1, which borders it anteriorly (Panels B and C). The pattern is similar for **VMV3** and PHA3, though the thickness differences are not as great (Panels B and C). Relative to their anterior neighbor PHA2, areas **VMV1** and **VMV2** have more myelin (Panel B), differ in functional connectivity, (Panel D), and are locally more deactivated in the BODY-AVG contrast (Panel K). **VMV1** and **VMV3** are thicker than VMV2, and thickness also helps distinguish **VMV1** from areas V2 and V3 (Panel C). Among the three areas, **VMV1** is the most heavily myelinated (Panel B) and **VMV2** is the thinnest (Panel C). Relative to its medial neighbor VMV2, area **VMV3** is more activated in the TOOL-AVG (Panel N), the SOCAL and RELATIONAL primary contrasts (e.g. Panel J), and is more deactivated in the FACES-SHAPES contrast (Panel O). Relative to its anterior neighbor PHA3, area **VMV2** is thinner (Panel C), is locally deactivated vs activated in the TOOL-AVG contrast (Panel N), and is activated vs deactivated in the FACES-SHAPES contrast (Panel O). However, the areal classifier did not perform as well at reliably identifying these areas in individuals compared to other cortical regions (see Main Text Figure 5). Notably, this region has not been previously well parcellated in either the human or the macaque, usually either being left unparcellated or parts of it being included in other areas. In humans, this is partly due to its largely representing high eccentricities that are difficult to map with retinotopic studies. That being said, our VMV3 may overlap partly with area VO2, VMV2 with area PHC1, and VMV1 with area PHC2 (Arcaro et al., 2009; Wandell and Winawer, 2011; Wang et al., 2015).

The **PIT** complex ((Abdollahi et al., 2014; Kolster et al., 2010); see Panel E) and the fusiform face complex (FFC) (Kanwisher and Yovel, 2006; Rajimehr et al., 2009; Tsao et al., 2008) are both strongly activated by the FACE-AVG contrast (Panel L) and the FACE-SHAPES contrast (Panel O). Compared to posterior neighbor V4 and inferior neighbor V8, the **PIT** complex has less myelin (Panel B) and does not have as organized visuotopy (Panels F and G). Relative to area V8, the **PIT** complex is activated vs deactivated in the FACE-AVG contrast (Panel L), deactivated vs activated in the PLACES-AVG contrast (Panel M), and more activated in the FACES-SHAPES contrasts (Panel O). Relative to its supero-lateral neighbor LO2, the **PIT** complex is more activated in the FACE-AVG (Panel L) and FACES-SHAPES contrasts (Panel O) and less activated in the TOOLS-AVG contrast (Panel N). Relative to its antero-superior neighbor PH, the **PIT** complex has more myelin (though the change is gradual, Panel B), is activated vs deactivated in the FACE-AVG (Panel L) and FACES-SHAPES (Panel O) contrasts, is less activated in the TOOL-AVG (Panel N) and TOM-RANDOM contrasts. Relative to anterior neighbor FFC, the **PIT** complex is thinner (Panel C) and there is a local reduction in the strength of the FACE-AVG activation at their boundary (Panel L). Overall the PIT/FFC border is only highly significant for the thickness modality (Panel C), so we relied also on published evidence (e.g., (Abdollahi et al., 2014; Kanwisher and Yovel, 2006; Rajimehr et al., 2009) supporting a boundary between this region and the rest of face selective cortex (Panel L). Our PIT is nearly co-extensive with areas phPITd and phPITv combined (Abdollahi et al., 2014), but we did not find strong evidence for these subdivisions and refer to our area as the PIT complex. It may overlap with the occipital face area (OFA) (Kanwisher and Yovel, 2006; Tsao et al., 2008) and part of hOC4la (Malikovic et al., 2015).

The Fusiform Face Complex (**FFC**) is called a complex because it has substantial intra-areal heterogeneity and thus may contain additional subparcels. Relative to its lateral neighbors PH and TE2p, the **FFC** has more myelin (Panel B), is more activated in the FACE-AVG (Panel L) and FACES-SHAPES contrasts (Panel O), is deactivated vs activated in the TOOL-AVG contrast (Panel N), and differs in resting state functional connectivity (Panel D). Finally, relative to its anterior neighbor TF, the **FFC** has more myelin (Panel B) and is more activated in the FACE-AVG (Panel L) and FACES-SHAPES contrasts (Panel O). There is some uncertainty about the anterior/posterior position of this border because the task activations may also decrease due to susceptibility dropout, and the myelin content changes relatively gradually. Some studies of the fusiform face area (FFA) have reported a patchy organization in individual subjects (e.g., (Kanwisher and Yovel, 2006; Tsao et al., 2008), but our results for the group average are more similar to the strip-like organization reported by (Rajimehr et al., 2009) in some individuals as well as their group average. The VVC and the FFC show substantial overlap with architecturally defined areas FG1 and FG2 (Caspers et al., 2013) including a boundary along the mid-fusiform sulcus (Weiner et al., 2014), which is visible in our group average data despite the use of areal feature-based registration, supporting the suggested areal/folding correlation in this region (Weiner et al., 2014).

5. MT+ Complex and Neighboring Visual Areas

This section covers nine visual areas in lateral occipital and posterior temporal cortex: V3CD, LO1, LO2, LO3, V4t, FST, MT, MST, and PH. These areas are surrounded by early visual cortex (V4) posteriorly, dorsal stream visual cortex (V3B) medially, ventral stream visual cortex (PIT and FFC) inferiorly, inferior parietal cortex (PGp, IP0) superiorly, and the temporal-parietal-occipital junction (TPOJ2 and TPOJ3) plus lateral temporal cortex (PHT and TE2p) anteriorly. These areas are generally more heavily myelinated than their neighbors in inferior parietal and lateral temporal association cortex, but less heavily myelinated than early visual areas. Exceptions are the very heavily myelinated areas MT and MST of the MT+ complex near the center of this region. Figure 6 shows architectural, functional, connectivity, and topographic information that was used to parcellate the MT+ region and neighboring cortex. Panel A shows the areas on a map of the group average folding pattern.

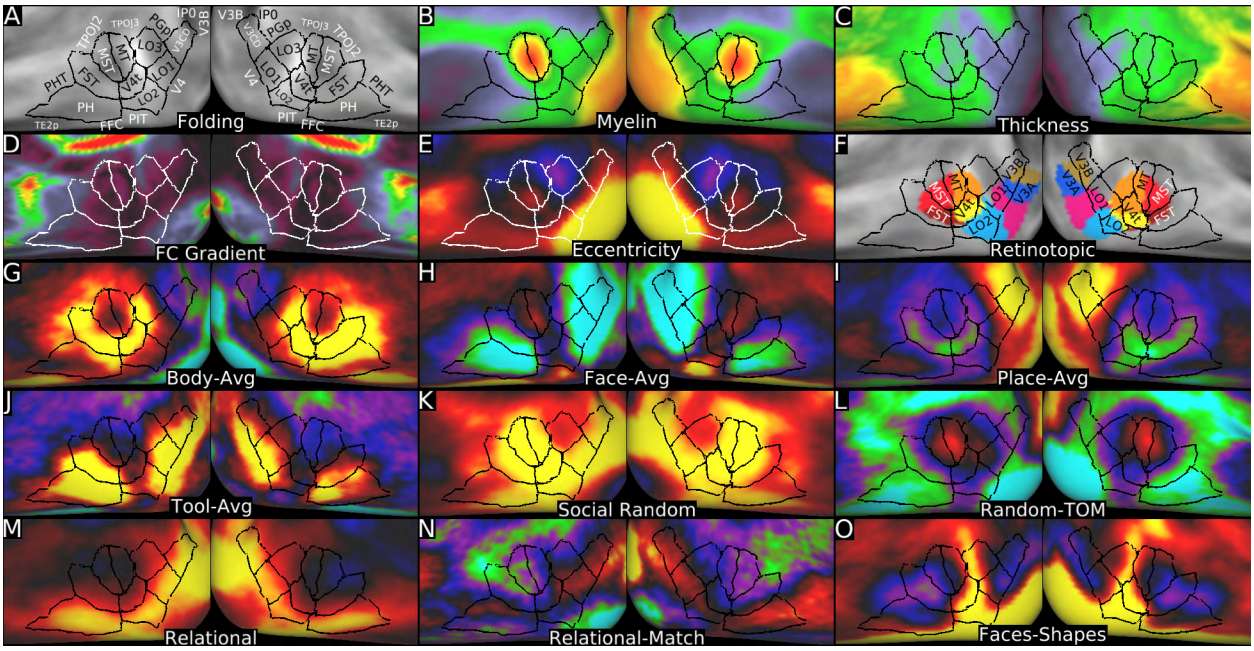

Figure 6 shows multi-modal information used to parcellate the MT+ complex and surrounding cortex. Panel A shows the areas on a group average cortical folding map. Panels B and C show myelin and cortical thickness maps. Panel D shows the resting state functional connectivity gradient. Panel E shows the foveal vs peripheral eccentricity contrast, highlighting the foveal confluence in the center of the MT+ complex. Panel F shows some retinotopic areas (Abdollahi et al., 2014). Panels G, H, I, and J show the BODY-AVG, FACE-AVG, PLACE-AVG, and TOOL-AVG contrasts. Panels K and L show the SOCIAL RANDOM primary contrast and RANDOM-TOM contrasts. Panels M, N and O show a RELATIONAL primary contrast, the RELATIONAL-MATCH contrast, and the FACES-SHAPES contrast. Data at http://balsa.wustl.edu/QqnB.

Areas **V3CD**, **LO1**, **LO2**, and **LO3** are moderately myelinated areas lying between the early visual cortex and the MT+ complex (Panel B). V3CD, LO1, and LO2 differ from adjacent area V4 because of myelin, thickness, and visuotopic transitions (see Panels B and C and Section #2 Early Visual Results). **V3CD's** medial border with V3B was described in Section #3 Dorsal Stream Visual Results. Relative to its supero-medial neighbor IP0, area **V3CD** differs in functional connectivity (Panel D), is activated vs deactivated in the TOOL-

AVG (Panel J) and RELATIONAL-MATCH (Panel N) contrasts, and is deactivated vs activated in the FACES-SHAPES (Panel O) contrast. Relative to its supero-anterior neighbor PGp, area **V3CD** has more myelin (Panel B), is much thinner (Panel C), differs more modestly in functional connectivity (Panel D), and is more activated in the working memory RELATIONAL and EMOTION primary contrasts, the TOOLS-AVG (Panel J), and RELATIONAL-MATCH contrast (Panel N). Relative to its infero-lateral neighbor LO1, area **V3CD** is less activated in the BODY-AVG (Panel G) and more activated in the PLACE-AVG (Panel I) task fMRI contrasts, and it is also slightly thicker (Panel C, more prominent in the right hemisphere). Relative to its superior neighbor LO1, area **LO2** is thicker (Panel C) and is strongly activated vs activated/deactivated in the FACES-SHAPES task contrast (Panel O). LO2's border with PIT was covered previously in Section #4 Ventral Visual Stream Results. Relative to its anterior neighbor V4t, area **LO2** is much less activated in the BODY-AVG contrast (Panel G), much more activated in the relational primary contrasts (e.g. Panel M), and differs modestly in functional connectivity (Panel D). Relative to its posterior neighbor LO1, area **LO3** is less activated in the TOOL-AVG contrast (Panel J) and in several primary task fMRI contrasts (e.g. Panels K and M) and is deactivated vs activated in the RELATIONAL-MATCH contrast (Panel N). On the other hand, LO1 and LO3 have similar architecture, and LO1 represents central visual fields whereas LO3 represents more peripheral visual fields (Panel E). A reasonable alternative would be to consider these areas to be a single area having significant internal heterogeneity. Relative to its superior neighbor PGp, area **LO3** has more myelin (Panel B), is strikingly thinner (Panel C), differs modestly in functional connectivity (Panel D), and is deactivated vs activated in the PLACE-AVG task contrast (Panel I). Relative to its inferior neighbor V4t, area **LO3** is thinner (Panel C), differs in functional connectivity (Panel D), is more deactivated in the FACE-AVG contrast (Panel H), and is less activated in the SOCIAL RANDOM primary contrast (Panel K). Relative to its anterior neighbor MT, area **LO3** has less myelin (Panel B), differs in functional connectivity (Panel D), and is less activated in the SOCIAL RANDOM task contrast (Panel K). Relative to its antero-superior neighbor TPOJ3, area **LO3** differs in functional connectivity (Panel D), is deactivated vs activated in the working memory 2BK-0BK contrast, and is less deactivated in the RELATIONAL-MATCH contrast (Panel N). Our LO1 and LO2 each overlap with anterior portions of published LO1 and LO2 maps (Panel F) (Abdollahi et al., 2014; Kolster et al., 2010), and for this reason we kept these names. Because we found that the Hansen et al parcellation of V4 best fit our data (Hansen et al., 2007), the posterior portion of LO1 and LO2 (Abdollahi et al., 2014) are a part of our area V4 and similarly our LO1 and LO2 areas do not match those of Larsson and Heeger (Larsson and Heeger, 2006) and their followers (their LO1 is part of our dorsal V4, and their LO1+LO2 have been subdivided into V4t, LO1, and LO2). Our area V3CD overlaps extensively with V3A and V3B (Abdollahi et al., 2014), but again parts of their areas overlap with our dorsal V4 (we reverse their V3A/V3B/V3C/V3D nomenclature to better match other studies, as noted above). Areas V3CD, LO1, LO2, and LO3 likely overlap with cytoarchitectonic hOC4la and perhaps parts of hOC4lp (Malikovic et al., 2015).

The MT+ complex contains four areas encircling a central foveal confluence (Panel E). The arrangement is similar to that reported for the motion-sensitive cluster mapped previously (Abdollahi et al., 2014; Kolster et al., 2010), so we use their terminology (Panel F). Areas **MT** and **MST** are both heavily myelinated, **V4t** is moderately myelinated, and **FST** is more lightly myelinated (Panel B). Relative to its anterior neighbor MST, area **MT** is

more activated in the RANDOM-TOM task contrast (Panel L; these task conditions differ in the pattern of moving objects); **MT** and MST also differ modestly in functional connectivity (Panel D). The MT/MST boundary is not as robust as most others reported here and additionally draws on visuotopic evidence (not shown) that MT and MST share an upper field representation as reported by others (Abdollahi et al., 2014; Kolster et al., 2010). **MT** and **MST** both differ from areas FST, V4t, and LO3 in being much less activated in the BODY-AVG task fMRI contrast (Panel G). Relative to its superior neighbor MT and anterior neighbor FST, area **V4t** is much more activated in the FACES-SHAPES contrast (Panel O). Relative to its inferior neighbor FST, area **MST** is activated vs deactivated in the FACE-AVG contrast (Panel H) and less activated in the TOOL-AVG contrast (Panel J). Relative to its posterior neighbor V4t, area **FST** is more activated in the TOOL-AVG contrast (Panel J) and is deactivated vs activated in the FACES-SHAPES task contrast (Panel O). Relative to their anterior neighbor TPOJ2 and superior neighbor TPOJ3, areas **MT** and **MST** have more myelin (Panel B), differ in functional connectivity (Panel D), and are less activated in the MOTOR CUE-AVG task contrast. Relative to its superior neighbor TPOJ2, area **FST** has less myelin (Panel B) and is more activated in the BODY-AVG contrast (Panel G), deactivated vs activated in the FACE-AVG contrast (Panel H), and activated vs deactivated in the TOOL-AVG contrast (Panel J). Relative to its inferior neighbor PH, area **FST** is thinner (Panel C) and is more deactivated in the PLACE-AVG contrast (Panel I) and less activated in the RELATIONAL primary contrast (Panel M). Relative to its anterior neighbor PHT, area **FST** is thinner (Panel C), differs in functional connectivity (Panel D), is more activated in the BODY-AVG contrast (Panel G), and more deactivated in the PLACES-AVG contrast (Panel I). Cytoarchitectonic areas hOC5v and hOC5d (Malikovic et al., 2007) likely correspond to areas MT and MST in our study, and our V4t may overlap with part of hOC4la (Malikovic et al., 2015).

Area **PH** lies between the MT+ complex and the ventral stream FFC. It has strong functional connectivity with other higher visual areas such as IPS1, V3CD, and the VVC, but has less myelin (Panel B) and is thicker (Panel C) than most other visual areas. The functional connectivity of **PH** differs from FFC and its anterior neighbors TE2p and PHT, (Panel D). Relative to its antero-superior neighbor PHT and supero-anterior neighbor TE2p, area **PH** has more myelin (Panel B) and is thinner (Panel C). Relative to PHT, area **PH** also is much more activated in the TOOL-AVG contrast (Panel J), much more deactivated in the FACE-AVG contrast (Panel H), and more activated in the RELATIONAL primary contrast (Panel M). PH in our parcellation corresponds to the superior part of PH in the Von Economo and Koskinas parcellation (Triarhou, 2007a, b; von Economo and Koskinas, 1925).

6. Somatosensory and Motor Cortex

The next four sections cover early and intermediate somatosensory and motor cortex, beginning with the core areas 4, 3a, 3b, 1, and 2. We previously (Glasser and Van Essen, 2011) used myelin mapping to identify boundaries between these areas and compared them to probabilistic surface-based cytoarchitectonic maps (Fischl et al., 2008), thereby providing a neuroanatomical validation of the T1w/T2w myelin mapping technique. Here we delineate these areas using multi-modal information that distinguishes them from surrounding areas (24dd, 6mp, 6d, FEF, 55b, 6v, 43, OP4, PFop, PFt, AIP, 7PC,

7AL, 5L, and 5m). We also present evidence for five somatotopic subregions within these early somatosensory and motor areas. Each subregion spans portions of multiple areas and the areas and subregions can be combined to be further subdivide this region of cortex into distinct subareas that represent topographic subdivisions of a single architectonic area. Figure 7 shows the multi-modal information used to define these areas (displayed on cortical flat maps because the entirety of the somatomotor strip cannot be seen from one perspective on inflated surfaces). The locations of the early sensory and motor areas are tightly correlated with cortical folding patterns, resulting in a sharp delineation of the fundus of the central sulcus and the crowns of the pre- and post-central gyri in the group average mean curvature map after MSMAll areal-feature-based registration (Panel A).

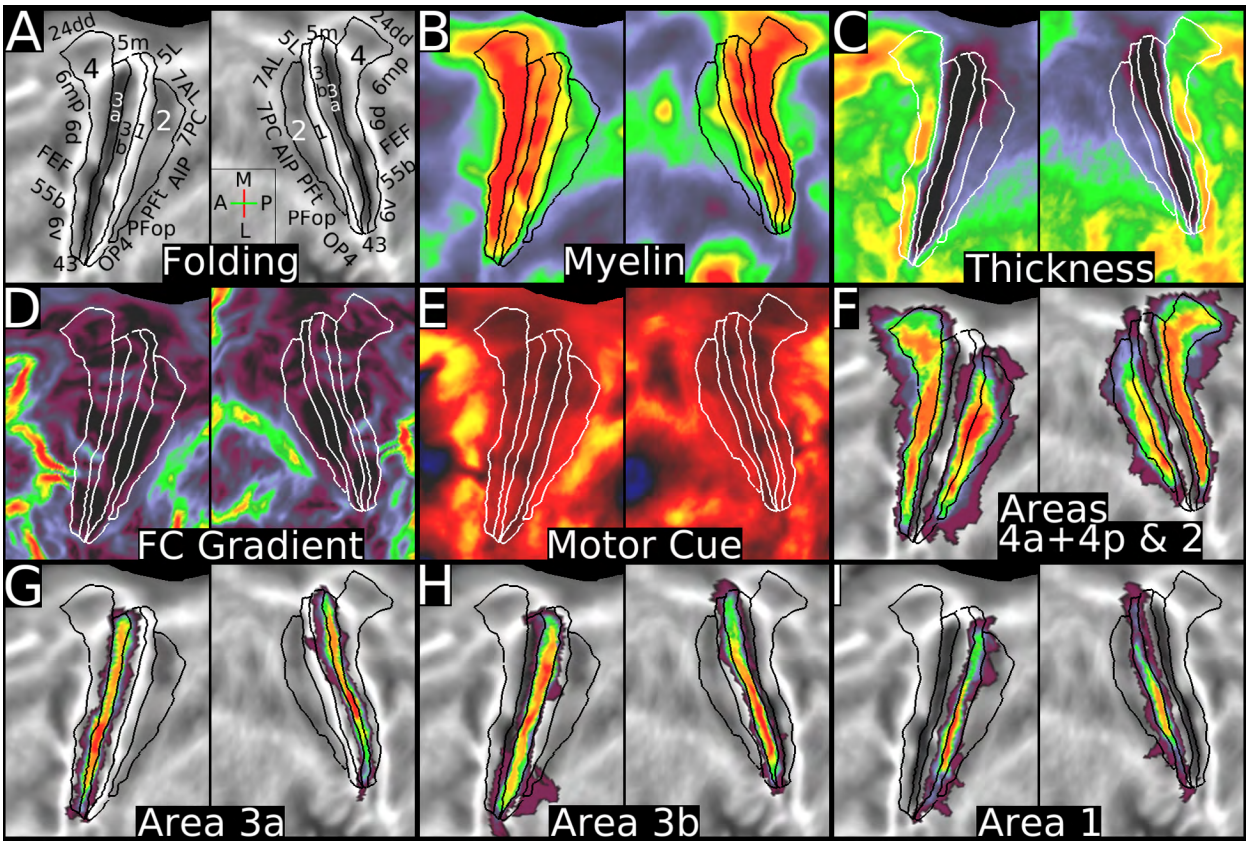

Figure 7 shows multi-modal information used to define early sensory and motor areas and surface-based probabilistic maps of these areas defined using post-mortem cytoarchitecture and the registered on the surface with FreeSurfer registration. The direction icon in Panel A shows Anterior (A), Posterior (P), Medial (M), and Lateral (L) directions (approximate orientation in 3D space) for the left surface (the A/P axis is reversed for the right surface). Panel A shows the areas on a mean curvature map, displayed on cortical flatmaps. Panels B and C show myelin and thickness maps. Panels D and E show the resting state functional connectivity gradient and the task fMRI MOTOR CUE contrast. Panels F, G, H, and I show probabilistic cytoarchitectonic areas. Panel F shows the sum of the probabilities of areas 4a and 4p and area 2. Panels G, H, and I show areas 3a, 3b and 1. Data at http://balsa.wustl.edu/Jjv2.

Area **4** (M1, or primary motor cortex) on the anterior bank of the central sulcus is perhaps the most architecturally distinct area in current non-invasive neuroimaging, as it is much more heavily myelinated than its anterior neighbors 6mp, 6d, FEF, 55b, and 6v (Panel B), and much thicker than its posterior neighbors 3a and 5m (Panel C). Additionally,

the body part task fMRI contrasts (T-AVG, ?H-AVG [? is a shorthand used here and below to mean both L and R for left and right hemispheres], ?F-AVG) each decrease in strength anterior to area **4**. Relative to its inferior neighbor 43, area **4** has more myelin (Panel B) and differs in functional connectivity (Panel D). Relative to its posterior neighbors 3a and 5m, area **4** has more myelin (Panel B), is thicker (Panel C), and (for 5m) differs in functional connectivity (Panel D). For the border with area 3a, the semiautomated border optimizer relied most on myelin because there is a narrow sharp gradient in myelin between areas 4 and 3a. Relative to its infero-medial neighbor 24dd (up on the flat map), area **4** has more myelin (Panel B) and differs in functional connectivity (Panel D). Our area 4 agrees well with the combined areas 4p and 4a from post-mortem cytoarchitecture registered on the surface (Fischl et al., 2008; Geyer et al., 1996)(Panel F).

Primary somatosensory cortex (S1) includes areas **3a** (in the fundus of the central sulcus) and **3b** (occupying the entire posterior bank of the sulcus). Relative to its posterior neighbor 3b, area **3a** has less myelin (Panel B) and is thicker (Panel C), and the semiautomated border optimizer relied most on myelin. Relative to its inferior neighbor OP4, area **3a** has more myelin (Panel B), is thinner (Panel C), and differs in functional connectivity (Panel D). Area **5m**, medial to 3a and 3b (up on the flatmap) has less myelin than either 3a or 3b (Panel B), differs modestly from 3a in functional connectivity (Panel D), and is much thicker than 3b (Panel C). Relative to its posterior neighbor area 1, area **3b** is much thinner (Panel C) and has more myelin (Panel B). Our areas 3a and 3b agree well with probabilistic areas 3a and 3b from post-mortem cytoarchitecture registered on the surface (Fischl et al., 2008; Geyer et al., 1999; Geyer et al., 2000) (Panels G and H).

Areas **1** and **2** are also part of the S1 primary somatosensory complex. Relative to its posterior neighbor area 2, area **1** has more myelin (Panel B), is less activated in the motor CUE task (Panel E) and in the LH and RH task fMRI contrasts (specifically in the ipsilateral hemisphere), and is more activated in the EMOTION FACES-SHAPES contrast. Relative to its inferior neighbors OP4 and PFop, area **1** has more myelin, is thinner, differs in functional connectivity (Panel D), and is less activated in the MOTOR CUE contrast (Panel E). Relative to their postero-medial neighbor 5L, both areas **1** and **2** have more myelin (Panel B) and are less activated in the MOTOR CUE task contrast (Panel E). Relative to the four areas (7AL, 7PC, AIP, and PFt) sharing a substantial common boundary along its posterior side, area **2**: (i) has more myelin than area 7AL, differs in functional connectivity, and is less activated in in the MOTOR CUE contrast (Panel E); (ii) has more myelin than area 7PC and is less activated in the MOTOR CUE contrast (Panel E); (iii) is thinner than area AIP, differs in functional connectivity, is less activated in the working memory 2BK-0BK, and more activated in the, FACE-AVG contrast (along with differences in at least four other contrasts); and (iv) has more myelin and is thinner than area PFt, differs in functional connectivity, is less activated in the BODY-AVG contrast and more activated in the ?H-AVG and FACES-SHAPES contrasts. Our areas 1 and 2 generally align well with the corresponding areas mapped using post-mortem cytoarchitecture and registered on the surface (Fischl et al., 2008; Geyer et al., 1999; Geyer et al., 2000; Grefkes et al., 2001), but there are some differences (Panel I, F). Our area 1 (Panel I) tends to be wider than the probabilistic map, especially in the left hemisphere, and area 2 (Panel F) extends more posteriorly in some regions (indeed, the maximum probabilities of areas 3b and 2 almost join in some locations). Also, our area 1 is symmetric in terms of its overall extent along the postcentral gyrus, whereas the probabilistic map is modestly asymmetric. The

differences in area 1 may be related to the strong distortion that occurs on the post-central gyral crown (Robinson et al., 2014) from the FreeSurfer registration used to register the post-mortem cytoarchitectonic maps. Our area 2's medial/superior extent also likely overlaps some with area 5L from Scheperjans, (Scheperjans et al., 2008a; Scheperjans et al., 2008b) though our border is placed at the maximum architectural and functional transition as for other areas.

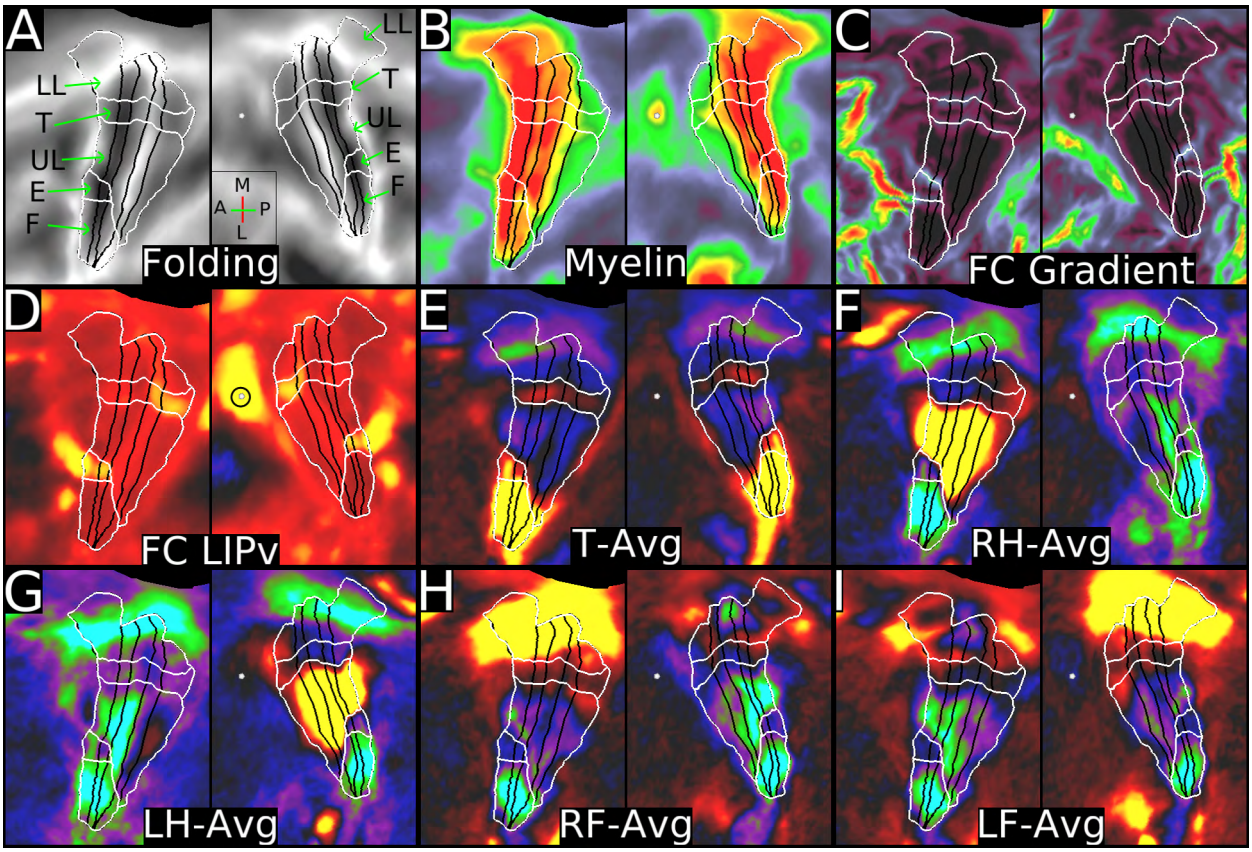

Figure 8 shows subregions and subareas of the sensorimotor strip, displayed on cortical flatmaps. Panel A shows folding maps. The direction icon in Panel A shows Anterior (A), Posterior (P), Medial (M), and Lateral (L) directions (approximate orientation in 3D space) for the left surface (the A/P axis is reversed for the right surface). Panel B shows myelin maps, which interestingly have some correspondence with the subareas (white). Areal boundaries remain black. Panel C shows the resting state functional connectivity gradients that were used to define the subregions using the semiautomated border drawing approach. Panel D shows functional connectivity from the heavily myelinated LIPv seed (black circle, which has functional connectivity with some parts of the sensori-motor strip. Panels E, F, G, H, and I show the task fMRI contrasts T-AVG, ?H-AVG (RH-AVG and LH-AVG), and ?F-AVG (RF-AVG and LF-AVG). Data at http://balsa.wustl.edu/QwnL.

Sensorimotor areas 4, 3a, 3b, 1, and 2 are largely architecturally defined. Previous fMRI studies have revealed highly inhomogeneous functional connectivity within the sensorimotor strip, but the heterogeneity is more related to somatotopic boundaries than areal boundaries, with distinct subregions related to representations of the face vs the rest of the body (Power et al., 2011; Van Essen et al., 2014; Yeo et al., 2011). Here, we provide evidence for a finer-grained somatotopic organization that includes 5 functional and connectional subdivisions within the sensorimotor strip (see Figure 8), based on resting state functional connectivity gradients (Panel C; see also Panel D of Figure 7) and

somatotopic task fMRI contrasts (Panels E, F, G, H, I). Each white-outlined region spans multiple architectonic areas but occupies a restricted portion of the somatotopic map and a small portion of each architectonic area. We label these five somatomotor subregions based on the known or presumed portion of the body involved: the F (face), E (eye), UL (upper limb), T (trunk), and LL (lower limb). The intersection of the somatomotor subregions with the architectonic areas can be used to define distinct 'subareas' (four or five subareas for each of the five architectonic areas), but our analysis here focuses mainly at the level of somatomotor subregions.

The most infero-lateral subregion, F (face) is activated in the T-AVG contrast (Panel E). Subregion E (eye) lies just posterior to the frontal eye fields (FEF, a heavily myelinated hotspot just anterior to area 4) and is clearly evident only in areas 4 and 3a. This approximate region was previously shown to be activated by squeezing (squinting) the muscles around the eyes (Meier et al., 2008). This was not explicitly tested in the HCP motor task fMRI paradigm, but subregion E has strong functional connectivity with the LIP/VIP complex (heavily myelinated hotspot posterior to area 2 marked by small white sphere), similar to that found in areas FEF and PEF (Panel D, hotspots of myelin and functional connectivity anterior to area 4). It is also activated in the T-AVG contrast (Panel E). The middle subregion UL is activated in the ?H-AVG task contrasts (Panels F and G). Interestingly, its proportional representation across the sensorimotor strip changes markedly: subarea 4_UL (upper limb) occupies about one-fourth of area 4, whereas subarea 2_UL occupies more than half of area 2. Subregion T (trunk) was not explicitly tested for in the motor task paradigm but its somatotopic assignment seems highly likely given its position between the upper and lower limb representations (Penfield and Rasmussen, 1950). It is intriguing but puzzling that subareas 1_T and 2_T show strong functional connectivity with the LIP/VIP complex (Panel D; same seed as correlates with subregion E). Subregion LL (lower limb) is strongly activated contralaterally in the ?F-AVG task contrasts but only moderately activated in subarea 2_LL (Panels H and I). In adjoining area 5L, the foot activation is strong, but bilateral – see Section #7 Paracentral Lobular and Mid Cingulate Cortex). Interestingly, some reproducible (see Supplementary Figure 1 in the Supplementary Results and Discussion and Main Text Figure 1) variations in myelin content within area 3b (see Panel B) align with the subareas described above, particularly the trunk subarea (3b_T) and the boundary between subareas 3b_F and 3b_UL. Somatotopic variations in myelin content have previously been reported in area 3b using histological methods, including a similar face/hand boundary myelin content decrease in the macaque (Krubitzer et al., 2004) and marmoset (Krubitzer and Kaas, 1990), and further variations in more superior regions (Krubitzer and Kaas, 1990).

7. Paracentral Lobular and Mid Cingulate Cortex

This section discusses areas in and around the paracentral lobule and mid-cingulate cortex. These are higher sensory and motor regions that include cingulate motor areas (24dd and 24dv), supplementary motor areas (6mp, 6ma, SCEF), and subdivisions of area 5 (5m, 5L and 5mv). They are surrounded by areas 4, 3a, 3b, 1, 2, 7AL, 7Am, PCV, 23c, p24pr, p32pr, 8BM, SFL, s6-8, 6a, and 6d. Figure 9 shows much of the multi-modal information used to parcellate this region, displayed on inflated maps that are viewed from a medio-superior perspective (lateral is up, medio-inferior is down, anterior is towards the center of

the panel, posterior is towards the outside of the panel). Area 4 extends medially, onto the anterior portion of the paracentral lobule (Fischl et al., 2008; Geyer et al., 1996; Rademacher et al., 1993), Panel A), whereas areas 3a, 3b, and 1 do not in our or previous studies (Fischl et al., 2008; Geyer et al., 1999; Geyer et al., 2000; Rademacher et al., 1993), Panel A). We first discuss subdivisions of Brodmann's area 5, then the cingulate motor areas, and finally some supplementary motor areas.

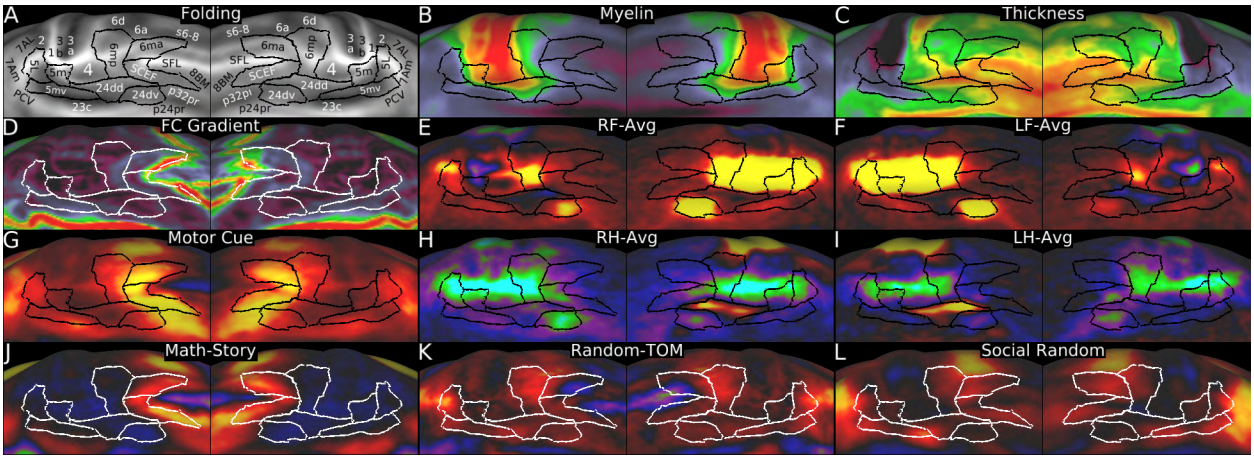

Figure 9 shows some of the multi-modal information used to delineate cortical areas in the paracentral lobular and mid cingulate cortical region. Panel A shows the areas delineated in this section overlaid on a folding map. Panels B and C show myelin and thickness maps. Panel D shows the resting state functional connectivity gradient. Panels E and F show the MOTOR RF-AVG and LF-AVG task fMRI contrasts (referred to as ?F-AVG in the text). Panel G shows the MOTOR CUE task contrast. Panels H and I show the RH-AVG and LH-AVG task contrasts (referred to as ?H-AVG in the text). Panels J, K and L show the MATH-STORY, RANDOM-TOM, and SOCIAL RANDOM task contrasts. Data at http://balsa.wustl.edu/J49j.

We identified 3 subdivisions of area 5. Area **5L** occupies a similar location to that reported previously, though our area 2 may overlap with its most lateral extent (Scheperjans et al., 2008a; Scheperjans et al., 2008b). Area **5m** occupies a similar location to that reported previously on the paracentral lobule (Scheperjans et al., 2008a; Scheperjans et al., 2008b), though the group definition does not extend past the fundus of the posterior cingulate sulcus (some individuals likely do, however). Area **5mv** overlaps with area 5ci reported previously and the most posterior extent of area 5m (Scheperjans et al., 2008a; Scheperjans et al., 2008b). Area 5L is a lightly myelinated area (Panel B) whose borders with areas 1 and 2 were described above in Section #6 Somatosensory and Motor Cortex. Relative to its posterior neighbors 7AL and 7Am, area **5L** differs in functional connectivity (Panel D) and is less activated in the CUE-AVG task contrast. **5L** is also much more strongly activated than 7Am in the ?F-AVG foot motor task contrasts (Panels E and F). Relative to its anterior neighbor 5m, area **5L** has much less myelin (Panel B) and is more activated in the MOTOR CUE task (Panel G), the ipsilateral hemisphere's ?F-AVG foot motor contrast (Panels E and F), and the RANDOM-TOM contrast (Panel K). Area **5L**'s inferior border with **5mv** is marked by a change in functional connectivity (Panel D) and decreased activation in the ?F-AVG foot motor contrasts (Panels E and F) and the MOTOR AVG contrast. Area 5m's borders with areas 3b, 3a, and 4 were covered previously in Section #6 Somatosensory and Motor Cortex. Relative to its anterior neighbor 24dd, area **5m** is thinner (Panel C) and differs in functional connectivity (Panel D). Relative to its inferior

neighbor 5mv, area **5m** has much more myelin (Panel B), differs in functional connectivity (Panel D) and is less activated in the SOCIAL RANDOM-TOM (Panel K) contrast. Relative to its anterior neighbor 24dd, area **5mv** has less myelin (Panel B), is thinner (Panel C), differs in functional connectivity (Panel D), is more strongly activated in the ?F-AVG foot motor contrast (Panels E and F), and is deactivated instead of strongly activated in the ?H-AVG contralateral hand motor contrast (Panels H and I). Relative to its inferior neighbor 23c, area **5mv** is thinner (Panel C), differs in functional connectivity (Panel D), and is more activated in the RANDOM-TOM task contrast (Panel K). Relative to its postero-inferior neighbor PCV, area **5mv** is thinner (Panel C), is deactivated vs activated in the working memory 2BK-0BK contrast, the GAMBLING primary contrasts, and less activated in the SOCIAL primary contrasts in the right hemisphere (Panel L). Relative to its posterior neighbor 7Am, area **5mv** differs in functional connectivity (Panel D) and is less activated in the working memory 2BK-0BK contrast, the MOTOR CUE contrast (Panel G), and the SOCIAL primary contrasts (Panel L).

Areas **24dd** and **24dv** constitute most of the cingulate motor cortex (Palomero-Gallagher et al., 2009; Vogt and Vogt, 2003). The borders of area 24dd with areas 4 and 5mv were already described above and in Section #6 Somatosensory and Motor Cortex. Relative to its inferior neighbor 23c, area **24dd** has more myelin (Panel B) and differs in functional connectivity (Panel D). Relative to its antero-inferior neighbor 24dv, area **24dd** has more myelin, differs in functional connectivity (Panel D), is strongly activated vs deactivated in the contralateral ?H-AVG hand motor contrast (Panels H and I) and is minimally activated vs strongly activated in the ?F-AVG contrast (Panels E and F). Relative to its antero-superior neighbor 6mp, area **24dd** differs in functional connectivity (Panel D), is strongly activated vs deactivated in the contralateral ?H-AVG hand motor contrast (Panels H and I) and less activated in the ?F-AVG foot motor contrasts (Panels E and F). Relative to the anteriorly neighboring supplementary and cingulate eye fields (SCEF), area **24dd** has more myelin (Panel B), differs in functional connectivity (Panel D), is strongly activated vs deactivated in the contralateral ?H-AVG hand motor contrast (Panels H and I), and is less activated in the T-AVG, MOTOR AVG contrast, CUE contrast (Panel G) and other task primary contrasts. Relative to its anterior neighbor p32pr, area **24dv** differs in functional connectivity (Panel D), is less activated in the CUE contrast (Panel G), more activated in the ?F-AVG foot motor contrast (Panels E and F), and deactivated instead of activated in the MATH-STORY contrast (Panel J). Relative to its inferior neighbor p24pr and posterior neighbor 23c, area **24dv** has more myelin (Panel B), differs modestly in functional connectivity (Panel D), and is more activated in the ?F-AVG foot motor contrasts (Panels E and F). The cingulate motor cortex is particularly active in the motor tasks and shows somatotopic organization, with 24dd more related to the upper limb and 24dv more related to the lower limb. It is in the expected location inferior and anterior to motor cortex as reported previously (Vogt et al., 1995; Vogt et al., 2005). Based only on topography, the foot (24dv) and hand (24dd) representations could be considered subareas within a single cingulate motor area (CMA) having a more complete body representation (perhaps even including the face representation in adjoining SCEF). However, the prominent architectural and other differences already noted above argue against combining these regions, as does the precedent set by other studies cited above.

The supplementary motor cortex was divided into three areas, **6mp**, **6ma**, and the supplementary and cingulate eye fields (**SCEF**). Area 6mp overlaps with SMAc of (Vorobiev

et al., 1998) on the medial surface, but extends supero-laterally into a region they did not map. Area 6ma overlaps partially with SMAr of (Vorobiev et al., 1998) but extends farther anteriorly and laterally and not as far inferiorly on the mesial surface. Collectively these areas overlap extensively with the region previously identified as the supplementary motor cortex (Roland and Zilles, 1996). The boundaries of 6mp with areas 4 posteriorly and 24dd inferiorly were already described in Section #6 Somatosensory and Motor Cortex and above. Relative to its anterior neighbor 6ma, area **6mp** has more myelin, differs in functional connectivity (Panel D), is less activated in the MOTOR CUE contrast (Panel G) and more activated in the FOOT-AVG contrast (Panels E and F). Relative to its anterior neighbor SCEF, area **6mp** has more myelin (Panel B), differs in functional connectivity (Panel D), is less activated in the MOTOR AVG and MATH-STORY contrasts (Panel J), and differs in a number of the primary contrasts including the RELATIONAL MATCH contrast. Relative to its lateral neighbor 6d, area **6mp** differs in functional connectivity (Panel D), and is deactivated vs activated in the contralateral ?H-AVG hand motor contrast (Panels H and I). Additionally, **6mp** is more deactivated than 6d in the LANGUAGE MATH, and STORY contrasts and less activated in the RANDOM-TOM contrast. Relative to area 6a anteriorly, **6mp** is slightly thinner (Panel C) and less activated in the working memory 2BK-0BK, MATH-STORY (Panel J), and many primary task contrasts, e.g. the SOCIAL RANDOM (Panel L) contrast. Relative to its latero-inferior neighbor 6a, area **6ma** has less myelin (Panel B), differs in functional connectivity (Panel D), and is less activated in the SOCIAL RANDOM (Panel L) and TOM contrasts. Relative to its anterior neighbor s6-8, area **6ma** differs dramatically in functional connectivity (Panel D), is more activated in the MOTOR CUE contrast and is deactivated vs activated in the RELATIONAL MATCH contrast. Relative to its anterior neighbor SFL, area **6ma** differs dramatically in functional connectivity (Panel D), is more activated in the MOTOR CUE contrast (Panel G), is deactivated vs activated in the LANGUAGE STORY contrast and activated vs deactivated in the MATH-STORY contrast (Panel J). Relative to its medial neighbor SCEF, area **6ma** is thinner (Panel C), has less myelin (Panel B), and is much less activated in the MOTOR AVG contrast. Areas 6ma and 6mp are parts of probabilistic cytoarchitectonic area 6 (Fischl et al., 2008; Geyer, 2004). The supplementary and cingulate eye fields (SCEF) are named because of their functional connectivity with the frontal and premotor eye fields (areas FEF and PEF) together with other visual regions. They also have a their similar location to that described in (Amiez and Petrides, 2009), but they also overlap with SMAr from (Vorobiev et al., 1998). Relative to its superior neighbor SFL, area **SCEF** differs in functional connectivity (Panel D), has more myelin (Panel B), is activated vs deactivated in the LANGUAGE MATH-STORY contrast, is deactivated vs activated in the LANGAUGE STORY contrast, and is activated vs deactivated in the RELATIONAL-MATCH contrast in the left hemisphere only (as will be highlighted in later sections, area SFL is one of several areas with substantial lateralization of functional activation). Relative to its anterior neighbor 8BM, **SCEF** has more myelin (Panel B), is thinner, differs substantially in functional connectivity (Panel D), is locally more activated in the primary gambling contrasts and the MOTOR CUE contrast (Panel G), and less activated in the RELATIONAL-MATCH contrast. Finally, relative to its inferior neighbor p32pr, area **SCEF** is more activated in multiple primary contrasts in the working memory and gambling tasks, the LANGUAGE MATH contrast, the SOCIAL RANDOM contrast (Panel L), RELATIONAL, and EMOTION-SHAPES and MATH-STORY task contrasts (Panel J). Area SCEF is part of probabilistic cytoarchitectonic area 6 (Fischl et al., 2008; Geyer, 2004)

8. Premotor Cortex

This section includes six areas that occupy what is typically called the premotor region anterior to area 4 (Roland and Zilles, 1996). Area 55b lies immediately anterior to area 4, splitting premotor cortex into superior and inferior subdivisions, but it is very different from all other areas within classical architectonic area 6 (Fischl et al., 2008; Geyer, 2004). The superior premotor subdivisions include areas 6d, 6a, and the frontal eye field (FEF), whereas the inferior premotor subdivisions include 6v, 6r, and the premotor eye field (PEF). These areas are surrounded by areas 4, 6mp 6ma, s6-8, i6-8, 8Av, 8C, IFJp, 44, FOP4, FOP1, and 43. Figure 10 shows some of the multi-modal information that we used to parcellate the premotor cortex, with Panel A showing the areas and their neighbors labeled on an inflated surface with an underlay of cortical folding.

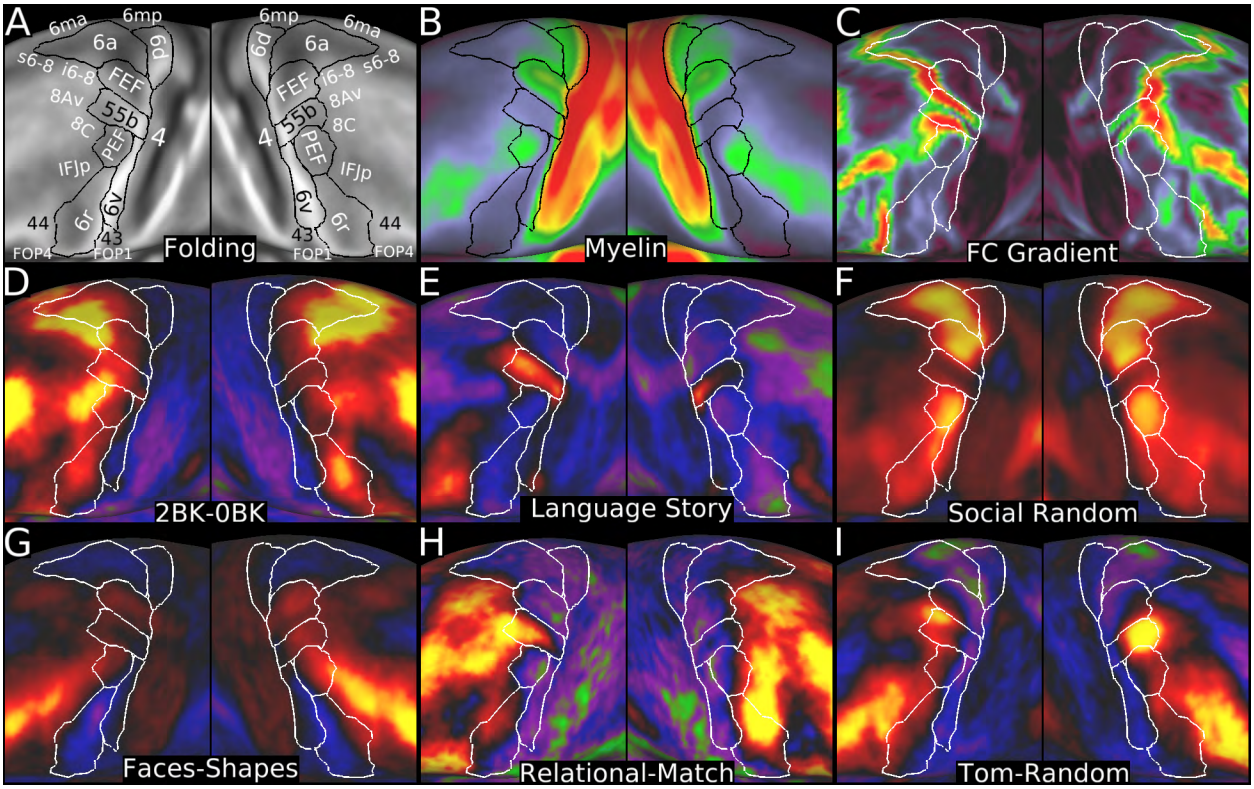

Figure 10 shows multi-modal information used to parcellate the premotor cortex. Panel A shows the 6 premotor areas plus 55b on a folding map. Panel B shows them on the myelin map. Panel C shows the functional connectivity gradient. Panels D, E, and F show the working memory 2BK-0BK contrast, the LANGUAGE STORY contrast, and the SOCIAL RANDOM contrast. Panels G, H, and I show the EMOTION FACES-SHAPES contrast, the RELATIONAL-MATCH contrast, and the SOCIAL TOM-RANDOM contrast. Data at http://balsa.wustl.edu/Qm5v.

The superior borders of **6a** and **6d** and the posterior border of area 6d were covered in the preceding two Sections (#6 Somatosensory and Motor Cortex and #7 Paracentral Lobular and Mid Cingulate Cortex). Relative to its anterior neighbor 6a, area **6d** differs in functional connectivity (Panel C), is less activated in the working memory 2BK-0BK (Panel D), MATH-STORY, and SOCIAL RANDOM (Panel F) contrasts, and is more activated in the ?H-AVG hand motor contrasts. Relative to its inferior neighbor FEF, area

6d has less myelin (Panel B), differs in functional connectivity (Panel C), and is less activated in many of the primary task contrasts, including the GAMBLING, SOCIAL (Panel F), RELATIONAL, and EMOTION contrasts. Relative to its antero-medial neighbor s6-8, area **6a** differs strongly in functional connectivity (Panel C), is more activated in the LANGUAGE MATH, SOCIAL (Panel F), and RELATIONAL primary contrasts, and is less deactivated in the STORY contrast (Panel E). Relative to its anterior neighbor area i6-8, area **6a** differs markedly in functional connectivity (Panel C), is more activated in the SOCIAL primary contrasts (Panel F), and is deactivated vs activated in the FACES-SHAPES (Panel G) and RELATIONAL REL-MATCH contrasts (Panel H). For this border, the semiautomated border optimizer relied most on functional connectivity. Relative to its latero-inferior neighbor FEF, area **6a** has less myelin (Panel B) and differs in several task contrasts including less activation in the GAMBLING and RELATIONAL primary contrasts, and the EMOTION SHAPES primary contrast. These superior subdivisions of area 6 are within the territory of probabilistic surface-registered cytoarchitectonic area 6 (Fischl et al., 2008; Geyer, 2004). The border between 6a and 6d may correspond to the border between 6aβ and 6aα (Geyer et al., 2000).

The premotor cortex contains two moderately myelinated eye fields, the Frontal Eye Field (**FEF**) and the Premotor Eye Field (**PEF**), separated by a lightly myelinated isthmus, area **55b** (Panel B). The eye fields share similar patterns of functional connectivity, which differs markedly from that of area 55b (Panel C). Also, they have similar patterns of task activation (being particularly activated during the primary contrasts of many tasks (e.g. Panel F), as distinct from 55b's lesser activation). The borders of FEF with 6a and 6d superiorly and with area 4 posteriorly were covered above and in Section #6 Somatosensory and Motor Cortex. Relative to its anterior neighbors i6-8, and 8Av, area **FEF** is deactivated vs activated in the RELATIONAL REL-MATCH contrast (Panel H). Relative to 8Av, **FEF** is also more activated in the MATH-STORY contrast and the CUE-AVG contrast. Relative to its inferior neighbor 55b, area **FEF** has more myelin (Panel B), differs markedly in functional connectivity (Panel C), and in primary task contrasts (e.g. Panel F), and is less activated in the STORY contrast (Panel E). Area **55b** (Hopf, 1956) was already covered in the Main Results (see Figure 2), and 55b's border with 8Av and 8C is covered below in Section #22 DorsoLateral Prefrontal Cortex. The Main Text and the Supplementary Results and Discussion sections #1.3-1.4 and Supplementary Figures 7-10 describe the distinct topologies that area 55b and the eye fields have in atypical individuals. Here, we focus on the typical relationships revealed in the group average analyses.

Relative to its superior neighbor 55b, area **PEF** has more myelin (Panel B), differs in functional connectivity (Panel C), is less activated in the LANGUAGE STORY contrast (Panel E), and is more activated in a number of primary task contrasts (e.g. SOCIAL RANDOM in Panel F). Relative to its anterior neighbor 8C, area **PEF** has more myelin (Panel B), differs in functional connectivity (Panel C), and is more activated in primary task contrasts (e.g. SOCIAL RANDOM in Panel F). Relative to its antero-inferior neighbor IFJp, area **PEF** differs in functional connectivity (Panel C), is more activated in the SOCIAL primary contrasts (Panel F), and is deactivated vs activated in the RELATIONAL-MATCH contrast (Panel H). Relative to its inferior neighbor 6r and infero-posterior neighbor 6v, area **PEF** has more myelin (Panel B), differs in functional connectivity (Panel C), and is more activated in the primary task contrasts (e.g. Panel F). **PEF** is also less activated than 6r in the BODY-AVG contrast and more activated in the PLACE-AVG contrast. The eye fields PEF and FEF

correspond closely to those identified in (Amiez and Petrides, 2009). PEF is also similar in location to 6v2 from (Amunts et al., 2010).

Premotor areas **6v** and **6r** appear in similar locations to those described in (Amunts et al., 2010), with their 6v1 matching our 6v. The borders of 6v with areas 4 posteriorly and PEF anteriorly have already been described (in Section #6 Somatosensory and Motor Cortex and above). Relative to its superior neighbor 55b, area **6v** differs in functional connectivity, is less activated in the STORY contrast and more activated in the MOTOR CUE contrast. Relative to its anterior neighbor 6r, area **6v** differs in functional connectivity, having particularly strong connectivity with areas 6d, 2, 24dd, and SII, along with the upper limb representation of the sensori-motor cortex, which is distinct from area 6r (gradient in Panel C). Area **6v** is also deactivated vs activated relative to 6r in the WORKING MEMORY 2BK-0BK (Panel D), RELATIONAL-MATCH (Panel H), and TOM-RANDOM (Panel I) contrasts, and less activated in the BODY-AVG and MATH-STORY contrasts. Relative to its inferior neighbor 43, area **6v** differs in functional connectivity (Panel C) and is activated vs deactivated in primary task contrasts (e.g. Panel F). Relative to its antero-inferior neighbor IFJp, area **6r** has less myelin (Panel B), is more activated in the BODY-AVG contrast, and is less activated or deactivated in the PLACE-AVG, FACES-SHAPES (Panel G) and several primary task contrasts. Relative to its anterior neighbor area 44, area **6r** differs in functional connectivity (Panel C), is more activated in the MOTOR AVG contrast, is deactivated vs activated in the LANGUAGE STORY contrast (Panel E) and STORY-MATH contrast, and activated vs deactivated in the FACES-SHAPES contrast (Panel G). Also relative to area 44, area 6r is less activated in the right hemisphere in the TOM-RANDOM contrast (Panel I), and less activated in the left hemisphere in the RELATIONAL-MATCH contrast (Panel H). Relative to its inferior neighbors FOP4 and FOP1, area **6r** differs in functional connectivity (Panel C), has more myelin (Panel B), and is thinner than FOP4. Relative to its posterior neighbor 43, area **6r** has less myelin (Panel B), differs in functional connectivity (Panel C), is more activated in primary task contrasts (e.g. Panel F), has differential activity in the T-AVG and ?H-AVG contrasts (more prominent in the ipsilateral hemisphere), and is more activated in the working memory 2BK-0BK contrast (Panel D).

9. Posterior Opercular Cortex

The posterior operculum of the Sylvian fissure, including the second somatosensory area, SII, is the fourth and final region of our parcellation that is related mainly to sensori-motor function, based on functional connectivity and task-fMRI activations. This region includes six areas, 43, FOP1 (Frontal Opercular area 1), OP4, OP1, OP2-3, and PFcm, which are surrounded by areas 1, 3b, 3a, 4, 6v, 6r, FOP4, FOP2, Ig, 52, RI, PSL, PF, PFop. Figure 11 shows multi-modal information that was used to parcellate this region of cortex on a very inflated view of the posterior operculum inside the Sylvian fissure, together with the six areas overlaid on a folding map (Panel A).

The superior borders of area **43** and **FOP1** with areas 4, 3a, 6v and 6r were covered earlier (Sections #6 Somatosensory and Motor Cortex, #8 Premotor Cortex). Relative to its anterior neighbor FOP4, area **FOP1** has more myelin (Panel B), differs in functional connectivity (Panel D) and is more activated in many MOTOR primary contrasts (exemplified by the MOTOR AVG contrast, Panel G). Relative to its infero-medial neighbor FOP2, area **FOP1** differs in functional connectivity (Panel D), is more activated in the ?F-

AVG foot (Panels H and I) contrasts, and is deactivated vs activated in the contralateral ?H-AVG hand (Panels K and L) and TOM-RANDOM contrasts. Relative to its posterior neighbor 43, area **FOP1** differs in functional connectivity and is much more activated in the MOTOR AVG contrast (Panel G). Relative to its inferior neighbor FOP2, area **43** has more myelin (Panel B), differs in functional connectivity (Panel D), and is deactivated vs activated in the SOCIAL TOM contrast. Relative to its posterior neighbor OP4, area **43** differs in functional connectivity (Panel D), and is deactivated or less activated in many primary task contrasts including LANGAGE MATH (Panel E) and GAMBLING, and is much less activated in the T-AVG motor contrast (Panel J). Area 43 is assigned this name for its similarity in location to area 43 as described by Brodmann (Brodmann, 1909; Brodmann, 2007) directly inferior to sensorimotor cortex (though OP4 may also correspond to the posterior part of Brodmann's 43, (Eickhoff et al., 2006a; Eickhoff et al., 2006b)). Our area 43 may correspond to area 41 from the Vogt-Vogt school (Nieuwenhuys et al., 2015).

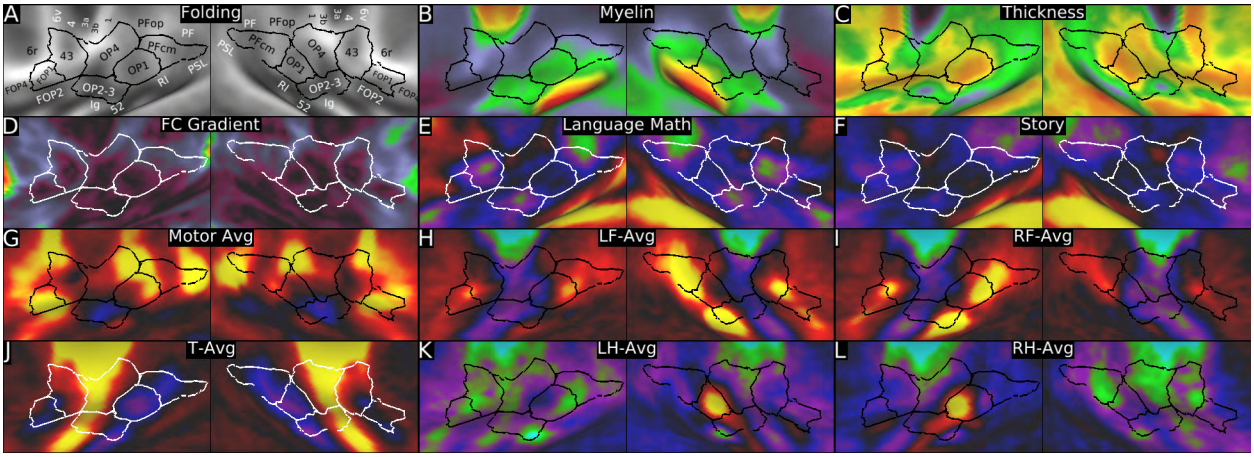

Figure 11 shows multi-modal information that was used to define the boundaries of the areas in the posterior opercular cortex. Panel A shows these areas on a folding map. Panels B and C show the myelin and thickness maps. Panel D shows the resting state functional connectivity gradients. Panels E and F show the LANGUAGE MATH and STORY task contrasts. Panels G, H, I, J, K, and L show the MOTOR AVG, LF-AVG, RF-AVG, T-AVG, LH-AVG, and RH-AVG task contrasts. Data at http://balsa.wustl.edu/JZ31.

Relative to its infero-medial neighbor OP2-3 (on the opercular surface; down in the figure), area **OP4** has less myelin, is activated vs deactivated in the MOTOR AVG task contrast (Panel G) and is more activated in the LANGUAGE MATH contrast (Panel E). Relative to its posterior neighbor OP1, area **OP4** is has less myelin, differs in functional connectivity (Panel D), is deactivated vs strongly and focally activated in the contralateral ?H-AVG hand motor contrasts (Panels K and L) and is strongly activated vs deactivated in the T-AVG contrast (Panel J). **OP4's** boundary with area 1 was covered previously in Section #6 Somatosensory and Motor Cortex. Relative to its supero-posterior neighbor PFop, area **OP4** differs in functional connectivity (Panel D) and is modestly activated vs strongly deactivated in the LANGUAGE STORY contrast (Panel F). Our area OP4 may correspond to area 68 from the Vogt-Vogt school (Nieuwenhuys et al., 2015).

Relative to its anterior neighbor FOP2, area **OP2-3** has more myelin (Panel B), differs in functional connectivity (Panel D), is deactivated vs activated in the MOTOR AVG contrast (Panel G) and in many primary contrasts including RELATIONAL and EMOTION

contrasts. Relative to its medio-inferior neighbor Ig (down in the figure; on the insula instead of the operculum), area **OP2-3** is thinner (Panel C), is deactivated vs activated in the MOTOR AVG contrast (Panel G), and is more deactivated in the working memory 2BK-0BK contrast. OP2-3 (and also Ig, covered in Section #12 Insular and Frontal Opercular Cortex) has an orderly somatotopic representation revealed in the MOTOR task contrasts (T-AVG, ?H-AVG, and ?F-AVG, Panels H, I, J, K, L) that involves contralateral activation for the foot and hand and bilateral activation for the tongue. Relative to its posterior neighbor retroinsular area RI, area **OP2-3** has less myelin (Panel B), is locally thicker (Panel C), differs in functional connectivity (Panel D), and is more deactivated in the working memory 2BK-0BK and LANGUAGE STORY contrasts (Panel F). Relative to its lateral neighbor OP1, area **OP2-3** has slightly less myelin (Panel B), differs in functional connectivity (Panel D), is more deactivated in the working memory 2BK-0BK task contrast, less activated in the ?H-AVG hand motor contrasts (Panels K and L), and more deactivated in the LANGUAGE MATH contrast (Panel E). Area OP2-3 is so named because it overlaps extensively with the locations of areas OP2 and OP3 (Eickhoff et al., 2006a; Eickhoff et al., 2006b), which we were unable to clearly distinguish in our data. Cortex activated by vestibular stimulation (sometimes called parieto-insular vestibular cortex, or PIVC) appears to include OP2 (Eickhoff et al., 2006c).

Area **OP1** has more myelin than all of its neighbors except area RI (Panel B), and likely corresponds to area SII (Burton et al., 2008; Eickhoff et al., 2006a; Eickhoff et al., 2006b). Relative to its medial neighbor RI, area **OP1** has less myelin (Panel B), is thicker (Panel C), differs in functional connectivity (Panel D), and is much more activated in the contralateral ?H-AVG hand motor contrasts (Panels K and L). Relative to its posterior neighbor PFcm, area **OP1** differs in functional connectivity (Panel D) and is much more activated in the contralateral ?H-AVG hand motor contrasts (Panels K and L). Our OP1 matches the location of OP1 previously reported (Eickhoff et al., 2006a; Eickhoff et al., 2006b) and is consistent with our previous report of it having more myelin (Glasser and Van Essen, 2011).

Relative to its superior neighbors PFop and PF and its posterior neighbor PSL, area **PFcm** has more myelin (Panel B) and differs in functional connectivity (Panel D). Relative to PFop and PF, area **PFcm** is less activated in the BODY-AVG contrast (in the left hemisphere for PFop and in both hemispheres for PF) and less deactivated in the LANGUAGE STORY contrast (Panel F). Relative to its lateral neighbor PSL, area **PFcm** is more activated in the contralateral ?F-AVG foot motor contrasts, (Panel H and I) and is deactivated vs activated in the STORY contrast (left hemisphere only, Panel F) and in the MATH contrast (Panel E). Relative to its inferior neighbor RI, area **PFcm** has less myelin (Panel B), differs in functional connectivity (Panel D), is more deactivated in the working memory 2BK-0BK contrast, and is more activated the MOTOR CUE contrast and in the ?F-AVG foot motor contrasts (Panels H and I). We previously identified **PFcm** as being more heavily myelinated (Glasser and Van Essen, 2011), having compared its location (Caspers et al., 2008; Caspers et al., 2006) with myelin maps.

10. Early Auditory Cortex

We now discuss auditory cortex, the last of the three large sensory domains in human neocortex. We divide the auditory cortex into the heavily myelinated early auditory

cortex and the more moderately myelinated auditory association cortex (Section #11). The early auditory areas include A1, LBelt (Lateral Belt), MBelt (Medial Belt), PBelt (Para-Belt), and the retro-insular cortex (RI). These areas are surrounded by areas, OP2-3, OP1, PFcm, PSL, A4, Ig, and TA2. The multi-modal information used to parcellate the auditory cortex is shown on flattened surfaces in Figure 12, with the areas identified shown in Panel A on a folding map.

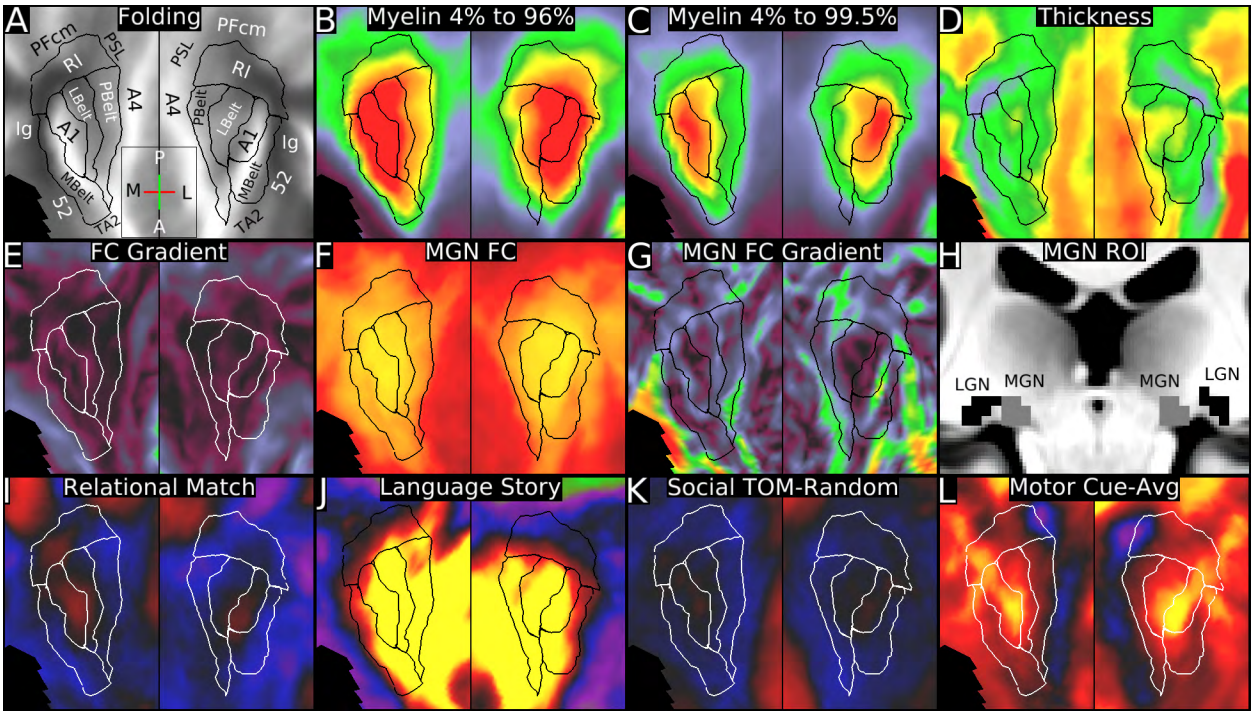

Figure 12 shows the multi-modal information used to parcellate the early auditory areas on flattened surfaces. The direction icon in Panel A shows Anterior (A), Posterior (P), Medial (M), and Lateral (L) directions (approximate orientation in 3D space) for the left surface (the M/L axis is reversed for the right surface). Panel A shows the early auditory areas on a folding map. Panels B and C show myelin maps with different scaling, 4% to 96% and 4% to 99.5% to highlight differences in myelin content of the very heavily myelinated auditory cortex. Panel D shows cortical thickness and Panel E shows functional connectivity gradients. Panel F shows the connectivity map from the MGN seed (Panel H) scaled from 2% to 99.5% to highlight differences in functional connectivity in the early auditory cortex, and Panel G shows the gradient of this map. Panels I, J, K, and L show the RELATIONAL MATCH, LANGUAGE STORY, SOCIAL TOM-RANDOM, and MOTOR CUE-AVG task contrasts. Data at http://balsa.wustl.edu/RV3p.

In contrast to early visual and somatomotor cortex, parcellation of the early auditory cortex has proven much more challenging in both macaques and humans (Baumann et al., 2013; Hackett et al., 2001; Kaas and Hackett, 2000; Moerel et al., 2014). In macaques there is evidence for a core auditory strip containing a primary area A1 plus one or two additional tonotopic areas. These areas are surrounded by medial and lateral belt complexes, each containing multiple tonotopic areas, plus a lateral parabelt complex that also contains multiple subdivisions (Hackett, 2007). Human architectonic and fMRI studies provide evidence for a similar overall arrangement, but a consensus is lacking on the number and precise locations of these areas (Baumann et al., 2013; Moerel et al., 2014). In our parcellation, we identify a very heavily myelinated core on medial and posterior

aspects of Heschl's gyrus (Panels A and C), which we consider likely to be primary auditory cortex, or A1. We identified three complexes surrounding our A1. Two are heavily myelinated (Panels B and C), (as are human and macaque belt areas – (Hackett et al., 2001). We identify them as MBelt (medial belt), LBelt (lateral belt) because they are similar but not identical to previous parcellations and hence warrant modified names (Moerel et al., 2014). The retro-insular area, RI, adjoining A1 postero-superiorly, is moderately-to-heavily myelinated (Panel B), corresponds to the retroinsular region identified by (Kurth et al., 2010; Pandya and Sanides, 1973), which we previously noted was heavily myelinated (Glasser and Van Essen, 2011), and overlaps with the postero-superior portion of the belt as delineated by (Moerel et al., 2014). We also identify PBelt as a lateral parabelt complex and area 52 medial to our MBelt complex. (Architectonic area 52 has been suggested to correspond to the medial belt (Moerel et al., 2014), but we consider this unlikely based on its location and degree of myelination, as discussed below.) Our arrangement of areas is also similar to that of Von Economo and Koskinas, with their TC corresponding to our A1, their TB corresponding to our MBelt and LBelt, their TA1 corresponding to our PBelt, and their TD corresponding to our RI (Triarhou, 2007a, b; von Economo and Koskinas, 1925). All of these areas are likely complexes of smaller fields (Moerel et al., 2014) that were not readily discernible in our data.

A1 (or the auditory core) is bordered by areas MBelt antero-medially, LBelt posteriorly, and RI supero-postero-medially. **A1** is very heavily myelinated, even relative to its heavily myelinated surrounding neighbors, as shown in Panel B (using our standard palette scale that saturates at a maximum of 96%) and in Panel C (using a saturation level of 99.5% to reveal the heavier myelination of A1 relative to its neighbors). **A1** is also moderate in thickness (Panel D), in contrast to the much thinner primary visual (area V1) and somatosensory (area 3b) cortex illustrated in previous sections (#1 Primary Visual Cortex (V1) and #6 Somatosensory and Motor Cortex). Using a different dataset acquired at 1mm isotropic resolution, we previously reported that A1 appeared notably thinner than its neighbors and speculated that this might reflect a bias in which FreeSurfer's segmentation of the gray/white boundary extended into deep cortical layers in heavily myelinated regions (Glasser and Van Essen, 2011). This speculation is confirmed insofar as the higher resolution (0.7mm) T1w and T2w images plus additional processing pipeline improvements for the HCP data (Glasser et al., 2013) indicate that A1 is indeed as thick as its neighbors (Panel D). The region of heaviest myelination is situated on the medial half of Heschl's gyrus, mostly on the posterior bank but extending over the crown of the gyrus. This overlaps with both areas TE1.0 and TE1.1 of (Morosan et al., 2001) (their Fig. 11, also see (Glasser and Van Essen, 2011)). Additionally, many primary task contrasts show modest differences in activation in **A1** relative to its neighbors (e.g., the RELATIONAL MATCH contrast, Panel I). Specifically, relative to its postero-lateral neighbor LBelt, **A1** has more myelin (Panel C), differs in functional connectivity (Panel E) and is more activated in the RELATIONAL MATCH contrast (Panel I). Relative to its antero-medial neighbor MBelt, area **A1** has more myelin (Panel C), differs in functional connectivity with a Medial Geniculate Nucleus (MGN) thalamic seed ROI (Panels F, G, and H), and is more activated in the RELATIONAL MATCH contrast (Panel I). Relative to its posterior neighbor RI, area **A1** has more myelin (Panels B and C), differs in functional connectivity both overall (Panel E) and when seeded from the MGN (Panels F, G), and is more activated in the LANGUAGE MATH and STORY contrasts (Panel J).

Relative to its antero-medial neighbor area 52, the **MBelt** complex has more myelin (Panel B), is thicker (Panel D), and is activated vs deactivated in the LANGUAGE MATH and STORY contrasts (Panel J). Relative to its antero-lateral neighbor area TA2, **MBelt** has more myelin (Panel B), is thinner (Panel D), and is more activated in the LANGUAGE MATH and STORY contrasts (Panel J). Relative to its lateral neighbor PBelt, the **MBelt** complex has more myelin (Panel C) and is less activated in the language MATH and STORY contrasts (Panel J) and more activated in the EMOTION FACES-SHAPES contrast. The antero-lateral portion of the MBelt complex likely overlaps with area TE1.0 of (Morosan et al., 2001) (Glasser and Van Essen, 2011). Relative to its lateral neighbor PBelt, the **LBelt** complex has more myelin (Panel C), has stronger functional connectivity with the MGN nucleus (Panels F and G), and is modestly activated vs deactivated in the TOM-RANDOM contrast (Panel K). Relative to its postero-superior neighbor RI, the **LBelt** complex has more myelin (Panel C), has stronger functional connectivity with the MGN (Panels F and G), and is more activated by the MATH and STORY contrasts (Panel J). Relative to its lateral neighbor A4, the **PBelt** complex has more myelin (Panel B and C), is thinner (Panel D), has greater functional connectivity with the MGN (Panels F and G), and is more activated in the CUE-AVG contrast (Panel L). Relative to its supero-medio-posterior (up on the map) neighbor RI, the **PBelt** complex has more myelin (Panels B and C; the myelin gradient is strong where **PBelt** and RI adjoin), and greater functional connectivity with the MGN (Panels F and G). Finally, relative to area PSL postero-laterally, area **RI** has more myelin (Panels B and C), is thinner (Panel D, more prominently in the right hemisphere), differs in functional connectivity (Panel E), is deactivated vs activated in primary contrasts (e.g. the GAMBLING primary contrasts), and is less activated in the MATH-STORY contrast. The anterior (OP2-3) and superior (OP1 and PFcm) borders of **RI** were covered in the Section #9 Posterior Opercular Cortex, and the inferior borders were covered above.

11. Auditory Association Cortex

We identified auditory association cortex as a region mainly on the superior temporal gyrus and within the superior temporal sulcus that is activated in the LANGUAGE STORY, MATH, and STORY-MATH contrasts. It is strongly functionally connected with the inferior frontal gyrus, including areas 44, 45, and 47l. This auditory region likely becomes progressively less purely auditory and more multi-modal as one progresses inferiorly, anteriorly, and posteriorly (away from early auditory cortex, e.g. Main Text Figure 3). Indeed, functional connectivity with early auditory cortex progressively decreases along those directions. This region includes eight areas that we identify as A4, A5, STSdp, STSda, STSvp, STSva, STGa, and TA2. Because our parcellation is finer grained than most previously attempted parcellations of the superior temporal gyrus and sulcus, we have introduced largely novel terminology here, except that TA2 is based on the Von Economo and Koskinas parcellation (Triarhou, 2007a, b; von Economo and Koskinas, 1925). These areas are surrounded by PBelt, MBelt, PI, TGd, TE1a, TE1m, TE1p, PHT, TPOJ1, STV, and PSL. Figure 13 shows multi-modal information used to parcellate this region's cortex into the areas displayed on a folding map in Panel A.

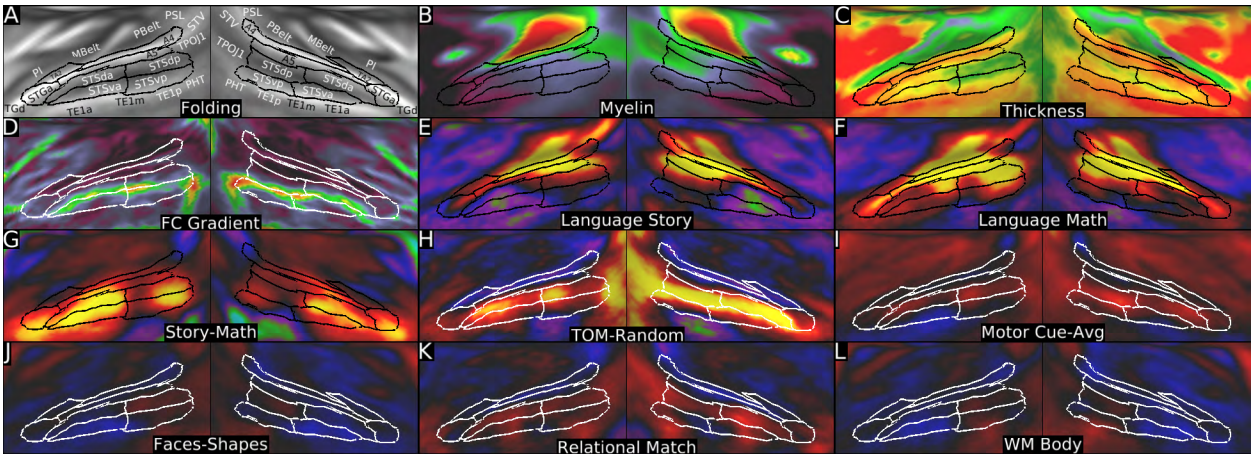

Figure 13 shows multi-modal information used to parcellate the auditory association cortex. Panel A shows the cortical areas overlaid on a folding map. Panels B and C show myelin and cortical thickness maps. Panel D shows the resting state functional connectivity gradient. Panels E, F, and G show the LANGUAGE STORY, MATH, and STORY-MATH contrasts. Panels H, I, and J show the TOM-RANDOM, MOTOR CUE-AVG, and FACES-SHAPES contrasts. Panels K and L show the RELATIONAL MATCH and WM BODY primary task contrasts. Data at http://balsa.wustl.edu/W3v5.

A4's supero-medial border with PBelt was covered in Section #10 Early Auditory Cortex. Relative to its inferior neighbor A5, area **A4** differs in functional connectivity, and this gradient was primarily used to define the boundary (Panel D). **A4** also has more myelin than **A5** assessed statistically (Panel B), though the myelin gradient peak does not align with the functional connectivity gradient peak. Relative to its antero-medial neighbor TA2, area **A4** has more myelin (Panel B), differs in functional connectivity (Panel D), is more activated in the LANGUAGE MATH and STORY contrasts (Panels E and F), and is less activated in the CUE-AVG contrast (Panel I). Based on its position on the crown of the superior temporal gyrus, area **A4** may correspond to cytoarchitectonic area Te3 (Morosan et al., 2005). The borders of A4, A5, and STSdp with areas PSL, STV, and TPOJ1 posteriorly will be covered in Section #15 Temporal-Parietal-Occipital Junction. Relative to its antero-medial neighbor TA2, area **A5** differs in functional connectivity (Panel D), and is more activated in the LANGAUGE STORY-MATH (Panel G) and TOM-RANDOM (Panel H) contrasts. Relative to its inferior neighbor STSdp, area **A5** differs in many primary and non-primary task contrasts including more activation in the LANGAUGE MATH (Panel E) and STORY (Panel F) contrasts and less activation in the working memory (e.g Panel L) and RELATIONAL (e.g. Panel J) primary contrasts, and the FACE-AVG, TOM-RANDOM (Panel H), and FACES-SHAPES (Panel K) contrasts. Relative to its inferior neighbor STSda, area **A5** again shows differences in a variety of task contrasts including markedly more activation in the LANGAUGE MATH contrast (Panel E), more activation in the TOOL-AVG contrast, markedly less activation in the TOM-RANDOM contrast (Panel H), and less activation in the CUE-AVG (Panel I) and FACES-SHAPES (Panel K) contrasts. Relative to its anterior neighbor STGa, area **A5** has more myelin (Panel B) and differs in functional connectivity (Panel D).

Relative to area STSvp on the inferior bank of the STS, area **STSdp** on the superior banks is has more myelin (Panel B), differs markedly in functional connectivity (Panel D), is more activated in the LANGUAGE MATH (Panel E), TOM-RANDOM (Panel H, especially in the right hemisphere), and MOTOR CUE-AVG (Panel I) contrasts. Relative to its anterior

neighbor STSda in the superior bank of the STS, area **STSdp** has more myelin (Panel B), and differs markedly in its functional activation profile, being more activated in the CUE-AVG contrast (Panel I) and the RELATIONAL MATCH (Panel J), working memory (e.g. Panel L), SOCIAL TOM and other primary contrasts, and less active in the STORY-MATH contrast (Panel G). Relative to its inferior neighbor STSva on the inferior bank of the STS, area **STSda** differs greatly in functional connectivity (Panel D) and is more activated in the in the MOTOR CUE-AVG contrast (Panel I) and less deactivated in the GAMBLING primary contrasts (more on the left than on the right). Relative to its anterior neighbor STGa, area **STSda** is has more myelin, is thinner, is less activated in the LANGUAGE MATH and STORY contrasts, and is more activated in the TOM-RANDOM contrast.

Relative to PHT anteriorly, area **STSvp** differs strongly in functional connectivity and is activated instead of deactivated in the LANGUAGE STORY contrast and the STORY-MATH contrast. Relative to its postero-inferior neighbor TE1p on the inferior temporal gyrus (MTG), area **STSvp** differs in functional connectivity (Panel D), is more activated in the STORY (Panel F) and STORY-MATH contrasts (Panel G), and is less activated in the FACES-SHAPES contrast (Panel K). Relative to its inferior neighbor TE1m, further anterior on the MTG, area **STSvp** differs in functional connectivity (Panel D) and is activated vs deactivated in the STORY (Panel F), STORY-MATH (Panel G), and TOM-RANDOM (Panel H) contrasts. Relative to its anterior neighbor STSva, area **STSvp** has more myelin (Panel B), differs in functional connectivity (Panel D), is more activated in working memory (e.g Panel L), GAMBLING, EMOTION, and other primary task contrasts, and differs in the STORY-MATH contrast (Panel G, especially in the right hemisphere). Relative to its infero-lateral neighbor area TE1a on the anterior MTG, area **STSva** has more myelin (Panel B), is thinner (Panel C), is more activated in the STORY-MATH contrast (Panel G), and differs in some primary contrasts including more deactivation in the RELATIONAL (Panel K), working memory (e.g. Panel L), GAMBLING, and EMOTION contrasts.

The final two auditory association areas, **TA2** and **STGa,** lie on the planum polare and STG anterior to Heschl's gyrus. **TA2**'s medial border with MBelt was covered in Section #10 Early Auditory Cortex and its borders with A4 and A5 were covered above. Relative to its antero-medial neighbor area PI, area **TA2** has more myelin (Panel B), is thicker (Panel C), and is activated vs deactivated in the LANGAUGE MATH (Panel E) and STORY (Panel F) contrasts. Relative to its lateral neighbor STGa, area **TA2** has more myelin (Panel B), differs in functional connectivity (Panel D), and is less activated in the STORY-MATH task contrast (Panel G) and deactivated vs activated in the TOM-RANDOM contrast (Panel H). Relative to its medio-inferior neighbor PI, area **STGa** is substantially thicker (Panel C) and is more activated in the LANGAUGE STORY-MATH (Panel G) and TOM-RANDOM task contrasts (Panel H). Relative to its anterior neighbor TGd (including the temporal pole), area **STGa** differs in functional connectivity (Panel D) and is more activated in the STORY (Panel F) and CUE-AVG (Panel I) contrasts. Area TA2 may overlap with TE1.2 from (Morosan et al., 2001).

12. Insular and Frontal Opercular Cortex

This section covers the insular and frontal opercular cortex. Previous architectonic studies have subdivided the insula into a superior and posterior granular region, an

anterior, inferior agranular region, and a dysgranular region lying in between (Kurth et al., 2010; Morel et al., 2013). We identified 13 areas in the insula and frontal operculum, including areas 52, PI (ParaInsular cortex), Ig (Insula granular), Posterior Insular areas PoI1 and PoI2, Frontal Opercular areas FOP2 and FOP3, a Middle Insular area MI, an Anterior Ventral Insular area AVI, an Anterior Agranular Insular Complex AAIC, the Piriform cortex Pir, and Frontal Opercular areas FOP4 and FOP5. These areas are surrounded by areas TGd, STGa, TA2, MBelt, OP2-3, 43, FOP1, 6r, 44, 45, 47l, 47s, and pOFC. Figure 14 shows multi-modal information used to define the cortical areas in the insular and frontal opercular cortex (areas on a folding map, Panel A).

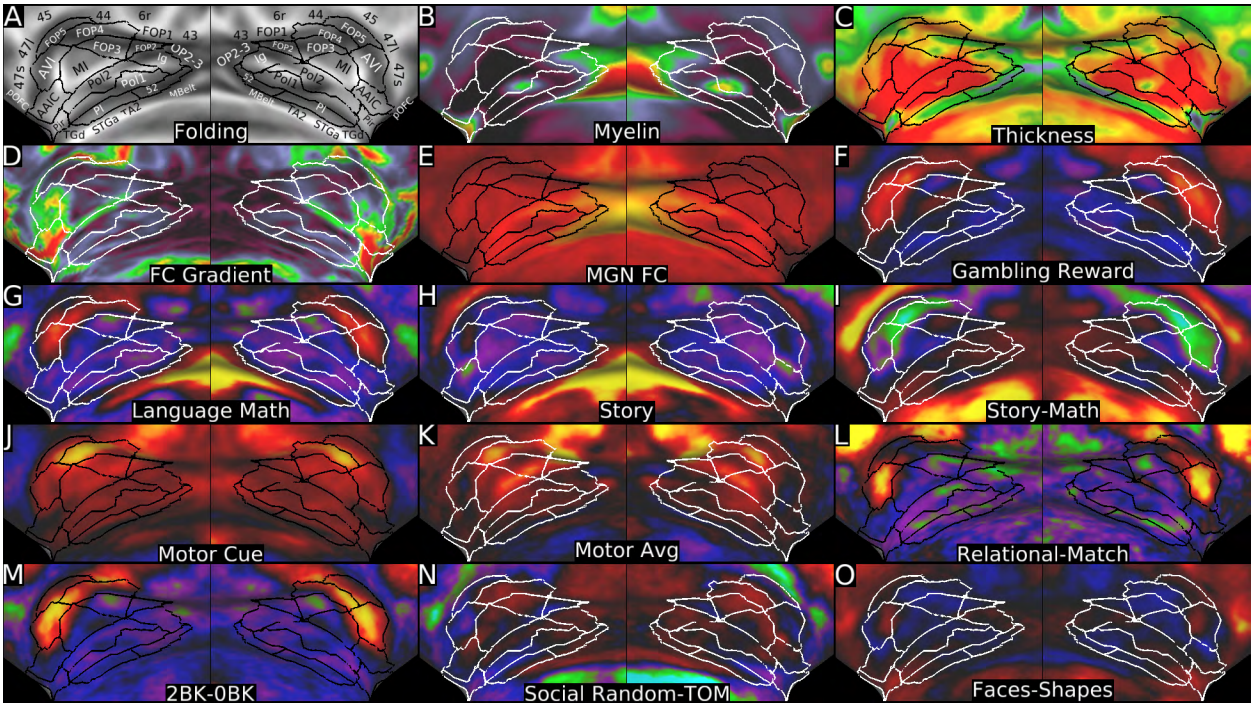

Figure 14 shows multi-modal information used to define cortical areas in the insula and frontal operculum. Panel A shows the areas on a folding map. Panels B and C show myelin and cortical thickness maps. Panels D and E show the resting state functional connectivity gradient and the map of functional connectivity with the MGN. Panel F shows an example primary task contrast (GAMBLING Reward). Panels G, H, and I show the LANGUAGE MATH, STORY, and STORY-MATH contrasts. Panels J, K, and L show the MOTOR CUE, MOTOR AVG, and RELATIONAL-MATCH contrasts. Panels M, N, and O show the working memory 2BK-0BK, SOCIAL RANDOM-TOM, and EMOTION FACES-SHAPES contrasts. Data at http://balsa.wustl.edu/Wznm.

Area **52** is a transitional region lying between an early auditory sensory area (MBelt) and a very different type of cortex (insular area PoI1, and granular insular area Ig). In this respect it is analogous to the Dorsal Visual Transitional area DVT described below (Section #18 Posterior Cingulate Cortex), which is transitional between early visual areas and very different cortex. Area **52** shares some properties with MBelt, including functional connectivity with the MGN (Panel E) and being relatively thin (Panel C), but it has important differences, including having much less myelin (Panel B) and net deactivation in the LANGUAGE STORY and MATH task contrasts (Panels G and H), features that it shares with its more anterior insular neighbors. Thus, it seems reasonable to consider area **52** as a transitional auditory area. We identify it as area **52** based on its similarity in location to

Brodmann's area **52** (Brodmann, 1909; Brodmann, 2007) (Figure 89) within the inferior portion of the circular sulcus, between early auditory cortex (his area 41) and the posterior insula. It appears to also correspond to the posterior portion of area IBT in von Economo and Koskinas's parcellation, as there is room for an MBelt-like set of areas between their auditory core and area IBT (Triarhou, 2007a, b; von Economo and Koskinas, 1925). The posterior granular insular cortex identified by (Morel et al., 2013) may include area **52**. The posterior border of area **52** with MBelt was described already (Section #10 Early Auditory Cortex). Relative to its anterior neighbor Ig, area **52** is thinner (Panel C), has stronger functional connectivity with the MGN (Panel E), and is more activated in the BODY-AVG task contrast and less deactivated in the LANGUAGE MATH and STORY contrasts (Panels G and H). Similarly, relative to area PoI1, area **52** is substantially thinner (Panel C) and has stronger functional connectivity with the MGN (Panel E). Area **52** is also statistically more activated than Pol1 in the LANGUAGE MATH contrast (Panel G). Relative to area PI (the anterior extension of Von Economo and Koskinas area IBT (Triarhou, 2007a, b; von Economo and Koskinas, 1925), area **52** has many similarities, but has more myelin (Panel B), is thinner (Panel C), and has stronger functional connectivity with the MGN (Panel E). Area **PI's** posterior borders with area TA2 and area STGa were previously covered (Section #11 Auditory Association Cortex). Relative to its antero-inferior neighbor TGd, area **PI** is thinner (Panel C), differs in functional connectivity (Panel D), is more activated in the LANGUAGE MATH contrast (Panel G) and less activated (or deactivated) in the STORY-MATH (Panel I), and the RANDOM-TOM contrasts. Relative to area PoI1 medially, area **PI** is substantially thinner (Panel C) and is less deactivated in the working memory 2BK-0BK contrast (Panel M). **PI** is also statistically less deactivated than Pol1 in the LANGUAGE MATH (Panel G) contrast. Area PI corresponds approximately to area PI in (Ding et al., 2009) lying in the inferior circular sulcus.

We identified area **Ig** as a region that appears to overlap extensively with area **Ig** of (Morel et al., 2013) and with areas Ig1 and Ig2 of (Kurth et al., 2010). As defined, **Ig** has some internal heterogeneity, but insufficient for us to unambiguously make a finer parcellation based on our data. The superior and posterior borders of **Ig** were already described (Section #9 Posterior Opercular Cortex, and above). As noted previously, area **Ig** contains a somatotopic representation of the body (see Figure 11). Relative to antero-inferior neighbors PoI1 and PoI2, area **Ig** has more myelin (Panel B), is thinner (Panel C), and is more activated in the FACES-SHAPES contrast (Panel O). Relative to its supero-medial neighbor FOP2, **Ig** has more myelin (Panel B), differs in functional connectivity (Panel D), and in a large number of task contrasts, including less activation in many primary contrasts (e.g. Panel F) and the MOTOR AVG contrast (Panel K) and more activation in the RANDOM-TOM (Panel N) and FACES-SHAPES (Panel O) contrasts.

We identified two areas, **PoI1** and **PoI2** overlapping the posterior portion of dysgranular areas Id1, Id2, and Id3 by (Morel et al., 2013) and (Kurth et al., 2010), and possibly the posterior portion of the agranular cortex. Unfortunately, parcellation of this region is confounded by a relatively consistent surface reconstruction artifact caused by the FreeSurfer white matter surface and the putamen subcortical segmentation encroaching into the claustrum, leading to artifactual peaks in the myelin maps (Panel B). In addition, because of the very deep white matter surface placement and overlap between the white matter surface and putamen segmentation, the reconstructed pial surface does not extend all the way out to the real pial surface, leading to an artifactual dip in estimated

cortical thickness, more prominent in the right hemisphere (Panel C). The parcellation of this region should be revisited when this artifact is removed in a future FreeSurfer version. Aside from these focal artifacts, both **PoI1** and **PoI2** are very thick (Panel C) and very lightly myelinated (Panel B). Relative to its supero-medial neighbor PoI2, area **PoI1** differs in functional connectivity (Panel D) and is deactivated or weakly activated vs strong activation of **PoI2** in the T-AVG tongue MOTOR contrast. Relative to their anterior-inferior neighbor Pir, areas **PoI1** and **PoI2** have much less myelin (Panel B) and are thicker (Panel C). Relative to anterior neighbor AAIC, area **PoI2** differs in functional connectivity (Panel D), is more deactivated in the working memory 2BK-0BK (Panel M) and RELATIONAL-MATCH (Panel L) contrasts and more activated in the MOTOR CUE contrast (Panel J). Relative to its superior neighbor MI (the middle insular area), area **PoI2** differs in functional connectivity, is deactivated vs activated in the GAMBLING primary contrast (Panel F) and activated vs deactivated the STORY-MATH contrast (Panel I). For area **FOP2**, its borders superiorly (FOP1 and 43) and posteriorly (OP2-3) were covered previously (Section #9 Posterior Opercular Cortex), and its inferior border with Ig was covered above. Relative to its anterior neighbors FOP3 and FOP4, **FOP2** has more myelin, but less than posteriorly adjoining granular cortex Ig (Panel B). Relative to FOP3, **FOP2** also differs in functional connectivity (Panel D) and is less deactivated in the LANGUAGE MATH and STORY contrasts (Panels G and H).

Along the antero-inferior margin of the insula, at the juncture of the frontal and temporal lobes (limen insula), the cortex is substantially more heavily myelinated and thinner (Panels B and C) than nearby AAIC antero-superiorly and TGd antero-inferiorly, and previously discussed borders with PoI1 and PoI2. This area likely corresponds to the piriform olfactory cortex (**Pir**) (Ding et al., 2009; Morel et al., 2013), as we noted previously (Glasser and Van Essen, 2011). Relative to its neighbors, area **Pir** shows apparent differences in functional connectivity and in a number of task contrasts. However, we do not consider these differences to be convincing because strong vascular artifacts were commonly identified in this region in the resting state data (i.e., as structured noise components in FIX+ICA denoising), and there is relatively little signal in the Pir in the denoised resting state connectivity data. The task data are thus suspect because they were not processed using ICA+FIX denoising. Medially, area Pir adjoins non-cortical gray matter that is outside of the grayordinates space (Glasser et al., 2013).

We identified two areas in the anterior insula, the anterior agranular insular complex (**AAIC**) and the Middle Insular area (**MI**). AAIC is called a complex because it includes inferior portions of the architectonic subdivisions Iai and Ial of (Ongur et al., 2003) and because it has considerable functional heterogeneity in our data that could potentially reveal subdivisions using higher resolution data. The agranular insula is among the most lightly myelinated and thickest cortical regions (Panels B and C; see also (Glasser and Van Essen, 2011). Relative to its neighbors 47s antero-laterally and AVI superiorly, area **AAIC** has less myelin (Panel B) and is thicker (Panel C). Additionally, area AAIC differs from area 47s in functional connectivity and being slightly activated vs deactivated in the MOTOR CUE-AVG contrast and less activated in the STORY-MATH (Panel I) and SOCIAL TOM contrasts. Area AAIC differs from AVI in being deactivated vs activated in many primary task fMRI contrasts (e.g. Panel F), the LANGUAGE MATH contrast (Panel G), the RELATIONAL-MATCH contrast (Panel L), and the working memory 2BK-0BK contrast (Panel M). Relative to superior neighbor MI, area **AAIC** differs in functional connectivity

(Panel D), is less activated in the MOTOR CUE (Panel J) and MOTOR AVG (Panel K) contrasts, and is deactivated vs activated in the EMOTION SHAPES contrast. Relative to anterior neighbor AVI, area **MI** has less myelin (Panel B), differs in functional connectivity (Panel D), is deactivated vs activated in the LANGUAGE MATH and STORY primary contrasts (Panels G and H) and in the RELATIONAL REL-MATCH (Panel L) and working memory 2BK-0BK (panel M) contrasts, and is more activated in the MOTOR AVG (Panel K) and RANDOM-TOM (Panel N) contrasts. Relative to superior neighbor FOP3, area **MI** has less myelin (Panel B), is thinner (Panel C), is less deactivated in the LANGUAGE MATH contrast (Panel G), deactivated vs activated in the LANGUAGE STORY-MATH contrast (Panel I), and less activated in the RANDOM-TOM contrast (Panel N). Architectonically, **MI** is likely a dysgranular area (Morel et al., 2013). The anterior portion of **MI** overlaps with superior portions of the architectonic subdivision Ial of (Ongur et al., 2003).

Cortex superior to the anterior insula includes areas **FOP3** (along the superior peri-insular sulcus) and **FOP4**. **FOP3** and **FOP4** are more lightly myelinated than their anterior, superior, and posterior neighbors (Panel B). The borders of **FOP3** with MI inferiorly and FOP2 posteriorly have already been described. Relative to its supero-lateral neighbor FOP4, area **FOP3** is thinner (Panel C), differs modestly in functional connectivity (Panel D), is deactivated vs activated in the primary task contrasts (e.g. Panel F) and the working memory 2BK-0BK (Panel M), MOTOR CUE (Panel J), and LANGUAGE MATH (Panel G) contrasts, is activated vs deactivated in the LANGUAGE STORY-MATH contrast (Panel I), and is more deactivated in the RELATIONAL-MATCH contrast. **FOP4's** posterior (FOP1) and superior (6r) borders have previously been described (Sections #8 Premotor Cortex and #9 Posterior Opercular Cortex). Relative to supero-lateral neighbor area 44, area **FOP4** has less myelin (Panel B), differs strongly in functional connectivity (Panel D), is more activated in the MOTOR CUE (Panel J) and MOTOR AVG contrasts (Panel K), and is deactivated vs activated in the RELATIONAL-MATCH contrast (Panel L). Relative to anterior neighbor FOP5, area **FOP4** has less myelin (Panel B), is more activated in the MOTOR AVG contrast (Panel K), is activated vs deactivated in the RANDOM-TOM contrast (Panel N), and is deactivated vs activated in the FACES-SHAPES contrast (Panel O). Relative to supero-anterior neighbor area AVI, area **FOP4** is more heavily myelinated, differs in functional connectivity, is more activated in the MOTOR CUE (Panel J) and MOTOR AVG (Panel K) contrasts, is activated vs deactivated in the RANDOM-TOM contrast (Panel N), and is less activated in the RELATIONAL-MATCH contrast (Panel L).

Areas **FOP5** and **AVI** are the most anterior pair of areas in this region. Relative to its postero-superior neighbor area 44, area **FOP5** differs in functional connectivity (Panel D, especially in the left hemisphere) and is more activated in the MOTOR CUE contrast (Panel J) and less activated in the RELATIONAL-MATCH contrast (in the left hemisphere, Panel K). Relative to its neighbors area 45 supero-laterally and area 47l antero-laterally, area **FOP5** differs in functional connectivity (Panel D) and is more activated in many primary task contrasts (e.g. Panel F), the MOTOR CUE-AVG contrast (greater difference in left than right), and is deactivated vs activated in the LANGUAGE STORY (Panel H) and the STORY-MATH (Panel I) contrasts. Relative to its inferior neighbor AVI, area **FOP5** differs in functional connectivity (Panel D), is less activated in the working memory 2BK-0BK contrast (Panel M), more activated in the MOTOR AVG contrast (Panel K), and less activated in the RELATIONAL-MATCH contrast (Panel L). Relative to its anterior neighbor 47l, area **AVI** differs in functional connectivity, and is more activated in many primary task contrasts (e.g.

Panel F), the working memory 2BK-0BK contrast (Panel M), and the MOTOR CUE-AVG contrast, and is deactivated vs activated in the LANGUAGE STORY (Panel H) and STORY-MATH (Panel I) contrasts. Finally, relative to its infero-lateral neighbor 47s, area **AVI** differs in functional connectivity (Panel D), is more activated in many primary task contrasts (Panel F), the MOTOR CUE-AVG contrast (greater difference in left than right), the LANGUAGE MATH contrast (Panel G), and the RELATIONAL-MATCH contrast (Panel L), and is deactivated vs activated in the STORY-MATH contrast (Panel I). Area FOP5 likely overlaps considerably with a locally more heavily myelinated region that we previously identified as area PrCO (Glasser and Van Essen, 2011). AVI overlaps with superior portions of the architectonic subdivision Iai of (Ongur et al., 2003).

13. Medial Temporal Cortex

The inferior medial temporal region contains a set of seven elongated areas, including the hippocampus (H), presubiculum (PreS), entorhinal cortex (EC), the peri-entorhinal and ectorhinal complex (PeEc), and peri-hippocampal areas 1, 2 and 3 (PHA1, PHA2, and PHA3). These areas are surrounded by the retrosplenial cortex (RSC), the prostriate cortex (ProS), V2, the ventromedial visual areas (VMV1-3), the ventral visual complex (VVC), and areas TF, TGv, and TGd. We include the hippocampus because the cortical grayordinates space includes a portion of the hippocampus (the full hippocampus is also segmented by FreeSurfer and is represented as a volume in the subcortical portion of the grayordinates space (Glasser et al., 2013)). Figure 15 shows multi-modal information that was used to parcellate the medial temporal cortex (on a folding map in Panel A).

The hippocampal complex (**H**), including the subiculum, includes the inferior bank of the hippocampal fissure extending laterally to its fundus, where it adjoins the non-cortical medial wall ROI of the grayordinates space. Relative to the presubiculum (**PreS**) medially, the hippocampal complex (**H**) has much less myelin (Panel B) and appears to be thicker in places (Panel C), though the latter likely reflects imperfect FreeSurfer segmentation of hippocampal subfields. The **PreS** contains the perforant path (Augustinack et al., 2010; Glasser and Van Essen, 2011) and is thus much more heavily myelinated than all of its neighbors except the retrosplenial cortex, RSC (Panel B). **PreS** is also thinner than V2 and the Prostriate area (ProS) posteriorly (Panel C). Relative to its supero-posterior neighbor retrosplenial cortex (RSC), **PreS** is also thinner (Panel C) and differs in functional connectivity (Panel D). Relative to its antero-lateral neighbor entorhinal cortex (EC), area **PreS** has much more myelin (Panel B) and is somewhat thinner (Panel C). Relative to its inferior neighbor area PHA1, the **PreS** has much more myelin (Panel B), is thinner (Panel C), is less activated in the PLACE-AVG (Panel K), LANGUAGE STORY-MATH (Panel G), and SOCIAL TOM-RANDOM (Panel H) contrasts, and is more activated in the BODY-AVG contrast (Panel I). Relative to its infero-medial neighbor PeEc, the **EC** has more myelin (Panel B), is much thinner (Panel C), differs in functional connectivity (Panel D), is less activated in the primary task contrasts (e.g. Panel F) and in the TOM-RANDOM (Panel H) and FACES-SHAPES (Panel M) contrasts, and is activated vs deactivated in the working memory 2BK-0BK contrast (Panel E). Relative to area PHA1 posteriorly, the **EC** has more myelin (Panel B), is thinner (Panel C), and is less activated in

the LANGUAGE STORY-MATH (Panel G) and SOCIAL TOM-RANDOM (Panel H) contrasts. Our area EC overlaps extensively with probabilistic EC from (Fischl et al., 2009) (Panel O).

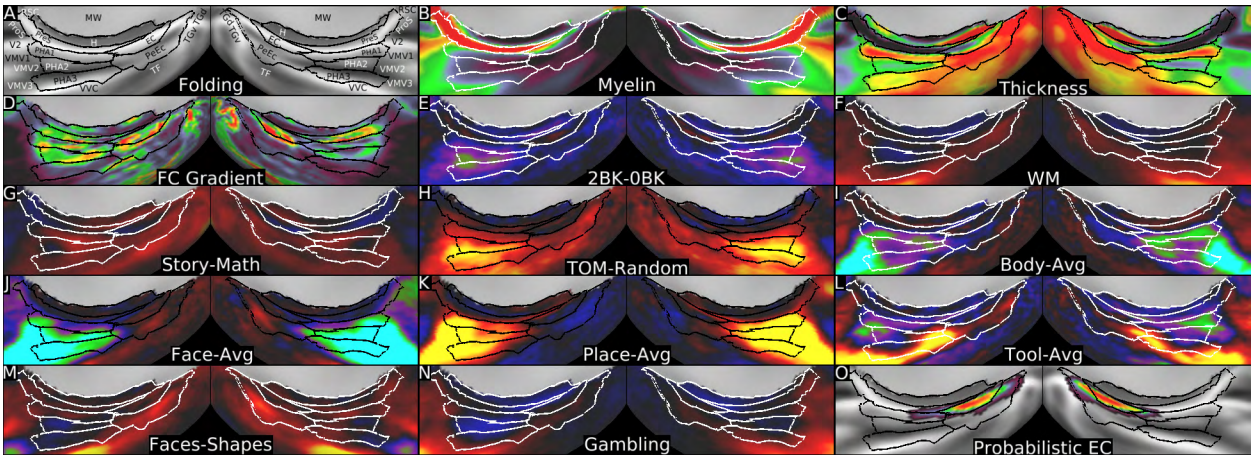

Figure 15 shows the multi-modal information used to parcellate the medial temporal cortex. Panel A shows the areas on a folding map. Panels B and C show the myelin and cortical thickness maps. Panel D shows the resting state functional connectivity gradient. Panels E and F show the working memory 2BK-0BK and an example working memory primary contrast. Panels G and H show the LANGAUGE STORY-MATH contrast and the SOCIAL TOM-RANDOM contrast. Panels I, J, K, and L show the categories contrasts, BODY-AVG, FACE-AVG, PLACE-AVG, and TOOL-AVG. Panels M and N show the EMOTION FACES-SHAPES contrast and the GAMBLING primary contrast. Panel O shows the probabilistic map of the entorhinal cortex (EC) from (Fischl et al., 2009). Data at http://balsa.wustl.edu/QXDP.

We were unable to reliably distinguish between the peri-entorhinal cortex (BA 35) and the ectorhinal cortex (BA 36), which together we identified as the **PeEc** complex, located outside of the entorhinal cortex (Augustinack et al., 2013; Ding et al., 2009). Relative to its anterior neighbor area TGd, **PeEc** is thicker (Panel C) and differs in functional connectivity (Panel D). Relative to its antero-inferior neighbor TGv, area **PeEc** has more myelin (Panel B) and is more activated in the working memory (Panel F) and relational primary task contrasts. Relative to its inferior neighbor TF, area **PeEc** has less myelin (Panel B), is thicker (Panel C), and has greater activation in the working memory primary contrasts (Panel F). Relative to its postero-inferior neighbor PHA3, area **PeEc** has less myelin (Panel B), is thicker (Panel C), is modestly less deactivated in the working memory 2BK-0BK contrast (Panel E), less deactivated in the BODY-AVG contrast (Panel I), activated vs deactivated in the FACE-AVG contrast (Panel J), deactivated vs activated in the PLACE-AVG contrast (Panel K), less activated in the TOM-RANDOM contrast (Panel H), and more activated in the FACES-SHAPES contrast (Panel M). Relative to its posterior neighbor PHA2, area **PeEc** is much thicker (Panel C) and differs in task activations similar to those just described for PHA3. Relative to its postero-medial neighbor PHA1, area **PeEc** is slightly thicker (Panel C) and is deactivated vs activated in the PLACES-AVG contrast (Panel K) and more activated in the GAMBLING primary contrasts (Panel N). The PeEc may be the site of the anterior temporal face patch (ATFP, AFP1) (Rajimehr et al., 2009; Tsao et al., 2008), given its activation in the FACE-AVG and FACES-SHAPES contrasts.

Relative to its medio-inferior neighbor PHA2, area **PHA1** is dramatically thicker (Panel C) and is less deactivated in the FACE-AVG contrast (Panel J). Relative to its inferior neighbor PHA3, area **PHA2** has less myelin (Panel B), is thinner (Panel C), and differs in

functional connectivity (Panel D). Relative to its antero-medial neighbor TF, area **PHA3** differs in functional connectivity (Panel D), is deactivated vs activated in the BODY-AVG (Panel I) and FACE-AVG (Panel J) contrasts, and is activated vs deactivated in the PLACE-AVG (Panel K) and TOOL-AVG (Panel L) contrasts. The borders of the PHA 1-3 areas with areas VMV1-3 and the VVC were covered in Section #4 Ventral Stream Visual Cortex.

14. Lateral Temporal Cortex

Lateral temporal cortex has expanded dramatically over the course of human evolution (Glasser et al., 2014; Hill et al., 2010). We identified nine areas in lateral temporal cortex and the temporal pole that are architecturally lightly myelinated, thick, and functionally multi-modal, and many are involved in the task negative network. The nine areas include PHT, TE1p, TE1m, TE1a, TE2p, TE2a, TGv, TGd, and TF. They are surrounded mainly by auditory and visual association areas, including STGa, STSda, STSva, STSvp, TPOJ1, TPOJ2, FST, PH, FFC, VVC, PHA3, PeEc, Pir, and PI. Figure 16 shows multi-modal information used to parcellate the lateral temporal cortex, and the areas on a folding map (Panel A). The area names in this region generally reflect correspondences with the Von Economo and Koskinas temporal lobe parcellation (Triarhou, 2007a, b; von Economo and Koskinas, 1925), but for several of their areas, we identified subdivisions along the anterior-posterior axis.

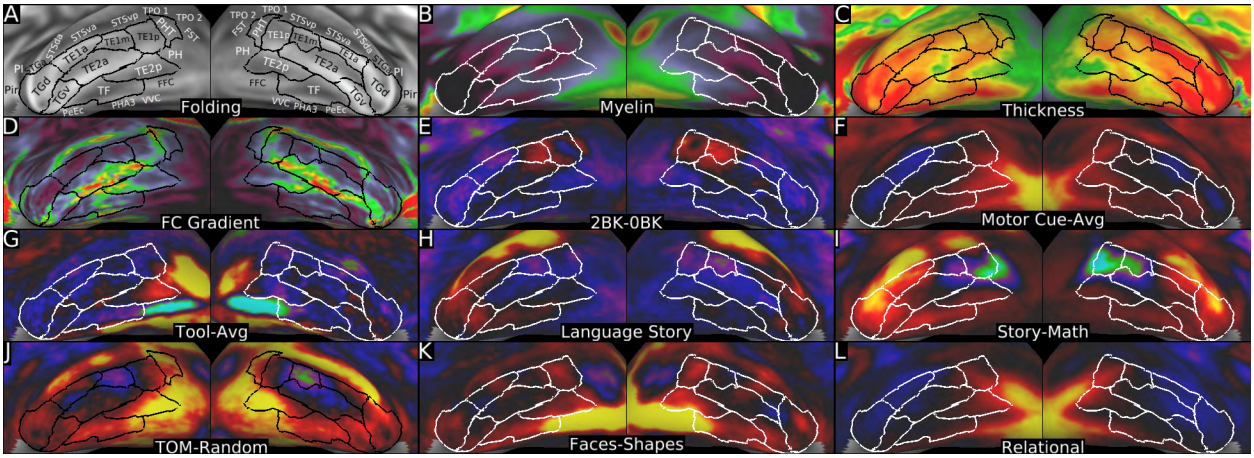

Figure 16 shows multimodal information used to parcellate the lateral and polar temporal cortex. Panel A shows the areas on a folding map. Panels B and C show the myelin map and cortical thickness map. Panel D shows the functional connectivity gradient. Panels E, F, and G show the working memory 2BK-0BK contrast, the MOTOR CUE-AVG contrast, and the categories TOOL-AVG contrast. Panels H and I show the LANGUAGE STORY and STORY-MATH contrasts. Panels J, K, and L show the SOCIAL TOM-RANDOM contrast, the EMOTION FACE-SHAPES contrast, and a RELATIONAL primary contrast. Data at http://balsa.wustl.edu/W8rz.

The temporal polar cortex was divided into two areas, **TGd** and **TGv**. Both are very lightly myelinated (Panel B) and thick (Panel C) relative to their neighbors. The superior (Pir, PI, STGa) and inferior borders (PeEc) of these areas were described already (Sections #12 Insular and Frontal Opercular Cortex insular, #11 Auditory Association Cortex, and #13 Medial Temporal Cortex). Relative to its inferior neighbor TGv, area **TGd** differs in functional connectivity (Panel D) and is deactivated vs activated in the MOTOR CUE-AVG

contrast (Panel F) and the RELATIONAL primary contrasts (Panel L). Relative to its posterior neighbor TE1a, area **TGd** differs modestly in functional connectivity (Panel D) and is more activated in the TOM-RANDOM contrast (Panel J). There is also a gradual decrease in myelin content progressing from the back of TE1a to **TGd** (Panel B). Relative to its infero-posterior neighbor TE2a, area **TGd** has less myelin (Panel B), is thicker (Panel C), differs in functional connectivity (Panel D), is deactivated vs weakly activated in the working memory 2BK-0BK (Panel E) and MOTOR CUE-AVG (Panel F) contrasts, and is more activated in the STORY-MATH contrast (Panel I). Relative to its posterior neighbor TE2a, area **TGv** is thicker (Panel C), differs in functional connectivity (Panel D), and is more activated in the MOTOR CUE-AVG (Panel F), LANGUAGE STORY (Panel H), and TOM-RANDOM (Panel J) contrasts. Relative to its infero-posterior neighbor TF, area **TGv** has less myelin (Panel B), is thicker (Panel C), and is less deactivated in the LANGUAGE MATH contrast.

Posterior to temporal polar cortex are three areas in the inferior temporal sulcus and gyrus, **TF**, **TE2a**, and **TE2p**. **TF's** anterior, medial (PeEc and PHA3), and posterior boundaries (FFC and VVC) have already been covered (above and Sections #4 Ventral Stream Visual Cortex and #13 Medial Temporal Cortex). Relative to its lateral-superior neighbor TE2a, area **TF** has more myelin (Panel B), differs in functional connectivity (Panel D), and is more activated in the MOTOR CUE-AVG (Panel F), LANGUAGE STORY (Panel H), and the TOM-RANDOM (Panel J) contrasts. Relative to its posterior neighbor TE2p, area **TF** differs in functional connectivity (Panel D) and is more activated in the LANGUAGE STORY (Panel H) and FACE-AVG contrasts (both more prominent on the left than the right). Relative to its antero-lateral neighbor TE2a, area **TE2p** has more myelin, differs in functional connectivity (Panel D), and is more activated in the CUE-AVG (Panel F) and the TOM-RANDOM (Panel J) contrasts. Because of noisier gradients in this region (near the temporal lobe susceptibility artifact), the automated border optimizer's penalty for taking circuitous paths was increased for this border. Relative to supero-lateral neighbor TE1a, area **TE2a** has more myelin (Panel B), is thinner (Panel C), differs in functional connectivity (Panel D), is weakly activated vs strongly deactivated in the working memory 2BK-0BK (Panel E) and MOTOR CUE-AVG (Panel F) contrasts, deactivated vs activated in the LANGUAGE STORY contrast (Panel H), and less activated in the LANGUAGE STORY-MATH contrast (Panel I). Relative to supero-lateral neighbor TE1m, area **TE2a** has less myelin (Panel B), is less activated in the working memory 2BK-0BK contrast (Panel E), less deactivated the LANGUAGE STORY contrast (Panel H), and less deactivated in the TOM-RANDOM contrast (Panel J). Relative to postero-superior neighbor TE1p, **TE2a** has less myelin (Panel B), differs in functional connectivity (Panel D), is less activated in the CUE-AVG (Panel F) and RELATIONAL-MATCH contrasts, less deactivated in the LANGUAGE STORY-MATH contrast (Panel I), and more activated in the FACES-SHAPES contrast (Panel K). Relative to medial neighbor TE1p, area **TE2p** differs in functional connectivity (Panel D), is deactivated vs activated in the working memory 2BK-0BK contrast (Panel E), activated vs strongly deactivated in the LANGUAGE STORY-MATH contrast (Panel I), and more activated in the TOM-RANDOM contrast (Panel J). Notably, area **TE2p** is activated in the TOOL-AVG contrast in the left hemisphere but deactivated in the right hemisphere (Panel G).

The middle temporal gyrus includes four areas, **TE1a**, **TE1m**, **TE1p**, and **PHT**. The first three are strongly associated with the task negative network, whereas PHT is strongly

associated with the task positive network. The inferior and anterior borders of these areas were covered above, and their posterior borders (FST and PH) and superior (STSva and STSvp) were covered previously (Sections #5 MT+ Complex and Neighboring Visual Areas and #11 Auditory Association Cortex). Relative to posterior neighbor TE1m, area **TE1a** has less myelin (Panel B), is thicker (Panel C), differs in functional connectivity (Panel D), is deactivated vs activated in many primary task contrasts (e.g. RELATIONAL Panel L) and in the working memory 2BK-0BK (Panel E) and the MOTOR CUE contrasts, and is more activated in the LANGUAGE STORY-MATH contrast (Panel I). Relative to posterior neighbor TE1p, area **TE1m** differs in functional connectivity (Panel D), is less activated in the MOTOR CUE-AVG (Panel F) and FACES-SHAPES (Panel K) contrasts, and is more deactivated in the TOM-RANDOM contrast (Panel J). Relative to posterior neighbor PHT, area **TE1p** differs markedly in functional connectivity (Panel D), is less activated in the BODY-AVG and SOCIAL TOM contrasts, deactivated vs activated in the MOTOR AVG contrast, and activated vs deactivated in the FACES-SHAPES contrast (Panel K). Relative to areas TPOJ1 and TPOJ2 supro-medially, area **PHT** has less myelin (Panel B), differs in functional connectivity (Panel D), is deactivated vs activated in the FACE-AVG contrast, and is less activated in the MOTOR AVG contrast.

15. Temporo-Parieto-Occipital Junction

We identified the temporo-parieto-occipital junction as a strip of cortex bounded by auditory, lateral temporal, inferior parietal and occipital (visual MT+ complex) regions. This region contains five multimodal areas, TPOJ1, TPOJ2, TPOJ3, STV, and PSL, that are surrounded by areas PGp, PGi, PFm, PF, PFcm, RI, A4, A5, STSdp, STSvp, PHT, FST, MST, MT, and LO3. Areas TPOJ1-3 are moderately myelinated and show strong functional connectivity among themselves and with STV. They form a bridge between higher auditory and higher visual areas, as they are correlated with both. Figure 17 shows the multi-modal information used to parcellate these areas, along with the areas on a folding map (Panel A). All five areas have novel names, as these areas to do not clearly correspond with previous parcellations of this region.

The anterior and inferior borders of areas **TPOJ2** and **TPOJ3** have previously been described previously (Sections #5 MT+ Complex and Neighboring Visual Areas, #11 Auditory Association Cortex, and #14 Lateral Temporal Cortex). Relative to its posterior neighbor PGp, area **TPOJ3** has more myelin (Panel B), is thinner (Panel C, especially on the left), differs in functional connectivity (Panel D), is activated vs deactivated in the working memory 2BK-0BK and BODY-AVG (Panel M) contrasts, weakly activated vs strongly deactivated in the FACE-AVG contrast, weakly deactivated vs strongly activated in the PLACE-AVG contrast, and strongly activated vs weakly activated or deactivated in the FACES-SHAPES contrast (Panel O). Relative to its superior neighbor PGi, area **TPOJ3** has more myelin (Panel B), is thinner (Panel C), differs strongly in functional connectivity (Panel D), is more activated in primary task contrasts (e.g., Panel J), the BODY-AVG contrast (Panel M), the MOTOR CUE contrast (Panel K), and is less activated in the LANGUAGE STORY (Panel H) and STORY-MATH (Panel I) contrasts. Relative to its anterior neighbor TPOJ2, area **TPOJ3** is thinner (Panel C), more activated in the working memory 2BK-0BK contrast, less activated in the RELATIONAL primary contrast (Panel J), MOTOR AVG (Panel L), and FACES-SHAPES (Panel O) contrasts. Relative to its superior neighbor PGi, area

TPOJ2 has more myelin (Panel B), differs strongly in functional connectivity (Panel D), and is more activated in primary task contrasts (e.g., Panel J), the BODY-AVG contrast (Panel M), the MOTOR CUE contrast (Panel K), and is less activated in the LANGUAGE STORY (Panel H) and STORY-MATH (Panel I) contrasts. Relative to its anterior neighbor TPOJ1, area **TPOJ2** is thinner (Panel C), differs in functional connectivity (Panel D), is more activated in the BODY-AVG contrast (Panel M), is deactivated in the PLACE-AVG contrast, and is deactivated vs activated in the LANGUAGE STORY contrast (Panel H).

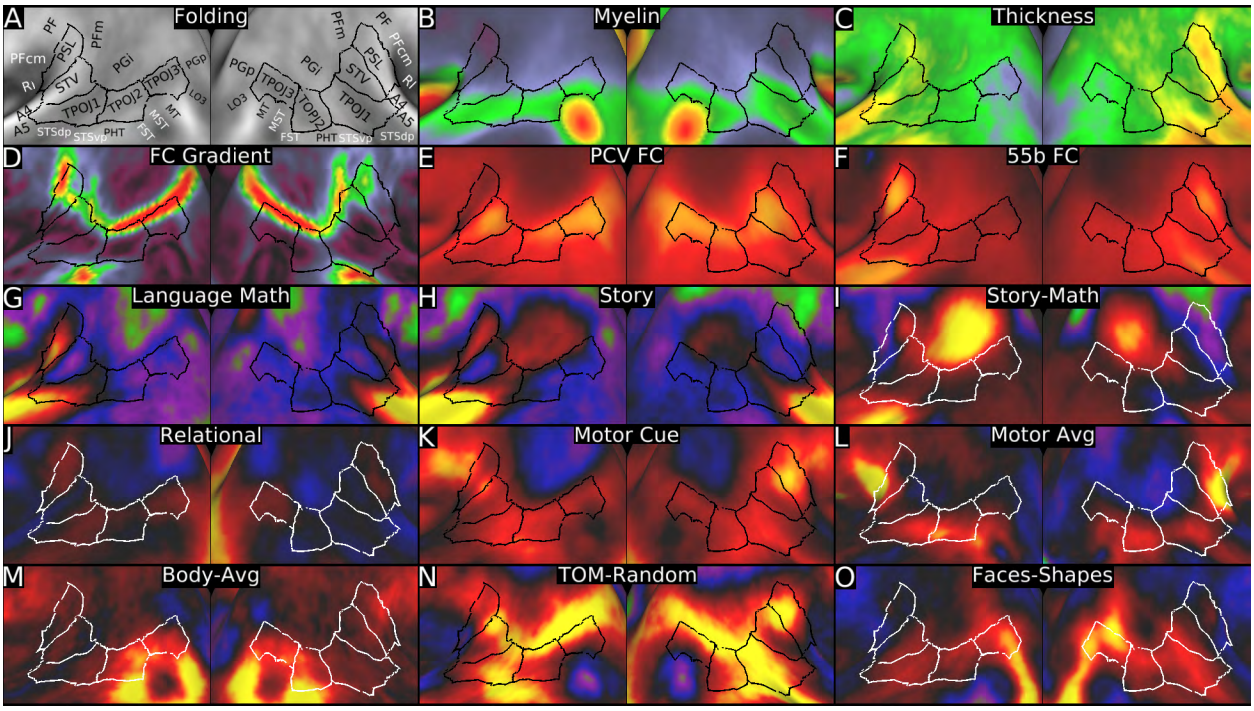

Figure 17 shows multi-modal information used to parcellate the cortex of the temporo-parieto-occipital junction. Panel A shows the five areas on a group average folding map. Panels B and C show the myelin and thickness maps. Panel D shows the overall resting state functional connectivity gradient. Panel E shows the functional connectivity map from seeding area PCV bilaterally. Panel F shows the functional connectivity map from seeding area 55b unilaterally (seeding left 55b shown on the left and seeding right 55b shown on the right). Panels G, H, and I show the LANGUAGE MATH, STORY, and STORY-MATH task fMRI contrasts. Panels J, K, and L show a RELATIONAL primary contrast, the MOTOR CUE contrast, and the MOTOR AVG contrast. Panels M, N, and O show the BODY-AVG contrast, the TOM-RANDOM contrast, and the FACES-SHAPES contrast. Data at http://balsa.wustl.edu/WKkq.

Relative to its postero-superior neighbor PGi, **TPOJ1** has more myelin (Panel B), differs in functional connectivity (Panel D), and is more activated in primary task contrasts (e.g. Panel J), the MOTOR CUE (Panel K) and MOTOR AVG (Panel L) contrasts, and less activated in the LANGUAGE STORY-MATH contrast (Panel I). **TPOJ1's** border with PHT was covered previously (Section #14 Lateral Temporal Cortex). In the right hemisphere relative to inferior neighbor STSvp, area **TPOJ1**, has more myelin (Panel B) and differs in functional connectivity (Panel D). Relative to its inferior neighbor STSdp, area **TPOJ1** has more myelin (Panel B), differs in functional connectivity (Panel D), and is more activated in the MOTOR AVG (Panel L, more on the left than the right) and the FACES-SHAPES (Panel O) contrasts and less activated in the LANGUAGE STORY-MATH contrast (Panel I). Relative to

anterior neighbor A5, area **TPOJ1** has more myelin (Panel B), differs in functional connectivity (Panel D), is deactivated vs activated in the TOOL-AVG contrast, more activated in the MOTOR CUE (Panel K) contrast, less activated in the STORY-MATH (Panel I) contrast, and activated vs deactivated in the TOM-RANDOM (Panel N) and FACES-SHAPES (Panel O) contrasts. Relative to its supero-anterior neighbor A4, area **TPOJ1** differs in functional connectivity (Panel D), is more activated in the MOTOR CUE contrast (Panel K), activated vs deactivated in the FACE-AVG, TOM-RANDOM (Panel N) and FACES-SHAPES (Panel O) contrasts, and deactivated vs activated in the TOOL-AVG contrast. The border of **TPOJ1** with STV will be discussed below. Unlike areas TPOJ2 and TPOJ3, area **TPOJ1** is both larger and more heavily myelinated in the right hemisphere (Panel B).

The remaining two areas in this region, **STV** (Superior Temporal Visual area) and **PSL** (Peri-Sylvian Language area) have several distinctive features in addition to the typical multi-modal gradients used to define other cortical areas. In terms of functional connectivity, STV is strongly connected with PCV (Posterior Cingulate Visual area, used as a bilateral seed in Panel E), and gradients from the functional connectivity map seeded from area PCV in both hemispheres were used in its definition. Similarly, gradients from the functional connectivity map seeded from unilateral area 55b (Panel F) were used to help define PSL. PSL also contains an anterior to posterior topographic organization of connectivity (which is also present in areas 55b, SFL, and 44, see Figure 18). In contrast to most other regions, there are prominent asymmetries of some features for these two areas. Below, the criteria used for the left and right hemispheres are described separately when it improves clarity.

The border between **STV** and area A4 is moderately long in the left hemisphere, but almost nonexistent on the right. In the **left** hemisphere, **STV** is more connected with PCV than is area A4 (Panel E), is deactivated vs activated in the TOOL-AVG, LANGUAGE MATH and STORY (Panels G and H) contrasts, more activated in the MOTOR CUE-AVG contrast, and activated vs deactivated in the SOCIAL primary contrasts and the TOM-RANDOM contrast (Panel N). Relative to inferior neighbor TPOJ1 in **both** hemispheres, **STV** has less myelin (Panel B), has stronger functional connectivity with the PCV (Panel E), and is deactivated vs activated in the LANGUAGE MATH and STORY contrasts (Panels G and H). In the **left** hemisphere, STV is less activated than TPOJ1 in the GAMBLING primary contrasts and the MOTOR AVG contrast (Panel L). In the **right** hemisphere, STV is less activated than TPOJ1 in the TOM-RANDOM contrast (Panel N). Relative to its posterior neighbor PGi in **both** hemispheres, **STV** differs strongly in functional connectivity (Panel D) and is less activated in the LANGUAGE STORY and STORY-MATH contrasts (Panels H and I) and more activated in the SOCIAL RANDOM contrast. Relative to its posterior neighbor PFm in **both** hemispheres, **STV** differs strongly in functional connectivity (Panel D) and is more activated in the SOCIAL primary contrasts. Relative to its superior neighbor PSL in **both** hemispheres, area **STV** is deactivated vs activated in the working memory primary contrasts, the MOTOR AVG contrast (Panel L), the LANGUAGE MATH (Panel G) and STORY (Panel H, left hemisphere only) contrasts, and the RELATIONAL primary contrasts (e.g. Panel J). **STV** also has stronger functional connectivity with PCV (Panel E), whereas **PSL** has stronger functional connectivity with 55b in the corresponding hemisphere (Panel F).

Relative to its antero-inferior neighbor A4, area **PSL** has stronger functional connectivity with area 55b (Panel F), is activated vs deactivated in the primary contrasts (e.g. Panel J), deactivated vs activated in the TOOL-AVG contrast, and more activated in the

MOTOR AVG (Panel L). Relative to its supero-posterior neighbor PFm, area **PSL** has stronger functional connectivity with area 55b (Panel F), is more activated in the LANGUAGE MATH and STORY contrasts (Panels G and H in the left hemisphere), the MOTOR CUE (Panel K) and TOM-RANDOM (Panel N in the right hemisphere) contrasts, and the relational primary contrasts in both hemispheres (e.g. Panel J). The left **PSL** is more activated in the RELATIONAL-MATCH contrast relative to the right hemisphere **PSL**, and it is much thicker on the right than the left (Panel C). Relative to its supero-anterior neighbor PF, area **PSL** has stronger functional connectivity with area 55b (Panel F) and is less activated in the MOTOR CUE contrast on the left (Panel K, but not on the right), more activated in the LANGUAGE MATH and STORY contrast (Panels G and H, less deactivated on the right), and more activated in the TOM-RANDOM contrast in the right but not the left (Panel N). Thus, area PSL is one of a handful of strikingly functionally lateralized areas in the cerebral cortex, having a number of left/right task activation differences and belonging to the strongly lateralized language network (see Figure 18).

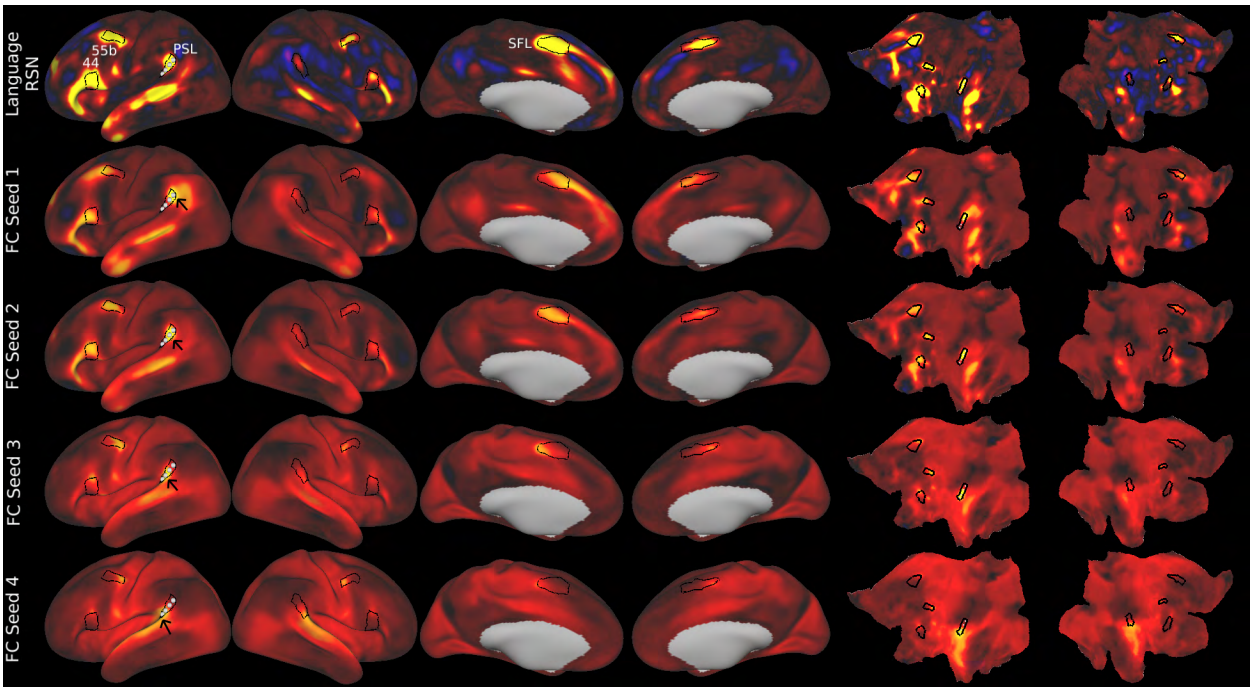

Figure 18 shows the topographic organization of the language network (Row 1 d=40 ICA RSN). Four seeds are placed along the anterior-posterior axis of area PSL in the left hemisphere (marked by black arrows from posterior to anterior). The functional connectivity pattern shows corresponding changes in the other major nodes of the language network, including 55b, SFL, and 44. The pattern is present when seeded in either hemisphere, but stronger in the left hemisphere. Data at http://balsa.wustl.edu/WNrX.

Area PSL**,** along with areas 55b, SFL, and 44, also shows topographic organization of functional connectivity along its anterior to posterior axis as illustrated in Figure 18. Row 1 shows a left-lateralized language RSN, with areas PSL, 55b, 44, and SFL outlined in white. Seed locations in left area PSL (black arrows) progressing from posterior (row 2) to anterior (rows 3 – 5) are associated with elevations in FC that progress from anterior to posterior in area 55b, inferior to superior in area 44, and anterior to posterior in area SFL in both hemispheres but more prominently on the left. In both hemispheres PSL appears in

a reasonably corresponding geographic location near the supero-posterior tip of the Sylvian fissure and extending onto the superior temporal gyrus (especially on the right), and it is functionally connected with a corresponding set of areas in each hemisphere.

16. Superior Parietal Cortex

The superior parietal region has some parallels to the cortex of the temporo-parieto-occipital junction, insofar as it lies between two major sensory modalities (in this case visual and somatosensory domains) and forms a bridge between these modalities. We include in the superior parietal region the medial bank of the intra-parietal sulcus (IPS) and superior medial parietal cortex and divided this region into ten areas: LIPv, LIPd, VIP, AIP, MIP, 7PC, 7AL, 7Am, 7PL, and 7Pm. These areas are surrounded by areas IP0, IP1, IP2, PFm, PF, PFt, 2, 5L, PCV, 7m, POS2, DVT, and IPS1. Figure 19 shows the multi-modal information used in parcellating the superior parietal cortex, with Panel A showing the areas on a folding map.

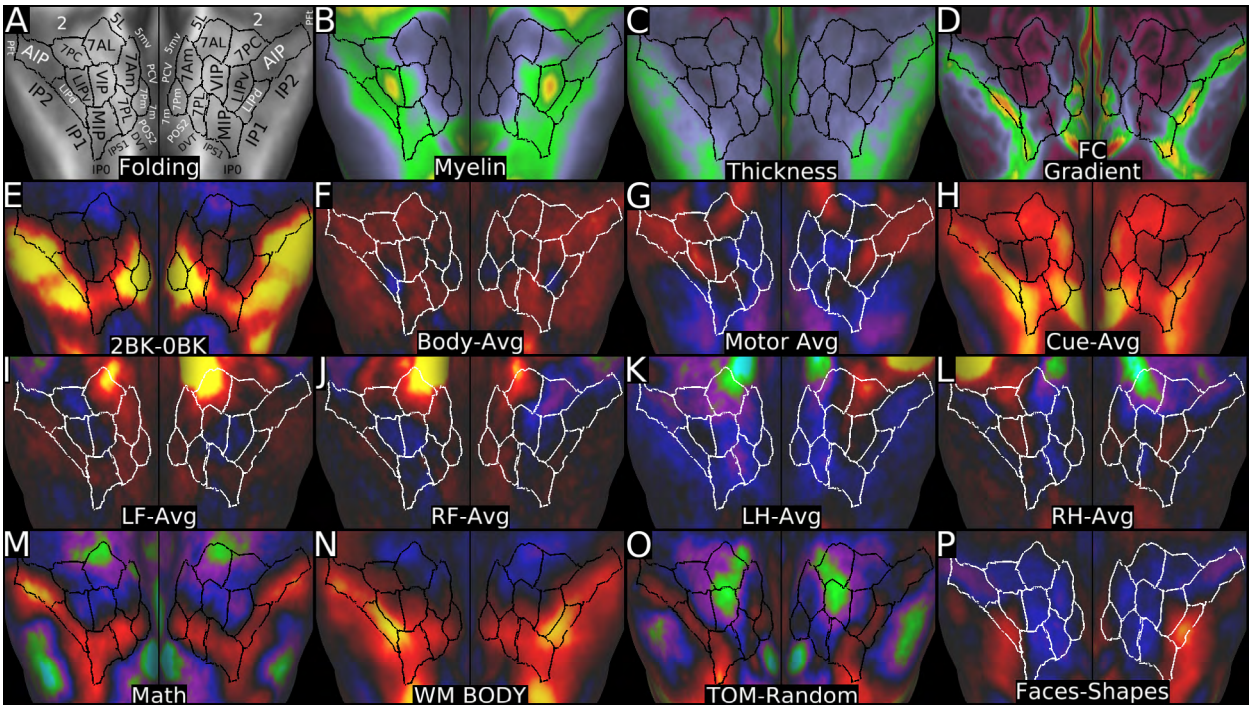

Figure 19 shows multi-modal information used in parcellating the superior parietal cortex. Panel A shows the areas on a group average folding map. Panels B and C show the myelin map and the cortical thickness map. Panel D shows the functional connectivity gradient. Panels E, F, G, and H show the working memory 2BK-0BK contrast, the BODY-AVG contrast, the MOTOR AVG contrast, and the MOTOR CUE-AVG contrast. Panels I, J, K, and L show the MOTOR LF-AVG, RF-AVG, LH-AVG, and RH-AVG contrasts. Panels M, N, O, and P show the LANGUAGE MATH, a working memory primary contrast, TOM-RANDOM contrast, and FACES-SHAPES contrast. Data at http://balsa.wustl.edu/RGGM.

Area **MIP** separates a more posterior region of the dorsal stream visual cortex from a more anterior region (containing putative homologues of macaque LIPv and VIP). We identified it as **MIP** because it is a candidate homologue of macaque **MIP**, lying between the putative LIP/VIP homologues and more posterior visual regions (Van Essen et al., 2012a).

MIP has strong functional connectivity with other areas along the medial bank of the IPS (e.g. LIPd and AIP) and less connectivity with either the posterior (e.g. IPS1, V7, V3A) or anterior portions (LIPv, VIP) of the dorsal visual stream. Area **MIP's** posterior border with IPS1 was covered previously (see Section #3 Dorsal Stream Visual Cortex). Relative to its anterior neighbors LIPv and VIP, area **MIP** is thicker (Panel C), differs in functional connectivity (Panel D), is more activated in the working memory 2BK-0BK contrast (Panel E), the MOTOR CUE-AVG contrast (Panel H), the LANGUAGE MATH (Panel M) and MATH-STORY contrasts, and the TOM-RANDOM contrast (Panel O). **MIP** also has less myelin than LIPv (Panel B). Relative to its medial neighbor 7PL, area **MIP** has more myelin (Panel B), is less activated in the working memory 2BK-0BK contrast (Panel E), more deactivated in the FACE-AVG contrast, and more activated in the TOOL-AVG and TOM-RANDOM (Panel O) contrasts. Relative to inferior neighbor IP0, **MIP** is thinner (Panel C) and differs in functional connectivity (Panel D). Relative to its lateral neighbor IP1, **MIP** has more myelin and is thinner (Panels B and C), differs strongly in functional connectivity (Panel D), is more deactivated in the FACE-AVG contrast, and is more activated in the TOOL-AVG, SOCIAL TOM, TOM-RANDOM (Panel O), and EMOTION SHAPES contrasts. Relative to its antero-lateral neighbor LIPd, **MIP** has less myelin (Panel B), differs in functional connectivity (Panel D), is less activated in the working memory and gambling primary contrasts, more activated in the BODY-AVG (Panel F) contrast, and deactivated vs activated in the FACE-AVG and FACES-SHAPES (Panel P) contrasts.

The **LIPv/VIP** complex is distinct from its neighbors both architecturally and functionally. The area names reflect a presumed homology with correspondingly named areas in the macaque, even though LIPv is on the lateral bank of the IPS in the macaque (where it is ventral to LIPd) but is on the medial bank of the IPS in humans. Thus, LIPv lies supero-medial to LIPd, reflecting the overall medial shift of parietal visual regions in humans compared to macaques. **LIPv** is heavily myelinated and **VIP** is moderately myelinated (Panel B). Both areas have much stronger functional connectivity with higher dorsal stream visual areas than do their neighbors, and they also have a distinct pattern of functional activation. Because of high intersubject variability of areal boundaries relative to cortical folds and the folding patterns themselves, this region benefits especially from areal-feature-based registration (the myelin maps presented here are much sharper than those made with folding-based registration in (Glasser and Van Essen, 2011), for example). The putative homologies are based on myelin maps that have been analyzed in macaques, chimpanzees, and humans showing a corresponding hotspot of increased myelin content in the IPS (Glasser et al., 2014). Relative to its inferolateral neighbor LIPd, area **LIPv** has more myelin, is thinner (Panels B and C), differs in functional connectivity (Panel D), is less activated in the working memory 2BK-0BK (Panel E), FACE-AVG, CUE-AVG (Panel H), LANGUAGE MATH (Panel M) and MATH-STORY contrasts, and is deactivated vs activated in the TOM-RANDOM contrast (Panel O). Relative to its anterior neighbor AIP, area **LIPv** has more myelin (Panel B), is thinner (Panel C), differs in functional connectivity (Panel D), is less activated in the working memory 2BK-0BK (Panel E), CUE-AVG (Panel H), LANGUAGE MATH (Panel M) and MATH-STORY contrasts, and is more deactivated in the TOM-RANDOM (Panel O) and RELATIONAL-MATCH contrasts. Relative to its anterior neighbor 7PC, area **LIPv** has more myelin (Panel B), is thinner (Panel C), differs in functional connectivity (Panel D), is less activated in the MOTOR CUE-AVG contrast (Panel H), but is more activated in the ipsilateral ?H-AVG contrast (Panels K and L). Relative to its medial

neighbor VIP, **LIPv** has more myelin (Panel B), differs modestly in functional connectivity (Panel D), is less activated in the working memory 2BK-0BK contrast (Panel E, more so on the right than the left), more activated in the MOTOR AVG (Panel G), ipsilateral ?H-AVG hand motor (Panels K and L), and FACES-SHAPES (Panel P) contrasts, and is less activated in the T-AVG face motor and SOCIAL RANDOM contrasts. Relative to its anterior neighbor 7AL, area **VIP** is has more myelin (Panel B), differs in functional connectivity (Panel D), is less activated in the MOTOR CUE and MOTOR AVG (Panel G) contrasts, and more activated in the EMOTION primary contrasts. Relative to its medial neighbor 7Am, area **VIP** has more myelin (Panel B), differs in functional connectivity (Panel D), is less activated in the MOTOR CUE-AVG contrast (Panel H), and more deactivated in the TOM-RANDOM contrast (Panel P). Relative to its postero-medial neighbor 7PL, area **VIP** has more myelin (Panel B), differs in functional connectivity (Panel D), is less activated in the working memory 2BK-0BK (Panel E), MOTOR CUE-AVG (Panel H), and LANGUAGE MATH (Panel M) and MATH-STORY contrasts, and is more deactivated in the TOM-RANDOM contrast (Panel O). We previously suggested (Glasser and Van Essen, 2011) that cytoarchitectonic area hIP3 (Scheperjans et al., 2008a; Scheperjans et al., 2008b) might overlap with the heavily myelinated patch now identified as LIPv (and perhaps also part of area LIPd), but confirmation would require surface based (and ideally areal feature-based alignment) of the post-mortem cytoarchitectonic data.

Areas **LIPd** and **AIP** are named after putative homologues in the macaque (Van Essen et al., 2012a), in part based on their relationship to the LIPv/VIP complex just discussed. **LIPd** is a moderately myelinated area inferolateral to area LIPv (Panel B). Relative to its lateral neighbors IP1 and IP2, **LIPd** differs strongly in functional connectivity (Panel D), is deactivated vs activated in the BODY-AVG contrast (Panel F), activated vs deactivated in the PLACE-AVG contrast, more activated in the MOTOR CUE and TOM-RANDOM contrasts (Panel O), and less activated in the RELATIONAL-MATCH contrast. Also **LIPd** was statistically more activated than IP1 and IP2 in the working memory (e.g. Panel N), gambling, and relational primary contrasts. Relative its anterior neighbor AIP, **LIPd** has more myelin (Panel B), differs in functional connectivity (Panel D), is less activated in the BODY-AVG (Panel F) and MOTOR AVG (Panel G) contrasts, more activated in the PLACE-AVG and MOTOR CUE-AVG (Panel H) contrasts, and activated vs deactivated in the FACES-SHAPES contrast (Panel P). Relative to its infero-lateral neighbor IP2, area **AIP** differs in functional connectivity (Panel D), is more activated in SOCIAL and EMOTION primary task contrasts and in the MOTOR CUE contrast, less deactivated in the FACE-AVG and LANGUAGE STORY contrasts, and more deactivated in the FACES-SHAPES contrast (Panel P). Relative to its anterior neighbor PFt, area **AIP** has more myelin (Panel B) and is more activated in several primary contrasts (e.g. Panel N). Relative to its medial neighbor 7PC, area **AIP** differs in functional connectivity (Panel D), is more activated in the primary contrasts (e.g. Panel N) and the working memory 2BK-0BK contrast (Panel E), and is deactivated vs activated in the contralateral ?H-AVG hand motor contrasts (Panels K and L).

The posterior, lateral, and anterior borders of area **7PC** have previously been covered (above and Section #6 Somatosensory and Motor Cortex). Relative to its anterior and posterior neighbors LIPv and area 2, area **7PC** has less myelin (Panel B) and has stronger functional connectivity with somatosensory area 2 than with more visually related LIPv. We assigned this name based on its location antero-lateral to areas hIP3 and

7A (Scheperjans et al., 2008a; Scheperjans et al., 2008b). Relative to its medial neighbor 7AL, area **7PC** has more myelin (Panel B), differs in functional connectivity (Panel D), is less activated in the MOTOR CUE and bilateral ?F-AVG foot MOTOR contrasts (Panels I and J), more activated in bilateral ?H-AVG hand MOTOR contrasts (Panels K and L), and less deactivated in the TOM-RANDOM contrast (Panel O). We identified medial and lateral subdivisions **7Am** and **7AL** of area 7A (though our area VIP may also overlap with the region identified as 7A by (Scheperjans et al., 2008a; Scheperjans et al., 2008b) and the anterior corner of **7AL** may overlap with 5L as well). Most of **7AL's** borders have already been covered (above and Sections #6 Somatosensory and Motor Cortex and #7 Paracentral Lobular and Mid Cingulate Cortex). Relative to posterior neighbor VIP and anterior neighbor area 2, area **7AL** has less myelin but is comparable in myelin content to its medial neighbors 5L and 7Am (Panel B). Its strongest distant functional connectivity is with superior premotor cortex. Relative to its medial neighbor 7Am, area **7AL** has slightly more myelin (Panel B), differs in functional connectivity (Panel D), is more activated in the MOTOR AVG contrast (Panel G) and more deactivated in the TOM-RANDOM contrast (Panel O). Area **7Am's** border with 5L has been covered previously (Section #7 Paracentral Lobular and Mid Cingulate Cortex). Relative to its infero-medial neighbor PCV, area **7Am** has less myelin (Panel B), is thinner (Panel C), differs in functional connectivity (Panel D), is more activated in the working memory 2BK-0BK (Panel E), MOTOR CUE-AVG (Panel H), and MATH-STORY contrasts (Panel M), and is activated vs deactivated in the FACES-SHAPES contrast (Panel P). Relative to its postero-lateral neighbor 7PL, area **7Am** has less myelin (Panel B), differs in functional connectivity (Panel D), is less activated in the primary contrasts (e.g. Panel N), working memory 2BK-0BK (Panel E), and LANGUAGE MATH (Panel M) and MATH-STORY contrasts. Relative to its postero-medial neighbor 7Pm, area **7Am** is thinner (Panel C), differs in functional connectivity (Panel D), is less activated in the working memory 2BK-0BK contrast (Panel E), deactivated vs activated in the RELATIONAL-MATCH contrast, and more deactivated in the FACES-SHAPES contrast (Panel P).

We identified medial and lateral areas **7Pm** and **7PL** within the region identified as area 7P by (Scheperjans et al., 2008a; Scheperjans et al., 2008b), lying posterior to 7A, medial to the intra-parietal sulcus (IPS), anterior to the partieto-occipital sulcus (POS), and superior to 7m. Relative to its anterior neighbor PCV, area **7Pm** has less myelin (Panel B), differs in functional connectivity (Panel D), is more activated in the working memory 2BK-0BK (Panel E), LANGUAGE MATH (Panel M), MATH-STORY, and RELATIONAL-MATCH contrasts, and is deactivated vs activated in the BODY-AVG contrast (Panel F). Relative to its inferior neighbor 7m, area **7Pm** differs in functional connectivity (Panel D), is deactivated vs activated in the BODY-AVG contrast (Panel F), less activated in the FACE-AVG and FACES-SHAPES (Panel P) contrasts, more activated in the PLACE-AVG and MATH-STORY contrasts, and less deactivated in the TOOL-AVG contrast. Relative to its infero-posterior neighbor POS2, area **7Pm** has less myelin (Panel B), is thicker (Panel C), differs in functional connectivity (Panel D), is more activated in some of the primary contrasts (SOCIAL and EMOTION) and the working memory 2BK-0BK contrast (Panel E), is deactivated vs activated in the BODY-AVG contrast (Panel F), is activated vs deactivated in the PLACE-AVG, LANGUAGE MATH (Panel M), and TOM-RANDOM (Panel O) contrasts, is less activated in the MOTOR CUE-AVG contrast (Panel H), and is less deactivated in the LANGUAGE STORY contrast. Relative to its supero-lateral neighbor 7PL, area **7Pm** has less

myelin (Panel B), is thicker (Panel C), differs in functional connectivity (Panel D), is deactivated vs activated in the BODY-AVG contrast (Panel F), and is less activated in the EMOTION and SOCIAL primary contrasts. Relative to its postero-inferior neighbor POS2, area **7PL** has less myelin (Panel B), differs in functional connectivity (Panel D), is more activated in some of the primary contrasts (SOCIAL and EMOTION), is activated vs deactivated in the PLACE-AVG, LANGUAGE MATH (Panel M), and TOM-RANDOM (Panel O) contrasts, and is less deactivated in the LANGUAGE STORY contrast. Finally, relative to its postero-inferior neighbor DVT, area **7PL** differs in functional connectivity (Panel D), is more activated in the working memory 2BK-0BK contrast (Panel E), is locally activated vs deactivated in the BODY-AVG contrast (Panel F), LANGUAGE MATH (Panel M), and MATH-STORY contrasts, less deactivated in the FACE-AVG contrast, and less activated in the PLACE-AVG contrast.

17. Inferior Parietal Cortex

The inferior parietal cortex is an association region similar in several respects to the lateral temporal cortex discussed previously. It is predominantly lightly myelinated (Panel B), moderately thick cortex (Panel C), and includes some areas strongly associated with the task positive network and others with the task negative network. Like the lateral temporal cortex, this region has expanded dramatically in humans relative to macaques and chimpanzees (Glasser et al., 2014; Hill et al., 2010). We identified ten areas in this region: PGp, PGs, PGi, PFm, PF, PFt, PFop, IP0, IP1, and IP2. The names reflect correspondences with areas identified by (Caspers et al., 2008; Caspers et al., 2006; Choi et al., 2006), except that their PF likely extends into portions of our PSL and STV, their PGa is subdivided into PGi and PGs (which also may include some of their PGp, as our PGp is somewhat smaller). Area IP0 is a new area posterior to IP1 along the lateral bank of the posterior IPS. These areas are surrounded by PFcm, OP4, 1, 2, AIP, LIPd, MIP, IPS1, V3B, V3CD, LO3, TPOJ1, TPOJ2, TPOJ3, STV, and PSL. Figure 20 shows multi-modal information used to parcellate this region, with the areas shown on a folding map in Panel A.

Area **PGp** is a transitional area insofar as its myelin content (Panel B) and thickness (Panel C) are similar to the rest of the inferior parietal cortex, but it has stronger functional connectivity with other transitional regions (e.g. the dorsal visual transitional area—DVT) and with higher visual cortex than does the rest of the inferior parietal cortex. Area **PGp's** posterior and inferior borders were previously covered in Sections #5 MT+ Complex and Neighboring Visual Areas (V3CD, LO3), and #15 Temporal-Parietal-Occipital Junction (TPOJ3). Relative to its supero-anterior neighbor PGs, area **PGp** differs strongly in functional connectivity (Panel D), is deactivated vs activated in the FACE-AVG contrast, and is activated vs deactivated in the PLACE-AVG, SOCIAL RANDOM, and MOTOR CUE-AVG (Panel F, deactivated on the left, less activated on the right and only assessed statistically) contrasts. Our area PGp corresponds to area PGp from (Caspers et al., 2008; Caspers et al., 2006), though it is somewhat smaller. Area **IP0** lies in the posterior IPS, and its borders with V3CD, V3B, and IPS1 were discussed previously (Sections #3 Dorsal Stream Visual Cortex and #5 MT+ Complex and Neighboring Visual Areas). Relative to its supero-lateral neighbor PGp, area **IP0** has more myelin (Panel B), is thinner (Panel C), differs modestly in functional connectivity (Panel D), and is more activated in primary contrasts (e.g. Panel I) and the FACES-SHAPES contrast (Panel J). Relative to its antero-superior neighbor IP1,

area **IP0** differs in functional connectivity (Panel D), is more activated in many primary contrasts (e.g. Panel I), is deactivated vs activated in the FACE-AVG and RELATIONAL-MATCH contrasts, activated vs deactivated in the PLACE-AVG contrast, and less deactivated in the LANGUAGE STORY contrast (Panel G).

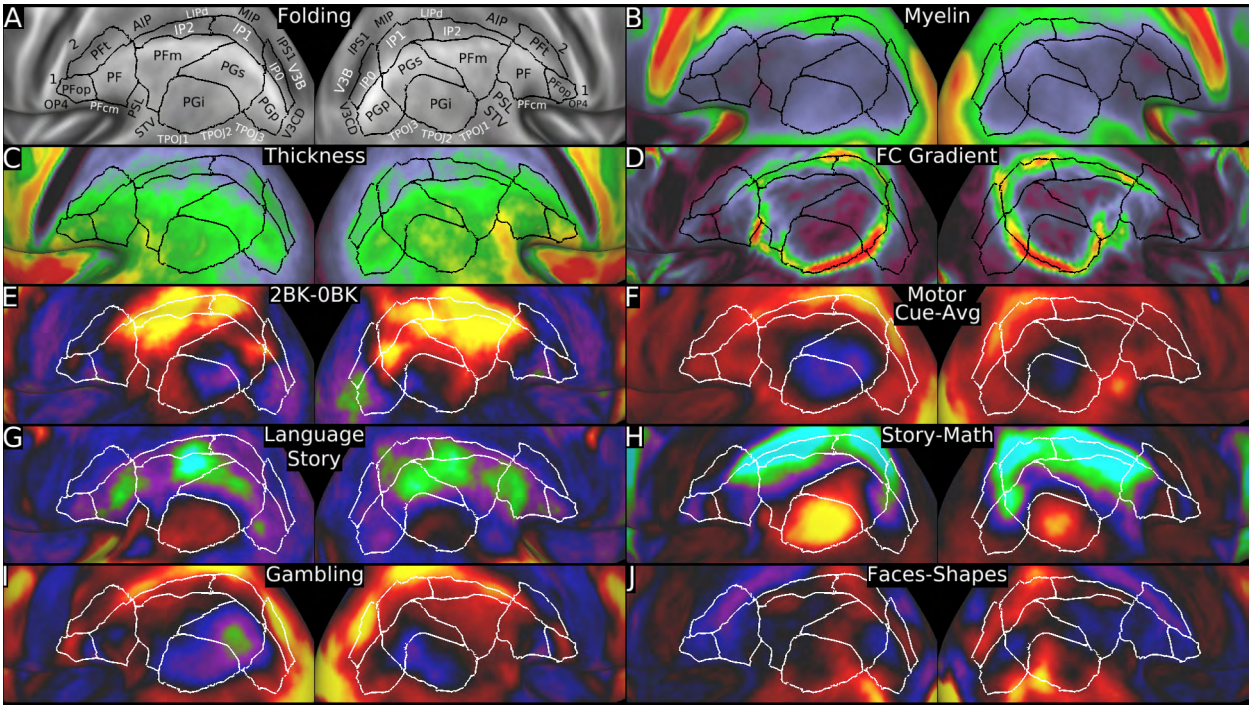

Figure 20 shows the multi-modal information used to parcellate the inferior parietal cortex. Panel A shows the areas on a folding map. Panels B and C show the myelin and cortical thickness maps. Panel D shows the resting state functional connectivity gradient. Panels E and F show the working memory 2BK-0BK contrast and the MOTOR CUE-AVG contrast. Panels G and H show the LANGUAGE STORY and STORY-MATH contrasts. Panels I and J show the GAMBLING PRIMARY contrast and the FACES-SHAPES contrasts. Data at http://balsa.wustl.edu/WL0P.

We identified two areas on the lateral bank of the intraparietal sulcus that correspond to areas **IP1** and **IP2** reported by (Choi et al., 2006). Relative to their neighbors on the medial bank (MIP, LIPd, and AIP), **IP1** and **IP2** differ strongly in functional connectivity (Panel D) and in various task contrasts (see Section #16 Superior Parietal Cortex). Relative to their lateral neighbors PGs and PFm, **IP1** and **IP2** have more myelin (Panel B) and differ modestly in functional connectivity (Panel D). Also, **IP1** is more activated in primary contrasts (e.g. Panel I), the MOTOR CUE-AVG contrast (Panel F), the LANGUAGE MATH contrast, less deactivated in the LANGUAGE STORY contrast (Panel G), and more activated in the FACES-SHAPES contrast (Panel J). Relative to its infero-lateral neighbor PGs, **IP1** is also more deactivated in the language STORY-MATH contrast (Panel H). Relative to its infero-lateral neighbor PFm, **IP2** is also more activated in the MOTOR CUE-AVG contrast (Panel F). Relative to its anterior neighbor IP2, area **IP1** differs modestly in functional connectivity (Panel D), is modestly more activated in RELATIONAL primary contrasts and FACES-SHAPES contrast (Panel J), and is less deactivated in the LANGUAGE STORY contrast (Panel G). Relative to anterior neighbor PF, area **IP2** differs in functional connectivity (Panel D) and in the FACES-SHAPES contrast (Panel J).

We subdivided classical area PF (BA 40) into 5 areas sufficiently similar to those identified by (Caspers et al., 2008; Caspers et al., 2006) that we use the same names: **PF**, **PFt**, **PFop**, PFm, and PFcm (previously covered in Section #9 Posterior Opercular Cortex). The three most anterior areas (PFt, PFop, and PF) have strong functional connectivity with other portions of the task positive network. Their superior (AIP), anterior (1, 2, OP4), and inferior borders (PFcm, PSL) have been covered previously in Sections #16 Superior Parietal Cortex, #6 Somatosensory and Motor Cortex, #9 Posterior Opercular Cortex, and #15 Temporal Parietal Occipital Junction. Relative to its posterior neighbor PF and inferior neighbor PFop, area **PFt** has more myelin and is thinner (Panels B and C), differs in functional connectivity (Panel D), and is less deactivated in the LANGUAGE STORY contrast (Panel G), more activated in the SOCIAL RANDOM contrast, and more deactivated in the FACES-SHAPES contrast (Panel J). **PFt** is also more activated than PF in the EMOTION SHAPES contrast. Relative to its posterior neighbor PF, area **PFop** is modestly thicker (Panel C), differs in functional connectivity (Panel D), and is less activated in the contralateral and ipsilateral ?F-AVG foot motor contrasts. Relative to its posterior neighbor PFm, area **PF** is thicker (Panel C), differs in functional connectivity (Panel D), and is more activated in the MOTOR CUE and SOCIAL TOM contrasts. Our areas PFop and PF may correspond to areas 72 and 88 from the Vogt-Vogt school (Nieuwenhuys et al., 2015).

The remaining three areas in the inferior parietal cortex are **PFm**, **PGi**, and **PGs**. Area **PFm** is a transitional region between PF, which is a major node in the task positive network, and **PGi** and **PGs**, which are major nodes in the task negative network. All three areas are lightly myelinated relative to most of their neighbors (Panel B) and are moderately thick (Panel C). Many of the outer borders of these areas were covered above or in Section #15 Temporal Parietal Occipital Junction (TPOJ1, TPOJ2, TPOJ3, STA, and PSL). Internally, these areas all differ from one another in functional connectivity (Panel D). Relative to its postero-inferior neighbor PGi, area **PFm** also has modestly less myelin (Panel B). Relative to PGi and posterior neighbor PGs, area **PFm** is also more activated in the working memory 2BK-0BK (Panel E), MOTOR CUE-AVG (Panel F), and the GAMBLING primary contrasts (Panel I), and is more deactivated in the STORY-MATH contrast (Panel H). Relative to PFm and superior-medial neighbor PGs, area **PGi** is more activated in the FACE-AVG, LANGAUGE STORY (Panel G) (only assessed statistically on the right), and the STORY-MATH (Panel H) contrasts. Our areas PGi and PGs correspond to area PGa from (Caspers et al., 2008; Caspers et al., 2006). Our areas PFm and PGi plus PGs may correspond to areas 89 and 90 from the Vogt-Vogt school (Nieuwenhuys et al., 2015).

18. Posterior Cingulate Cortex

The posterior cingulate cortex contains a diversity of architecturally and functionally distinct areas that we group together based on geographic proximity rather than functional similarity. It includes 14 areas: DVT, ProS, POS1, POS2, RSC, v23ab, d23ab, 31pv, 31pd, 31a, 23d, 23c, PCV, and 7m, which are surrounded by areas PreS, V2, V1, V6, V6A, IPS1, 7PL, 7Pm, 7Am, 5mv, 24dd, 24dv, p24pr, and 33pr. Figure 21 shows the multi-modal information used to parcellate this region. Panel A shows the areas on a group average folding map.

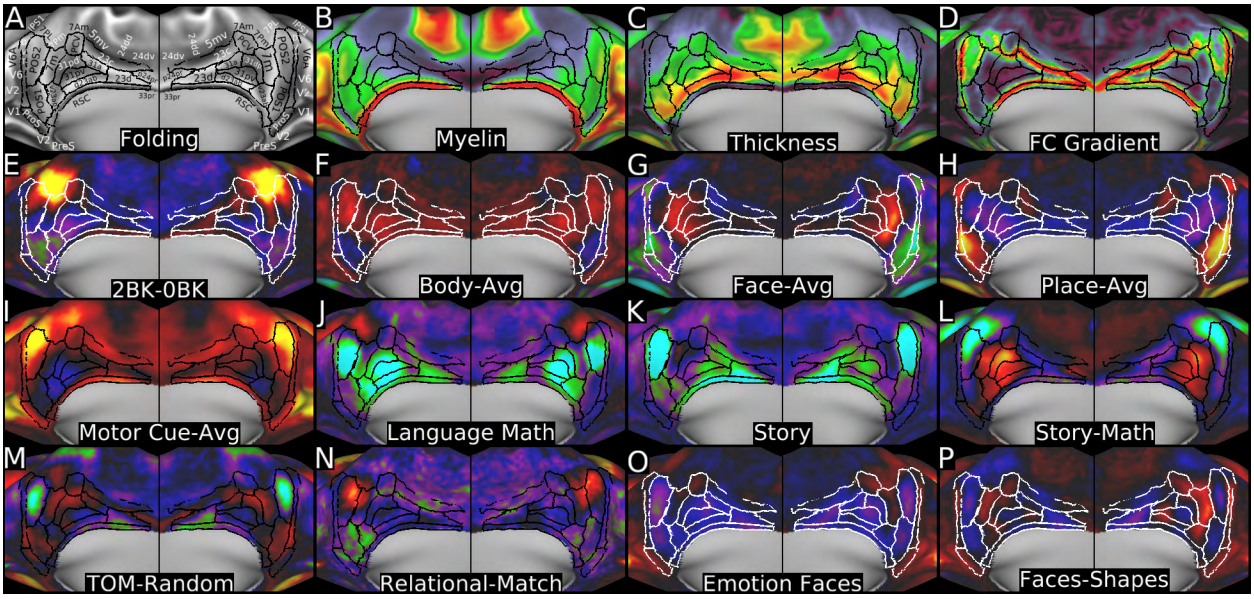

Figure 21 shows the multi-modal information used to parcellate the posterior cingulate cortex. Panel A shows the areas on a folding map. Panels B and C show the myelin and cortical thickness maps. Panel D shows the resting state functional connectivity gradients. Panels E, F, G, and H show the working memory 2BK-0BK, BODY-AVG, FACE-AVG, and PLACE-AVG contrasts. Panel I shows the MOTOR CUE-AVG contrast. Panels J, K, and L show the LANGUAGE MATH, STORY, and STORY-MATH contrasts. Panels M, N, O, and P show the TOM-RANDOM, RELATIONAL-MATCH, EMOTION FACES primary, and FACES-SHAPES contrasts. Data at http://balsa.wustl.edu/Jp5j.

The anterior bank of the parietal-occipital sulcus (POS) is an intriguing but poorly understood region that is transitional between early visual cortex and posterior cingulate association cortex. It includes 3 newly identified areas (though see (Glasser and Van Essen, 2011), where we suggested the existence of POS1 and POS2 based on myelin maps alone), plus one previously described area. The Dorsal Visual Transitional cortex (**DVT**) and Prostriate (**ProS**) cortex are transitional areas having architectural properties similar to their anterior neighbors and functional and connectional patterns more similar to their posterior neighbors (analogous to area 52 in Section #12 Insular and Frontal Opercular Cortex). The prostriate cortex **ProS** lies anterior to V1 (Sanides, 1970; Sanides and Vitzthum, 1965; Vogt, 2001), and its borders with V1, V2, and PreS were covered previously (Sections #1 Primary Visual Cortex (V1), #2 Early Visual Cortex, and #13 Medial Temporal Cortex). Despite its dramatically lower myelin content (Panel B), area **ProS** has strong functional connectivity with the early visual cortex. Relative to its superior neighbor POS1, area **ProS** is more lightly myelinated (Panel B), differs in functional connectivity (Panel D), and is more activated in the working memory primary contrasts and the FACES-SHAPES contrast (Panel P). Relative to its superior neighbor **DVT**, area **ProS** has less myelin (Panel B), is more activated in the working memory and relational primary contrasts, and is locally less deactivated in the FACE-AVG contrast (Panel G). Area **DVT's** posterior and superior borders were covered previously (Sections #2 Early Visual Cortex, #3 Dorsal Stream Visual Cortex, and #16 Superior Parietal Cortex). Although area **DVT** appears to be a very narrow strip when viewed on the inflated surface, it actually spans the entire fundus of the superior POS and is only slightly narrower than neighboring area V6. **DVT** has strong functional connectivity with higher dorsal stream visual cortex

and posterior superior parietal cortex, and weaker connectivity with its anterior neighbors POS1 and POS2. Relative to its antero-medial neighbor POS1, area **DVT** has less myelin (Panel B), is thinner (Panel C), differs in functional connectivity (Panel D), and is more activated in the working memory PLACE primary contrast. Relative to its antero-medial neighbor POS2, **DVT** has less myelin (Panel B), is thinner (Panel C), differs dramatically in functional connectivity (Panel D), is activated vs deactivated in the PLACE-AVG contrast (Panel H), EMOTION primary contrasts (e.g. Panel O), and FACES-SHAPES contrast (Panel P), is less deactivated in the LANGUAGE STORY and STORY-MATH contrasts (Panels K and L), is more activated in the SOCIAL primary contrasts, and is less deactivated in the TOM-RANDOM contrast (Panel M).

Area **POS2** is a highly distinctive area, as it differs dramatically from its neighbors in the four major feature categories (myelin, thickness, resting state connectivity, and task activations). Additionally, **POS2** has notably large BOLD fluctuations, and thus high Contrast to Noise Ratio (CNR) in functional neuroimaging. Particularly distinctive is the strong functional connectivity of POS2 with the retrosplenial complex (RSC). Because of its distinctiveness, the area is an excellent candidate for more detailed study with neuroanatomically informed and careful functional neuroimaging methods. The borders of **POS2** with DVT postero-laterally and 7PL and 7Pm superiorly have already been described (above and in Section #16 Superior Parietal Cortex). Relative to its antero-medial neighbor 7m, area **POS2** has more myelin (Panel B), is thinner (Panel C), differs strongly in functional connectivity (Panel D), is less activated in the FACE-AVG contrast (Panel G), and is more deactivated in the LANGUAGE MATH and STORY (Panels J and K), TOM-RANDOM (Panel M), and FACES-SHAPES (Panel P) contrasts. Relative to its inferior neighbor POS1, area **POS2** has more myelin (Panel B), is thinner (Panel C), differs in functional connectivity (Panel D), is activated vs deactivated in the BODY-AVG (Panel F) and FACE-AVG contrasts (Panel G), is deactivated vs activated in the PLACE-AVG contrast (Panel H), is more activated in the MOTOR CUE-AVG (Panel I) contrast, is more deactivated in the LANGUAGE MATH and STORY contrasts (Panels J and K), and is strongly deactivated vs activated in the TOM-RANDOM contrast (Panel M).

Relative to its supero-medial neighbor 7m, area **POS1** has more myelin (Panel B), differs in functional connectivity (Panel D), is strongly deactivated vs mixed activated/deactivated in the working memory 2BK-0BK contrast (Panel E), is deactivated vs activated in the FACE-AVG (Panel G) and FACES-SHAPES (Panel P) contrasts, is activated vs deactivated in the PLACE-AVG contrast (Panel H), is more deactivated in the LANGUAGE STORY contrast (Panel K), is deactivated vs activated in the STORY-MATH contrast (Panel L), and is more deactivated in the RELATIONAL-MATCH contrast (Panel N). Relative to its antero-medial neighbor v23ab, **POS1** differs in functional connectivity (Panel D), is deactivated vs activated in the FACE-AVG contrast (Panel G), activated vs deactivated in the PLACE-AVG contrast (Panel H), less deactivated in the MOTOR CUE-AVG contrast (Panel I), and deactivated vs activated in the STORY-MATH (Panel L) and FACES-SHAPES (Panel P) contrasts. Finally, relative to its antero-medial neighbor, the retrosplenial complex (RSC), area **POS1** has much less myelin (Panel B), is much thicker (Panel C), differs in functional connectivity (Panel D), is deactivated vs activated in the BODY-AVG contrast (Panel F), more activated in the PLACE-AVG contrast (Panel H), and less activated in the MOTOR CUE-AVG contrast (Panel I). Given the strong activation of area **POS1** in the PLACE-AVG task contrast, it likely corresponds to the scene-selective region identified as 'retrosplenial

cortex' in some neuroimaging studies (e.g., (Nasr et al., 2011)). However, it is a misnomer to call this region retrosplenial cortex, perhaps fostered by Brodmann's schematic drawing in which cortex behind the splenium of the corpus callosum was expanded so that areas 29 and 30 within the callosal sulcus could be more easily viewed. In reality these areas do not actually extend onto the anterior bank of the parietal occipital sulcus where POS1 resides (Palomero-Gallagher et al., 2009; Vogt, 2009).

The real retrosplenial complex (**RSC**) is a very distinct complex of areas (including Brodmann's areas 29 and 30, (Palomero-Gallagher et al., 2009; Vogt, 2009) that lies within the posterior callosal sulcus. Besides being very tightly coupled with area POS2, the RSC is dramatically more heavily myelinated and thinner than most of its neighbors (Panels B, C, and (Glasser and Van Essen, 2011)). The border between RSC and PreS inferiorly was already covered (Section #13 Medial Temporal Cortex). Relative to its posterior neighbor area v23ab, the **RSC** has more myelin (Panel B), is thinner (Panel C), differs in functional connectivity (Panel D), is less deactivated in the working memory 2BK-0BK (Panel E) and GAMBLING primary contrasts, is activated vs deactivated in the MOTOR CUE-AVG contrast (Panel I), is more deactivated in the LANGUAGE STORY contrast (Panel K), and is deactivated vs activated in the STORY-MATH contrast (Panel L). Relative its superior neighbor d23ab, the **RSC** is more heavily myelinated (Panel B), thinner (Panel C), differs in functional connectivity (Panel D), is activated vs deactivated in the 2BK-0BK (Panel E) and GAMBLING primary contrasts, is more activated in the MOTOR-AVG contrast, is more deactivated in the LANGUAGE STORY contrast (Panel K), is deactivated vs activated in the LANGUAGE STORY-MATH contrast (Panel L), and is more deactivated in the TOM-RANDOM contrast (Panel M). Relative to its superior neighbor 23d, the **RSC** has more myelin (Panel B), is thinner (Panel C), differs in functional connectivity (Panel D), is more activated in the MOTOR CUE-AVG contrast (Panel I) and more deactivated in the LANGUAGE STORY-MATH contrast (Panel L). Relative to its anterior neighbor 33pr, the **RSC** has more myelin (Panel B), differs in functional connectivity (Panel D), is more activated in the MOTOR CUE-AVG contrast (Panel I) and is more deactivated in the LANUGAGE STORY (Panel K) and TOM-RANDOM (Panel M) contrasts. Like POS2, the real retrosplenial cortex is an excellent candidate for further neuroimaging study using methods that accurately align cortical areas across subjects and avoid excessive spatial blurring.

The most superior portion of the medial parietal cortex was already covered in Section #16 Superior Parietal Cortex (7PL, 7Pm, 7Am), but two areas, **7m** and **PCV** remain to be covered here. Area **7m**, corresponding to area 7m of (Scheperjans et al., 2008a; Scheperjans et al., 2008b), has strong functional connectivity with task negative network areas PGi and PGs in lateral parietal cortex. Its posterior and superior borders with POS2, POS1, and 7Pm have been covered already (above and in Section #16 Superior Parietal Cortex). Relative to its inferior neighbor v23ab, area **7m** is less myelinated (Panel B), is more activated in the working memory 2BK-0BK (Panel E) and TOM-RANDOM (Panel M) contrasts and in the RELATIONAL and EMOTION primary contrasts (e.g. Panel O), is less deactivated in the LANGUAGE MATH contrast (Panel J), and is activated vs deactivated in the LANGUAGE STORY contrast (Panel K). Relative to its anterior neighbor 31pd, area **7m** is thicker (Panel C), differs in functional connectivity (Panel D), is more activated in the working memory 2BK-0BK (Panel E), FACE-AVG (Panel G), and FACES-SHAPES (Panel P) contrasts, is less deactivated in the LANGUAGE MATH contrast (Panel J), and is activated vs deactivated in the LANGUAGE STORY contrast (Panel K, in the right hemisphere). Relative

to its superior neighbor **PCV**, area **7m** differs in functional connectivity (Panel D), is more activated in the FACE-AVG (Panel G), STORY-MATH (Panel L), and FACES-SHAPES (Panel P) contrasts, and more deactivated in the PLACE-AVG contrast (Panel H). The newly identified PreCuneus Visual area, **PCV,** is distinctive in its strong functional connectivity with areas STV, TPOJ3, and DVT. Area **PCV's** superior (7Am), posterior (7Pm), and anterior neighbors (5mv) have already been covered in Sections #16 Superior Parietal Cortex and #7 Paracentral Lobular and Mid Cingulate Cortex. Relative to its inferior neighbor 31pd, area **PCV** differs strongly in functional connectivity (Panel D), is less activated in the STORY-MATH contrast (Panel L), and is more activated in the EMOTION primary contrasts (e.g. Panel O). Relative to its anterior neighbor 31a, area **PCV** is more heavily myelinated (Panel B), is thinner (Panel C), differs strongly in functional connectivity, is activated instead of deactivated in the FACE-AVG contrast (Panel G), is less activated in the PLACE-AVG contrast (Panel H), and is activated/less deactivated in the STORY-MATH (Panel L) contrast. Relative to its anterior neighbor 23c, area **PCV** has more myelin (Panel B), differs in functional connectivity (Panel D), is more activated in the FACE-AVG (Panel G) and STORY-MATH (Panel L) contrasts, is less activated in the PLACE-AVG contrast (Panel H), and is activated vs deactivated in the FACES-SHAPES contrast (Panel P). Area PCV likely corresponds to a precuneus ('PrCu') visual area showing retinotopic organization (Sereno et al., 2013). Also, it is noteworthy that the functional connectivity gradients in this region are strikingly affected by global or mean grey signal regression, which shifts the gradient ridge that lies along the inferior and posterior border (Panel D) towards the center of area **PCV**.

Brodmann's area 23 in posterior cingulate cortex has been subdivided in a variety of ways in previous architectonic studies. Our parcellation agrees most closely with that of (Palomero-Gallagher et al., 2009; Vogt, 2009), in which 23a and 23b were combined into 23ab, but then split into inferior and superior subdivisions, which we identify respectively as **v23ab** and **d23ab**. (Vogt's parcellation of area 23 also includes areas 23c and 23d discussed below.) The posterior (7m), inferior (POS1), and anterior (RSC) borders of area **v23ab** were already covered above. Relative to its superior neighbor 31pd, area **v23ab** is thicker (Panel C), differs modestly in functional connectivity (Panel D), is less activated in the STORY-MATH contrast (Panel L), and is more deactivated in the RELATIONAL-MATCH contrast (Panel N). Relative to its superior neighbor area 31pv, area **v23ab** is thicker (Panel C), differs modestly in functional connectivity (Panel D), is more deactivated in the RELATIONAL-MATCH contrast (Panel N), and is locally deactivated vs activated in the FACES-SHAPES contrast (Panel P). Relative to its supero-anterior neighbor area d23ab, area **v23ab** differs modestly in functional connectivity (Panel D) and is more deactivated in the RELATIONAL-MATCH contrast (Panel N). Relative to superior neighbor area 31pv, area **d23ab** is dramatically thicker (Panel C), as was previously shown in (Glasser and Van Essen, 2011). Relative to its anterior neighbor area 23d, area **d23ab** differs in functional connectivity (Panel D), is deactivated vs activated in the working memory 2BK-0BK contrast (Panel E), and is less deactivated in the STORY-MATH (Panel L), TOM-RANDOM (Panel M), and FACES-SHAPES (Panel P) contrasts.

Superior to areas v23ab and d23ab is area 31 (Palomero-Gallagher et al., 2009; Vogt, 2009), which we have divided into three areas, **31pv**, **31pd**, and **31a**. Relative to is supero-posterior neighbor area 31pd, area **31pv** has more myelin (Panel B), is thicker (Panel C), is more deactivated in the LANGUAGE STORY contrast (Panel K), and is deactivated vs

activated in the TOM-RANDOM contrast (Panel M). Relative to its superior neighbor area 31a, area **31pv** has more myelin (Panel B), differs modestly in functional connectivity (Panel D), is more activated in the BODY-AVG contrast (Panel F), is activated vs deactivated in the FACE-AVG (Panel G) and STORY-MATH (Panel L) contrasts, and is deactivated vs activated in the PLACE-AVG (Panel H) and TOM-RANDOM (Panel M) contrasts. The borders of area **31pd** with area v23ab, 7m, and PCV were already described above. Relative to its anterior neighbor area 31a, area **31pd** has more myelin (Panel B), is thinner (Panel C), differs modestly in functional connectivity (Panel D), and is less activated in the BODY-AVG contrast (Panel F), is more activated in the FACE-AVG contrast (Panel G), is deactivated vs activated in the PLACE-AVG contrast (Panel H), is more deactivated in the LANGUAGE MATH contrast (Panel J), and is activated vs deactivated in the STORY-MATH contrast (Panel L). Relative to its superior neighbor area 23c, area **31a** is thicker (Panel C), differs dramatically in functional connectivity (Panel D), and is less activated in the MOTOR CUE-AVG contrast (Panel I). Relative to its anterior neighbor area 23d, area **31a** differs modestly in functional connectivity (Panel D), and is less activated in the BODY-AVG contrast (Panel F), is deactivated vs activated in the FACE-AVG contrast (Panel G), is activated vs deactivated in the PLACE-AVG (Panel H), TOM-RANDOM (Panel M), and FACES-SHAPES (Panel P) contrasts, and is less deactivated in the LANGUAGE MATH contrast (Panel J).

Areas **23c** and **23d** both lie superior and anterior to the other areas in the posterior cingulate region (Palomero-Gallagher et al., 2009; Vogt, 2009). Area **23d** is a very thick (Panel C), lightly myelinated area (Panel B) that differs strongly from its superior neighbors in functional connectivity (Panel D). Relative to its anterior neighbor p24pr, area **23d** differs in functional connectivity (Panel D), and is deactivated vs weakly activated in the TOOL-AVG contrast, is less activated in the CUE-AVG contrast (Panel I), is more deactivated in the LANGUAGE MATH contrast (Panel J), is activated vs deactivated in the SOCIAL primary contrasts, and is deactivated vs activated in the FACES-SHAPES contrast (Panel P). Area **23d** is also statistically more heavily myelinated (Panel B) and more activated in the LANGUAGE STORY contrast (Panel K) than p24pr. Relative to its superior neighbor area **23c**, area **23d** is thicker (Panel C), differs strongly in functional connectivity (Panel D), and is less activated in the CUE-AVG contrast (Panel I) and deactivated vs activated in the TOM-RANDOM contrast (Panel M). Area **23c** is a lightly myelinated (Panel B), moderately thick area (Panel C) that lies between the task negative posterior cingulate cortex and the sensorimotor cortex that has strong functional connectivity with the task positive network. Most of its borders have already been covered (above or in Section #7 Paracentral Lobular and Mid Cingulate Cortex: 5mv, 24dd, 24dv). Relative to its anterior neighbor p24pr, area **23c** is more heavily myelinated (Panel B) and thinner (Panel C).

19. Anterior Cingulate and Medial Prefrontal Cortex

The anterior cingulate and medial prefrontal cortex, lying along the medial aspect of each hemisphere and anterior to motor/premotor areas, is generally lightly myelinated and thick. It has functional connectivity with a variety of networks and differential functional activations in many different tasks. We divided this region into 15 areas: 33pr, p24pr, a24pr, p24, a24, p32pr, a32pr, d32, p32, s32, 8BM, 9m, 10v, 10r, and 25, surrounded by areas RSC, 23d, 23c, 24dv, SCEF, SFL, 8BL, 9a, 9p, 10d, 10pp, OFC, and pOFC. The

organization of the region reflects two dominant principles: 1) Architecturally, there are three major bands of cingulate cortex: a narrow strip of thin and lightly myelinated periallocortex (classical area 33) lying inferiorly; a very thick, very lightly myelinated proisocortex (classical area 24) in the middle; and a thick, lightly myelinated paralimbic region (classical area 32) superiorly (Glasser and Van Essen, 2011; Paus, 2001). The medial prefrontal cortex lies outside these regions superiorly, anteriorly, and inferiorly. 2) Based on functional connectivity, there is a very strong gradient ridge that runs obliquely, from supero-posterior to antero-inferior. Behind this transition (posterior and inferior) cortex is more connected with higher somatosensory and motor regions and the task positive network. In front of the transition, cortex is strongly associated with the task negative network. The multi-modal information used to parcellate the anterior cingulate and medial prefrontal cortex is shown in Figure 22. Panel A shows the areas on a folding map.

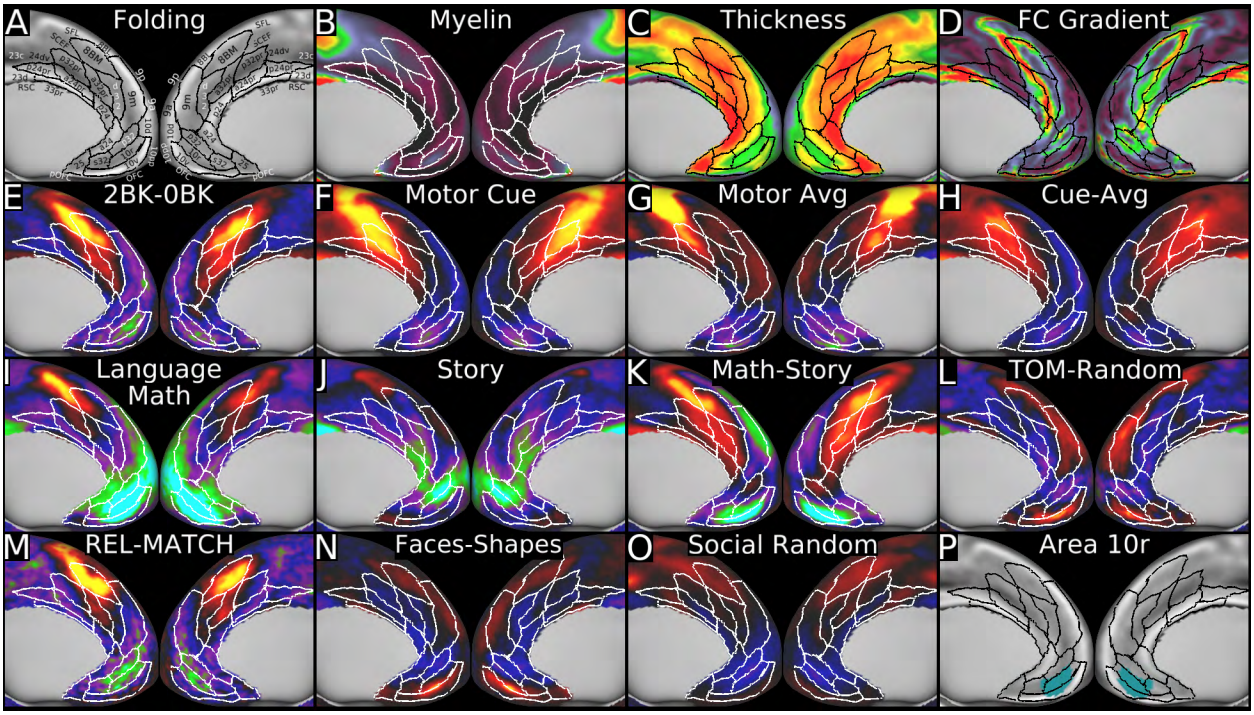

Figure 22 shows multi-modal information used to parcellate the anterior cingulate cortex. Panel A shows the areas on a group average folding map. Panels B and C show the myelin and cortical thickness maps. Panel D shows the resting state functional connectivity gradients. Panels E, F, G, and H show the working memory 2BK-0BK, MOTOR CUE, AVG, and CUE-AVG task contrasts. Panels I, J, K, and L show the LANGUAGE MATH, STORY, MATH-STORY and SOCIAL TOM-RANDOM contrasts. Panels M, N, and O show the RELATIONAL-MATCH and EMOTION FACES-SHAPES contrasts and the SOCIAL RANDOM primary contrast. Panel P shows area 10r from the (Ongur et al., 2003) publication. Data at http://balsa.wustl.edu/Q9xk.

The periallocortex (classical area 33) is a thin (Panel C), lightly myelinated strip (Panel B) that lies in front of the retrosplenial cortex (RSC). Vogt recognized three subdivisions of area 33: area 33 proper plus a33' and p33' (Vogt, 2009). Our data provides evidence for a single area in this region that we identify as **33pr** (pr represents ' because the latter is a reserved character in many programming languages), corresponding to the location of Vogt's a33' and p33'. The more anterior area 33 subdivision of Vogt may be

largely excluded from the grayordinates space established by the medial wall mask (though part of it may be visible in the right hemisphere), which likely also encroaches on part of 33pr (more so in the left hemisphere). A future higher resolution standard grayordinates space would benefit from improvements to the medial wall mask here (as well as exclusion of the hippocampal complex, as noted above). The posterior border of area **33pr** with the RSC was covered in Section #18 Posterior Cingulate Cortex. Relative to its superior neighbor p24pr, area **33pr** is much thinner (Panel C), has slightly more myelin (Panel B), differs modestly in resting state functional connectivity (Panel D), is less deactivated in the LANGUAGE MATH contrast (Panel I), and is more activated in the MATH-STORY contrast (Panel K). Relative to its superior neighbor a24pr, area **33pr** (Panel C) is again much thinner (Panel C) and has slightly more myelin (Panel B). It also is modestly activated vs deactivated in the TOM-RANDOM contrast (Panel L) and is less deactivated in the LANGUAGE STORY contrast (Panel J). In both cases, cortical thickness was a primary criterion for delineating the border using the semi-automated border optimize tool. Our 33pr may correspond to area 16 from the Vogt-Vogt school (Nieuwenhuys et al., 2015).

The proisocortex (area 24) is a thick (Panel C), very lightly myelinated (Panel B) strip that lies superior to area 33. Vogt (Vogt, 2009) recognized three subdivisions of area 24 (area 24 proper and a24' and p24'). We identified four areas, including a more anterior pair (a24 and p24, which are anterior and posterior subdivisions of Vogt's area 24 proper) and a more posterior pair (**a24pr** and **p24pr**, corresponding to Vogt's a24' and p24', with pr substituting for '). Vogt also identified a more superior triplet, areas 24c, a24c', and p24c', and these areas likely partially overlap with our areas p24, a24, a24pr, and p24pr. The borders of the most posterior subdivision, **p24pr** with area 23d, 23c, and 24dv were already covered (Sections #18 Posterior Cingulate Cortex and #7 Paracentral Lobular and Mid Cingulate Cortex). Relative to its anterior neighbor a24pr, area **p24pr** differs in functional connectivity (Panel D), is less activated in the MOTOR CUE (Panel F) and CUE-AVG (Panel H) contrasts, is less deactivated in the contralateral ?H-AVG hand motor and LANGUAGE STORY contrasts (Panel J), is deactivated vs activated in the T-AVG face motor contrast, and is activated vs deactivated in the SOCIAL RANDOM primary contrast (Panel O). Moving anteriorly, relative to its superior neighbor p32pr, area **a24pr** has dramatically less myelin (Panel B), is less activated in the MOTOR CUE (Panel F), AVG (Panel G), and LANGUAGE MATH-STORY (Panel K) contrasts and in a variety of primary contrasts (e.g. Panel O), is deactivated vs activated in the LANGUAGE MATH contrast (Panel I), and is more deactivated in the LANGUAGE STORY contrast (Panel J). Relative to its superior neighbor a32pr, area **a24pr** has dramatically less myelin (Panel B), differs in functional connectivity (Panel D), and is deactivated vs activated in the LANUAGE MATH (Panel I) and RELATIONAL-MATCH (Panel M) contrasts and the SOCIAL RANDOM primary contrast (Panel O). Relative to its anterior neighbor p24, area **a24pr** differs in functional connectivity (Panel D), is more activated in the MOTOR CUE contrast (Panel E), is weakly activated vs weakly deactivated in the MOTOR AVG contrast (Panel F), and is less deactivated in the LANGUAGE STORY contrast (Panel J).

Further anteriorly, relative to its superior neighbor a32pr, area **p24** has less myelin (Panel B), is thicker (Panel C), differs in functional connectivity (Panel D), is less activated in the working memory 2BK-0BK contrast (Panel E), is deactivated vs activated in the LANGUAGE MATH (Panel I) and RELATIONAL-MATCH (Panel M) contrasts and in primary contrasts such as the SOCIAL RANDOM contrast (Panel O), and is less activated in the

LANGUAGE MATH-STORY contrast (Panel K). Relative to its superior neighbor d32, area **p24** has less myelin (Panel B), is thicker (Panel C), differs strongly in functional connectivity (Panel D), and is more activated in the MOTOR CUE (Panel F) and CUE-AVG (Panel H) contrasts. Relative to its anterior neighbor a24, area **p24** differs strongly in functional connectivity (Panel D), is activated vs deactivated in the MOTOR CUE (Panel F) and CUE-AVG (Panel H) contrasts, and is less deactivated in the LANGUAGE MATH contrast (Panel I). Further anteriorly, relative to its superior neighbor 9m, area **a24** has less myelin (Panel B), is thicker (Panel C), differs modestly in functional connectivity (Panel D), is more deactivated in the LANGUAGE STORY contrast (Panel J), and is deactivated vs activated in the TOM-RANDOM (Panel L) and FACES-SHAPES (Panel N) contrasts. Relative to its anterior neighbor p32, area **a24** has less myelin (Panel B), is thicker (Panel C) and differs in functional connectivity (Panel D). Relative to its inferior neighbor s32, area **a24** has less myelin (Panel B), is thicker (Panel C), and differs in functional connectivity (Panel D). Relative to its posterior neighbor 25, area **a24** has less myelin (Panel B) and differs in functional connectivity (Panel D).

The paralimbic cortex (area 32) is a thick (Panel C), lightly myelinated (Panel B) strip that surrounds the area 24 complex on its superior and anterior sides. Vogt recognized four subdivisions of area 32: area 32' most posteriorly followed by areas d32, p32, and s32 progressing anteriorly then inferiorly (Vogt, 2009). We subdivide area 32 into five subdivisions that are split by area 9m (see below). The three most posterior areas are **p32pr**, **a32pr** (posterior and anterior subdivisions of Vogt's 32') and **d32** (overlapping with d32 of Vogt). Anterior to 9m we identified areas p32 and s32 (overlapping with p32 and s32 of Vogt). Our areas 32 may include portions of Vogt's areas 24c, a24c', and p24c'. The borders of the most posterior subdivision of area 32, **p32pr**, with areas 24dv and SCEF were already covered (Section #7 Paracentral Lobular and Mid Cingulate Cortex), and its border with a24pr was covered above. Relative to its anterior neighbor a32pr, area **p32pr** differs in functional connectivity (Panel D), is more activated in the MOTOR CUE (Panel F), MOTOR AVG (Panel G), and EMOTION primary contrasts and in the RELATIONAL REL-MATCH contrast (Panel M). Moving anteriorly and relative to its superior neighbor 8BM, area **a32pr** differs strongly in functional connectivity (Panel D), is more activated in the working memory 2BK-0BK (Panel E), MOTOR CUE (Panel F), and CUE-AVG (Panel H) contrasts, is less activated in the SOCIAL primary contrasts (e.g. Panel O) and RELATIONAL-MATCH contrast (Panel M), and is deactivated vs activated in the FACES-SHAPES contrast (Panel N). Relative to its anterior neighbor d32, area **a32pr** differs strongly in functional connectivity (Panel D), is more activated in the MOTOR CUE (Panel F) and CUE-AVG (Panel H) contrasts and in the RELATIONAL primary contrasts. Further anterior and relative to its superior neighbor 8BM, area **d32** has modestly less myelin (Panel B), differs modestly in functional connectivity (Panel D), is less activated in the working memory 2BK-0BK contrast (Panel E) and in the SOCIAL and RELATIONAL primary contrasts (e.g. Panel O), is more deactivated in the LANGUAGE STORY contrast (Panel J), is strongly activated vs weakly activated or deactivated in the RELATIONAL-MATCH contrast (Panel M), and is deactivated vs activated in the FACES-SHAPES contrast (Panel N). Relative to its anterior neighbor 9m, area **d32** has modestly more myelin on the left (Panel B), differs in functional connectivity (Panel D), is activated vs deactivated in the working memory 2BK-0BK (Panel E) and LANGUAGE MATH-STORY (Panel K) contrasts, and is deactivated vs activated in the TOM-RANDOM contrast (Panel L).

In our parcellation, and contrary to Vogt's parcellation, we find a region of cortex that intercedes between area d32 and area **p32** that is more similar to area 9m than to either area d32 or p32. There may be substantially inter-individual heterogeneity in this region, as this portion of cortex shares some properties with d32 as well. Further anteriorly and relative to its superior neighbor 9m, area **p32** differs in functional connectivity (Panel D), is activated vs deactivated in the MOTOR CUE-AVG (Panel H) and LANGUAGE MATH-STORY (Panel K) contrasts, is strongly deactivated vs weakly deactivated or activated in the LANGUAGE STORY contrast (Panel J), and is deactivated vs activated in the TOM-RANDOM (Panel L) and FACES-SHAPES (Panel N) contrasts. Relative to its anterior neighbor 10d, area **p32** has less myelin (Panel B), is thicker (Panel C), differs in functional connectivity (Panel D), and is activated vs deactivated in the MOTOR CUE-AVG (Panel H) and MATH-STORY (Panel K) contrasts. Relative to its inferior neighbor 10r, area **p32** is more lightly myelinated (Panel B), thicker (Panel C), differs in functional connectivity (Panel D), and is activated vs deactivated in the MOTOR CUE-AVG (Panel H) and LANGUAGE MATH-STORY (Panel K) contrasts. Relative to its inferior neighbor s32, area **p32** differs in functional connectivity (Panel D), is weakly activated/deactivated vs strongly deactivated in the LANGUAGE MATH-STORY contrast (Panel K) and deactivated vs activated in the TOM-RANDOM contrast (Panel L). Moving inferiorly and relative to its anterior neighbor 10r, area **s32** has less myelin (Panel B), is thicker (Panel C), differs modestly in functional connectivity (Panel D), and is less deactivated in the CUE-AVG contrast (Panel H). Relative to its inferior neighbor 10v, area **s32** has more myelin (Panel B) and differs modestly in functional connectivity (Panel D). Relative to its posterior neighbor 25, area **s32** has less myelin (Panel B) and is thinner (Panel C).

The remaining areas in this region are largely medial or orbital prefrontal areas. Most superior and posterior is area **8BM**, whose posterior border with SCEF was covered in Section #7 Paracentral Lobular and Mid Cingulate Cortex and whose inferior borders were covered above. Area 8BM is so named because it overlaps with the medial portion of area 8B from (Petrides and Pandya, 1999). Relative to its supero-posterior neighbor SFL, area **8BM** differs strongly in functional connectivity (Panel D), is more activated in the working memory 2BK-0BK (Panel E) and MATH-STORY (Panel K) contrasts, and is more activated in the RELATIONAL-MATCH contrast (areas are more different on the right, Panel M). Relative to its supero-lateral neighbor 8BL, area **8BM** is thicker (Panel C), differs in functional connectivity (Panel D), is activated vs deactivated in the working memory 2BK-0BK (Panel E), MOTOR CUE-AVG (Panel H), LANGUAGE MATH-STORY (Panel K), and RELATIONAL-MATCH (Panel M) contrasts. Relative to its superior neighbor 9m, area **8BM** has more myelin (Panel B), differs in functional connectivity (Panel D), is activated vs deactivated in the working memory 2BK-0BK (Panel E), MOTOR CUE (Panel F) and CUE-AVG (Panel H), LANGUAGE MATH (Panel I) and MATH-STORY (Panel K), and RELATIONAL-MATCH (Panel M) contrasts, and is deactivated vs activated in the TOM-RANDOM contrast (Panel L).

Also lying mostly on the medial surface is area **9m,** the medial portion of area 9 from (Petrides and Pandya, 1999). The inferior borders of area **9m** with 8BM, d32, a24, and p24 were covered above. Relative to its posterior neighbor 8BL, area **9m** has modestly less myelin (Panel B), differs modestly in functional connectivity (Panel D), is more activated in the TOM-RANDOM contrast (Panel L), and is deactivated vs activated in the RELATIONAL-MATCH contrast (Panel M). Relative to its superior neighbor 9p, area **9m** has

less myelin (Panel B), is much thicker (Panel C), differs modestly in functional connectivity (Panel D), is activated/less deactivated vs more deactivated in the LANGUAGE STORY contrast (Panel J), and is more activated in the TOM-RANDOM contrast (Panel L). Relative to its lateral neighbor 9a, area **9m** has less myelin (Panel B), is thicker (Panel C), and differs in functional connectivity (Panel D) in the right hemisphere and is deactivated instead of activated in the RELATIONAL-MATCH contrast in the left hemisphere (Panel M). Relative to its antero-lateral neighbor 10d, area **9m** has less myelin (Panel B), is thicker (Panel C), and differs in functional connectivity (Panel D).

We identified two medial subdivisions of area 10 (in contrast to (Ongur et al., 2003), who reported three, and the most posterior of theirs overlaps most with our area 25 and s32). The first area, **10r**, corresponds reasonably closely to area 10r as mapped by (Ongur et al., 2003) (Panel P). The posterior and superior borders of area **10r** with s32 and p32 were covered above. Relative to its superior neighbor 10d, area **10r** differs in functional connectivity (Panel D) and is more deactivated in the working memory 2BK-0BK (Panel E) and MOTOR CUE-AVG (Panel H) contrasts. Relative to its inferior neighbor 10v, area **10r** has more myelin (Panel B), is thinner (Panel C), differs modestly in functional connectivity (Panel D), is activated/less deactivated vs more deactivated in the LANGUAGE MATH-STORY contrast (Panel K), is deactivated vs activated in the TOM-RANDOM contrast (Panel L), and is more deactivated in the RELATIONAL-MATCH contrast (Panel M). Relative to its superior neighbor 10d, area **10v** is thicker (Panel B), differs in functional connectivity (Panel D), is more deactivated in the LANGUAGE MATH-STORY contrast (Panel K), is activated vs deactivated in the TOM-RANDOM contrast (Panel L), and is more activated in the FACES-SHAPES contrast (Panel N). Relative to its antero-lateral neighbor 10pp, area **10v** has less myelin (Panel B, in the left hemisphere), is thicker (Panel C), differs in functional connectivity (Panel D), and is more deactivated in the MATH-STORY contrast (Panel K). Relative to its infero-lateral neighbor OFC, area **10v** has less myelin (Panel B) and is thicker (Panel C, left border defined primarily using thickness). In the orbito-frontal complex, signal loss greatly reduced the quality of resting state and task fMRI data. This region will need to be revisited in the future, once MR technology allows improved signal quality (e.g. by better shimming or by using spin echo fMRI). Relative to its posterior neighbor 25, area **10v** has less myelin (Panel B) and is thinner (Panel C). Area **25** is a very thick (Panel C), lightly myelinated (Panel B) cortical area beneath the genu of the corpus callosum. Its borders with a24, s32, and 10v have been covered above. Its borders with OFC and pOFC are primarily delineated by a difference in cortical thickness (Panel C), given the above issue with signal loss. The area is so named because of its similarity in position to area 25 in Vogt's parcellation (Vogt, 2009). Area **25** also appears to be in a similar location to that reported in (Palomero-Gallagher et al., 2015). Their s24 may correspond to our a24 and their s32 to our s32. One difference is that they usually find at least a narrow strip of s24 between 25 and s32, which we did not observe. An alternative explanation is that the medial wall mask that defines the grayordinates space may exclude a portion or even most of area 25 (in addition to their anterior area 33, which is definitely excluded) and that what we call area 25 is their s24 (Palomero-Gallagher et al., 2015). Importantly, this region is also challenging to map because the functional imaging modalities are lower in quality in this region, which is strongly effected by b0-related gradient echo fMRI signal loss. Future studies with an expanded grayordinates space and better MRI acquisitions may revisit the parcellation and areal identifications in the subgenual cingulate region.

20. Orbital and Polar Frontal Cortex

The orbital and polar frontal cortex contains cortical areas with a variety of architectural and functional properties. We have subdivided this region into 11 areas and complexes: 47s, 47m, a47r, 11l, 13l, a10p, p10p, 10pp, 10d, OFC, and pOFC. They are surrounded by areas 25, 10v, 10r, p32, 9m, 9a, 9-46d, a9-46v, p47r, 47l, AVI, AAIC, and Pir. The (Ongur et al., 2003) surface-based parcellation aided in naming many of these areas (Ongur et al., 2003); see Panel O). The multi-modal information used to parcellate the orbital and polar frontal cortex is shown in Figure 23. Panel A shows the areas on a folding map.

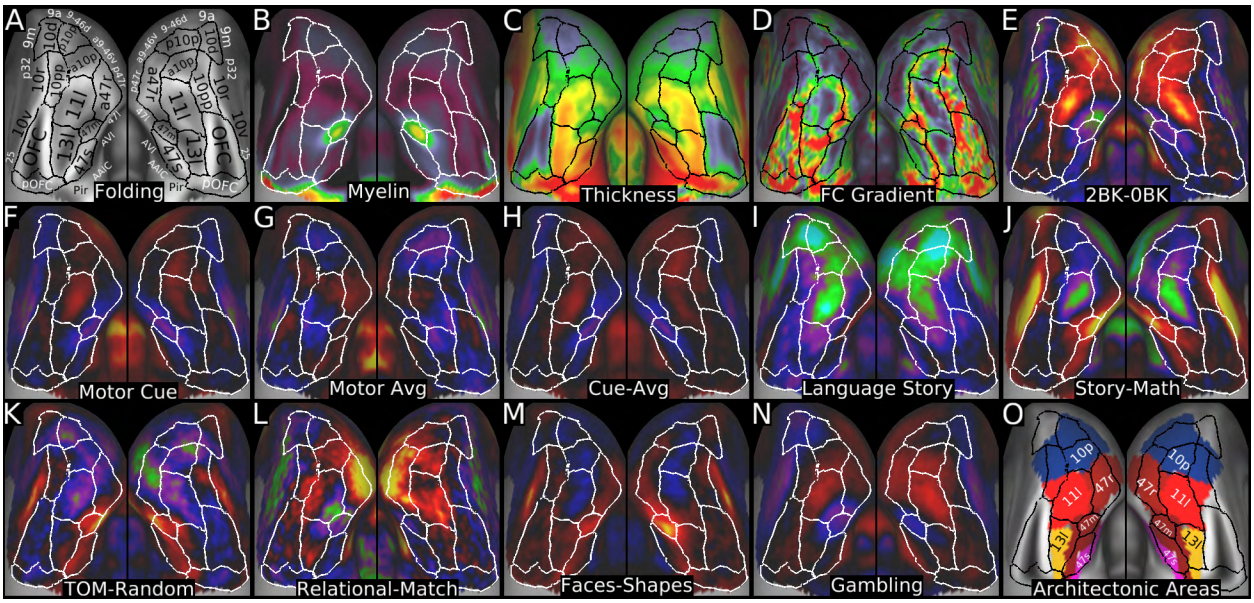

Figure 23 shows the multi-modal information that was used to parcellate the orbital and polar frontal cortex. Panel A shows the areas on a folding map. Panels B and C show myelin and cortical thickness maps. Panel D shows the resting state functional connectivity gradient. Panel E shows the working memory 2BK-0BK contrast. Panels F, G, and H show the MOTOR CUE, AVG, and CUE-AVG contrasts. Panels I and J show the LANGUAGE STORY and STORY-MATH contrasts. Panels K, L, M, and N show the TOM-RANDOM, RELATIONAL-MATCH, FACES-SHAPES, and GAMBLING primary contrasts. Panel O shows some areas (13l, 11l, 47m, 47s, 47r, and 10p) from the (Ongur et al., 2003) parcellation that were used to name areas in our parcellation. Data at http://balsa.wustl.edu/RkD2.

As mentioned in the preceding section, substantial b0-releated fMRI signal loss in the orbitofrontal cortex was an impediment to a fine-grained parcellation of this region. Using mainly architectural criteria, we identified two distinct complexes, the orbitofrontal complex (**OFC**) and the posterior orbitofrontal complex (**pOFC**) that include multiple architectonic areas by other parcellations (e.g. (Ongur et al., 2003). In particular, pOFC overlaps with areas 13a and 14c, and OFC overlaps with areas 11m, 13b, 13m, and 14r of (Ongur et al., 2003). With improved fMRI data quality (e.g. better shimming or spin echo fMRI), this region should be revisited. The medial borders of OFC and pOFC with 10v and 25 were covered previously in Section #20 Anterior Cingulate and Medial Prefrontal Cortex. Relative to its posterior neighbor pOFC, the **OFC** is thinner (Panel C) and has less myelin (Panel B), with cortical thickness being primarily used to delineate the boundary.

Relative to its lateral neighbor Pir, the **pOFC** is thicker (Panel C) and has less myelin (Panel B). Relative to its anterior neighbor 13l and antero-lateral neighbor 47s, the **pOFC** is thicker (Panel C) and has more myelin (Panel B). Relative to its lateral neighbor 13l, the **OFC** is thinner (Panel C) and has less myelin (Panel B). Relative to anterior-lateral neighbor 11l, the **OFC** is thinner (Panel C) and has slightly less myelin (Panel B). Relative to its antero-superior neighbor 10pp, the **OFC** is thinner (Panel C) and has slightly more myelin near the border (Panel B). The relative thinness of the OFC does not appear to be artifactual, insofar as histological studies also report this region to be thinner (Triarhou, 2007a, b; von Economo and Koskinas, 1925). Nonetheless, some of OFC cortex (particularly on inferiorly facing gyral crowns) may still be impacted by signal loss in the gradient echo T1w image, leading to artifactually thinner cortex. Artifacts in the myelin maps in this region were reduced relative to our previous study (Glasser and Van Essen, 2011) by using readout distortion correction of the T1w and T2w images so that they are not distorted relative to one another (Glasser et al., 2013), though signal loss in the T1w image likely still produces some artifacts on the inferiorly facing gyral crowns. Within this region, OFC and pOFC overlap with Fo1 and Fo2, though the boundary between OFC and pOFC is posterior to the boundary between Fo1 and Fo2 (Henssen et al., 2016).

Lateral to OFC, we identified areas **13l** and **11l**, based on their overlap with areas reported by (Ongur et al., 2003) (Panel O). Relative to its postero-lateral neighbor 47s, area **13l** differs in functional connectivity (Panel D) and is less activated in the TOM-RANDOM contrast (Panel K). Relative to its heavily myelinated lateral neighbor 47m, area **13l** has less myelin (Panel B), is thicker (Panel C), differs in functional connectivity (Panel D), is less deactivated in the MOTOR CUE-AVG contrast (Panel H), and is less activated in the LANGUAGE STORY-MATH (Panel J), TOM-RANDOM (Panel K), and FACES-SHAPES (Panel M) contrasts. Relative to its anterior neighbor 11l, area **13l** differs in functional connectivity (Panel D), is deactivated vs activated in the MOTOR CUE (Panel F) contrast, and is activated vs deactivated in the TOM-RANDOM (Panel K) and LANGUAGE STORY-MATH contrasts (Panel J). Relative to its postero-lateral neighbor 47m, area **11l** has much less myelin (Panel B), is thicker (Panel C), differs in functional connectivity (Panel D), is activated vs deactivated in the MOTOR CUE (Panel F) and CUE-AVG contrasts (Panel H), is more deactivated in the LANGUAGE STORY contrast (Panel I), is deactivated vs activated in the TOM-RANDOM contrast (Panel K), and is less activated/deactivated vs strongly activated in the FACES-SHAPES contrast (Panel M). Relative to its lateral neighbor a47r, area **11l** is thicker (Panel C), differs in functional connectivity (Panel D), is activated vs deactivated in the MOTOR CUE-AVG contrast (Panel H), and is deactivated vs activated in the LANGUAGE STORY-MATH (Panel J) and FACES-SHAPES (Panel M) contrasts. Relative to its superior neighbor a10p, area **11l** has less myelin near the border (Panel B), is thicker (Panel C), differs in functional connectivity (Panel D), and is more deactivated in the LANGUAGE STORY-MATH contrast (Panel J). Relative to its supero-medial neighbor 10pp, area **11l** is thicker (Panel C), differs in functional connectivity (Panel D), is more activated in the working memory 2BK-0BK contrast (Panel E), and is more deactivated in the STORY-MATH contrast (Panel J). These areas overlap extensively with area Fo3 (Henssen et al., 2016).

We subdivided area 47 into five areas, three of which (**47s**, **47m**, and **a47r**) are covered in this section, with the remaining two (47l, p47r) covered in the next Section #21 Inferior Frontal Cortex. The names of these areas reflect correspondences with the (Ongur

et al., 2003) parcellation, though in our parcellation, 47m does not extend as far posteriorly, and 47s extends more medially and does not extend as far laterally (Panel O). The most anterior area is **47s**, a lightly myelinated (Panel B), thick area (Panel C) that is connected to the language network and is more activated in the language task contrasts than many of its neighbors (Panels I and J). Its posterior borders with AAIC and AVI were covered in Section #12 Insular and Frontal Opercular Cortex, and its borders with 13l and pOFC were covered above. Relative to its superior neighbor 47m, area **47s** has less myelin (Panel B), differs in functional connectivity (Panel D), and is less activated by the STORY-MATH (Panel J), TOM-RANDOM (Panel K), and FACES-SHAPES (Panel M) contrasts. Relative to its supero-lateral neighbor 47l, area **47s** is thicker (Panel C), differs in functional connectivity (Panel D), and is less activated by the LANGUAGE STORY contrast (Panel I). Area **47m** is one of the more distinctive areas in the cerebral cortex. Unlike the rest of prefrontal cortex, area 47m is a hot spot of heavily myelination (Panel B), as we have noted previously (Glasser and Van Essen, 2011). It has strong functional connectivity with areas 10r and s32, and it shows more pronounced differential activation in various category task contrasts (BODY-AVG, FACE-AVG, PLACE-AVG, and TOOL-AVG) than do other prefrontal cortical areas (except perhaps area 10r). The borders of area 47m with 47s, 13l, and 11l have already been described above. Relative to its lateral neighbor 47l, area **47m** has more myelin (Panel B), differs in functional connectivity (Panel D), is deactivated vs activated in the LANGUAGE STORY contrast (Panel I), and is more activated in the FACES-SHAPES contrast (Panel M). Relative to its antero-lateral neighbor a47r, area **47m** has more myelin (Panel B), differs in functional connectivity (Panel D), is more deactivated in the LANGUAGE MATH contrast, and is more activated in the FACES-SHAPES contrast (Panel M).

Relative to its posterior neighbor 47l, area **a47r** differs in functional connectivity (Panel D), is deactivated vs activated in the LANGUAGE STORY contrast (Panel I), is less activated/deactivated vs activated in the LANGUAGE STORY-MATH (Panel J) and TOM-RANDOM (Panel K) contrasts, is activated vs deactivated in the RELATIONAL primary contrasts, and is more activated in the RELATIONAL-MATCH contrast (Panel L). Relative to its superior neighbor p47r, area **a47r** is more lightly myelinated (Panel B), thicker (Panel C), differs in functional connectivity (Panel D), and is more deactivated in the LANGUAGE MATH contrast, and is less deactivated in the STORY-MATH contrast (Panel J). Relative to its supero-medial neighbor a9-46v, area **a47r** differs in functional connectivity (Panel D), is modestly less activated in the working memory 2BK-0BK contrast (Panel E), is deactivated vs activated in the MOTOR CUE contrast (Panel F), less deactivated in the LANGUAGE STORY-MATH contrast (Panel J), and is activated vs deactivated in the FACES-SHAPES contrast (Panel M). The topology of area **a47r**'s superior border differs in the left and right hemispheres, as it adjoins both a10p and p10p in the right hemisphere, but only a10p on the left. Interestingly the (Yeo et al., 2011) functional network parcellation shows an analogous asymmetry in this region. Relative to its medial neighbor a10p, area **a47r** differs in functional connectivity (Panel D), differs in the MOTOR CUE-AVG contrast (Panel H, deactivated vs activated on the left and less activated on the right), and is less deactivated in the LANGUAGE STORY-MATH contrast (Panel J), is more activated in the RELATIONAL-MATCH contrast (Panel L), and is activated vs deactivated in the FACES-SHAPES contrast (Panel M). In the right hemisphere relative to its postero-medial neighbor p10p, area **a47r** differs in functional connectivity (Panel D), is more activated in the

primary GAMBLING contrasts (e.g. Panel N) and the RELATIONAL-MATCH (Panel L) contrasts and is less activated in the MOTOR CUE-AVG (Panel H).

We now discuss the remaining four subdivisions of area 10: **10pp**, **a10p**, **p10p** and **10d**. These largely overlap with area Fp1 of (Bludau et al., 2014), whereas areas 10r and 10v (covered in Section #19 Anterior Cingulate and Medial Prefrontal Cortex) largely overlap with Fp2 (though 10d likely also overlaps partly with Fp2). Our polar divisions of area 10 overlap extensively with area 10p in (Ongur et al., 2003) (which was incompletely defined along its superior extent). The most polar subdivision of area 10, 10pp, has medial (10v), inferior (OFC), and lateral (11l) borders that were covered already (above or in Section #19 Anterior Cingulate and Medial Prefrontal Cortex). Relative to its lateral neighbor a10p, area **10pp** differs in functional connectivity (Panel D), is less activated in the working memory 2BK-0BK contrast (Panel E), and is activated vs deactivated in the LANGUAGE STORY-MATH (Panel J), TOM-RANDOM (Panel K), and FACES-SHAPES (Panel M) contrasts. Relative to its superior neighbor 10d, area **10pp** differs in functional connectivity (Panel D) and is activated vs deactivated in many primary task contrasts (e.g. Panel N). Parcellation of cortex in the vicinity of area 10pp should be revisited once better methods of suppressing susceptibility-induced signal loss from the frontal sinus are available, as this process may affect its borders. The lateral (a47r), inferior (11l), and medial (10pp) borders of area **a10p** were already covered above. Relative to supero-posterior neighbor p10p, area **a10p** is thicker (Panel C), differs in functional connectivity (Panel D), and is activated vs deactivated in the GAMBLING primary contrasts (e.g. Panel N). Corresponding to the above asymmetry in areal topology of a47r, area **a10p** adjoins area a9-46v only in the left hemisphere. In the left hemisphere relative to posteriorly bordering area a9-46v, area **a10p** differs in functional connectivity (Panel D), is less deactivated in the LANGUAGE STORY-MATH contrast (Panel J), and is more activated in the RELATIONAL primary contrasts. Relative to its lateral neighbor a9-46v, area **p10p** differs in functional connectivity (Panel D), is deactivated vs activated in the GAMBLING and EMOTION primary contrasts (e.g. Panel N), and is less deactivated in the STORY-MATH contrast (Panel J). Relative to its posterior neighbor 9-46d, area **p10p** is thinner (Panel C), differs in functional connectivity (Panel D), is deactivated vs activated in the GAMBLING and EMOTION primary contrasts (Panel N), is more activated in the MOTOR CUE contrast (Panel F), and is less deactivated in the LANGUAGE STORY-MATH contrast (Panel J). Relative to its postero-medial neighbor 9a, area **p10p** has more myelin (Panel B), differs in functional connectivity (Panel D), is activated vs deactivated in the working memory 2BK-0BK contrast (Panel E), and is deactivated vs activated in the MOTOR AVG contrast (Panel G). Relative to its medial neighbor 10d, area **p10p** differs in functional connectivity (Panel D), is activated vs deactivated in the working memory 2BK-0BK contrast (Panel E) and the MOTOR CUE-AVG contrast (Panel H), and is deactivated vs activated in the LANGUAGE STORY-MATH contrast (Panel J). Relative to its posterior neighbor 9a, area **10d** has more myelin (Panel B), differs in functional connectivity (Panel D), and is more deactivated in the GAMBLING primary contrasts (Panel N).

21. Inferior Frontal Cortex

The inferior frontal cortex contains language-associated areas, including Broca's area, plus a number of moderately myelinated areas in the inferior frontal sulcus. We

subdivided inferior frontal cortex into eight areas: 44, 45, IFJp, IFJa, IFSp, IFSa, 47l, and p47r, which are surrounded by areas FOP4, FOP5, AVI, 47s, 47m, a47r, a9-46v, 46, p9-46v, 8C, PEF, and 6r. Figure 24 shows multi-modal information used to parcellate the inferior frontal cortex. Panel A shows the areas on a folding map.

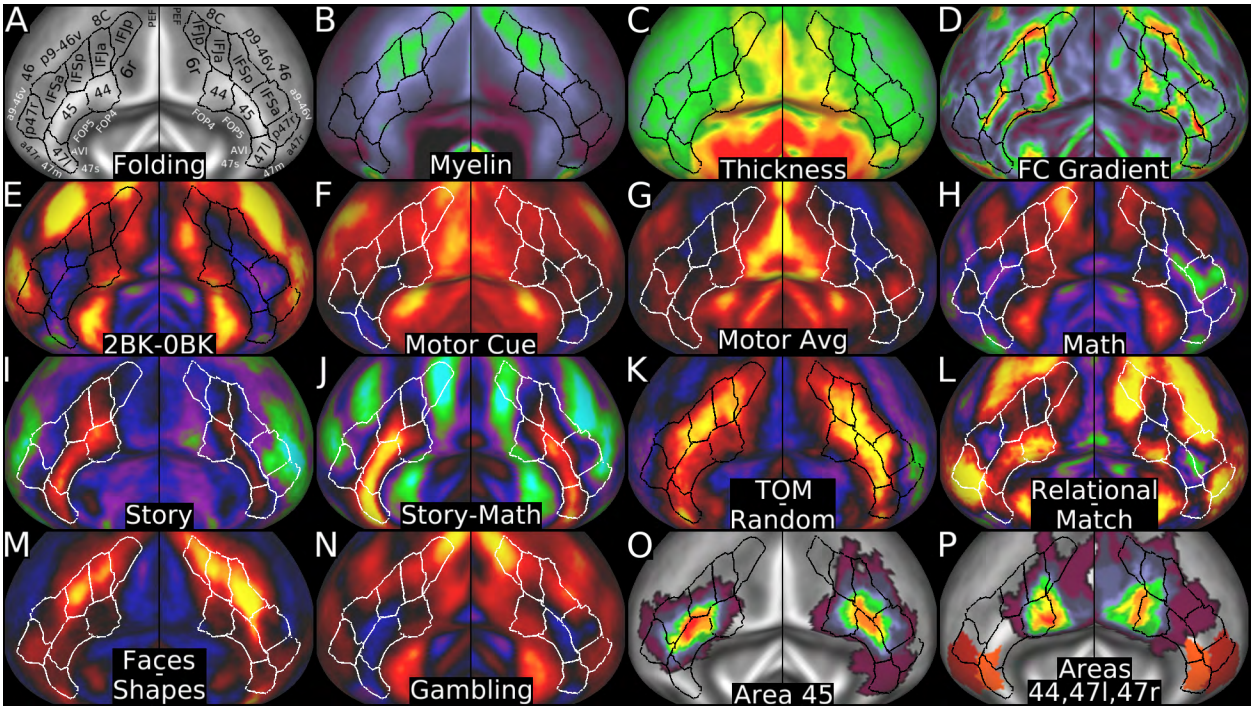

Figure 24 shows multi-modal information used to parcellate the inferior frontal cortex. Panel A shows the areas on a folding map. Panels B and C show myelin and cortical thickness maps. Panel D shows the resting state functional connectivity gradients. Panels E, F, G, and H show the working memory 2BK-0BK contrast, the MOTOR CUE contrast, the MOTOR AVG contrast, and the LANGUAGE MATH contrast. Panels I, J, K and L show the LANGUAGE STORY contrast, the STORY-MATH contrast, the SOCIAL TOM-RANDOM contrast, and the RELATIONAL-MATCH contrast. Panels M and N show the EMOTION FACES-SHAPES contrast and a GAMBLING primary contrast. Panel O shows the surface-based probabilistic map of area 45 from (Fischl et al., 2008). Panel P shows the surface-based probabilistic map of area 44 from (Fischl et al., 2008) and maps of area 47l and 47r from (Ongur et al., 2003). While the parcellation is reasonably symmetric (parcel boundaries in the same locations relative to folding and areal features) the probabilistic maps have some asymmetries, suggesting that registration drift may contribute to some of the mismatches. Data at http://balsa.wustl.edu/W0Nl.

Areas **44**, 45, and 47l are so named because of their substantial overlap with correspondingly named areas in previous studies (Panels O and P, (Amunts et al., 1999; Fischl et al., 2008; Ongur et al., 2003), though the overlap is not perfect. Broca's area is commonly described as including Brodmann's areas 44 and 45 (Amunts et al., 2010; Amunts et al., 1999). In the LANGUAGE STORY primary contrast (Panel I) and STORY-MATH contrast (Panel J), the strongest activations in the inferior frontal region included areas 44, 45, and 47l on the left, with more modest activations of areas 45 and 47l on the right. These three areas also show strong functional connectivity with one another and with other areas activated in the language task contrasts. Area **44**'s posterior border with 6r was covered in Section #8 Premotor Cortex and its borders with FOP4 and FOP5 were covered in Section #12 Insular and Frontal Opercular Cortex. Relative to its superior

neighbor IFJa, area **44** has less myelin (Panel B), is thicker (Panel C), differs modestly in functional connectivity (Panel D), is more activated in the RELATIONAL-MATCH contrast in the left hemisphere (Panel L) and less activated in the FACES-SHAPES contrast (Panel M). Relative to its antero-superior neighbor IFSp, area **44** has less myelin (Panel B), is thicker (Panel C), differs modestly in functional connectivity (Panel D), is more activated in the working memory 2BK-0BK (Panel E) and MOTOR AVG (Panel G) contrasts, and is less activated in the FACES-SHAPES contrast (Panel M). In the left hemisphere, area **44** is also more activated in the LANGUAGE STORY (Panel I) and RELATIONAL-MATCH (Panel L) contrasts and less activated in the TOM-RANDOM (Panel K) contrast relative to area IFSp. Relative to its anterior neighbor 45, area **44** has modestly less myelin (Panel B), is thicker (Panel C), differs in functional connectivity in the right hemisphere (Panel D), is activated vs deactivated in primary task contrasts (e.g. Panel N) and in the working memory 2BK-0BK (Panel E) and LANGUAGE MATH (Panel H) contrasts, and is less activated in the LANGUAGE STORY-MATH contrast (Panel J). Area **44** shows strongly lateralized functional activation in the LANGUAGE STORY contrast (Panel I) and to some extent in the RELATIONAL-MATCH task contrast (Panel L). Areas 44 and 45 have been subdivided respectively into cytoarchitectonic areas 44d and 44v and 45a and 45p (Amunts et al., 2010). We found intra-areal heterogeneity in the right hemisphere consistent with similar subdivisions of both areas 44 and 45, but not in the left hemisphere (Panel D; see also panel L) in our in vivo multi-modal data.

Relative to its supero-posterior neighbor IFSp, area **45** has less myelin (Panel B), is thicker (Panel C), differs modestly in functional connectivity (Panel D), is more activated in the LANGUAGE STORY contrast (Panel I, more on the right), and is less activated in the FACES-SHAPES contrast (Panel M). Area **45** is activated in the RELATIONAL-MATCH contrast in the left hemisphere (Panel L), but mainly deactivated in the right hemisphere, whereas IFSp is more activated on the right. Relative to its superior neighbor IFSa, area **45** differs in functional connectivity (Panel D), is activated vs deactivated in the LANGUAGE STORY (Panel I) and STORY-MATH (Panel J) contrasts, and in the RELATIONAL-MATCH contrast in the left hemisphere (Panel L). Relative to its supero-anterior neighbor p47r, area **45** differs in functional connectivity (Panel D), is deactivated vs activated in many primary task contrasts (e.g. Panel N) and in the working memory 2BK-0BK (Panel E) and LANGUAGE STORY (Panel I) contrasts, is activated vs deactivated in the LANGUAGE STORY-MATH contrast (Panel J), and is less activated in the TOM-RANDOM (Panel K) and RELATIONAL-MATCH (Panel L) contrasts. Relative to its inferior neighbor 47l, area **45** has more myelin (Panel B), differs in functional connectivity (in the right hemisphere only, Panel D), is more activated in the MOTOR CUE contrast (Panel F), and is deactivated vs activated in the EMOTION SHAPES primary contrast. Relative to its supero-anterior neighbor p47r, area **47l** is thicker (Panel C), differs in functional connectivity (Panel D), is deactivated vs activated in the working memory 2BK-0BK contrast (Panel E), is activated vs deactivated in the LANGUAGE STORY (Panel I) and STORY-MATH (Panel J) contrasts, and is less activated in the RELATIONAL-MATCH contrast (Panel L). The remaining borders of **47l** (with a47r, 47m, and 47s anteriorly and inferiorly, and with AVI and FOP5 posteriorly and inferiorly) were covered in Sections #20 Orbital and Polar Frontal Cortex and #12 Insular and Frontal Opercular Cortex.

The inferior frontal sulcus includes areas **IFJp**, **IFJa**, IFSp, IFSa that are named because of their similarity in location to areas ifj2, ifj1, ifs2, and ifs1 that were partly

described in (Amunts et al., 2010), but with some differences in relation to a future, yet to be published parcellation (Katrin Amunts, personal communication). It also includes area p47r, so named because it overlaps with the posterior part of area 47r of (Ongur et al., 2003) (Panel P). Area **IFJp's** posterior borders with PEF and 6r were discussed in Section #8 Premotor Cortex. Relative to its superior neighbor 8C, area **IFJp** has more myelin (Panel B), differs in functional connectivity (Panel D), is more activated in primary task contrasts (e.g. Panel N) and in the PLACE-AVG, TOM-RANDOM (Panel K), and FACES-SHAPES (Panel M) contrasts, and is more deactivated in the FACE-AVG and LANGUAGE STORY-MATH (Panel J) contrasts. Relative to its anterior neighbor IFJa, area **IFJp** is thicker (Panel C), differs in functional connectivity (Panel D), is deactivated vs activated in the FACE-AVG contrast, is less activated in the LANGUAGE STORY contrast (Panel I), is strongly deactivated vs weakly activated in the STORY-MATH contrast (Panel J), and is more activated in the RELATIONAL-MATCH contrast (Panel L, particularly on the right). Relative to its superior neighbor 8C, area **IFJa** has more myelin (Panel B), differs in functional connectivity (Panel D), is more activated in the MOTOR CUE (Panel F), TOM-RANDOM (Panel K) and FACES-SHAPES (Panel M) contrasts, and is less activated in the RELATIONAL-MATCH contrast (Panel L). Relative to its anterior neighbor IFSp, area **IFJa** is thicker (Panel C), differs in functional connectivity (Panel D), is more activated in the MOTOR AVG contrast (Panel G), and is weakly deactivated vs activated in the RELATIONAL-MATCH contrast (Panel L).

Further anterior and relative to its supero-posterior neighbor 8C, area **IFSp** has more myelin (Panel B), differs in functional connectivity (Panel D), is activated vs deactivated in the LANGUAGE STORY contrast in the left hemisphere (Panel I), is more activated in the TOM-RANDOM (Panel K) and FACES-SHAPES (Panel M) contrasts, and is less activated in the RELATIONAL-MATCH contrast in the left hemisphere (Panel L). Relative to its superior neighbor p9-46v, area **IFSp** has more myelin (Panel B), differs in functional connectivity (Panel D), is deactivated vs strongly activated in the working memory 2BK-0BK contrast (Panel E), is more activated in the LANGUAGE STORY contrast in the left hemisphere (Panel I) and in the TOM-RANDOM (Panel K) and FACES-SHAPES (Panel M) contrasts, and is less activated in the RELATIONAL-MATCH contrast (Panel L). Relative to its anterior neighbor IFSa, area **IFSp** has more myelin (Panel B), differs in functional connectivity (Panel D), is deactivated vs activated in the MOTOR AVG contrast (Panel G), is activated/less deactivated vs more deactivated in the LANGUAGE STORY contrast (Panel I), and is more activated in the FACES-SHAPES contrast (Panel M). Further anterior and relative to its supero-posterior neighbor p9-46v, area **IFSa** differs in functional connectivity (Panel D), is activated vs deactivated in the working memory 2BK-0BK contrast (Panel E), is more activated in the TOM-RANDOM contrast (Panel K), and is deactivated vs activated in the RELATIONAL-MATCH contrast in the left hemisphere (Panel L). Relative to its superior neighbor 46, area **IFSa** has more myelin (Panel B), differs in functional connectivity (Panel D), is more activated in the 2BK-0BK (Panel E) and FACES-SHAPES (Panel M) contrasts, and is activated vs deactivated in the TOM-RANDOM contrast (Panel K). Relative to its antero-superior neighbor a9-46v, area **IFSa** differs in functional connectivity (Panel D), is deactivated vs activated in the working memory 2BK-0BK contrast (Panel E), is less deactivated in the STORY-MATH contrast (Panel J), and is activated vs deactivated in the TOM-RANDOM contrast (Panel K). Relative to its anterior neighbor p47r, area **IFSa** has more myelin (Panel B), differs in functional connectivity

(Panel D), is deactivated vs activated in the working memory 2BK-0BK (Panel E) and RELATIONAL-MATCH (Panel L) contrasts, is more deactivated in the LANGUAGE MATH contrast (Panel H), and is less deactivated in the LANGUAGE STORY-MATH contrast (Panel J). Finally, relative to its superior neighbor a9-46v, area **p47r** differs in functional connectivity (Panel D), is activated/less deactivated vs more deactivated in the LANGUAGE MATH (Panel H) and STORY contrasts on the left (Panel I), is more activated in the RELATIONAL-MATCH contrast (Panel L), and is activated vs deactivated in the FACES-SHAPES contrast (Panel M). The anterior border of **p47r** with area a47r was covered in Section #20 Orbital and Polar Frontal Cortex.

22. DorsoLateral Prefrontal Cortex

The dorsolateral prefrontal cortex is one of the larger and more functionally heterogeneous regions of human neocortex, and thus the often-used term "DLPFC" is not a particularly specific spatial localization. The DLPFC region is generally lightly myelinated, of moderate thickness, participates strongly in both the task positive and task negative networks, and shows substantial heterogeneity in functional contrasts. Thus it has many similarities with the inferior parietal cortex and lateral temporal cortex, as well as with the other prefrontal regions (including inferior frontal, orbital and polar frontal, and medial frontal). Like lateral temporal cortex and inferior parietal cortex, the dorsolateral prefrontal cortex has also expanded dramatically in humans relative to monkeys and apes (Glasser et al., 2014; Hill et al., 2010). We have subdivided DLPFC into 13 areas: 8C, 8Av, i6-8, s6-8, SFL, 8BL, 9p, 9a, 8Ad, p9-46v, a9-46v, 46, and 9-46d. They are surrounded by areas 55b, FEF, 6a, 6ma, SCEF, 8BM, 9m, 10d, p10p, a10p, a47r, p47r, IFSa, IFSp, IFJa, IFJp, and PEF. Figure 25 shows the multi-modal information used to parcellate this region of cortex. Panel A shows the areas on a cortical folding map.

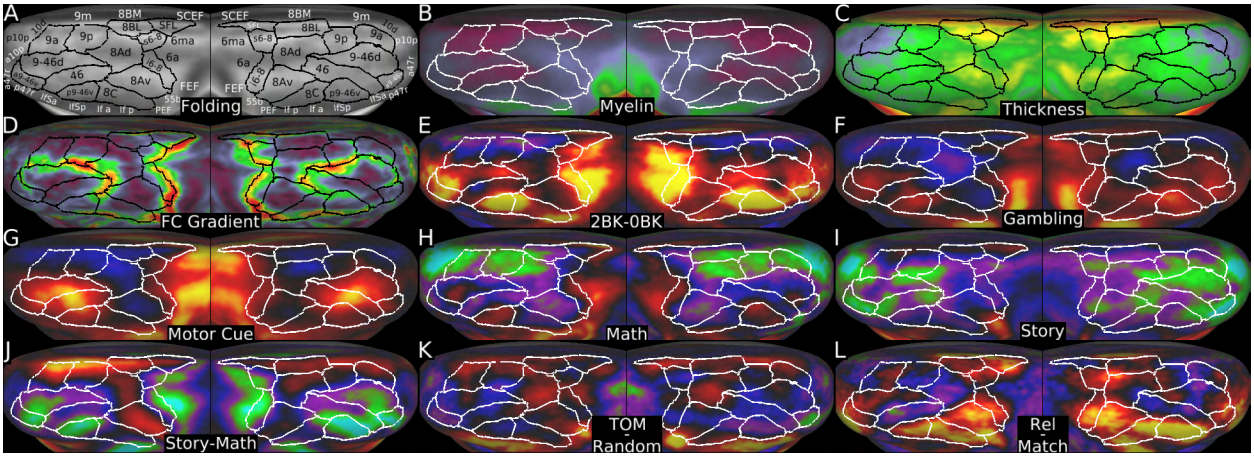

Figure 25 shows multi-modal information used to parcellate the dorsolateral prefrontal cortex. Panel A shows the areas on a group average folding map. Panels B and C show the myelin and cortical thickness maps. Panel D shows the resting state functional connectivity gradient map. Panels E and F show the working memory 2BK-0BK contrast and a GAMBLING primary contrast. Panels G, H, and I show the MOTOR CUE contrast, the LANGUAGE MATH contrast, and the LANGUAGE STORY contrast. Panels J, K, and L show the STORY-MATH contrast, the TOM-RANDOM contrast, and the RELATIONAL-MATCH contrast. Data at http://balsa.wustl.edu/Q2LG.

A notably distinct area in dorsolateral prefrontal cortex is the hemispherically asymmetric Superior Frontal Language (**SFL**) area, located posteriorly on the superior frontal gyrus. The **SFL** area is larger on the left, shows more activation in the LANGUAGE STORY contrast in the left hemisphere (Panel I), and strong activation in the RELATIONAL-MATCH contrast in the left hemisphere compared with deactivation in the right hemisphere (Panel L). It is also part of the language network in the left hemisphere and the corresponding network in the right hemisphere (see Supplementary Figure 4 in the Supplementary Results and Discussion). The lateral (6ma) and medial (SCEF and 8BM) borders of area **SFL** were already covered (in Sections #8 Premotor Cortex and #19 Anterior Cingulate and Medial Prefrontal Cortex). Relative to its anterior neighbor 8BL, area **SFL** is thicker (Panel C), differs in functional connectivity (Panel D), is less deactivated in the LANGUAGE MATH contrast (Panel H), and is more activated in the LANGUAGE STORY contrast (particularly on the left, Panel I), in the TOM-RANDOM contrast (in the right hemisphere, Panel K), and in the RELATIONAL-MATCH contrast in the left hemisphere (Panel L). Relative to its lateral neighbor s6-8, area **SFL** is thicker (Panel C), differs in functional connectivity (Panel D), is less activated in the working memory 2BK-0BK contrast in the right hemisphere (Panel E), is activated (left) or activated/deactivated (right) vs strongly deactivated in the LANGUAGE STORY (Panel I) and STORY-MATH (Panel J) contrasts, is activated vs deactivated in the TOM-RANDOM contrast in the right hemisphere (Panel K), and is deactivated vs activated in the RELATIONAL-MATCH contrast in the right hemisphere (Panel L).

We identified two areas, **s6-8** and **i6-8**, in a transitional region similar to the transitional region of cortex between areas FB (BA6) and FC (BA8) in the von Economo and Koskinas parcellation (Talavage and Hall, 2012; Triarhou, 2007a, b; von Economo and Koskinas, 1925). We consider the region transitional because of differences across task contrasts as to whether their strongest gradient is located at the anterior or posterior border of the region. The posterior borders of area **s6-8** with 6ma and 6a were covered in Section #8 Premotor Cortex. Relative to its medial neighbor 8BL, area **s6-8** has more myelin (Panel B), differs in functional connectivity (Panel D), is activated vs deactivated in the working memory 2BK-0BK (Panel E), MOTOR CUE (Panel G), and CUE-AVG contrasts, is activated/deactivated vs strongly deactivated in the LANGAUGE MATH (Panel H) contrast, and is deactivated vs activated in the STORY-MATH contrast (Panel J). Relative to its anterior neighbor 8Ad, area **s6-8** differs in functional connectivity (Panel D), is more activated in the working memory 2BK-0BK contrast (Panel E), is activated vs deactivated in the MOTOR CUE contrast (Panel G), is less deactivated in the LANGUAGE MATH contrast (Panel H), and is deactivated vs activated in the STORY-MATH contrast (Panel J). Relative to its infero-lateral neighbor i6-8, area **s6-8** has less myelin (Panel B), differs in functional connectivity (Panel D), and is less activated in the RELATIONAL primary contrasts. Relative to its anterior neighbor 8Ad, area **i6-8** differs in functional connectivity (Panel D), is activated vs deactivated in many primary task contrasts (e.g. Panel F), is more activated in the working memory 2BK-0BK (Panel E), MOTOR CUE (Panel G), CUE-AVG and LANGUAGE MATH contrasts (Panel H), and is deactivated vs activated in the LANGAUGE STORY-MATH contrast (Panel J). Relative to its antero-lateral neighbor 8Av, area **i6-8** differs in functional connectivity (Panel D), is more activated in the working memory 2BK-0BK contrast (Panel E), and is deactivated vs activated in the STORY-MATH contrast (Panel J).

Anterior to the 6-8 transitional areas are five subdivisions of area 8 (8BM, 8BL, 8Ad, 8Av, and 8C), whose names largely reflect correspondences with architectonic areas defined by (Petrides and Pandya, 1999), except that their 8Av is subdivided into 8Av plus a new area 8C and their 8B is subdivided into 8BM and 8BL. Area 8BM was covered previously in Section #19 Anterior Cingulate and Medial Prefrontal Cortex. The medial and posterior borders of **8BL** with 8BM, 9m, SFL, and s6-8 were covered in #19 Anterior Cingulate and Medial Prefrontal Cortex or above. Relative to its anterior neighbor 9p, area **8BL** is thicker (Panel C), is more activated/less deactivated in the LANGUAGE STORY contrast (Panel I), and is more activated in the RELATIONAL-MATCH contrast in the left hemisphere (Panel L) and in the TOM-RANDOM (Panel K) and FACES-SHAPES contrasts in the right hemisphere. Relative to its inferior neighbor 8Ad, area **8BL** has less myelin (Panel B), is thicker (Panel C), differs in functional connectivity (Panel D), is deactivated vs activated in the working memory 2BK-0BK contrast (Panel E) and activated vs deactivated in the RELATIONAL-MATCH contrast in the left hemisphere (Pane L). Relative to its anterior neighbor 9p, area **8Ad** has more myelin (Panel B), is thicker (Panel C), differs in functional connectivity (Panel D), is more deactivated in the GAMBLING primary contrasts (e.g. Panel F), and is less activated/deactivated vs activated in the MOTOR AVG contrast. Relative to its anterior neighbor 9-46d, area **8Ad** differs strongly in functional connectivity (Panel D), is less activated in the working memory 2BK-0BK contrast (Panel E), and is deactivated vs activated in the GAMBLING and RELATIONAL primary contrasts (e.g. Panel F) and in the MOTOR CUE (Panel G) and CUE-AVG contrasts. Relative to its antero-lateral neighbor 46, area **8Ad** has more myelin (Panel B), is thicker (Panel C), differs strongly in functional connectivity (Panel D), and is deactivated vs activated in the MOTOR CUE (Panel G) and CUE-AVG contrasts. Relative to its infero-lateral neighbor 8Av, area **8Ad** differs in functional connectivity (Panel D), is deactivated vs activated in the working memory, GAMBLING, and RELATIONAL primary contrasts (e.g. Panel F), and is deactivated/less activated vs more activated in the RELATIONAL-MATCH contrast (Panel L). Relative to its postero-lateral neighbor 55b, area **8Av** differs in functional connectivity (Panel D), is less activated in the STORY (Panel I) and MOTOR CUE contrasts (Panel G), and is less activated in the TOM-RANDOM contrast in the right hemisphere only (Panel K). Relative to its anterior neighbor 46, area **8Av** differs in functional connectivity (Panel D), is deactivated vs activated in the MOTOR CUE (Panel G) and CUE-AVG contrasts, and is activated vs deactivated in the RELATIONAL-MATCH contrast (Panel L). Relative to its infero-lateral neighbor 8C, area **8Av** differs modestly in functional connectivity (Panel D), is less activated in the working memory 2BK-0BK contrast (Panel E), is deactivated vs activated in the MOTOR CUE (Panel G) and CUE-AVG contrasts, and is activated vs deactivated in the STORY-MATH contrast (Panel J). Relative to its antero-medial neighbor 46, area **8C** has more myelin (Panel B), differs strongly in functional connectivity (Panel D), and is locally more activated in the 2BK-0BK contrast (Panel E), is less activated in the MOTOR CUE (Panel G) and CUE-AVG contrasts, and is activated vs deactivated in the RELATIONAL-MATCH contrast (Panel L). Relative to its anterior neighbor p9-46v, area **8C** differs in functional connectivity (Panel D), is less activated in primary contrasts (e.g. Panel F) and in the MOTOR CUE (Panel G) and CUE-AVG contrasts, and is deactivated vs activated in the LANGUAGE MATH contrast (Panel H). Relative to its posterior neighbor 55b, area **8C** differs strongly in functional connectivity (Panel D) and is deactivated/less-activated in the LANGUAGE STORY contrast (Panel I). The inferior borders of area **8C** with PEF, IFJp, IFJa,

and IFSp were covered previously (Sections #8 Premotor Cortex and #21 Inferior Frontal Cortex).

We subdivided area 9 into three areas: 9m (covered previously in Section #19 Anterior Cingulate and Medial Prefrontal Cortex) and areas **9p** and **9a** (based on splitting the lateral portion of area 9 of (Petrides and Pandya, 1999). The medial (9m) and posterior (8BL, 8Ad) borders of area **9p** have already been covered (Section #19 Anterior Cingulate and Medial Prefrontal Cortex and above). Relative to its infero-lateral neighbor 9-46d, area **9p** has less myelin (Panel B), differs strongly in functional connectivity (Panel D), is deactivated vs activated in the working memory 2BK-0BK (Panel E), MOTOR CUE (Panel G, assessed only statistically) and CUE-AVG contrasts, and is mostly activated vs deactivated in the STORY-MATH contrast (Panel J). Relative to its anterior neighbor 9a, area **9p** is slightly thicker (Panel C), differs modestly in functional connectivity (Panel D), is deactivated vs activated in the SOCIAL primary contrasts in the left hemisphere, is less activated in the TOM-RANDOM contrast in the right hemisphere (Panel K), is mainly deactivated vs activated in the left hemisphere, and is mainly activated vs deactivated in the right hemisphere in the RELATIONAL-MATCH contrast (Panel L). Relative to its infero-lateral neighbor 9-46d, area **9a** has less myelin (Panel B), differs strongly in functional connectivity (Panel D), is deactivated vs activated in the working memory and RELATIONAL primary contrasts and in the working memory 2BK-0BK (Panel E), MOTOR CUE (Panel G), and CUE-AVG contrasts, and is activated vs deactivated in the STORY-MATH contrast (Panel J). The medial (9m) and anterior (10d and p10p) borders of **9a** have already been covered (Sections #19 Anterior Cingulate and Medial Prefrontal Cortex and #20 Orbital and Polar Frontal Cortex).

We identified four areas in the central portion of the dorsolateral prefrontal cortex region: **9-46d**, **46**, **a9-46v**, and **p9-46v**. The names are based on approximate correspondences with areas 9-46d, 46, and 9-46v of (Petrides and Pandya, 1999) except that we identify discontinuous anterior and posterior subdivisions of their area 9-46v. The anterior (p10p, a10p, a47r) and inferior (p47r) borders of area **a9-46v** were covered already (Sections #20 Orbital and Polar Frontal Cortex and #21 Interior Frontal Cortex). Relative to its superior neighbor 9-46d, area **a9-46v** differs in functional connectivity (Panel D), is deactivated vs activated in the SOCIAL TOM primary contrast, and is more deactivated in the TOM-RANDOM contrast (Panel K). Relative to its posterior neighbor 46, area **a9-46v** has slightly more myelin (Panel B), differs modestly in functional connectivity (Panel D), is more activated in the working memory, GAMBLING, and RELATIONAL primary contrasts (e.g. Panel F) and in the working memory 2BK-0BK contrast in the left hemisphere (Panel E), is more deactivated in the LANGUAGE STORY-MATH contrast in the left hemisphere (Panel J) and in the TOM-RANDOM contrast in both hemispheres (Panel K), and is more activated in the RELATIONAL-MATCH contrast in the left hemisphere (Panel L). The borders of **p9-46v** inferiorly with IFSa and IFSp and posteriorly with 8C were already covered (Section #21 Interior Frontal Cortex and above). Relative to its superior neighbor 46, area **p9-46v** has more myelin (Panel B), differs in functional connectivity (Panel D), is more activated in the working memory 2BK-0BK contrast (Panel E) and in the working memory, GAMBLING, and RELATIONAL primary task contrasts (e.g. Panel F), is activated vs deactivated in the LANGUAGE MATH (Panel H) and RELATIONAL-MATCH (Panel L) contrasts, and is more deactivated in the STORY-MATH contrast (Panel J). In the left hemisphere, the primary contrasts and RELATIONAL-MATCH contrasts were only

assessed statistically. Relative to its supero-medial neighbor 9-46d in the left hemisphere, area **46** has less myelin (Panel B), differs modestly in functional connectivity (Panel D), and is less activated in the working memory, GAMBLING, and RELATIONAL primary task contrasts (e.g. Panel F) and in the working memory 2BK-0BK (Panel E) and LANGUAGE MATH (Panel H) contrasts, is more deactivated in the STORY-MATH contrast (Panel J), and is deactivated vs activated in the RELATIONAL-MATCH contrast (Panel L). Relative to area 9-46d in the right hemisphere, area **46** differs modestly in functional connectivity (Panel D), is modestly less deactivated in the LANGUAGE STORY-MATH contrast (Panel J), and is modestly more deactivated in the RELATIONAL-MATCH contrast (Panel L). This central region of the DLPFC (including area 46) is also a hotspot of individual variability, including topologically incompatible areal configurations (Rajkowska and Goldman-Rakic, 1995a, b).

Table 1 lists the 180 areas of the cortical parcellation with index number, short name, description, whether or not the area is new or not, the sections the area is described in, synonyms or 'quasi-synonyms' for the area, and key studies used for the area's identification. A "Yes" in the 'New?' column signifies an area that was not previously described in the neuroanatomical literature as far as we are aware. For some areas, "Yes*" signifies subdivisions of a previously described area, homologues, or similarity to a previously described area but not the same. "No" means that the area was previously described in a very similar form to what we found here. The **bold** section number is the primary section in which the area is described. **Bold** studies are those that had surface-mapped data available for us to make direct comparisons on the same atlas mesh.

Parcel Index	Area Name	Area Description	New?	Sections	Other Names	Key Studies
1	V1	Primary Visual Cortex	No	**1**,2	17, hOC1, OC, BA17	Amunts et al 2000, **Fischl et al 2008**, **Abdollahi et al 2014**
2	MST	Medial Superior Temporal Area	No	**5**,15	MSTv, hOC5, hOC5v	**Abdollahi et al 2014**, Kolster et al 2010, Malikovic et al 2007, **Fischl et al 2008**
3	V6	Sixth Visual Area	No	2,**3**,18	112	Pitzalis et al 2006, Pitzalis et al 2013, Sereno et al 2012, Nieuwenhuys et al 2014
4	V2	Second Visual Area	No	1,**2**	18, hOC2, OB, BA18	Amunts et al 2000, **Fischl et al 2008**, Schira et al 2009, **Abdollahi et al 2014**, Wang et al 2015, Wandell and Winawer 2011
5	V3	Third Visual Area	No	**2**	V3d, V3v, VP, hOC3d, hOC3v	**Abdollahi et al 2014**, Rottschy et al 2007, Schira et al 2009, Kujovic et al 2012, Wang et al 2015, Wandell and Winawer 2011
6	V4	Fourth Visual Area	No	**2**,3,4,5	V4d, V4v, hV4, hOC4v, hOC4lp, LO1	Hansen et al 2007, **Abdollahi et al 2014**, Rottschy et al 2007, Malikovic et al 2015
7	V8	Eighth Visual Area	No	2,**4**,5	VO1	Hadjikhani et al 1998, **Abdollahi et al 2014**
8	4	Primary Motor Cortex	No	**6**,7,8,9	BA4, 4a, 4p, M1, PMC, F1	**Fischl et al 2008,** Geyer et al 1996
9	3b	Primary Sensory Cortex	No	**6**,7,9	S1, 3	**Fischl et al 2008,** Geyer et al 1999, Geyer et al 2000
10	FEF	Frontal Eye Fields	No	6,**8**,22		**Glasser and Van Essen 2011**, Amiez and Petrides 2009
11	PEF	Premotor Eye Field	No	6,**8**,21,22	6v2	Amiez and Petrides 2009, Amunts et al 2010
12	55b	Area 55b	No	6,**8**,22		Hopf 1956
13	V3A	Area V3A	No	2,**3**	V3D, hOC4d	**Abdollahi et al 2014**, Swisher et al 2007, Kujovic et al 2012, Wandell and Winawer 2011, Larsson and Heeger 2006, Tootell et al 1997
14	RSC	RetroSplenial Complex	No	13,**18**	29,30	**Glasser and Van Essen 2011,** Vogt, 2009, Palomero-Gallagher et al 2009
15	POS2	Parieto-Occipital Sulcus Area 2	Yes*	16,**18**		**Glasser and Van Essen 2011**
16	V7	Seventh Visual Area	No	**3**	IPS0	**Abdollahi et al 2014**, Swisher et al 2007, Larsson and Heeger 2006, Tootell et al 1998, Hagler et al 2007, Wang et al., 2015
17	IPS1	IntraParietal Sulcus Area 1	No	**3**,16,17		Swisher et al 2007, Wang et al., 2015, Hagler et al 2007
18	FFC	Fusiform Face Complex	No	**4**,5,14	FFA, FG2	**Glasser and Van Essen 2011,** Kanwisher and Yovel, 2006, Caspers et al 2013, Weiner et al 2014
19	V3B	Area V3B	No	**3**,5,17	V3C	**Abdollahi et al 2014**, Larsson and Heeger 2006, Swisher et al 2007, Wandell and Winawer 2011, Smith et al 1998
20	LO1	Area Lateral Occipital 1	No	2,**5**	LO2, hOC4la	**Abdollahi et al 2014,** Hansen et al 2007, Malikovic et al 2015, Larsson and Heeger 2006
21	LO2	Area Lateral Occipital 2	No	2,4,**5**	LO1, hOC4la	**Abdollahi et al 2014,** Hansen et al 2007, Malikovic et al 2015, Larsson and Heeger 2006
22	PIT	Posterior InferoTemporal	No	2,**4**,5	phPITv, phPITd, OFA, hOC4la	**Abdollahi et al 2014,** Kolster et al 2010, Malikovic et al 2015, Kanwisher and Yovel, 2006, Tsao et al 2008

		Complex				
23	MT	Middle Temporal Area	No	**5**,15	hOC5, hOC5d	**Abdollahi et al 2014**, Kolster et al 2010, Malikovic et al 2007, **Fischl et al 2008**
24	A1	Primary Auditory Cortex	No	10	Core, R1, TC, TE1.0, TE1.1, 41	**Glasser and Van Essen 2011**, Moerel et al 2014, von Economo and Koskinas 1925, Triarhou 2007, Morosan et al 2001
25	PSL	PeriSylvian Language Area	Yes	9,10,11, **15**,17		
26	SFL	Superior Frontal Language Area	Yes	7,19,**22**		
27	PCV	PreCuneus Visual Area	No	7,16,**18**	PrCu	Sereno et al 2012
28	STV	Superior Temporal Visual Area	Yes	11,**15**,17		
29	7Pm	Medial Area 7P	Yes	**16**,18	7P	Scheperjans et al 2008a, Scheperjans et al 2008b
30	7m	Area 7m	No	16,**18**		Scheperjans et al 2008a, Scheperjans et al 2008b
31	POS1	Parieto-Occipital Sulcus Area 1	Yes*	**18**	"Retrosplenial Cortex"	**Glasser and Van Essen 2011**
32	23d	Area 23d	No	**18**,19		Vogt, 2009, Palomero-Gallagher et al 2009
33	v23ab	Area ventral 23 a+b	No	**18**	23a, 23b, v23	Vogt, 2009, Palomero-Gallagher et al 2009
34	d23ab	Area dorsal 23 a+b	No	**18**	23a, 23b, d23	Vogt, 2009, Palomero-Gallagher et al 2009
35	31pv	Area 31p ventral	Yes*	**18**	31, 31d, 31v	Vogt, 2009, Palomero-Gallagher et al 2009
36	5m	Area 5m	No	6,**7**		Scheperjans et al 2008a, Scheperjans et al 2008b
37	5mv	Area 5m ventral	Yes*	**7**,16,18	5ci	Scheperjans et al 2008a, Scheperjans et al 2008b
38	23c	Area 23c	No	**7**,18,19		Vogt, 2009, Palomero-Gallagher et al 2009
39	5L	Area 5L	No	6,**7**,16		Scheperjans et al 2008a, Scheperjans et al 2008b
40	24dd	Dorsal Area 24d	No	6,**7**,18	24d	Palomero-Gallagher et al 2009, Vogt and Vogt 2003
41	24dv	Ventral Area 24d	No	**7**,19	24d	Palomero-Gallagher et al 2009, Vogt and Vogt 2003
42	7AL	Lateral Area 7A	Yes*	6,7,**16**		Scheperjans et al 2008a, Scheperjans et al 2008b
43	SCEF	Supplementary and Cingulate Eye Field	Yes*	**7**,19,22	SEF, CEF, 6, SMA, SMAr	Amiez and Petrides 2009
44	6ma	Area 6m anterior	Yes*	**7**,8,22	SMAr, 6, SMA	**Fischl et al 2008**, Vorobiev et al 1998, Geyer 2004
45	7Am	Medial Area 7A	Yes*	7,**16**,18		Scheperjans et al 2008a, Scheperjans et al 2008b
46	7Pl	Lateral Area 7P	Yes*	**16**,18		Scheperjans et al 2008a, Scheperjans et al 2008b
47	7PC	Area 7PC	No	6,**16**		Scheperjans et al 2008a, Scheperjans et al 2008b
48	LIPv	Area Lateral IntraParietal ventral	Yes*	**16**	hIP3	**Van Essen et al 2012a**, Scheperjans et al 2008a, Scheperjans et al 2008b
49	VIP	Ventral IntraParietal Complex	Yes*	**16**		**Van Essen et al 2012a**
50	MIP	Medial IntraParietal Area	Yes*	3,**16**,17		**Van Essen et al 2012a**
51	1	Area 1	No	**6**,7,9,17		**Fischl et al 2008,** Geyer et al 1999, Geyer et al 2000
52	2	Area 2	No	**6**,7,16,17		**Fischl et al 2008,** Grefkes et al 2000
53	3a	Area 3a	No	**6**,7,9,17		**Fischl et al 2008,** Geyer et al 1999, Geyer et al 2000
54	6d	Dorsal area 6	Yes*	6,7,**8**	6, 6aα	**Fischl et al 2008,** Geyer 2004, Geyer et al 2000
55	6mp	Area 6mp	Yes*	6,**7**,8	SMAc, 6, SMA	**Fischl et al 2008**, Vorobiev et al 1998, Geyer 2004
56	6v	Ventral Area 6	No	6,**8**,9	6, 6v1	**Fischl et al 2008**, Amunts et al 2010, Geyer 2004
57	p24pr	Area Posterior 24 prime	No	7,18,**19**	p24'	Vogt, 2009
58	33pr	Area 33 prime	No	18,**19**	33', 16	Vogt, 2009, Nieuwenhuys et al 2014
59	a24pr	Anterior 24 prime	No	**19**	a24'	Vogt, 2009
60	p32pr	Area p32 prime	Yes*	7,**19**	32'	Vogt, 2009
61	a24	Area a24	Yes*	**19**	24, s24	Vogt, 2009, Palomero-Gallagher et al 2015
62	d32	Area dorsal 32	No	**19**	32	Vogt, 2009
63	8BM	Area 8BM	Yes*	7,**19**,22	8B	Petredes and Pandya 1999
64	p32	Area p32	No	**19**,20	32ac, 32	**Van Essen et al 2012b,** Ongur et al 2003**,** Vogt, 2009, Palomero-Gallagher et al 2009
65	10r	Area 10r	Yes*	**19**,20		**Van Essen et al 2012b,** Ongur et al 2003
66	47m	Area 47m	No	**20**,21		**Van Essen et al 2012b,** Ongur et al 2003, **Glasser and Van Essen 2011**
67	8Av	Area 8Av	Yes*	8,**22**		Petredes and Pandya 1999
68	8Ad	Area 8Ad	Yes*	**22**		Petredes and Pandya 1999

69	9m	Area 9 Middle	Yes*	**19**,20,22	9	Petredes and Pandya 1999
70	8BL	Area 8B Lateral	Yes*	19,**22**	8B	Petredes and Pandya 1999
71	9p	Area 9 Posterior	Yes*	19,**22**	9	Petredes and Pandya 1999
72	10d	Area 10d	Yes*	19,**20**,22	10, Fp1, Fp2	Petredes and Pandya 1999, Bludau et al 2014
73	8C	Area 8C	Yes*	8,21,**22**	8Av	Petredes and Pandya 1999
74	44	Area 44	No	8,12,**21**	44d, 44v	**Fischl et al 2008,** Amunts et al 1999, Amunts et al 2010
75	45	Area 45	No	12,**21**	45a, 45p	**Fischl et al 2008,** Amunts et al 1999, Amunts et al 2010
76	47l	Area 47l (47 lateral)	No	12,20,**21**		**Van Essen et al 2012b,** Ongur et al 2003
77	a47r	Area anterior 47r	Yes*	20,**21**,22	47r	**Van Essen et al 2012b,** Ongur et al 2003
78	6r	Rostral Area 6	No	**8**,9,12,21		Amunts et al 2010
79	IFJa	Area IFJa	Yes	8,**21**,22		
80	IFJp	Area IFJp	Yes	8,**21**,22		
81	IFSp	Area IFSp	Yes	**21**,22		
82	IFSa	Area IFSa	Yes	**21**,22		
83	p9-46v	Area posterior 9-46v	Yes*	21,**22**	9-46v	Petredes and Pandya 1999
84	46	Area 46	No	21,**22**		Petredes and Pandya 1999, Rajkowska and Goldman-Rakic 1995a, Rajkowska and Goldman-Rakic 1995b
85	a9-46v	Area anterior 9-46v	Yes*	20,21,**22**	9-46v	Petredes and Pandya 1999
86	9-46d	Area 9-46d	No	20,**22**		Petredes and Pandya 1999
87	9a	Area 9 anterior	Yes*	19,20,**22**	9	Petredes and Pandya 1999
88	10v	Area 10v	Yes	**19**,20	10, Fp2	Bludau et al 2014
89	a10p	Area anterior 10p	Yes*	**20**,22	10p, 10, Fp1	**Van Essen et al 2012b,** Ongur et al 2003, Bludau et al 2014
90	10pp	Polar 10p	Yes*	19,**20**	10p, 10, Fp1	**Van Essen et al 2012b,** Ongur et al 2003, Bludau et al 2014
91	11l	Area 11l	No	**20**	Fo3	**Van Essen et al 2012b,** Ongur et al 2003, Henssen et al 2016
92	13l	Area 13l	No	**20**	Fo3	**Van Essen et al 2012b,** Ongur et al 2003, Henssen et al 2016
93	OFC	Orbital Frontal Complex	Yes*	19,**20**	11m, 13b, 13m, 14r, Fo1	**Van Essen et al 2012b,** Ongur et al 2003, Henssen et al 2016
94	47s	Area 47s	No	12,**20**		**Van Essen et al 2012b,** Ongur et al 2003
95	LIPd	Area Lateral IntraParietal dorsal	Yes*	**16**,17		**Van Essen et al 2012a**
96	6a	Area 6 anterior	Yes	7,**8**,22	6, 6aβ	**Fischl et al 2008,** Geyer 2004, Geyer et al 2000
97	i6-8	Inferior 6-8 Transitional Area	Yes*	8,**22**	FC(B)	von Economo and Koskinas 1925, Triarhou 2007
98	s6-8	Superior 6-8 Transitional Area	Yes*	7,8,**22**	FC(B)	von Economo and Koskinas 1925, Triarhou 2007
99	43	Area 43	No	6,8,**9**,12	41	Brodmann 1909, Brodmann 2007, Nieuwenhuys et al 2014
100	OP4	Area OP4/PV	No	6,**9**,17	68	Eickhoff et al 2006a, Eickhoff et al 2006b, Nieuwenhuys et al 2014
101	OP1	Area OP1/SII	No	**9**,10		Eickhoff et al 2006a, Eickhoff et al 2006b
102	OP2-3	Area OP2-3/VS	Yes*	**9**,10,12	OP2,OP3	Eickhoff et al 2006a, Eickhoff et al 2006b
103	52	Area 52	No	**10**,12	IBT	Brodmann 1909, Brodmann 2007, von Economo and Koskinas 1925, Triarhou 2007
104	RI	RetroInsular Cortex	No	9,**10**,12,15	reI, reIt, RetroInsular, Belt, TD	**Glasser and Van Essen 2011,** Pandya and Sanides 1973, Kurth et al 2009,von Economo and Koskinas 1925, Triarhou 2007
105	PFcm	Area PFcm	No	9,**10**,15,17		Caspers et al 2006, Caspers et al 2008
106	PoI2	Posterior Insular Area 2	Yes*	**12**	Id1, Id2, Id3	Kurth et al 2009, Morel et al 2013
107	TA2	Area TA2	No	10,**11**,12	TE1.2	von Economo and Koskinas 1925, Triarhou 2007, Morosan et al 2001
108	FOP4	Frontal OPercular Area 4	Yes	9,**12**,21		
109	MI	Middle Insular Area	Yes*	**12**	Ial	**Van Essen et al 2012b,** Ongur et al 2003

110	Pir	Pirform Cortex	No	**12,**14,20	Poc	**Glasser and Van Essen 2011**, Ding et al 2009, Morel et al 2013
111	AVI	Anterior Ventral Insular Area	Yes*	**12**,20,21	Iai	**Van Essen et al 2012b,** Ongur et al 2003
112	AAIC	Anterior Agranular Insula Complex	Yes*	**12**,20	Iai, Ial	**Van Essen et al 2012b,** Ongur et al 2003
113	FOP1	Frontal OPercular Area 1	Yes	8,**9**,12		
114	FOP3	Frontal OPercular Area 3	Yes	**12**		
115	FOP2	Frontal OPercular Area 2	Yes	9,**12**		
116	PFt	Area PFt	No	6,16,**17**		Caspers et al 2006, Caspers et al 2008
117	AIP	Anterior IntraParietal Area	Yes*	6,**16**,17		**Van Essen et al 2012a**
118	EC	Entorhinal Cortex	No	**13**	28	**Fischl et al 2009**
119	PreS	PreSubiculum	No	2,**13**,18	Sub, Subicular	**Glasser and Van Essen 2011,** Amunts et al 2005
120	H	Hippocampus	No	**13**		
121	ProS	ProStriate Area	No	1,2,13,**18**		**Glasser and Van Essen 2011**, Vogt et al 2001, Sanides and Vitzthum 1965, Sanides, 1970
122	PeEc	Perirhinal Ectorhinal Cortex	Yes*	**13**,14	ATFP, AFP1, Ectorhinal, Perirhinal, 35, 36	Augustinack et al 2013, Ding et al 2009, Ding and Van Hoesen 2010, Rajimehr et al 2009, Tsao et al 2008
123	STGa	Area STGa	Yes	**11**,12,14		
124	PBelt	ParaBelt Complex	Yes*	**10**,11	ParaBelt, TA1	Moerel et al 2014, von Economo and Koskinas 1925, Triarhou 2007
125	A5	Auditory 5 Complex	Yes	**11**,15		
126	PHA1	ParaHippocampal Area 1	Yes	2,4,**13**		
127	PHA3	ParaHippocampal Area 3	Yes	4,**13**,14		
128	STSda	Area STSd anterior	Yes	**11**,14		
129	STSdp	Area STSd posterior	Yes	**11**,15		
130	STSvp	Area STSv posterior	Yes	**11**,14,15		
131	TGd	Area TG dorsal	Yes*	11,12,13,**14**	TG	Ding et al 2009, von Economo and Koskinas 1925, Triarhou 2007
132	TE1a	Area TE1 anterior	Yes*	11,**14**		von Economo and Koskinas 1925, Triarhou 2007
133	TE1p	Area TE1 posterior	Yes*	5,11,**14**		von Economo and Koskinas 1925, Triarhou 2007
134	TE2a	Area TE2 anterior	Yes*	**14**		von Economo and Koskinas 1925, Triarhou 2007
135	TF	Area TF	No	4,**13**,14		von Economo and Koskinas 1925, Triarhou 2007
136	TE2p	Area TE2 posterior	Yes*	4,5,**14**		von Economo and Koskinas 1925, Triarhou 2007
137	PHT	Area PHT	No	5,11,**14**,15		von Economo and Koskinas 1925, Triarhou 2007
138	PH	Area PH	No	4,**5**,14		von Economo and Koskinas 1925, Triarhou 2007
139	TPOJ1	Area TemporoParietoOccipital Junction 1	Yes	11,14,**15**,17		
140	TPOJ2	Area TemporoParietoOccipital Junction 2	Yes	5,14,**15**,17		
141	TPOJ3	Area TemporoParietoOccipital Junction 3	Yes	5,**15**,17		
142	DVT	Dorsal Transitional Visual Area	Yes	2,3,16,**18**		
143	PGp	Area PGp	No	5,15,**17**	39,PG	Caspers et al 2006, Caspers et al 2008
144	IP2	Area IntraParietal 2	No	16,**17**		Choi et al 2006
145	IP1	Area IntraParietal 1	No	16,**17**		Choi et al 2006
146	IP0	Area IntraParietal 0	Yes	3,5,16,**17**		
147	PFop	Area PF opercular	No	6,9,**17**	40, 72	Caspers et al 2006, Caspers et al 2008, Nieuwenhuys et al 2014
148	PF	Area PF Complex	No	9,15,**17**	40, 88	Caspers et al 2006, Caspers et al 2008, Nieuwenhuys et al 2014

149	PFm	Area PFm Complex	No	15,**17**	40, 89	Caspers et al 2006, Caspers et al 2008, Nieuwenhuys et al 2014
150	PGi	Area PGi	No	15,**17**	PGa, 39, PG, 90	Caspers et al 2006, Caspers et al 2008, Nieuwenhuys et al 2014
151	PGs	Area PGs	No	15,**17**	PGa, 39, PG, 90	Caspers et al 2006, Caspers et al 2008, Nieuwenhuys et al 2014
152	V6A	Area V6A	No	**3**,18	112	Pizalis et al 2013, Nieuwenhuys et al 2014
153	VMV1	VentroMedial Visual Area 1	Yes*	2,**4**,13	PHC2, PHC-2	Arcaro et al 2009, Wang et al 2015
154	VMV3	VentroMedial Visual Area 3	Yes*	2,**4**,13	VO2	Arcaro et al 2009, Wang et al 2015, Wandell and Winawer 2011
155	PHA2	ParaHippocampal Area 2	Yes	4,**13**		
156	V4t	Area V4t	No	**5**	LO2	**Abdollahi et al 2014,** Kolster et al 2010, Larsson and Heeger 2006
157	FST	Area FST	No	**5**,14,15		**Abdollahi et al 2014,** Kolster et al 2010
158	V3CD	Area V3CD	Yes	2,3,**5**,17	V3A,V3B, hOC4la	**Abdollahi et al 2014,** Malikovic et al 2015
159	LO3	Area Lateral Occipital 3	Yes	**5**,15,17	hOC4la	
160	VMV2	VentroMedial Visual Area 2	Yes*	2,**4**,13	PHC1, PHC-1	Arcaro et al 2009, Wang et al 2015
161	31pd	Area 31pd	Yes*	**18**	31, 31d, 31v	Vogt, 2009, Palomero-Gallagher et al 2009
162	31a	Area 31a	Yes*	**18**	31, 31d, 31v	Vogt, 2009, Palomero-Gallagher et al 2009
163	VVC	Ventral Visual Complex	Yes*	**4**,13,14	VO1, VO2, PHC1, PHC2, PHC-1, PHC-2, FG1	Arcaro et al 2009, Wang et al 2015, Wandell and Winawer 2011, Caspers et al 2013, Weiner et al 2014
164	25	Area 25	No	**19**,20		Vogt, 2009, Palomero-Gallagher et al 2015
165	s32	Area s32	No	**19**	32pl, 32	Vogt, 2009, Palomero-Gallagher et al 2015, **Van Essen et al 2012b**, Ongur et al 2003
166	pOFC	posterior OFC Complex	Yes*	12,**19**,20	13a, 14c, Fo2	**Van Essen et al 2012b,** Ongur et al 2003, Henssen et al 2016
167	PoI1	Area Posterior Insular 1	Yes*	**12**	Id1, Id2, Id3	Kurth et al 2009, Morel et al 2013
168	Ig	Insular Granular Complex	Yes*	9,**12**	Ig1, Ig2	Kurth et al 2009, Morel et al 2013
169	FOP5	Area Frontal Opercular 5	Yes	**12**,21	PrCO	**Glasser and Van Essen 2011**
170	p10p	Area posterior 10p	Yes*	**20**,22	10p, 10, Fp1	**Van Essen et al 2012b,** Ongur et al 2003, Bludau et al 2014
171	p47r	Area posterior 47r	Yes*	20,**21**,22	47r	**Van Essen et al 2012b,** Ongur et al 2003
172	TGv	Area TG Ventral	Yes*	13,**14**		Ding et al 2009, von Economo and Koskinas 1925, Triarhou 2007
173	MBelt	Medial Belt Complex	Yes*	**10**,12	Belt, TB	Moerel et al 2014, von Economo and Koskinas 1925, Triarhou 2007
174	LBelt	Lateral Belt Complex	Yes*	**10**	Belt, TB	Moerel et al 2014, von Economo and Koskinas 1925, Triarhou 2007
175	A4	Auditory 4 Complex	Yes*	**11**,15	TE3	Morosan et al 2005
176	STSva	Area STSv anterior	Yes	**11**,14		
177	TE1m	Area TE1 Middle	Yes*	11,**14**		von Economo and Koskinas 1925, Triarhou 2007
178	PI	Para-Insular Area	No	11,**12**,14	IBT	von Economo and Koskinas 1925, Triarhou 2007, Ding et al 2009
179	a32pr	Area anterior 32 prime	Yes*	**19**	32'	Vogt, 2009
180	p24	Area posterior 24	Yes*	**19**	24	Vogt, 2009

Table 2 lists the neuroanatomical studies used to identify areas in this parcellation. Our area name is given and the study's area name is in parentheses.

Short Citation	Our Area Names (The Study's Area Names)
Abdollahi et al 2014	V1, V2, V3, V4 (V4 + LO1 + LO2 + V3A + V3B), V3A (V3D), V3B (V3C), V3CD (V3A + V3B), V7, V8 (VO1), LO1, LO2, PIT(PITd + PITv), MT, MST, FST, V4t
Amiez and Petrides 2009	SCEF (SEF + CEF), FEF, PEF
Amunts et a 2000	V1 (17), V2 (18)
Amunts et al 1999	44, 45
Amunts et al 2005	PreS (Subicular Complex)
Amunts et al 2010	6r, 6v (6v1), PEF (6v2), 44 (44d + 44v), 45 (45a + 45p)
Arcaro et al 2009	V8 (VO1), VVC (VO1 + VO2 + PH1 + PH2), VMV3 (VO2), VMV2 (PHC1), VMV1 (PHC2)
Augustinack et al 2013	PeEc (Perirhinal)
Bludau et al 2014	10pp + a10p + p10p + 10d (Fp1), 10r + 10v + 10d (Fp2)
Brodmann 1909, Brodmann 2007	43, 52, V1 (17), V2 (18), 4, 3a + 3b (3), 1, 2, A1 (41)
Caspers et al 2006	PFcm, PGp, PGs PGi (PGa), PFm, PF, PFt, PFop
Caspers et al 2008	PFcm, PGp, PGs PGi (PGa), PFm, PF, PFt, PFop
Caspers et al 2013	FFC (FG2), VVC (FG1)
Choi et al 2006	IP1, IP2
Ding et al 2009	PI, Pir, PeEc (35 + 36), TGd + TGv (TG)
Eickhoff et al 2006a	OP1, OP4, OP2-3 (OP2 + OP3)
Eickhoff et al 2006b	OP1, OP4, OP2-3 (OP2 + OP3)
Fischl et al 2008	V1 (17), V2 (18), 4 (4a + 4p), 3a, 3b, 1, 2, MT (hOC5), MST (hOC5), 44, 45, 6v (6), 55b (6), FEF (6), 6d (6), 6a (6), 6mp (6), 6ma (6), SCEF (6), SFL (6), 24dd (6)
Fischl et al 2009	EC
Geyer 2004	6v (6), 55b (6), FEF (6), 6d (6), 6a (6), 6mp (6), 6ma (6), SCEF (6), SFL (6), 24dd (6)
Geyer et al 1996	4 (4a + 4p)
Geyer et al 1999	3a, 3b, 1
Geyer et al 2000	3a, 3b, 1
Geyer et al 2000	6a (6aβ), 6d (6aα)
Glasser and Van essen 2011	FOP5 (PrCO), PreS (Sub)
Grefkes et al 2000	2
Hadjikhani et al 1998	V8
Hagler et al 2007	V7, IPS1
Hansen et al 2007	V4, LO1 + LO2 (LOC)
Henssen et al 2016	pOFC (Fo2), OFC (Fo1), 11l+13l (Fo3)
Hopf 1956	55b
Kanwisher and Yovel 2006	PIT (OFA), FFC (FFA)
Kolster et al 2010	MT (MT/V5), MST (pMST), V4t (pV4t), FST (pFST), PIT (phPITd + phPITv), LO1, LO2
Kujovic et al 2012	V3 (hOC3d), V3A (hOC4d)
Kurth et al 2009	RI (RetroInsular), Ig (Ig1 + Ig2), PoI1 + PoI2 (Id1 + Id2 + Id3)
Larsson and Heeger 2006	V3A, V3B, V7, V4 (hV4 + LO1), LO1 (LO1 + LO2), LO2 (LO1 + LO2), V4t (LO2)
Malikovic et al 2007	MT (hOC5d), MST (hOC5v)
Malikovic et al 2015	V4 (hOC4lp), V4t + LO1 + LO2 + LO3 + PIT + V3CD (hOC4la)
Moerel et al 2014	A1 (Core), MBelt (Belt), LBelt (Belt), PBelt (ParaBelt), RI (Belt)
Morel et al 2013	Ig, PoI1 + PoI2 (Id1 + Id2 + Id3), Pir (Poc)
Morosan et al 2001	A1 (TE1.0 + TE1.1), TA2 (TE1.2)
Morosan et al 2005	A4 (TE3)
Nieuwenhuys et al 2014	V6 + V6A (112), 43 (41), OP4 (68), PFop (72), PF (88), PFm (89), PGs+PGi (90), 33pr (16)
Ongur et al 2003	AAIC (Iai + Ial), AVI (Iai), MI (Ial), 10r, a10p + p10p + 10pp (10p), 47s, 47m, 47l, a47r + p47r (47r), 11l, 13l, OFC (11m + 13b + 13m + 14r), and pOFC (13a + 14c)
Palomero-Gallagher et al 2009	24dd, 24dv, v23ab (v23), d23ab (d23), 31pv (31), 31pd (31), 31a (31), 23d, 23c
Palomero-Gallagher et al 2015	25, a24 (s24), s32
Pandya and Sanides 1973	RI (reIt)
Petrides and Pandya 1999	8BM + 8BL (8B), 9m + 9a + 9p (9), 10d + 10r + 10v + a10p + p10p + 10pp (10), 8C + 8Av (8Av), 8Ad, p9-46v + a9-46v (9-46v), 46, 9-46d
Pitzalis et al 2006	V6
Pitzalis et al 2013	V6, V6A
Rajimehr et al 2009	FFC (FFA), PeEc (ATFP)
Rajkowska and Goldman-Rakic 1995a	46
Rajkowska and Goldman-Rakic 1995b	46
Rottschy et al 2007	V3 (hOC3v), V4 (hOC4v)

Sanides and Vitzthum 1965, Sanides, 1970	ProS (pStr)
Scheperjans et al 2008a	5L, 5m, 5mv (5ci), 7PC, 7AL + 7Am (7A), 7PL + 7Pm (7P), LIPv (hIP3)
Scheperjans et al 2008b	5L, 5m, 5mv (5ci), 7PC, 7AL + 7Am (7A), 7PL + 7Pm (7P), LIPv (hIP3)
Schira et al 2009	V1, V2, V3
Sereno et al 2012	V6
Smith et al 1998	V3B
Swisher et al 2007	V3A, V3B, V7, IPS1
Tootell et al 1997	V3A
Tootell et al 1998	V7
Tsao et al 2008	PIT (OFA), FFC (FFA), PeEc (ATFP)
Van Essen et al 2012a	LIPv, LIPd, VIP (VIPd + VIPv), MIP, AIP
Van Essen et al 2012b	AAIC (Iai + Ial), AVI (Iai), MI (Ial), 10r, a10p + p10p + 10pp (10p), 47s, 47m, 47l, a47r + p47r (47r), 11l, 13l, OFC (11m + 13b + 13m + 14r), and pOFC (13a + 14c)
Vogt 2009	v23ab (v23), d23ab (d23), 31pv (31), 31pd (31), 31a (31), 23d, 23c, 33pr (31a' + 31p'), p24pr (p24'), a24pr (a24'), p24 + a24 (24), p32pr + a32pr (32'), d32, p32, s32, 25
Vogt and Vogt 2003	24dd, 24dv
Vogt et al 2001	ProS
von Economo and Koskinas 1925, Triarhou 2007	V1 (OC), V2 (OB), A1 (TC), MBelt + LBelt (TB), RI (TD), PBelt (TA1), TA2, 52 + PI (IBT), TE1a + TE1m + TE1p (TE1), TE2a + TE2p (TE2), TF, PHT, PH, TGv + TGd (TG), s6-8 + i6-8 (FC(B))
Vorobiev et al 1998	6mp (SMAc), 6ma (SMAr), SCEF (SMAr)
Wandell and Winawer 2011	V1, V2, V3, V3A, V3B, V4 (hV4), V8 (VO1), VVC (VO1 + VO2), VMV3 (VO2)
Wang et al 2015	V1 (V1d + V1v), V2 (V2d + V2v), V3 (V3d +V3v), V3A, V3B, V7 (IPS0), IPS1, VVC
Weiner et al 2014	FFC (FG2), VVC (FG1)

Table 3 lists the task contrasts used above including the contrast index in the composite HCP task battery, the task name, the contrast index (cope number) within the task, the contrast name, and a brief description of the contrast.

Primary Contrast Differential Contrast Duplicate Contrast

Contrast Index	Task short name	Cope number	Task Contrast Name	Brief Description
1	WM [1]	1	2BK_BODY	Two-back task, body images(vs fixation) [2]
2	WM	2	2BK_FACE	Two-back task, face images (vs fixation)
3	WM	3	2BK_PLACE	Two-back task, place images (vs fixation)
4	WM	4	2BK_TOOL	Two-back task, tool images (vs fixation)
5	WM	5	0BK_BODY	Zero-back task, body images (vs fixation) [3]
6	WM	6	0BK_FACE	Zero-back task, face images (vs fixation)
7	WM	7	0BK_PLACE	Zero-back task, place images (vs fixation)
8	WM	8	0BK_TOOL	Zero-back task, tool images (vs fixation)
9	WM	9	2BK	Two-back task, all images (vs fixation)
10	WM	10	0BK	Zero-back task, all images (vs fixation)
11	WM	11	2BK-0BK	2BK vs 0BK
12	WM	12	neg_2BK	
13	WM	13	neg_0BK	
14	WM	14	0BK-2BK	0BK vs 2BK
15	WM	15	BODY	All body images (vs fixation)
16	WM	16	FACE	All face images (vs fixation)
17	WM	17	PLACE	All place images (vs fixation)
18	WM	18	TOOL	All tool images (vs fixation)
19	WM	19	BODY-AVG	All body images vs average of other 3 categories
20	WM	20	FACE-AVG	All face images vs average of other 3 categories
21	WM	21	PLACE-AVG	All place images vs average of other 3 categories
22	WM	22	TOOL-AVG	All tool images vs average of other 3 categories
23	WM	23	neg_BODY	
24	WM	24	neg_FACE	
25	WM	25	neg_PLACE	
26	WM	26	neg_TOOL	
27	WM	27	AVG-BODY	
28	WM	28	AVG-FACE	
29	WM	29	AVG-PLACE	
30	WM	30	AVG-TOOL	
31	GAMBLING [4]	1	PUNISH	Money loss blocks (vs fixation)
32	GAMBLING	2	REWARD	Money win blocks (vs fixation)
33	GAMBLING	3	PUNISH-REWARD	PUNISH vs REWARD
34	GAMBLING	4	neg_PUNISH	
35	GAMBLING	5	neg_REWARD	
36	GAMBLING	6	REWARD-PUNISH	REWARD vs PUNISH
37	MOTOR [5]	1	CUE	visual instruction cue (vs fixation)
38	MOTOR	2	LF	squeeze left toes (vs fixation)
39	MOTOR	3	LH	tap left fingers (vs fixation)
40	MOTOR	4	RF	squeeze right toes (vs fixation)
41	MOTOR	5	RH	tap right fingers (vs fixation)
42	MOTOR	6	T	move tongue (vs fixation)
43	MOTOR	7	AVG	Average of LF,LH,RF,RH,T (vs fixation)
44	MOTOR	8	CUE-AVG	CUE vs average of other 4 effectors
45	MOTOR	9	LF-AVG	LF vs average of other 4 effectors
46	MOTOR	10	LH-AVG	LH vs average of other 4 effectors
47	MOTOR	11	RF-AVG	RF vs average of other 4 effectors
48	MOTOR	12	RH-AVG	RH vs average of other 4 effectors
49	MOTOR	13	T-AVG	T vs average of other 4 effectors
50	MOTOR	14	neg_CUE	
51	MOTOR	15	neg_LF	

52	MOTOR	16	neg_LH	
53	MOTOR	17	neg_RF	
54	MOTOR	18	neg_RH	
55	MOTOR	19	neg_T	
56	MOTOR	20	neg_AVG	
57	MOTOR	21	AVG-CUE	
58	MOTOR	22	AVG-LF	
59	MOTOR	23	AVG-LH	
60	MOTOR	24	AVG-RF	
61	MOTOR	25	AVG-RH	
62	MOTOR	26	AVG-T	
63	LANGUAGE [6]	1	MATH	Answer arithmetic questions (vs intercept of GLM)
64	LANGUAGE	2	STORY	Listen to stories (vs intercept of GLM)
65	LANGUAGE	3	MATH-STORY	MATH vs STORY
66	LANGUAGE	4	STORY-MATH	STORY vs MATH
67	LANGUAGE	5	neg_MATH	
68	LANGUAGE	6	neg_STORY	
69	SOCIAL [7]	1	RANDOM	View randomly moving geometric objects (vs fixation)
70	SOCIAL	2	TOM	"Theory Of Mind": View "socially" interacting geometric objects (vs fixation)
71	SOCIAL	3	RANDOM-TOM	RANDOM vs TOM
72	SOCIAL	4	neg_RANDOM	
73	SOCIAL	5	neg_TOM	
74	SOCIAL	6	TOM-RANDOM	TOM vs RANDOM
75	RELATIONAL [8]	1	MATCH	Match objects based on verbal category (vs fixation)
76	RELATIONAL	2	REL	Compare featural dimensions distinguishing two pairs of objects (vs fixation)
77	RELATIONAL	3	MATCH-REL	MATCH vs REL
78	RELATIONAL	4	REL-MATCH	REL vs MATCH
79	RELATIONAL	5	neg_MATCH	
80	RELATIONAL	6	neg_REL	
81	EMOTION [9]	1	FACES	Emotional faces (vs intercept of GLM)
82	EMOTION	2	SHAPES	Neutral objects (vs intercept of GLM)
83	EMOTION	3	FACES-SHAPES	FACES vs SHAPES
84	EMOTION	4	neg_FACES	
85	EMOTION	5	neg_SHAPES	
86	EMOTION	6	SHAPES-FACES	SHAPES vs FACES

[1] WM = Working Memory
[2] Two-back: respond if current stimulus matches the item two back
[3] Zero-back: respond if current stimulus matches target cue presented at start of block
[4] adapted from (Delgado et al., 2000)
[5] adapted from (Buckner et al., 2011)
[6] Adapted from (Binder et al., 2011)
[7] Adapted from (Castelli et al., 2000; Wheatley et al., 2007)
[8] Adapted from (Smith et al., 2007)
[9] Adapted from (Hariri et al., 2002)

References

Abdollahi, R.O., Kolster, H., Glasser, M.F., Robinson, E.C., Coalson, T.S., Dierker, D., Jenkinson, M., Van Essen, D.C., Orban, G.A., 2014. Correspondences between retinotopic areas and myelin maps in human visual cortex. Neuroimage 99, 509-524.

Amiez, C., Petrides, M., 2009. Anatomical organization of the eye fields in the human and non-human primate frontal cortex. Prog Neurobiol 89, 220-230.

Amunts, K., Lenzen, M., Friederici, A.D., Schleicher, A., Morosan, P., Palomero-Gallagher, N., Zilles, K., 2010. Broca's region: novel organizational principles and multiple receptor mapping. PLoS Biol 8.

Amunts, K., Malikovic, A., Mohlberg, H., Schormann, T., Zilles, K., 2000. Brodmann's areas 17 and 18 brought into stereotaxic space-where and how variable? Neuroimage 11, 66-84.

Amunts, K., Schleicher, A., Burgel, U., Mohlberg, H., Uylings, H.B., Zilles, K., 1999. Broca's region revisited: cytoarchitecture and intersubject variability. J Comp Neurol 412, 319-341.

Arcaro, M.J., McMains, S.A., Singer, B.D., Kastner, S., 2009. Retinotopic organization of human ventral visual cortex. J Neurosci 29, 10638-10652.

Augustinack, J.C., Helmer, K., Huber, K.E., Kakunoori, S., Zollei, L., Fischl, B., 2010. Direct visualization of the perforant pathway in the human brain with ex vivo diffusion tensor imaging. Front Hum Neurosci 4, 42.

Augustinack, J.C., Huber, K.E., Stevens, A.A., Roy, M., Frosch, M.P., van der Kouwe, A.J., Wald, L.L., Van Leemput, K., McKee, A.C., Fischl, B., Alzheimer's Disease Neuroimaging, I., 2013. Predicting the location of human perirhinal cortex, Brodmann's area 35, from MRI. Neuroimage 64, 32-42.

Barch, D.M., Burgess, G.C., Harms, M.P., Petersen, S.E., Schlaggar, B.L., Corbetta, M., Glasser, M.F., Curtiss, S., Dixit, S., Feldt, C., Nolan, D., Bryant, E., Hartley, T., Footer, O., Bjork, J.M., Poldrack, R., Smith, S., Johansen-Berg, H., Snyder, A.Z., Van Essen, D.C., Consortium, W.U.-M.H., 2013. Function in the human connectome: task-fMRI and individual differences in behavior. Neuroimage 80, 169-189.

Baumann, S., Petkov, C.I., Griffiths, T.D., 2013. A unified framework for the organization of the primate auditory cortex. Front Syst Neurosci 7, 11.

Binder, J.R., Gross, W.L., Allendorfer, J.B., Bonilha, L., Chapin, J., Edwards, J.C., Grabowski, T.J., Langfitt, J.T., Loring, D.W., Lowe, M.J., 2011. Mapping anterior temporal lobe language areas with fMRI: a multicenter normative study. Neuroimage 54, 1465-1475.

Bludau, S., Eickhoff, S.B., Mohlberg, H., Caspers, S., Laird, A.R., Fox, P.T., Schleicher, A., Zilles, K., Amunts, K., 2014. Cytoarchitecture, probability maps and functions of the human frontal pole. Neuroimage 93 Pt 2, 260-275.

Brodmann, K., 1909. Vergleichende Lokalisationslehre der Grosshirnrinde in ihren Prinzipien dargestellt auf Grund des Zellenbaues. Leipzig, J.A. Barth; English translation available in Garey, L.J. Brodmann's Localization in the Cerebral Cortex (Smith Gordon, London, 1994).

Brodmann, K., 2007. Brodmann's: Localisation in the Cerebral Cortex. Springer Science & Business Media.

Buckner, R.L., Krienen, F.M., Castellanos, A., Diaz, J.C., Yeo, B.T., 2011. The organization of the human cerebellum estimated by intrinsic functional connectivity. Journal of neurophysiology 106, 2322-2345.
Burton, H., Sinclair, R.J., Wingert, J.R., Dierker, D.L., 2008. Multiple parietal operculum subdivisions in humans: tactile activation maps. Somatosens Mot Res 25, 149-162.
Caspers, J., Zilles, K., Eickhoff, S.B., Schleicher, A., Mohlberg, H., Amunts, K., 2013. Cytoarchitectonical analysis and probabilistic mapping of two extrastriate areas of the human posterior fusiform gyrus. Brain Struct Funct 218, 511-526.
Caspers, S., Eickhoff, S.B., Geyer, S., Scheperjans, F., Mohlberg, H., Zilles, K., Amunts, K., 2008. The human inferior parietal lobule in stereotaxic space. Brain Struct Funct 212, 481-495.
Caspers, S., Geyer, S., Schleicher, A., Mohlberg, H., Amunts, K., Zilles, K., 2006. The human inferior parietal cortex: cytoarchitectonic parcellation and interindividual variability. Neuroimage 33, 430-448.
Castelli, F., Happé, F., Frith, U., Frith, C., 2000. Movement and mind: a functional imaging study of perception and interpretation of complex intentional movement patterns. Neuroimage 12, 314-325.
Choi, H.J., Zilles, K., Mohlberg, H., Schleicher, A., Fink, G.R., Armstrong, E., Amunts, K., 2006. Cytoarchitectonic identification and probabilistic mapping of two distinct areas within the anterior ventral bank of the human intraparietal sulcus. J Comp Neurol 495, 53-69.
Delgado, M.R., Nystrom, L.E., Fissell, C., Noll, D., Fiez, J.A., 2000. Tracking the hemodynamic responses to reward and punishment in the striatum. Journal of neurophysiology 84, 3072-3077.
Ding, S.L., Van Hoesen, G.W., Cassell, M.D., Poremba, A., 2009. Parcellation of human temporal polar cortex: a combined analysis of multiple cytoarchitectonic, chemoarchitectonic, and pathological markers. J Comp Neurol 514, 595-623.
Eickhoff, S.B., Amunts, K., Mohlberg, H., Zilles, K., 2006a. The human parietal operculum. II. Stereotaxic maps and correlation with functional imaging results. Cereb Cortex 16, 268-279.
Eickhoff, S.B., Schleicher, A., Zilles, K., Amunts, K., 2006b. The human parietal operculum. I. Cytoarchitectonic mapping of subdivisions. Cereb Cortex 16, 254-267.
Eickhoff, S.B., Weiss, P.H., Amunts, K., Fink, G.R., Zilles, K., 2006c. Identifying human parieto-insular vestibular cortex using fMRI and cytoarchitectonic mapping. Hum Brain Mapp 27, 611-621.
Felleman, D.J., Van Essen, D.C., 1991. Distributed hierarchical processing in the primate cerebral cortex. Cereb Cortex 1, 1-47.
Fischl, B., Rajendran, N., Busa, E., Augustinack, J., Hinds, O., Yeo, B.T., Mohlberg, H., Amunts, K., Zilles, K., 2008. Cortical folding patterns and predicting cytoarchitecture. Cereb Cortex 18, 1973-1980.
Fischl, B., Stevens, A.A., Rajendran, N., Yeo, B.T., Greve, D.N., Van Leemput, K., Polimeni, J.R., Kakunoori, S., Buckner, R.L., Pacheco, J., Salat, D.H., Melcher, J., Frosch, M.P., Hyman, B.T., Grant, P.E., Rosen, B.R., van der Kouwe, A.J., Wiggins, G.C., Wald, L.L., Augustinack, J.C., 2009. Predicting the location of entorhinal cortex from MRI. Neuroimage 47, 8-17.

Gennari, F., 1782. De peculiari structura cerebri nonnullisque ejus morbis: paucae aliae anatom. observat. accedunt. ex regio typographeo.
Geyer, S., 2004. The microstructural border between the motor and the cognitive domain in the human cerebral cortex. Advances in anatomy, embryology, and cell biology 174.
Geyer, S., Ledberg, A., Schleicher, A., Kinomura, S., Schormann, T., Burgel, U., Klingberg, T., Larsson, J., Zilles, K., Roland, P.E., 1996. Two different areas within the primary motor cortex of man. Nature 382, 805-807.
Geyer, S., Schleicher, A., Zilles, K., 1999. Areas 3a, 3b, and 1 of human primary somatosensory cortex. Neuroimage 10, 63-83.
Geyer, S., Schormann, T., Mohlberg, H., Zilles, K., 2000. Areas 3a, 3b, and 1 of human primary somatosensory cortex. Part 2. Spatial normalization to standard anatomical space. Neuroimage 11, 684-696.
Glasser, M.F., Goyal, M.S., Preuss, T.M., Raichle, M.E., Van Essen, D.C., 2014. Trends and properties of human cerebral cortex: correlations with cortical myelin content. Neuroimage 93 Pt 2, 165-175.
Glasser, M.F., Sotiropoulos, S.N., Wilson, J.A., Coalson, T.S., Fischl, B., Andersson, J.L., Xu, J., Jbabdi, S., Webster, M., Polimeni, J.R., Van Essen, D.C., Jenkinson, M., Consortium, W.U.-M.H., 2013. The minimal preprocessing pipelines for the Human Connectome Project. Neuroimage 80, 105-124.
Glasser, M.F., Van Essen, D.C., 2011. Mapping human cortical areas in vivo based on myelin content as revealed by T1- and T2-weighted MRI. J Neurosci 31, 11597-11616.
Goddard, E., Mannion, D.J., McDonald, J.S., Solomon, S.G., Clifford, C.W., 2011. Color responsiveness argues against a dorsal component of human V4. Journal of vision 11, 3.
Goodale, M.A., Milner, A.D., 1992. Separate visual pathways for perception and action. Trends in neurosciences 15, 20-25.
Grefkes, C., Geyer, S., Schormann, T., Roland, P., Zilles, K., 2001. Human somatosensory area 2: observer-independent cytoarchitectonic mapping, interindividual variability, and population map. Neuroimage 14, 617-631.
Hackett, T., 2007. Organization and correspondence of the auditory cortex of humans and nonhuman primates. Evolution of the nervous system, 109-119.
Hackett, T.A., Preuss, T.M., Kaas, J.H., 2001. Architectonic identification of the core region in auditory cortex of macaques, chimpanzees, and humans. J Comp Neurol 441, 197-222.
Hadjikhani, N., Liu, A.K., Dale, A.M., Cavanagh, P., Tootell, R.B.H., 1998. Retinotopy and color sensitivity in human visual cortical area V8. Nature Neurosci 1, 235-241.
Hagler, D.J., Jr., Riecke, L., Sereno, M.I., 2007. Parietal and superior frontal visuospatial maps activated by pointing and saccades. Neuroimage 35, 1562-1577.
Hansen, K.A., Kay, K.N., Gallant, J.L., 2007. Topographic organization in and near human visual area V4. J Neurosci 27, 11896-11911.
Hariri, A.R., Tessitore, A., Mattay, V.S., Fera, F., Weinberger, D.R., 2002. The amygdala response to emotional stimuli: a comparison of faces and scenes. Neuroimage 17, 317-323.
Heinzle, J., Kahnt, T., Haynes, J.D., 2011. Topographically specific functional connectivity between visual field maps in the human brain. Neuroimage 56, 1426-1436.

Henssen, A., Zilles, K., Palomero-Gallagher, N., Schleicher, A., Mohlberg, H., Gerboga, F., Eickhoff, S.B., Bludau, S., Amunts, K., 2016. Cytoarchitecture and probability maps of the human medial orbitofrontal cortex. Cortex 75, 87-112.
Hill, J., Dierker, D., Neil, J., Inder, T., Knutsen, A., Harwell, J., Coalson, T., Van Essen, D., 2010. A surface-based analysis of hemispheric asymmetries and folding of cerebral cortex in term-born human infants. J Neurosci 30, 2268-2276.
Hopf, A., 1956. Über die Verteilung myeloarchitektonischer Merkmale in der Stirnhirnrinde beim Menschen. J Hirnforsch 2, 311-333.
Kaas, J.H., Hackett, T.A., 2000. How the visual projection map instructs the auditory computational map. J Comp Neurol 421, 143-145.
Kanwisher, N., Yovel, G., 2006. The fusiform face area: a cortical region specialized for the perception of faces. Philos Trans R Soc Lond B Biol Sci 361, 2109-2128.
Kolster, H., Peeters, R., Orban, G.A., 2010. The retinotopic organization of the human middle temporal area MT/V5 and its cortical neighbors. J Neurosci 30, 9801-9820.
Krubitzer, L., Huffman, K.J., Disbrow, E., Recanzone, G., 2004. Organization of area 3a in macaque monkeys: contributions to the cortical phenotype. Journal of Comparative Neurology 471, 97-111.
Krubitzer, L.A., Kaas, J.H., 1990. The organization and connections of somatosensory cortex in marmosets. Journal of Neuroscience 10, 952.
Kujovic, M., Zilles, K., Malikovic, A., Schleicher, A., Mohlberg, H., Rottschy, C., Eickhoff, S.B., Amunts, K., 2013. Cytoarchitectonic mapping of the human dorsal extrastriate cortex. Brain Struct Funct 218, 157-172.
Kurth, F., Eickhoff, S.B., Schleicher, A., Hoemke, L., Zilles, K., Amunts, K., 2010. Cytoarchitecture and probabilistic maps of the human posterior insular cortex. Cereb Cortex 20, 1448-1461.
Larsson, J., Heeger, D.J., 2006. Two retinotopic visual areas in human lateral occipital cortex. J Neurosci 26, 13128-13142.
Malikovic, A., Amunts, K., Schleicher, A., Mohlberg, H., Eickhoff, S.B., Wilms, M., Palomero-Gallagher, N., Armstrong, E., Zilles, K., 2007. Cytoarchitectonic analysis of the human extrastriate cortex in the region of V5/MT+: a probabilistic, stereotaxic map of area hOc5. Cereb Cortex 17, 562-574.
Malikovic, A., Amunts, K., Schleicher, A., Mohlberg, H., Kujovic, M., Palomero-Gallagher, N., Eickhoff, S.B., Zilles, K., 2015. Cytoarchitecture of the human lateral occipital cortex: mapping of two extrastriate areas hOc4la and hOc4lp. Brain Struct Funct.
Meier, J.D., Aflalo, T.N., Kastner, S., Graziano, M.S., 2008. Complex organization of human primary motor cortex: a high-resolution fMRI study. J Neurophysiol 100, 1800-1812.
Mishkin, M., Ungerleider, L.G., 1982. Contribution of striate inputs to the visuospatial functions of parieto-preoccipital cortex in monkeys. Behav Brain Res 6, 57-77.
Moerel, M., De Martino, F., Formisano, E., 2014. An anatomical and functional topography of human auditory cortical areas. Front Neurosci 8, 225.
Morecraft, R.J., Rockland, K.S., Van Hoesen, G.W., 2000. Localization of area prostriata and its projection to the cingulate motor cortex in the rhesus monkey. Cerebral Cortex 10, 192-203.
Morel, A., Gallay, M.N., Baechler, A., Wyss, M., Gallay, D.S., 2013. The human insula: Architectonic organization and postmortem MRI registration. Neuroscience 236, 117-135.

Morosan, P., Rademacher, J., Schleicher, A., Amunts, K., Schormann, T., Zilles, K., 2001. Human primary auditory cortex: cytoarchitectonic subdivisions and mapping into a spatial reference system. Neuroimage 13, 684-701.
Morosan, P., Schleicher, A., Amunts, K., Zilles, K., 2005. Multimodal architectonic mapping of human superior temporal gyrus. Anat Embryol (Berl) 210, 401-406.
Nasr, S., Liu, N., Devaney, K.J., Yue, X., Rajimehr, R., Ungerleider, L.G., Tootell, R.B., 2011. Scene-selective cortical regions in human and nonhuman primates. J Neurosci 31, 13771-13785.
Nieuwenhuys, R., Broere, C.A., Cerliani, L., 2015. A new myeloarchitectonic map of the human neocortex based on data from the Vogt-Vogt school. Brain Struct Funct 220, 2551-2573.
Ongur, D., Ferry, A.T., Price, J.L., 2003. Architectonic subdivision of the human orbital and medial prefrontal cortex. J Comp Neurol 460, 425-449.
Palomero-Gallagher, N., Eickhoff, S.B., Hoffstaedter, F., Schleicher, A., Mohlberg, H., Vogt, B.A., Amunts, K., Zilles, K., 2015. Functional organization of human subgenual cortical areas: Relationship between architectonical segregation and connectional heterogeneity. Neuroimage 115, 177-190.
Palomero-Gallagher, N., Vogt, B.A., Schleicher, A., Mayberg, H.S., Zilles, K., 2009. Receptor architecture of human cingulate cortex: evaluation of the four-region neurobiological model. Hum Brain Mapp 30, 2336-2355.
Pandya, D.N., Sanides, F., 1973. Architectonic parcellation of the temporal operculum in rhesus monkey and its projection pattern. Z Anat Entwicklungsgesch 139, 127-161.
Paus, T., 2001. Primate anterior cingulate cortex: where motor control, drive and cognition interface. Nature Reviews Neuroscience 2, 417-424.
Penfield, W., Rasmussen, T., 1950. The cerebral cortex of man; a clinical study of localization of function.
Petrides, M., Pandya, D.N., 1999. Dorsolateral prefrontal cortex: comparative cytoarchitectonic analysis in the human and the macaque brain and corticocortical connection patterns. Eur J Neurosci 11, 1011-1036.
Pitzalis, S., Galletti, C., Huang, R.S., Patria, F., Committeri, G., Galati, G., Fattori, P., Sereno, M.I., 2006. Wide-field retinotopy defines human cortical visual area v6. J Neurosci 26, 7962-7973.
Pitzalis, S., Sereno, M.I., Committeri, G., Fattori, P., Galati, G., Tosoni, A., Galletti, C., 2013. The human homologue of macaque area V6A. Neuroimage 82, 517-530.
Power, J.D., Cohen, A.L., Nelson, S.M., Wig, G.S., Barnes, K.A., Church, J.A., Vogel, A.C., Laumann, T.O., Miezin, F.M., Schlaggar, B.L., Petersen, S.E., 2011. Functional network organization of the human brain. Neuron 72, 665-678.
Rademacher, J., Caviness Jr, V., Steinmetz, H., Galaburda, A., 1993. Topographical variation of the human primary cortices: implications for neuroimaging, brain mapping, and neurobiology. Cerebral Cortex 3, 313.
Rajimehr, R., Young, J.C., Tootell, R.B., 2009. An anterior temporal face patch in human cortex, predicted by macaque maps. Proc Natl Acad Sci U S A 106, 1995-2000.
Rajkowska, G., Goldman-Rakic, P.S., 1995a. Cytoarchitectonic definition of prefrontal areas in the normal human cortex: I. Remapping of areas 9 and 46 using quantitative criteria. Cereb Cortex 5, 307-322.

Rajkowska, G., Goldman-Rakic, P.S., 1995b. Cytoarchitectonic definition of prefrontal areas in the normal human cortex: II. Variability in locations of areas 9 and 46 and relationship to the Talairach Coordinate System. Cereb Cortex 5, 323-337.
Robinson, E.C., Jbabdi, S., Glasser, M.F., Andersson, J., Burgess, G.C., Harms, M.P., Smith, S.M., Van Essen, D.C., Jenkinson, M., 2014. MSM: a new flexible framework for Multimodal Surface Matching. Neuroimage 100, 414-426.
Roland, P.E., Zilles, K., 1996. Functions and structures of the motor cortices in humans. Curr Opin Neurobiol 6, 773-781.
Rottschy, C., Eickhoff, S.B., Schleicher, A., Mohlberg, H., Kujovic, M., Zilles, K., Amunts, K., 2007. Ventral visual cortex in humans: cytoarchitectonic mapping of two extrastriate areas. Hum Brain Mapp 28, 1045-1059.
Sanides, F., 1970. Functional architecture of motor and sensory cortices in primates in the light of a new concept of neocortex evolution. The primate brain: Advances in primatology 1, 137-201.
Sanides, F., Vitzthum, H.G., 1965. Zur Architektonik der menschlichen Sehrinde und den Prinzipien ihrer Entwicklung. J, Neurology 18, 680-707.
Scheperjans, F., Eickhoff, S.B., Homke, L., Mohlberg, H., Hermann, K., Amunts, K., Zilles, K., 2008a. Probabilistic maps, morphometry, and variability of cytoarchitectonic areas in the human superior parietal cortex. Cereb Cortex 18, 2141-2157.
Scheperjans, F., Hermann, K., Eickhoff, S.B., Amunts, K., Schleicher, A., Zilles, K., 2008b. Observer-independent cytoarchitectonic mapping of the human superior parietal cortex. Cereb Cortex 18, 846-867.
Schira, M.M., Tyler, C.W., Breakspear, M., Spehar, B., 2009. The foveal confluence in human visual cortex. J Neurosci 29, 9050-9058.
Sereno, M.I., Dale, A.M., Reppas, J.B., Kwong, K.K., Belliveau, J.W., Brady, T.J., Rosen, B.R., Tootell, R.B., 1995. Borders of multiple visual areas in humans revealed by functional magnetic resonance imaging. Science 268, 889-893.
Sereno, M.I., Lutti, A., Weiskopf, N., Dick, F., 2013. Mapping the human cortical surface by combining quantitative T(1) with retinotopy. Cereb Cortex 23, 2261-2268.
Sereno, M.I., McDonald, C.T., Allman, J.M., 1994. Analysis of retinotopic maps in extrastriate cortex. Cereb Cortex 4, 601-620.
Smith, A.T., Greenlee, M.W., Singh, K.D., Kraemer, F.M., Hennig, J., 1998. The processing of first- and second-order motion in human visual cortex assessed by functional magnetic resonance imaging (fMRI). J Neurosci 18, 3816-3830.
Smith, R., Keramatian, K., Christoff, K., 2007. Localizing the rostrolateral prefrontal cortex at the individual level. Neuroimage 36, 1387-1396.
Swisher, J.D., Halko, M.A., Merabet, L.B., McMains, S.A., Somers, D.C., 2007. Visual topography of human intraparietal sulcus. J Neurosci 27, 5326-5337.
Talavage, T.M., Hall, D.A., 2012. How challenges in auditory fMRI led to general advancements for the field. Neuroimage 62, 641-647.
Tootell, R.B., Hadjikhani, N., Hall, E.K., Marrett, S., Vanduffel, W., Vaughan, J.T., Dale, A.M., 1998. The retinotopy of visual spatial attention. Neuron 21, 1409-1422.
Tootell, R.B., Mendola, J.D., Hadjikhani, N.K., Ledden, P.J., Liu, A.K., Reppas, J.B., Sereno, M.I., Dale, A.M., 1997. Functional analysis of V3A and related areas in human visual cortex. J Neurosci 17, 7060-7078.

Triarhou, L.C., 2007a. The Economo-Koskinas atlas revisited: cytoarchitectonics and functional context. Stereotact Funct Neurosurg 85, 195-203.
Triarhou, L.C., 2007b. A proposed number system for the 107 cortical areas of Economo and Koskinas, and Brodmann area correlations. Stereotact Funct Neurosurg 85, 204-215.
Tsao, D.Y., Moeller, S., Freiwald, W.A., 2008. Comparing face patch systems in macaques and humans. Proc Natl Acad Sci U S A 105, 19514-19519.
Van Essen, D., Glasser, M.F., Robinson, E., Chen, X.J., Jenkinson, M., Dierker, D., Nichols, T., Smith, S., 2014. Heritability of brain structure, function, and connectiviity in Human Connectome Project data. Annual Meeting of the Organization for Human Brain Mapping. (Hamburg, Germany; June 8-12 2014).
Van Essen, D., Newsome, W.T., Bixby, J.L., 1982. The middle temporal visual area in the macaque: myeloarchitecture, connections, functional properties and topographic organization. J Neurosci 2, 265-283.
Van Essen, D.C., Glasser, M.F., Dierker, D.L., Harwell, J., 2012a. Cortical parcellations of the macaque monkey analyzed on surface-based atlases. Cereb Cortex 22, 2227-2240.
Van Essen, D.C., Glasser, M.F., Dierker, D.L., Harwell, J., Coalson, T., 2012b. Parcellations and hemispheric asymmetries of human cerebral cortex analyzed on surface-based atlases. Cereb Cortex 22, 2241-2262.
Vogt, B., 2009. Cingulate neurobiology and disease. Oxford University Press.
Vogt, B., Nimchinsky, E., Vogt, L., Hof, P., 1995. Human cingulate cortex: surface features, flat maps, and cytoarchitecture. The Journal of comparative neurology 359, 490-506.
Vogt, B.A., Vogt, L., 2003. Cytology of human dorsal midcingulate and supplementary motor cortices. Journal of Chemical Neuroanatomy 26, 301-309.
Vogt, B.A., Vogt, L., Farber, N.B., Bush, G., 2005. Architecture and neurocytology of monkey cingulate gyrus. J Comp Neurol 485, 218-239.
Vogt, B.A., Vogt, L. J., Perl, D. P., & Hof, P. R., 2001. Cytology of human caudomedial cingulate, retrosplenial, and caudal parahippocampal cortices. J. Comp. Neurol, 438, 353-376.
von Economo, C., Koskinas, G.N., 1925. E Die Cytoarchitektonik der Hirnrinde des erwachsenen Menschen. Textband und Atlas. Wien, Springer.
Vorobiev, V., Govoni, P., Rizzolatti, G., Matelli, M., Luppino, G., 1998. Parcellation of human mesial area 6: cytoarchitectonic evidence for three separate areas. Eur J Neurosci 10, 2199-2203.
Wade, A.R., Brewer, A.A., Rieger, J.W., Wandell, B.A., 2002. Functional measurements of human ventral occipital cortex: retinotopy and colour. Philos Trans R Soc Lond B Biol Sci 357, 963-973.
Wandell, B.A., Winawer, J., 2011. Imaging retinotopic maps in the human brain. Vision Res 51, 718-737.
Wang, L., Mruczek, R.E., Arcaro, M.J., Kastner, S., 2015. Probabilistic Maps of Visual Topography in Human Cortex. Cereb Cortex 25, 3911-3931.
Weiner, K.S., Golarai, G., Caspers, J., Chuapoco, M.R., Mohlberg, H., Zilles, K., Amunts, K., Grill-Spector, K., 2014. The mid-fusiform sulcus: a landmark identifying both cytoarchitectonic and functional divisions of human ventral temporal cortex. Neuroimage 84, 453-465.
Wheatley, T., Milleville, S.C., Martin, A., 2007. Understanding animate agents distinct roles for the social network and mirror system. Psychological science 18, 469-474.

Winawer, J., Horiguchi, H., Sayres, R.A., Amano, K., Wandell, B.A., 2010. Mapping hV4 and ventral occipital cortex: the venous eclipse. J Vis 10, 1.
Yeo, B.T., Krienen, F.M., Sepulcre, J., Sabuncu, M.R., Lashkari, D., Hollinshead, M., Roffman, J.L., Smoller, J.W., Zollei, L., Polimeni, J.R., Fischl, B., Liu, H., Buckner, R.L., 2011. The organization of the human cerebral cortex estimated by intrinsic functional connectivity. J Neurophysiol 106, 1125-1165.

Supplementary Results and Discussion For A Multi-modal Parcellation of Human Cerebral Cortex

Matthew F. Glasser[1], Timothy S. Coalson[1]*, Emma C. Robinson[2,3]*, Carl D. Hacker[4]*, John Harwell[1], Essa Yacoub[5], Kamil Ugurbil[5], Jesper Andersson[2], Christian F. Beckmann[6], Mark Jenkinson[2], Stephen M. Smith[2], David C. Van Essen[1]

[1]Department of Neuroscience, Washington University Medical School, Saint Louis, Missouri 63110, USA. [2]FMRIB Centre, Nuffield Department of Clinical Neurosciences, John Radcliffe Hospital, University of Oxford, Oxford OX3 9DU, UK. [3]Department of Computing, Imperial College, London SW7 2AZ, UK. [4]Department of Biomedical Engineering, Washington University, Saint Louis, Missouri 63110, USA. [5]Center for Magnetic Resonance Research (CMRR), University of Minnesota, Minneapolis, Minnesota 55455, USA. [6]Donders Institute for Brain, Cognition and Behavior, Radboud University, Nijmegen 6525 EN, The Netherlands. [7]Department of Cognitive Neuroscience, Radboud University Medical Centre Nijmegen, Postbus 9101, Nijmegen 6500 HB, The Netherlands.

**These authors contributed equally to this work.*

1. Supplementary Results

1.1 Reproducibility of group average multi-modal data

Expanding on the striking similarities between 210P and 210V datasets highlighted in Main Text Figure 1, Figure 1 shows group average midthickness surfaces, FreeSurfer sulc and curvature folding measures, myelin maps, and cortical thickness maps corrected for surface curvature. All of these measures are highly reproducible across the 210P and 210V group averages (see legend to Figure 1). Because MSMAll areal feature-based registration was used to register the data (using myelin maps, resting state network maps, and visuotopic maps, see Methods section on image preprocessing), folding features that are well correlated with cortical areas remain sharp, whereas folding features that are poorly correlated with cortical areas are blurred away. This results in sharp folding patterns for the central sulcus, calcarine sulcus, and the insula, where areal boundaries are closely related to folds, whereas the folding patterns are blurred out in more cognitive regions where areas and folds are not well as correlated (see Figure 7 below for a side by side comparison of group and individual folding maps). This blurring effect on folding patterns in many cortical regions is also visible in the group average midthickness surfaces of Figure 1. Fine details in the average myelin maps and thickness maps are preserved because these features are correlated more strongly with cortical areas.

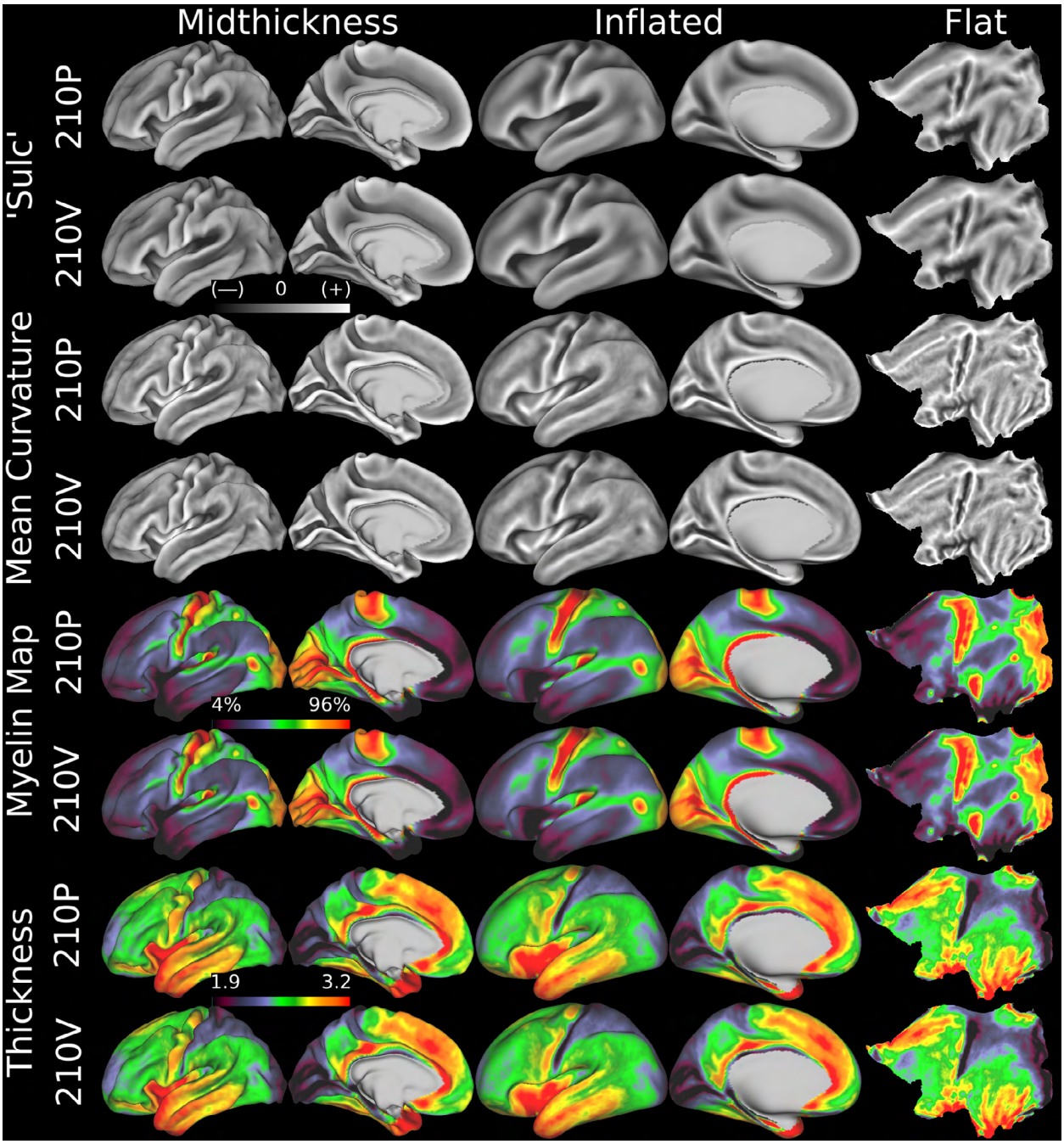

Figure 1 | **HCP group average architectural and folding map reproducibility.** Here we show group average left midthickness surfaces in Columns 1 and 2, left inflated surfaces in Columns 3 and 4 and left flat maps in Column 5. The 210P group averages are the odd rows and the 210V group averages are the even rows. The top two rows are FreeSurfer 'sulc' (r=0.996), the next two are FreeSurfer 'curv' (r=0.979), the next two are myelin (r=0.998), and the final two are thickness corrected for folding effects (r=0.994); all show extremely high cross-group reproducibility (both hemispheres were used in computing spatial map correlation coefficents). Folding patterns (sulc and curv) become blurry in many higher association regions of cortex, though they remain sharp in primary regions such as the central sulcus, calcarine sulcus, and insula, indicating that these regions have cortical areas that are well correlated with folding patterns. Areal feature-based surface registration also preserves fine spatial details in myelin maps and thickness maps that are consistent across groups. An example is the reproducible variation in the myelin maps of the primary somatosensory cortex, which appears to be related to somatotopic subdivisions (see Supplementary

Neuroanatomical Results #6, where these variations are compared with functional and connectivity-based somatotopic subdivisions). Sulcal folding is dark and gyral folding is bright, with grey in between. High myelin and thick cortex are red, low myelin and thin cortex are dark. T1w/T2w myelin content maps are a relative measure depicted on a percentile scale that indicates which cortical areas have more or less myelin. For brevity, we refer to them as 'myelin maps' in this report (as in previous reports). We consider them akin to an in vivo, MRI-based "myelin stain," analogous to histological myelin stains long used neuroanatomists rather than a truly quantitative measure of intracortical myelin (Glasser et al., 2014; Glasser and Van Essen, 2011). Data at http://balsa.wustl.edu/JpM6.

Figure 2 shows the spatial detail and quantitative reproducibility achievable without using spatial smoothing of the effect size (beta) maps for three example task fMRI contrasts (highest reproducibility, median reproducibility, least reproducible; Z statistic maps are similarly reproducible). Figure 3 shows the reproducibility for all 86 task contrasts, both for all grayordinates and for just surface grayordinates.

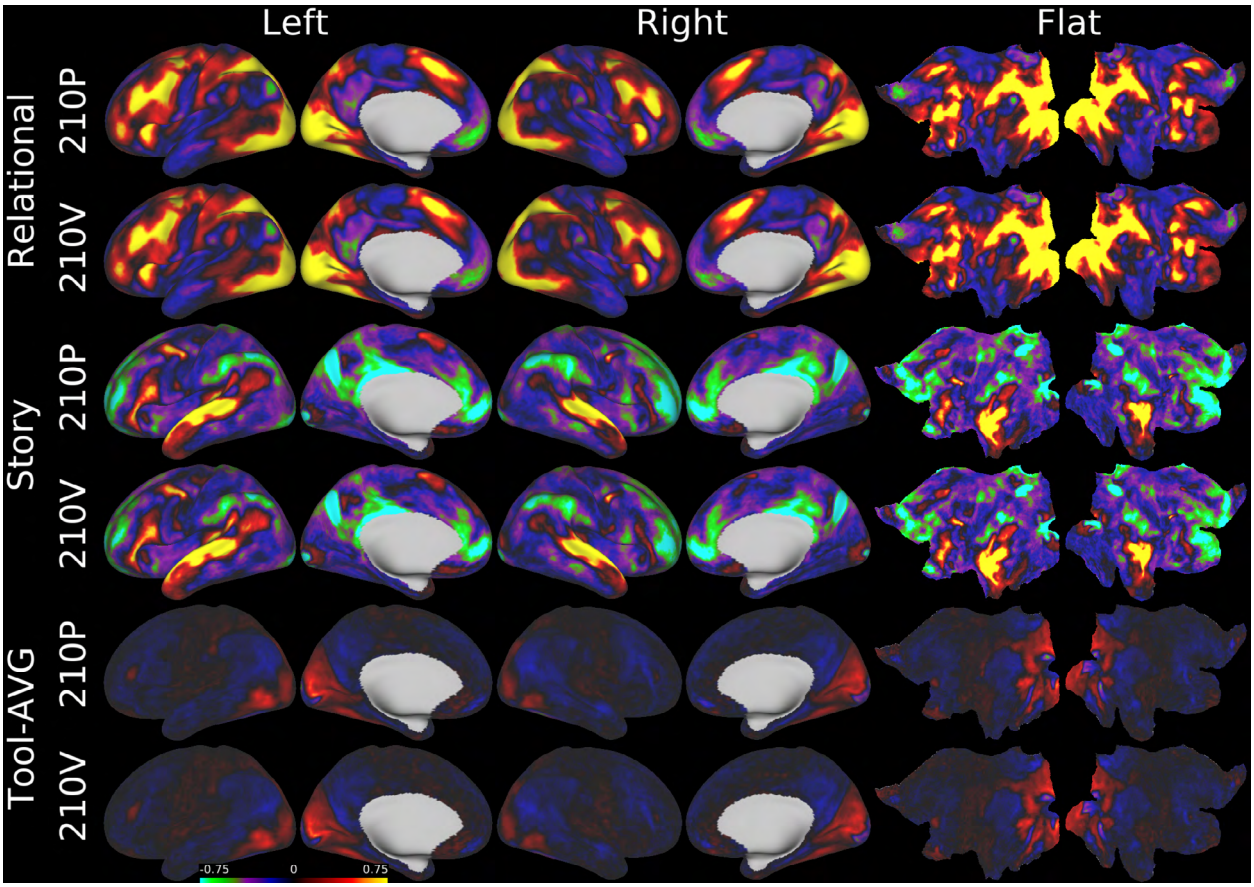

Figure 2 | **HCP group average task fMRI reproducibility.** Images are scaled from beta =+/-0.75. The odd rows are from the 210P dataset whereas the even rows are from the 210V dataset. These data are shown on left inflated views (Columns 1 and 2), right inflated views (Columns 3 and 4), and left and right flat maps (Columns 5 and 6, respectively). The top two rows are the task fMRI contrast with the highest reproducibility (Relational vs Baseline: r=0.995), the middle two rows are the task fMRI contrast with the median reproducibility (Language: Story vs Baseline: r=0.984), and the last two rows are the task fMRI contrast with the lowest reproducibility (Working Memory/Categories: Tool-Avg: r=0.944) that is not a known outlier (see Figure 3 legend). See (Robinson et al., 2014) for a comparison of the sharpness of task fMRI maps generated with areal feature-based registration versus folding-based registration. Data at http://balsa.wustl.edu/Q94z.

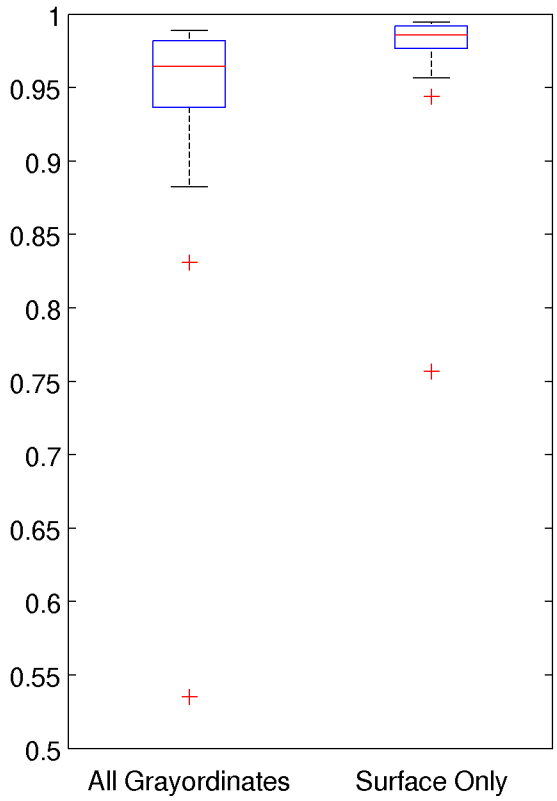

Figure 3 | **HCP group average task fMRI reproducibility for all contrasts.** Here we show box and whisker plots demonstrating the reproducibility of all 86 task contrasts (47 unique, 39 sign reversed) determined for all grayordinates (left) or surface grayordinates only (right, as shown in Figure 2 and whose r-values are mentioned in the figure legend). The bottom outlier (red cross) is the Gambling Reward-Punishment task contrast, which did not work as intended by the HCP and has very low information content in individual subjects. See Figure 2 legend for corresponding image data.

The top four rows of Figure 4 show the spatial patterns of two different resting state network maps (RSNs) from a d=137 ICA decomposition after computation of the individual subject maps using weighted regression and then averaging across the 210P group and the 210V group. (Weighted regression produces more accurate individual subject maps than the more standard dual regression approach, see Supplementary Methods #2.3.) The bottom four rows of Figure 4 show the reproducibility of dense functional connectivity maps for two different seeds. Figure 5 shows the reproducibility of all the non-artifactual RSNs and for all dense functional connectivity maps. Using the d=130 RSNs computed from the 210V subjects yielded similar reproducibility numbers (data not shown). The method for choosing the ICA dimensionalities is explained in Supplementary Methods #3.3.

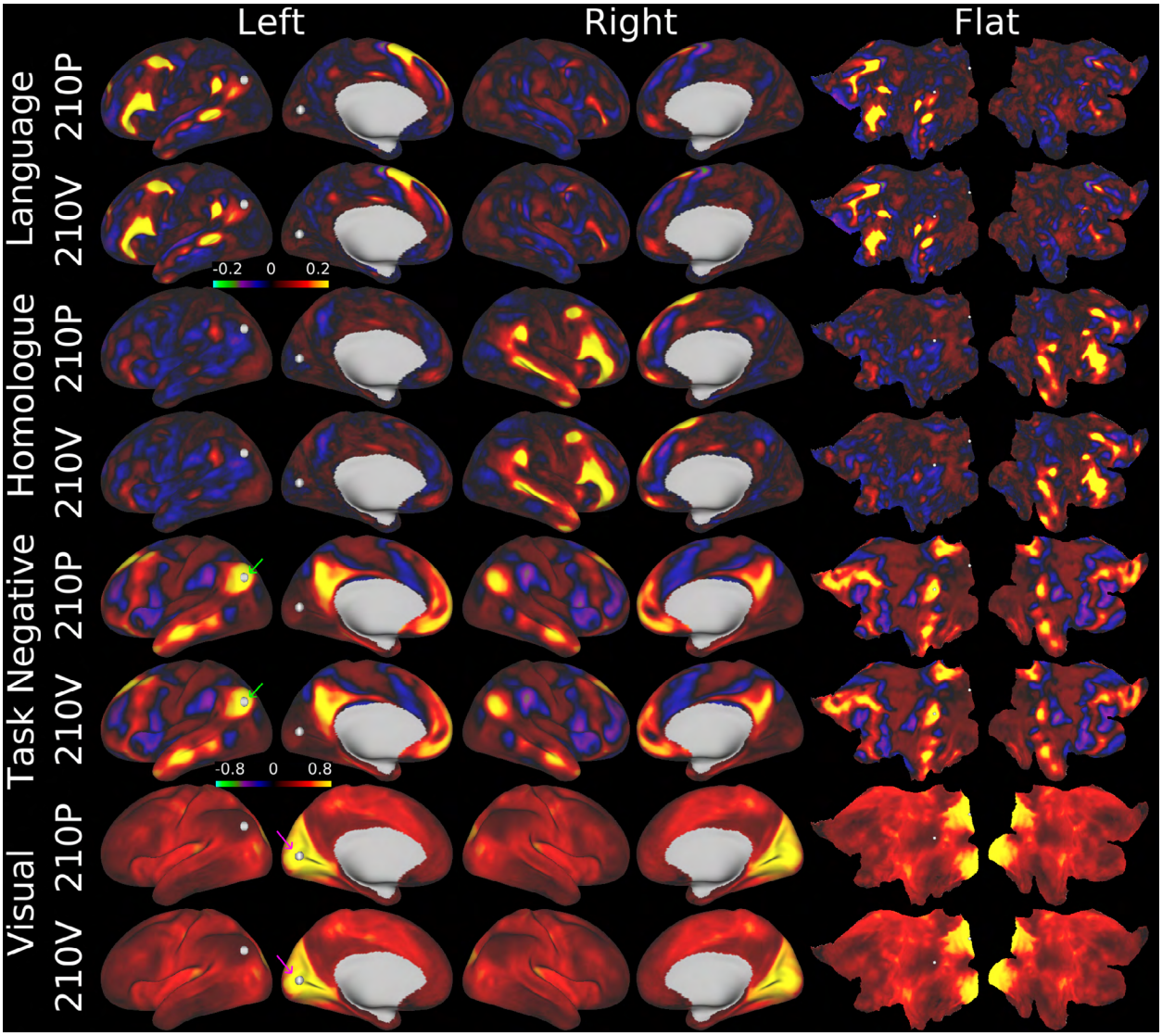

Figure 4 | **HCP group average resting-state fMRI reproducibility.** Here we show the reproducibility of Resting State Networks (RSNs, ICA d=137) and dense Functional Connectivity maps. The odd rows are the 210P dataset and the even rows are the 210V dataset. The RSNs were produced using ICA on the 210P dataset and then weighted regression of the group spatial maps onto the individual subject dense timeseries to produce individual subject spatial maps in all 449 subjects. The individual subject maps were then separately averaged across the 210P and 210V groups. The top two rows show the left lateralized language network and the next two rows show its right hemisphere homologue, both scaled between beta=+/-0.2. The next two rows show dense functional connectivity (FC) of the bilateral task negative (default mode) network seeded from a posterior inferior parietal grayordinate (green arrow, white sphere on left lateral surface), which has strong anti-correlation with the task positive network. The last two rows show the early visual network seeded from a grayordinate in the center of the calcarine sulcus (purple arrow, white sphere on left medial surface), which shows positive correlation with the entire brain. The dense FC maps are scaled from r=-0.8 to 0.8. Data at http://balsa.wustl.edu/RkMg.

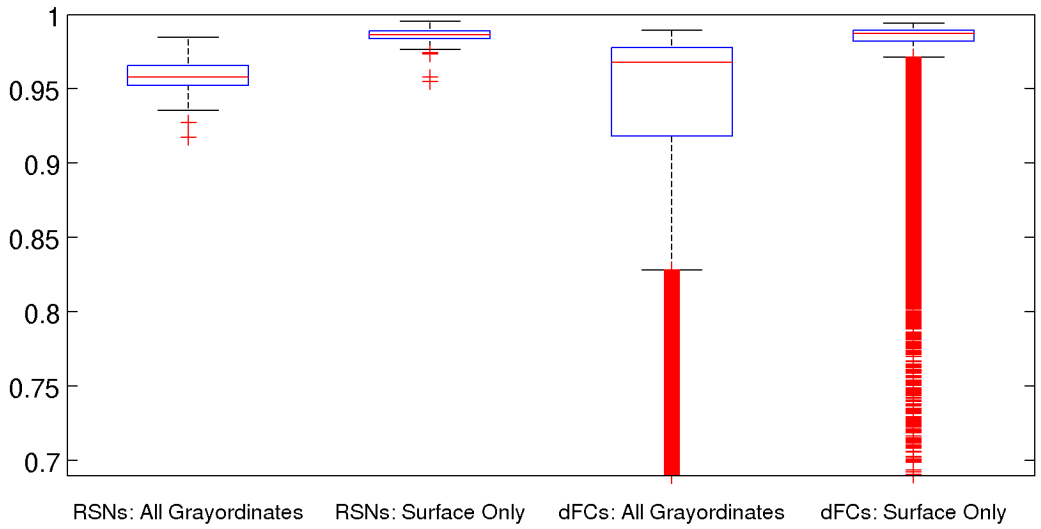

Figure 5 | **HCP group average resting state fMRI reproducibility all data.** Here we show the reproducibility of the 210P and 210V subject groups of resting state network maps (RSNs) (d=137) and dense Functional Connectivity maps (dFCs) for all grayordinates and for only surface grayordinates. Group level artifactual components (3) are not included (#RSNs=134) for either measure and only primarily surface components (#RSNs=77) are included for the surface only measure. See Figure 4 legend for how the RSNs were produced. For RSNs, the all grayordinates median reproducibility is r=0.978 and for surface only it is r=0.989. For dense FC maps, the all grayordinates median reproducibility is r=0.973 and for surface only it is r=0.989. Dense FC maps contain a considerable number of outliers (e.g. seeds in low CNR grayordinates in cortical and subcortical susceptibility regions. For dense FC, some outliers (red pluses more than 2.7 standard deviations below the median) extend below r=0.7, however the 134 RSN maps contain few outliers (as they have values largely close to zero in these low CNR susceptibility regions). Some of the dense map outliers may reflect the very large number of samples (over 4 billion) in a dense connectome. See Figure 4 for corresponding image data.

1.2 Cross-validation of the multi-modal parcellation

For the statistical cross-validation, the 210V dataset was parcellated using the 210P-derived multi-modal parcellation (i.e., architectural measures and fMRI timeseries for each 210V subject were averaged within the 210P-defined parcels prior to functional or connectivity-based analyses). We then computed paired t-tests (for significance) and effect sizes (Cohen's d, for robustness) across all subjects for each pair of neighboring areas and for all 266 distinct feature maps within the four independent feature categories: cortical thickness, myelin content, task fMRI contrast map betas, and full correlation functional connectivity with the other 178 areas (i.e. excluding the diagonal) (see Supplementary Methods, #7.2). To determine whether each of these parcellated feature maps was indeed robustly and statistically significantly different across the area pair's border in individual subjects, the results were thresholded at a Cohen's d>1 effect size threshold and a statistical significance threshold of $p<9*10^{-8}$ (Bonferroni-corrected for both hemispheres and two tails, see Methods section on statistical cross validation).

Figure 6 shows results displayed at each of the 1,050 borders shared by a pair of areas in the left or the right hemisphere. Colors in the top row indicate that 205 areal

borders are robustly and statistically significantly different across all four feature categories (red, 19.5% of border pairs), 535 across three categories (yellow, 51.0%), 268 across two categories (green, 25.5%), and 40 across one category (blue, 3.8%). Only two areal borders (black, 0.2%) were below the robust effect size threshold for all feature categories (but nonetheless passed the statistical significance threshold for multiple categories, see Figure 6 legend). Rows 2 - 5 show which areal borders passed the thresholds for each feature category. These results demonstrate that the areas of the multi-modal parcellation differ from their neighbors across multiple modalities in an independent group of subjects.

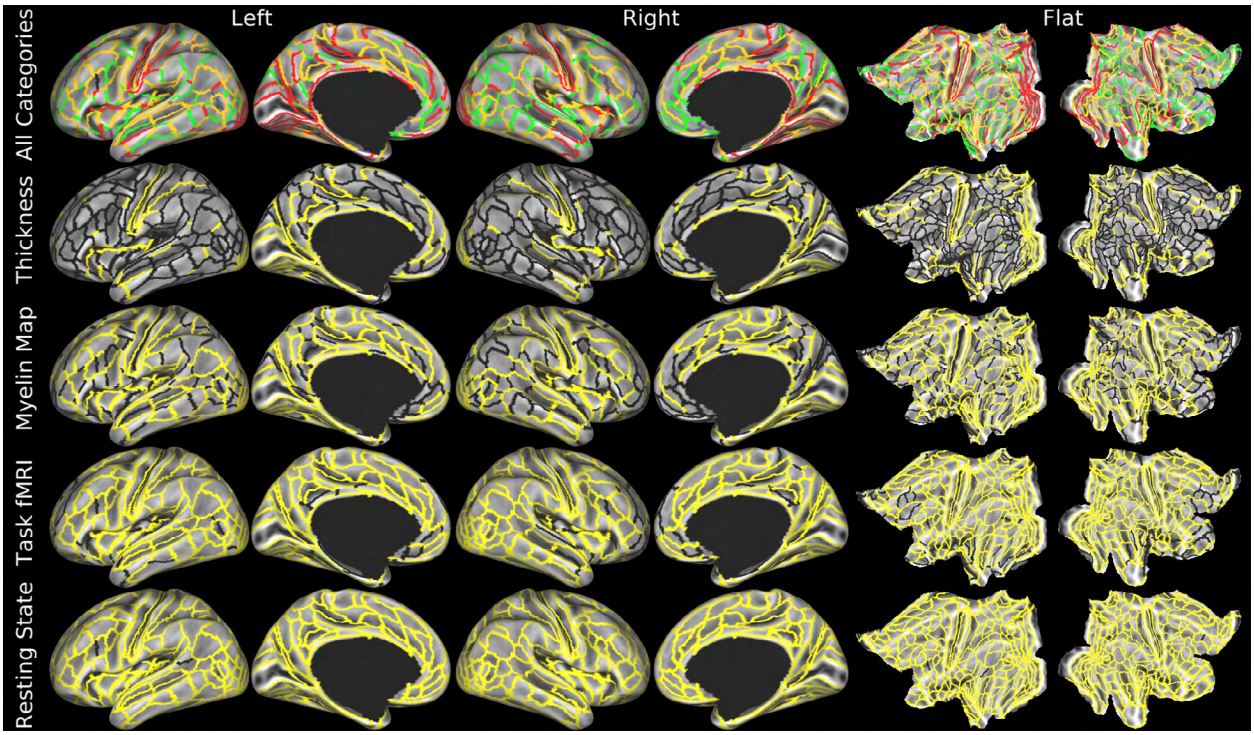

Figure 6 | **Cross-validation of the multi-modal parcellation.** Here we show the results of paired t-tests between each pair of neighboring areas' mean values across subjects in the 210V dataset but using the borders from the 210P parcellation. These tests were thresholded at Cohen's d>1 (abs(mean paired difference) / standard deviation of paired differences) and $p<9*10^{-8}$ for both hemispheres (Bonferroni corrected across two hemispheres, two-tailed significance threshold, see Methods section on statistical cross validation) to identify robust and statistically significant differences across each border pair. Row 1 shows how many of the four categories of features (thickness, myelin, tfMRI, rfMRI) passed these thresholds (Red=4, Orange=3, Green=2, Blue=1, Black=0). Rows 2 - 5 show which borders passed the thresholds (yellow=passed, black=not passed) respectively for thickness, myelin, any task fMRI contrast, and any difference in connectivity with an area in the full correlation parcellated connectome (excluding the diagonal). Two borders do not pass the d>1 effect size threshold for any category but still pass the significance threshold for multiple modalities (Black in Row 1): IFJa/IFSp in the left hemisphere (myelin: d=0.91, $p=3 * 10^{-29}$, tfMRI most different contrast LANGUAGE Story-Math: d=0.62, $p=2 * 10^{-16}$, rfMRI most different connectivity with area 47m: d=-0.85, $p=9 * 10^{-27}$) and 9a/9p in the right hemisphere (myelin: d=-0.84, $p=4 * 10^{-26}$, rfMRI most different connectivity with area 8Ad: d=-0.56, $p=3 * 10^{-14}$). Data at http://balsa.wustl.edu/W0N5.

1.3 Typical and atypical areal topologies of 55b and its neighbors

Although area 55b is a notably well defined cortical area (see Main Text Figure 2), it also exhibits a striking degree of individual variability in location and shape, even after MSMAll areal-feature-based surface registration. A substantial minority of subjects have topologically incompatible organizations of 55b and surrounding areas and areal features. These atypical topologies include spatial shifts, in which 55b is shifted relative to nearby areas and features, and splits of 55b, in which 55b is bisected by another area. Figure 7 illustrates spatial shifts in area 55b relative to another major nearby feature, the upper limb somatosensory-motor subregion. Fig. 7a-e show the group average areal features and pattern, in which 55b is strongly connected with the language network (RSN in column 1, task in column 3), is located between more heavily myelinated areas FEF, PEF, and 4 (column 2), and is elongated along an axis that points towards the postero-infero-lateral tip of the upper limb subregion of the somato-motor strip (RSN in column 4). Fig. 7f-j show a typical individual subject whose areal features closely match those of the group average. Fig. 7k-t show two subjects with an atypical organization in and around area 55b. Instead of 55b's long axis pointing ventrally, in both subjects it is tilted up towards the supero-anterior portion of the upper limb region, actually contacting it at the white sphere (columns 1 and 4). Although MSMAll attempts to align all of these areal features, the much larger upper limb region "wins," and hence area 55b remains misaligned with the group average. Because the patterns are topologically incompatible, MSMAll would generate large distortions in this region if the regularization penalty were relaxed. Column 5 shows the corresponding folding maps for the group average and individual subjects, which show both substantial variability and relatively poor correlation between areal boundaries and folding patterns in the region anterior to the central sulcus.

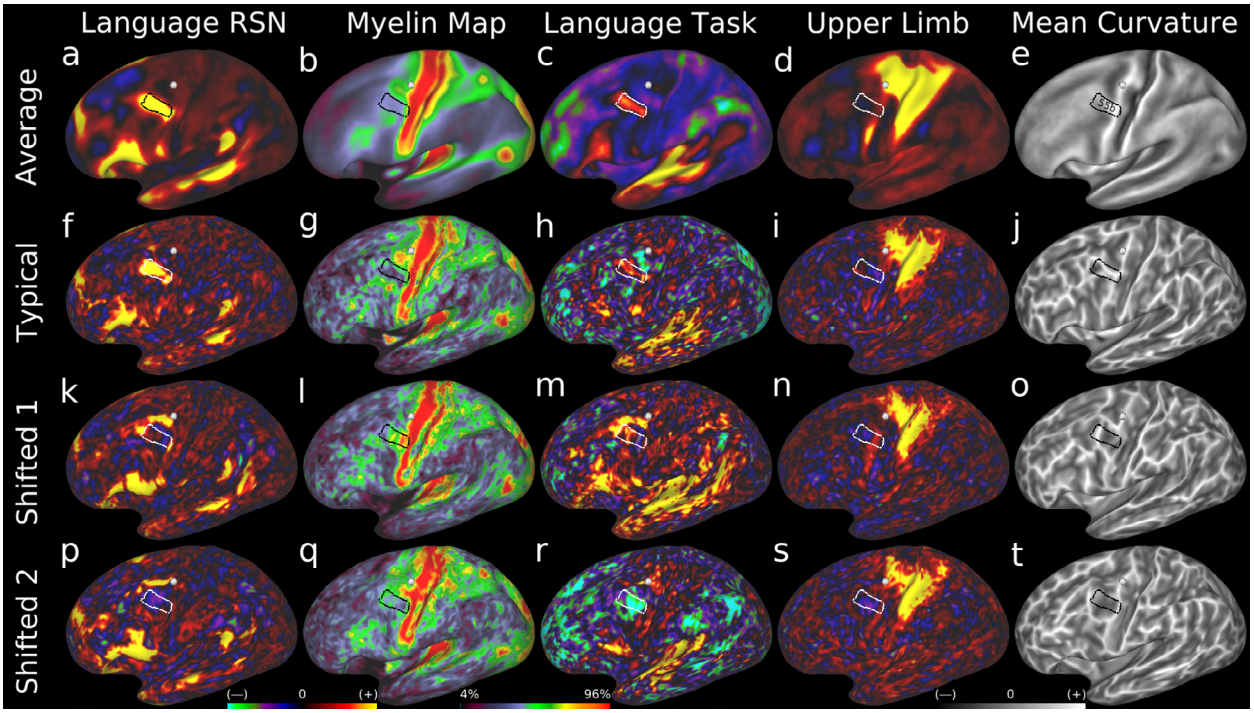

Figure 7 | **Atypical shifts of area 55b.** Here we show examples of one type of topological incompatibility between the typical layout of areal features near area 55b and a minority of subjects with an alternative 'shifted' layout. The first row shows the group average areal features: **a,** a d=40 RSN map corresponding to parts of the language network, **b,** a myelin map, **c,** a LANGUAGE Story-Baseline task contrast beta map, **d,** a d=40 RSN map corresponding to the upper limb somatosensory-motor topographic subregion, and, **e,** a mean curvature map illustrating the folding pattern. The group delineation of area 55b is a white or black line. **f-j** show these maps in a typical individual subject. **k-o** show an atypical subject whose 55b areal features are shifted relative to the typical pattern. **p-t** show a second atypical subject with a very similar pattern. In both cases, the posterior portion of area 55b is located near the white sphere instead of lying within the group delineated area 55b. Data at http://balsa.wustl.edu/Q2LV.

Besides the atypical shifted pattern just illustrated, area 55b and adjoining areas FEF and PEF show an additional atypical pattern. Typically, FEF and PEF are two moderately heavily myelinated areas that share very similar functional activation and connectivity patterns, but are split by lightly myelinated area 55b, which has very different functional activation and connectivity patterns. In a minority of subjects, however, it is 55b that is split, and FEF and PEF merge so that they are spatially adjoining. Figure 8 shows examples of this alternative topology. Fig. 8a-e show the group average areal features and pattern, in which 55b is strongly connected with the language network and is located between more heavily myelinated areas FEF, PEF, and 4. Also FEF and PEF are connected with the dorsal visual stream (RSN in column 4). Fig. 8f-j show a typical individual subject whose areal features closely match those of the group average. Fig. 8k-t show two subjects having the split 55b, joined FEF and PEF pattern. Importantly, the gap within the expected location of 55b in columns 1 and 3 (Fig. 8k, 8p, 8m, & 8r), indicating a lack of association (connectivity and function) with the language network, aligns with the region of increased connectivity with the dorsal stream visual cortex (column 4, Fig. 8n & 8s) and with elevated myelin content (column 2, Fig. 8l & 8q). The multi-modal nature of these individual differences argues strongly against attributing these findings simply to "noise in the data"; instead, the evidence indicates genuine individual differences in the topology of cortical functional and structural organization. As with the shifted patterns, the folding patterns in and near 55b, FEF, and PEF are both variable across subjects and variable in their relationship to areal features.

The neuroanatomists' survey of the left hemisphere of the 210P group of subjects using these multi-modal areal features revealed that ~89% (n=186) have the typical topology, ~4% (n=9) have the shifted topology, ~6% (n=12) have the split topology, and ~1% (n=3) have some other topology. While the canonical parcellation is best defined on the basis of the typical topology, it is highly desirable to map the alternative areal topologies as well as possible so that functional or connectivity-based measures are comparing the same areas across subjects. This is a major reason for using an areal classifier to delineate individual subject parcellations instead of simply imposing an atlas parcellation on the data. No topology preserving registration algorithm can bring these atypical subjects into precise alignment with an atlas parcellation. We found that area 55b is a notable hotspot of variability in areal topology (that is correlated with a hotspot in areal distortion from the MSMAll registration). Such variability in areal topologies will likely occur in varying degrees throughout the cortex, however. Presumably, as one examines finer levels of the neural hierarchy (e.g. within-area modularity), analogous kinds of spatially incompatible topologies will be increasingly prevalent. To take an extreme, it is

presumably not possible to register brains at the level of individual neurons or even cortical columns in a topology preserving way.

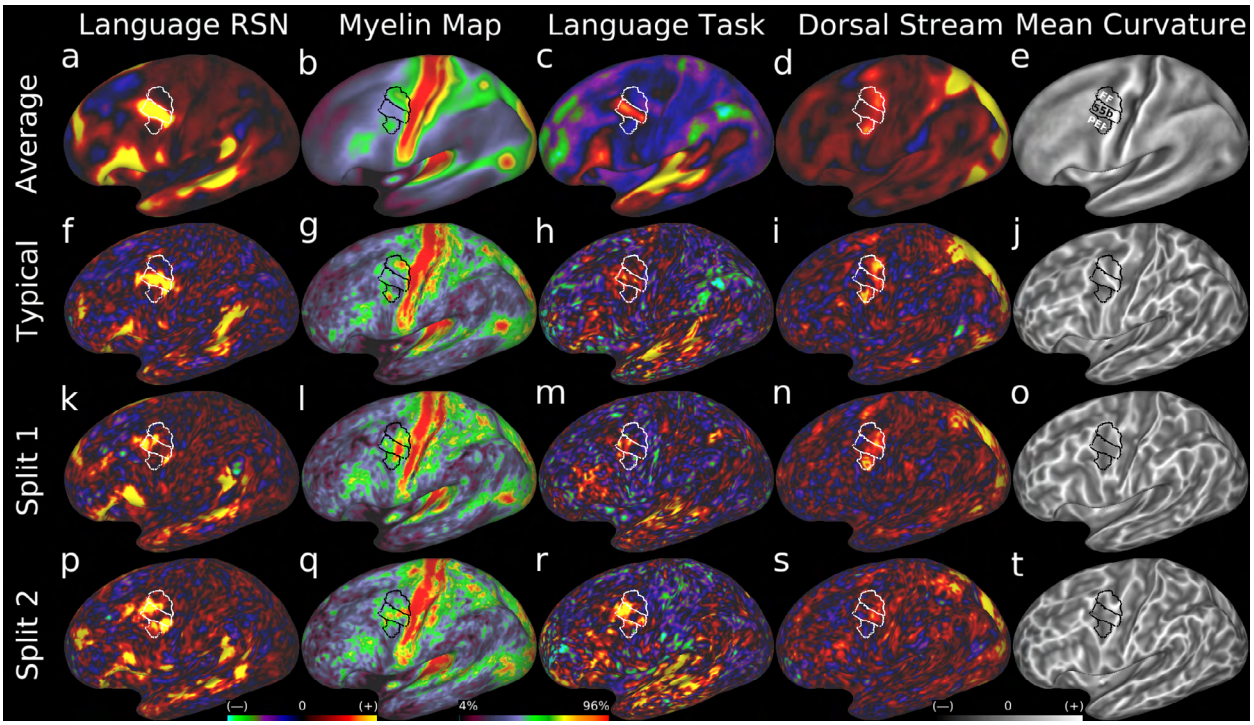

Figure 8 | **Atypical splits of area 55b.** Here we show examples of a second type of topological incompatibility between the typical layout of areal features near area 55b and a minority of subjects with alternative 'split' layouts. Row 1 shows the group average areal features: **a,** a d=40 RSN map corresponding to parts of the language network, **b,** a myelin map, **c,** a LANGUAGE Story-Baseline task contrast beta map, **d,** a d=40 RSN map corresponding to the dorsal visual stream, and, **e,** a mean curvature map illustrating the folding pattern. The group delineation of areas 55b, FEF, and PEF are white or black lines. **f-j** show these maps in a typical individual subject. **k-o** show an atypical subject whose area 55b is split and FEF and PEF are joined. **p-t** show a second atypical subject with a similar pattern. In both cases the split of 55b is visible in multiple independent areal features. Data at http://balsa.wustl.edu/Wrn2.

1.4 Automated individual subject multi-modal parcellations

The differing areal topologies of 55b and its neighbors not only demonstrate the need for individual subject parcellation (as opposed to atlas-based parcellation) but also serve as an excellent test case to evaluate critically whether an individual subject parcellation method is performing as desired. Figure 9 shows parcellation results for three example subjects, with Fig. 9a-j showing a typical 55b subject, Fig. 9k-t showing a shifted 55b subject, and Fig. 9u-dd showing a split 55b subject. The classifier output from the typical subject shows areas PEF (column 3), 55b (column 4), and FEF (column 5) in roughly the same places as in the group average (i.e. this subject has been well aligned with the areal-feature-based registration). In the shifted 55b subject, FEF and 55b have swapped places, and PEF extends into the region normally classified as 55b. Despite the atypical topology, the classifier was able to identify all three areas in their atypical locations based on their multi-modal areal fingerprints. In the split 55b subject, the classifier indicates that 55b is divided into two pieces, whereas FEF and PEF adjoin one another. Examples like this motivated us not to enforce a strict spatial contiguity criterion on the individual subject

parcellations. Instead, these split-area cases argue that it is possible for some areas to be spatially non-contiguous in some individuals, even if they are contiguous in most individuals. That the classifier was able to identify these atypical cases indicates that it is performing as desired, identifying cortical areas in many individuals even when their areal topology differs from the group average.

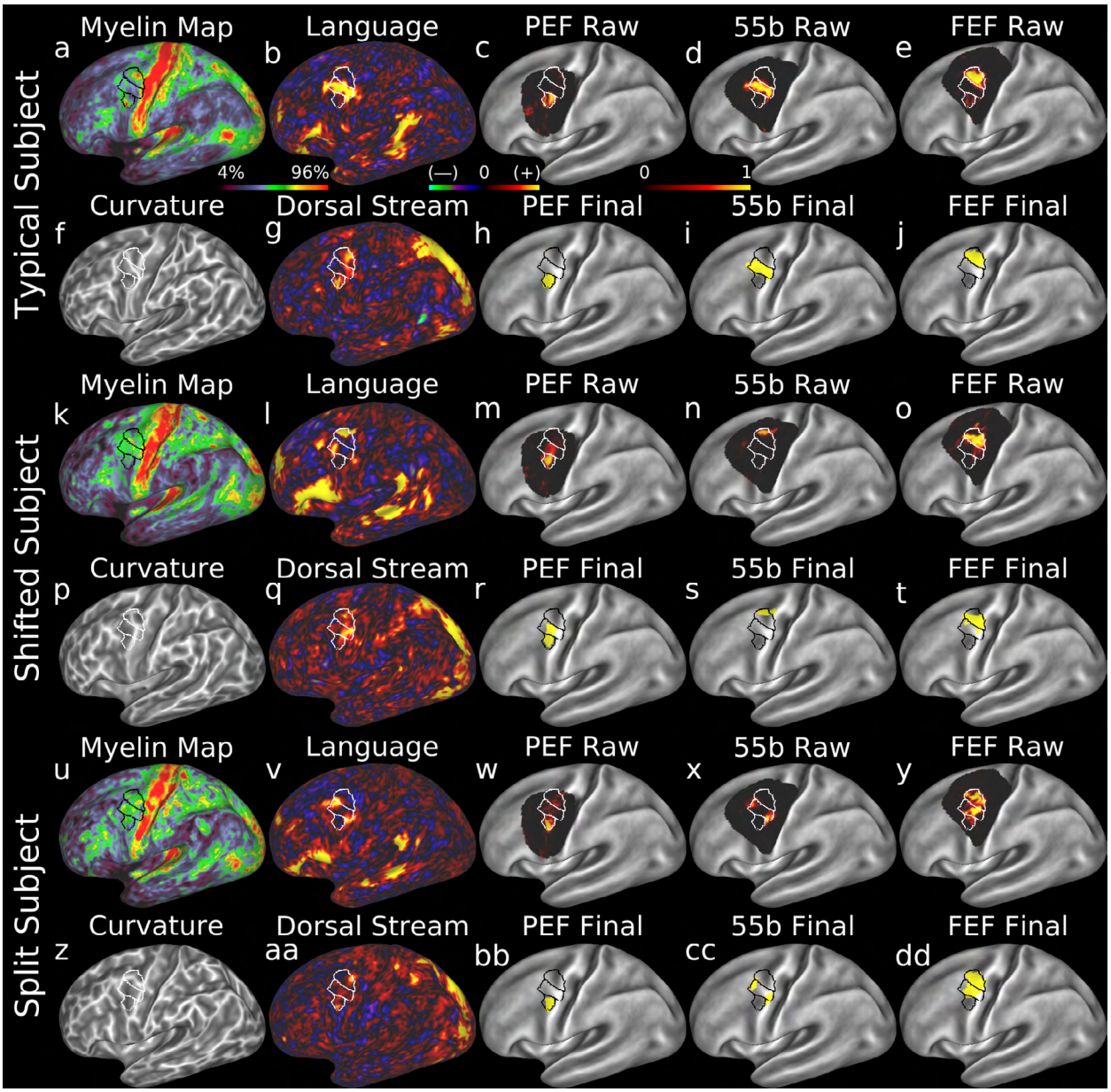

Figure 9 | **Areal classification of typical and atypical areas 55b.** Here we show classification of areas PEF, 55b, and FEF in three example individual subjects with typical, shifted, and split 55b areal topologies respectively (group parcels are black or white outlines). **a, k, & u** show the individual subject myelin maps. **b, l, & v** show the individual subject language resting-state network maps (d=40). **f, p, & z** show the individual subject folding maps. **g, q, aa** show the individual subject dorsal stream visual network maps (d=40). **c, d, e, m, n, o, w, x, & y** show the raw classifier output likelihood maps (scaled 0-1 black to yellow) for PEF, 55b, and FEF from left to right. **h, I, j, r, s, t, bb, cc, & dd** show the final parcels after combining across classifiers for PEF, 55b, and FEF. For all subjects, the areal classifier is able to identify area 55b sensibly. Data at http://balsa.wustl.edu/QxB9.

Another key indicator of the robustness of our classification method (and of the quality of the HCP data and analysis) comes from evaluating the reproducibility of results across repeat scans of individual HCP test-retest subjects. Figure 10 shows results from three subjects who were scanned through the full HCP protocol twice and processed through completely separate runs of the HCP's processing pipelines. Rows 1 and 2 show test-retest results for a subject with a typical 55b topology, rows 3 and 4 show results for a split-topology subject, and rows 5 and 6 show results for a shifted-topology subject. Columns 1 – 3 indicate a high degree of reproducibility for cortical folding (column 1, correlations for cases 1/2/3 are r=0.88/0.84/0.83), cortical myelin (column 2, correlations for cases 1/2/3 are r=0.91/0.88/0.87), and RSN maps (column 3, correlations for the illustrated d=40 RSN maps for cases 1/2/3 are r=0.64/0.62/0.5). As shown in columns 4 and 5, the classifier was able to delineate and identify area 55b in a consistent location in all three cases (correlation coefficients for the final parcels shown in cases 1/2/3 are r=0.87/0.79/0.82). Thus, while not as high as the group map correlations, the individual subject maps are reasonably reproducible.

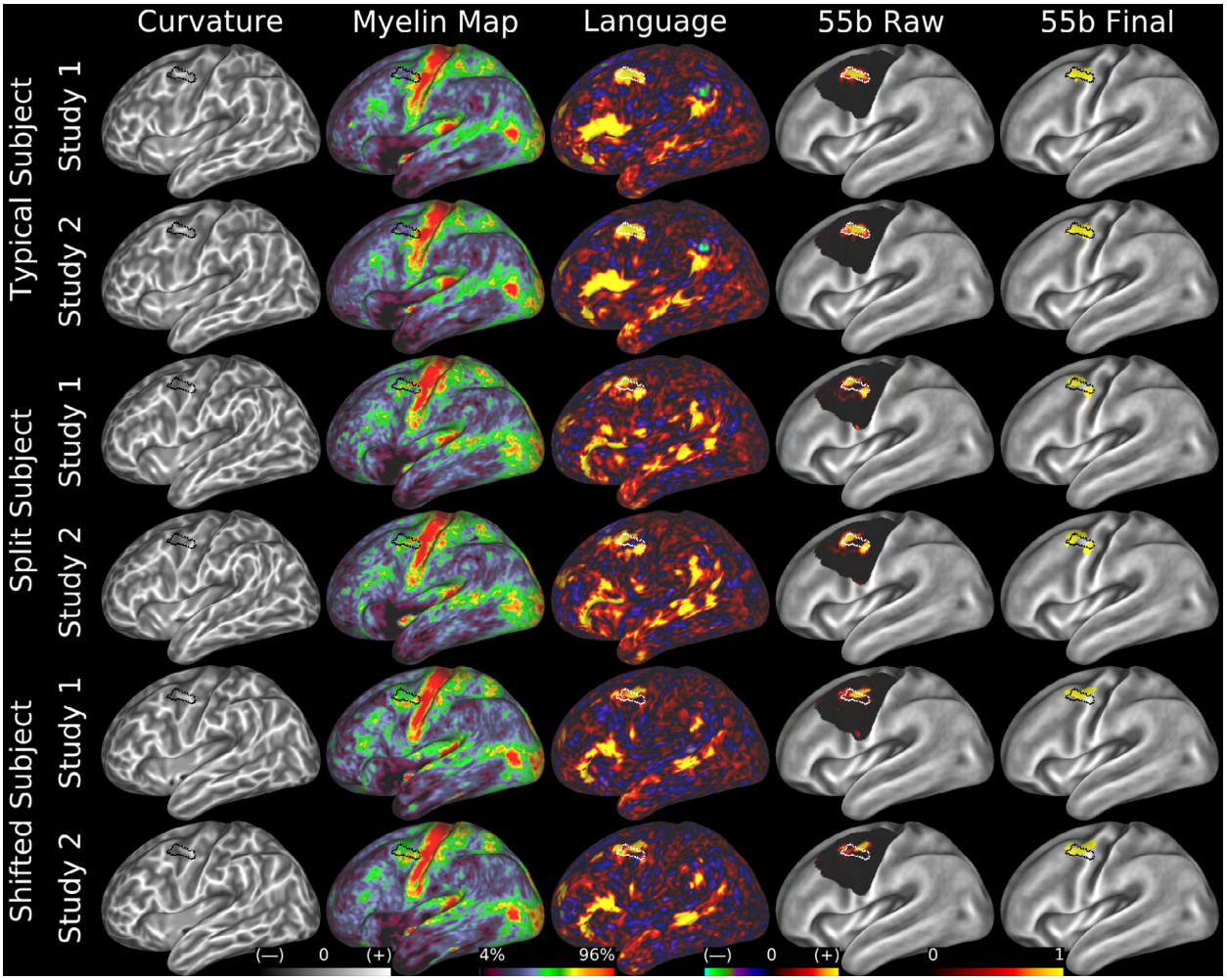

Figure 10 | **Reproducible areal classification of typical and atypical areas 55b.** Here we show individual subject curvature maps (column 1), myelin maps (column 2), d=40 RSN maps of the language network (column 3), classifier raw probability maps (column 4), and final parcel maps (column 5) of subjects scanned and analyzed through the HCP protocol and software pipelines twice. The group 55b definition is shown in a

black or white outline. Rows 1 and 2 show a subject with a typical 55b topology, rows 3 and 4 show a split 55b topology, and rows 5 and 6 show a shifted topology. Data at http://balsa.wustl.edu/WPPn.

Figure 11 shows the group parcellation and compares it with parcellations from a different set of three HCP test-retest subjects. The first row shows the group parcellation, which serves as the reference for rows 2-6 (reproducibility scores are correlation or Dice coefficients of the parcellations represented as 180 binary ROIs). Results are shown in row 2 for the subject with the highest overall parcellation reproducibility (r=0.79, Dice=0.75), row 3 for the subject with the median overall parcellation reproducibility (r=0.77, Dice=0.72), and row 4 for the subject with the lowest overall parcellation reproducibility (r=0.73, Dice=0.65), with individual-subject parcel boundaries shown in blue (test), red (retest), and purple (overlap) and group-average boundaries underlaid in black. Inspection of these maps reveals numerous examples in which deviation of an individual area boundary from the group mean is similar in both test and retest data but also examples of differences (likely errors). Rows 5 and 6 show the mean reproducibility of each area across the 27 test-retest subjects for the correlation and Dice measures. Larger areas tend to have higher reproducibility than smaller areas. While not as high as the group MPM reproducibility, the individual MPMs are reasonably reproducible. A topic for future study will be elucidating what causes differences across runs (see discussion below, #2.2-2.3).

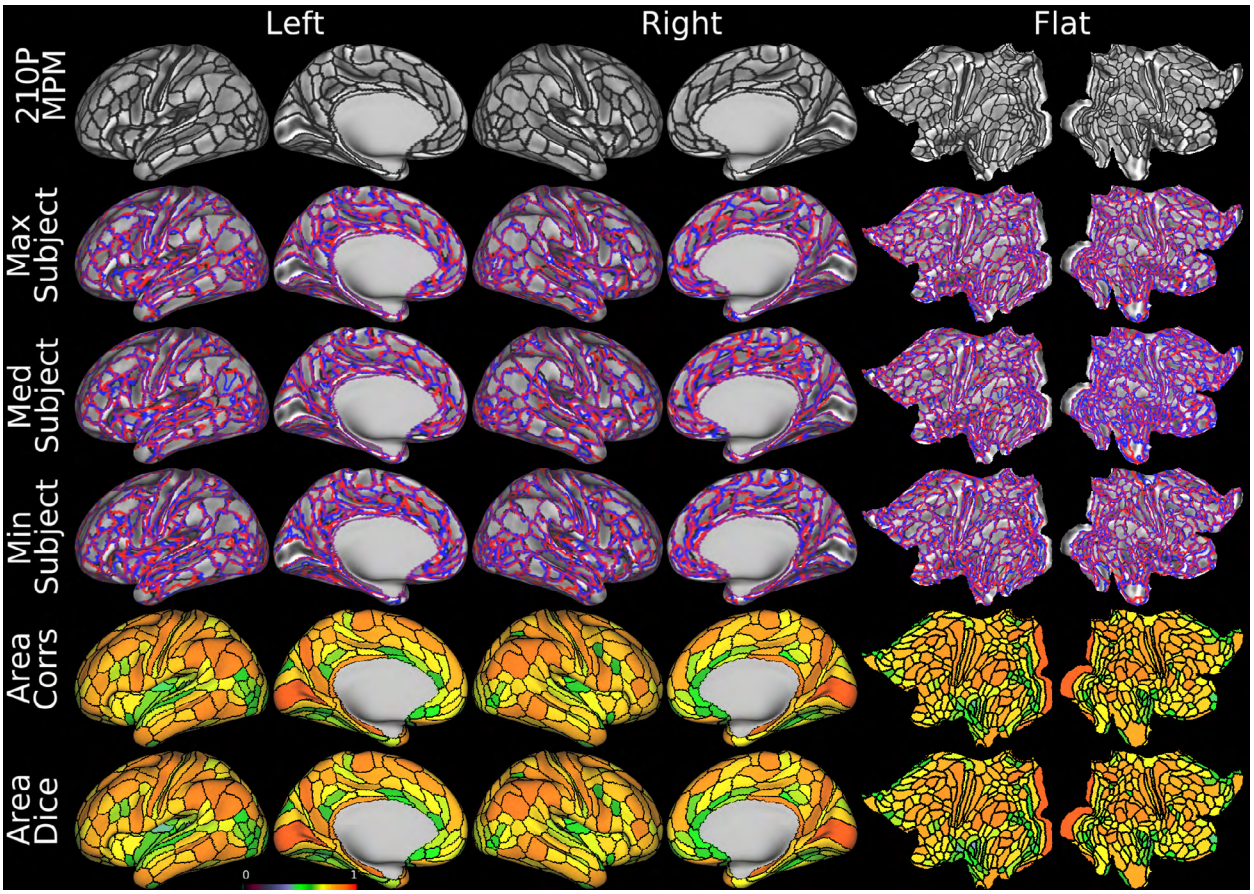

Figure 11 | **Individual subject parcellation reproducibility.** Here we show the group parcellation in comparison with three individuals' parcellations (who were each scanned twice). Row 1 shows the group parcellation (black outlines). Row 2 is the individual having the highest parcellation reproducibility (blue

outlines are 'test' individual areal boundaries and red outlines are 'retest' areal boundaries with purple as overlap and group boundaries as an underlay of black outlines). Row 3 is a second individual, who had the median parcellation reproducibility. Row 4 is a third individual, who had the lowest parcellation reproducibility. Rows 5 and 6 show the mean parcel reproducibility for each area across all 27 subjects that were scanned and analyzed twice for both the correlation and Dice measures (the full range is r=0.93, r=0.44, Dice=0.93. Dice=0.41). Data at http://balsa.wustl.edu/W72X.

1.5 Variability in surface areas across group cortical areas and in individual subjects

The availability of individual-subject parcellations in which a large majority of areas were identified in a large majority of individuals enabled interesting initial analyses of the sizes of cortical areas in the group average and variability in areal sizes across individuals. In individuals from the 210P group, the average size (i.e. surface area) of each cortical parcel spans a 26-fold range. V1 is the largest area (3292 mm^2 and 3229 mm^2 in the left and right hemispheres); nearly 80% of areas (142/180) are substantially smaller and within a four-fold range (150 – 600 mm^2, averaged across hemispheres). Across individuals, V1 is the least variable, with a total range slightly exceeding 2-fold, and a full-width at half maximum (FWHM) of 32% of the mean on the left and 30% on the right. Other areas larger than 500 mm^2 have variability with FWHM between 40% and 80% of the mean, while areas smaller than 500 mm^2 are generally more variable (mostly with FWHM 50% - 120% of the mean, in all cases excluding areas that were not identified in a given individual). These values represent the upper range of possible 'true' anatomical variability, given known methodological variability from subjects who had repeat scanning sessions. These data are amenable to future analyses of how individual variability in areal sizes correlates with behavioral and other phenotypic characteristics.

1.6 Peeking inside the areal classifier

We can "peek inside the black box" to examine the areal fingerprints learned by the classifier and ascertain to what degree it used the multiple modalities. We measured how sensitive the classifier is to changes in each feature map for each area as an indicator of the influence that each feature map has on generating the classification of each area (see Methods section on the cortical areal classifier). This sensitivity measure is positive or negative depending on whether the feature's value is larger or smaller inside the area, and its absolute magnitude indicates how important the feature is to the area's classification relative to its neighbors.

This sensitivity measure can be interrogated in multiple ways, as illustrated in Figure 12. Fig. 12a-b show the sensitivity measure at a 'dense' (vertex-wise) level for the demeaned myelin map in and around area 55b. The classifier 'sees' (Fig. 12b) area 55b as having much less myelin than area 4 posteriorly, slightly less myelin than FEF (superiorly) and PEF (inferiorly), and slightly more myelin than areas 8Av and 8C anteriorly, consistent with the pattern in the myelin map (Fig. 12a). We summarized this sensitivity measure for each area across all of its borders with neighboring areas by taking the maximum absolute value while retaining the sign, as shown in the parcellated sensitivity map for the myelin feature in Fig. 12c. Fig. 12d shows the matrix of these values for all 180 areas in the left hemisphere and all 112 features. Overall, all modalities are indeed useful for delineating and identifying cortical areas with the fully automated approach, just as with the semi-

automated neuroanatomical approach. Of the different areal properties, architectural features and resting state connectivity features drove the classifier's choices most strongly. Resting state visuotopic features were heavily used for specific areas (particularly early visual areas), but as expected are of limited value elsewhere. Task fMRI is also used, but clearly not as much as the other modalities (it has few yellows and cyans indicating high positive or negative sensitivity values). One possible explanation is that task fMRI maps are noisier than other feature maps and the information they do contain is largely redundant with other features (e.g. resting state) that have higher contrast to noise ratios in individual subjects.

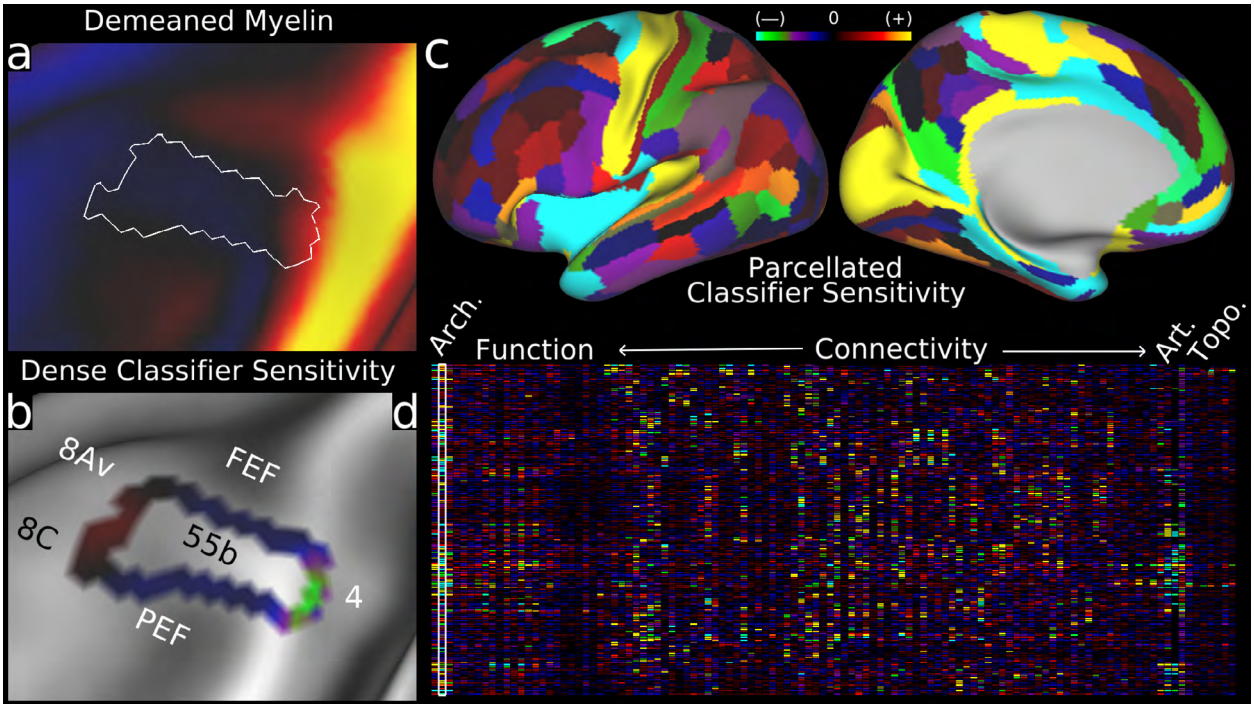

Figure 12 | **Signed classifier sensitivity measures. a,** shows the demeaned group average myelin map (what the classifier operates on) with area 55b outlined in white. **b,** shows the sensitivity measure for the myelin map and area 55b (only measured near the 55b border). Note that the measure is especially negative for the 55b/4 border (posteriorly), modestly negative for the 55b/FEF and 55b/PEF borders (superiorly and inferiorly), and modestly positive for the anterior border of 55b with 8Av and 8C. **c,** shows the maximum absolute value (shown with sign) of each area for the myelin map feature, indicating that myelin is useful for defining many, but by no means all, cortical areas. **d,** shows the matrix of all areas and all features (myelin is outlined white). The feature categories Architecture (Arch.), Function, Connectivity, Artifacts (Art.), and Topography (Topo.) are labeled along the top of the matrix. Data at http://balsa.wustl.edu/W60l.

2. Supplementary Discussion

2.1 Group average cortical parcellation.

The 180 cortical areas per hemisphere identified in this study are likely fewer than the actual number, because: (i) we have focused on particularly robust borders (consistent across at least two measures with a Cohen's effect size of at least 1 for 96% of borders), so it is unlikely that parcels were split too finely; and (ii) some parcels likely could be split

more finely, as our parcellation may be too coarse in some regions. For example, in orbitofrontal cortex we were unable to replicate known architectonic parcels (Ongur et al., 2003), likely in part because of susceptibility induced fMRI signal loss in that region. We also did not identify as many retinotopic areas in higher visual cortex as some studies have reported (Abdollahi et al., 2014; Wandell and Winawer, 2015; Wang et al., 2005). We identified some parcels as 'complexes' because we could not identify convincing subdivisions of a region that was previously reported to have a finer-grained parcellation. Hence, 180 areas is likely a lower bound on the actual number of areas, and ~200 per hemisphere might be closer to reality (though of course there will be finer levels of organization than cortical areas; see also point (v) in #2.8 below).

In this context, we hope that our parcellation, which we identify as HCP-MMP1.0 (Human Connectome Project Multi-Modal Parcellation v1.0), serves as version 1.0 of a progressively improving entity (analogous to open source software in which bugs may be fixed and new features implemented). Refinements to our cortical parcellation may come from multiple sources: (i) additional HCP data from the final 3T release (~1100 subjects with MRI data to be released in ~June, 2016) and/or the 7T data (~180 subjects and including retinotopy and movie paradigms, as well as rfMRI and dMRI). (ii) HCP tractography data, which may provide evidence for finer-grained parcellation in some regions (though see below #2.5); (iii) higher resolution structural and fMRI data that enable laminar-based cortical parcellation of myelin maps and resting-state networks; (iv) customized task fMRI experiments with high quality spatial localization that focus on particular regions; and (v) improved data acquisition, such as whole brain spin echo fMRI at high field that would ameliorate regional gradient echo fMRI signal loss. It will be important to use areal-feature-based registration and de-drifting in future studies to maximize the accuracy of cross-study comparisons, including with this parcellation.

The bilateral symmetry in the position, size, and functional connectivity profile of corresponding areas in the two hemispheres is striking (see Main Text Figure 3). The pattern is much more symmetric than those reported in several recent fully automated parcellations based only on resting-state functional connectivity (Gordon et al., 2014; Shen et al., 2013; Yeo et al., 2011), but is consistent with the bilateral symmetry generally reported in observer-independent postmortem architectonic parcellations (e.g. (Caspers et al., 2013)). Nevertheless, a number of interesting asymmetries are evident, some of which are described in the Supplementary Neuroanatomical Results.

2.2 Individual-subject parcellations.

Using a machine learning classifier, we successfully identified 98% of areas in the 210P group and 96.6% of areas in the 210V group that was not used to generate the parcellation. An important feature of the areal classifier is its ability to delineate and identify the 'non-standard' topology of some areas in some individuals. Area 55b was a notable hotspot for nonstandard topologies (indicated by higher average registration distortion in this region), including shifts in the local order of areas and splitting of area 55b into topologically discontinuous segments separated by joined areas FEF and PEF. Topological irregularities are evident for other areas as well, but their overall pattern and frequency, as well as the heritability of such patterns have yet to be systematically examined. It also is intriguing to speculate on how topological irregularities arise during

development, what degree of heritability they show (e.g., to what degree are atypical patterns shared by monozygotic twins), and whether they are associated with behavioral or other phenotypic correlates, but such topics are outside the scope of this study.

Although the areal classifier detects areas at a high rate, it does not detect them at a rate of 100% across all subjects. There are several possible causes for areas not detected by the classifier: 1) Some areas may neurobiologically truly not exist in some subjects. 2) Noise or artifacts (e.g. gradient echo fMRI dropout or the effects from large veins) may make some areas undetectable in some subjects (particularly smaller areas, areas near dropout regions, and areas that are not as distinct from their neighbors as are better detected areas). 3) Nonstationarity in the data (particularly in rfMRI scans, see #2.3) may lead to some areas being undetectable (if they are sufficiently similar to a neighbor across the available data to not be separated by the areal classifier). Better understanding the causes of undetected areas is an issue for future work: with more or better data, these areas might be detectable, or their absence might persist, suggesting that they represent genuine inter-subject variability like the atypical areal topologies. For now, we recommend that these areas be treated as having zero surface area for morphometric analyses and be controlled for using covariates of no interest for functional/connectivity cross-subject designs (i.e. a regressor with all zeros except for a 1 for the missing area in each subject that is missing it). Also, the group parcellation can be used as an atlas to parcellate (i.e. average data within the parcels) individual-subject data based on the individual subject to atlas alignment of the areal feature-based registration, though at the cost of reduced accuracy for atypical topologies that cannot be aligned using a topology preserving registration.

2.3 Aligning and parcellating future 'HCP-style' datasets.

In addition to high resolution T1w and T2w, the HCP acquired one hour of resting state fMRI data and one hour of task fMRI data (total across all tasks), which were used to derive the original semi-automated parcellation and for areal classification. MSMAll areal-feature-based alignment was driven solely by the resting state fMRI data and the T1w/T2w myelin maps. We tested the areal classification without the task fMRI data, finding that it detected areas at almost the same rate (96.4% vs 96.6% for the 210V data). Future work is needed to determine the minimum amount and type of fMRI data required for successful application of MSMAll and the areal classifier, but we can make several reasonable predictions: 1) It is likely that what will prove most important is the total amount of available fMRI data that has been cleaned using data-driven methods such as ICA+FIX (Griffanti et al., 2014; Salimi-Khorshidi et al., 2014) and then combined across runs. Whether the data is resting state fMRI, task fMRI, or movie fMRI is likely to be less important (for example, HCP resting state and task fMRI data, when analyzed similarly, are reported to produce similar results, (Cole et al., 2014). 2) The minimum amount of fMRI data needed to produce accurate MSMAll registrations and areal classifications is not yet known. Two considerations drive the need for more fMRI data. The first is that more fMRI data will improve the quality of connectivity estimates relative to unstructured (i.e. Gaussian) noise. The second is that fMRI data contain substantial nonstationarities, and thus connectivity estimates from a limited amount of time may not reflect the true average connectivity estimates, (irrespective of the effects of unstructured noise). This is expected

because the connectivity is thought to reflect what is going on in a person's brain at a given time, and shorter time windows are more likely to be different from a large average time window. The first consideration is amenable to improvement using better scanners (e.g. higher field strength), better head coils, and better pulse sequences (spin echo might help with dropout or large veins), but the second will be an intrinsic limitation of this kind of functional imaging, requiring that enough minutes of fMRI data are acquired. Perhaps this issue could be improved by using a more controlled experimental setting (e.g. a naturalistic movie that both holds the subject's attention and covers a wide range of stimuli). In general, optimizing the quality of the individual subject multi-modal parcellations (increasing the areal detection rate and the test-retest reproducibility of the parcellations) is an important subject for follow up work, enabled by what has been presented here.

Altogether, we anticipate that the methods described here will work for the 'HCP-style' data acquisition recommendations being used in forthcoming NIH-funded projects on the Lifespan Connectome and on Connectomes Related to Human Disease even though these projects will acquire less data per subject (see also Glasser et al., 2016). This will likely include ~30 min of multiband rfMRI data and another ~20 min of multiband tfMRI data. These datasets can likely be cleaned and combined to enable identification of RSNs using close to the 1 hour of rfMRI data used in this study for MSMAll alignment and the areal classifier. Other topics for future work include investigating how poor subject compliance (subject motion, subject going to sleep in the scanner, etc.) affects these methods. We strongly recommend the use of a method such as ICA+FIX (Griffanti et al., 2014; Salimi-Khorshidi et al., 2014) in order to remove spatially specific structured noise. The methods presented here for alignment and individual subject parcellation will not otherwise be affected by global signal differences (because they rely on multiple regression to generate resting state network maps, which represent partial betas more akin to partial correlation than full correlation). Thus, decisions to use or not use global signal regression or partial correlation can be postponed until one has generated parcellated timeseries. Ideally, however, one would eliminate the artifactual, likely physiologically induced (Golestani et al., 2015) global noise while retaining the genuine global neural signal and hopefully move the field past the divisive debate about global signal regression (see Glasser et al., 2016). Low spatial (>2.6 mm, the mean thickness of cortex) and temporal resolution (>1 s TR) data may not give as good results as the 2 mm, 0.72 s data used in this study because of blurring across cortical folds and worse data cleanup with slow TR data (Griffanti et al., 2014; Salimi-Khorshidi et al., 2014).

2.4 Circularity Considerations.

One potential concern regarding areal-feature-based alignment is whether it introduces circularity into the analyses. Two points are worth raising in this context: 1) Previous analysis of folding patterns, cortical thickness, or volume-based morphometric analyses are susceptible to a similar criticism (given that folding-based surface registration or T1w image intensities in a volume registration are used to drive the alignment in these cases). 2) We previously showed that areal-feature-based alignment using myelin maps and resting state network maps produces higher cross-subject statistics for an independent areal feature (task fMRI) that was not used to drive the registration, relative to alignment using folding-based registration (Robinson et al., 2014). Also, our implementation of the

MSMAll areal feature-based registration includes relatively strong regularization, generating substantially less distortion than standard folding-based methods (e.g. FreeSurfer, see Methods section on image preprocessing), and making it less likely that the registration would convert random noise into imputed areal features.

2.5 Diffusion imaging and tractography.

For technical reasons, we did not use diffusion imaging and tractography data as a source of information for our parcellation, even though tractography has been used in other studies to distinguish between gray matter parcels based on 'connectional contrast' (Behrens and Johansen-Berg, 2005; Jbabdi and Behrens, 2013). A primary reason was that tractography is susceptible to folding-related biases, including a tendency for streamlines to terminate preferentially on gyral crowns and to avoid sulcal fundi (Reveley et al., 2015; Van Essen et al., 2014). Given such biases, gradients in tractography connectivity may tend to correlate more with folding patterns for artifactual rather than neurobiological reasons. Understanding and improving the performance of tractography, especially near the gray/white border as fibers exit and enter the gray matter, is a topic of on-going work (e.g., (Canales-Rodríguez et al., 2015)). The ability to confirm consensus multi-modal borders using more advanced tractography algorithms will be a good test of how well these algorithms perform in individuals and group averages. One automated way of doing this would be to include tractography features from the 210P and 29T datasets in a classifier training and see if the tractography behaved more like the resting state connectivity or more like the task fMRI in an analysis like Figure 12 (i.e. does the areal classifier make use of the tractography?). Should this be successful, tractography may aid in identifying new boundaries as well. In any event, the current HCP parcellation provides a neuroanatomical framework that will enable quantitative comparisons of parcellated connectomes based on tractography with those based on functional connectivity, at the level of individual subjects as well as group averages.

2.6 Integration with other parcellations.

Substantial work remains in order to integrate our parcellation with information currently only available from post mortem histological methods, such as cytoarchitecture, laminar myeloarchitecture, and transmitter-receptor architecture (e.g., (Caspers et al., 2013; Zilles et al., 2015)). Simply bringing histological data into register with MRI data and into traditional MRI standard spaces has been a highly challenging but very successful methodological undertaking (Caspers et al., 2013). That said, it will be critical to apply the same sorts of spatial localization approaches to such histological data as was used for the in vivo data in this study to enable precise neuroanatomical comparisons between post-mortem and in vivo data. Early steps in this direction (Fischl et al., 2008) proved beneficial both in the present study and in previous work (Glasser and Van Essen, 2011).

2.7 Subcortical and cerebellar parcellation.

Many of the methods and approaches used in the present study could be readily extended to subcortical grey matter. This will be of particular interest for the HCP 7T data,

as the fMRI data have markedly higher CNR at 7T relative to the 3T scans and higher resolution at 1.6 mm vs 2 mm. Future higher resolution versions of the CIFTI grayordinates space may enable parcellation of additional subcortical structures (e.g. the claustrum).

It will also be of interest to use HCP data to parcellate the cerebellum, along the lines of a previous RSN-based cerebellar segmentation (Buckner et al., 2011), but using the rfMRI and tfMRI data from the HCP 3T and/or 7T scans. Ideally, such analyses would be done using cerebellar surface reconstructions of individual subjects, and then mapped to a group average cerebellar atlas surface. However, because cerebellar cortex is much thinner than cerebral neocortex, this is not yet feasible using existing segmentation algorithms, even though the high-resolution (0.7 mm) HCP T1w and T2w scans reveal many details of cerebellar folding. Nonetheless, a volume-based HCP cerebellar parcellation followed by mapping to an existing cerebellar surface-based atlas (Van Essen, 2002) would represent a considerable advance.

2.8 Sub-parcels and internal areal heterogeneity.

In general, a brain parcel is a region that has greater commonality of features within the parcel than with neighboring parcels (and this is explicitly what the areal classifier learns as a multi-modal areal fingerprint). However, within-parcel heterogeneity is profoundly important for understanding detailed aspects of brain circuitry and function. Internal heterogeneity extends across multiple levels, including within-area modularity and columnar organization all the way down to cellular and subcellular levels, but the heterogeneity accessible to the noninvasive 3T HCP neuroimaging data studied here is much coarser. We identified several types of within-parcel heterogeneity. (i) The somatosensory-motor strip contains five well-defined sub-regions, representing the lower limb, trunk, upper limb, face, and (surprisingly) a small patch of motor cortex likely representing muscles that control squinting of eyes (Meier et al., 2008), among other things. (ii) Within visual cortex, we demonstrated orderly gradients in the visuotopic maps of polar angle and eccentricity, which were made using resting state data. Our results are analogous to previous reports of visuotopy based on resting state fMRI (Gravel et al., 2014; Heinzle et al., 2011) but they benefitted from a number of analysis methods introduced here (see Supplementary Methods). (iii) Analogous orderly topographic gradients were evident in several higher cognitive regions – e.g., language-related areas 55b, PSL, and SFL (see Supplementary Neuroanatomical Results #15 Figure 18) though their functional significance is currently unknown. (iv) Many areas in our parcellation showed internal heterogeneity in one or more features, including task-fMRI, which were modest in magnitude and/or not consistent across multiple modalities. The reproducibility across independent datasets (see Figures 1-5 above) suggests that these heterogeneities mostly represent neurobiologically interesting variation, though some may reflect task-induced 'artifacts' (e.g. button box pressing, activation of only part of the visual field, etc). (v) Finally, although the topographic organization of early visual, somatosensory-motor, and auditory regions is reasonably well understood, we know much less about such organization in higher cognitive regions. One major impediment to this understanding in humans has been the use of brain imaging analysis methods that blur the fine details of functional and structural organization, obscuring such topographic patterns. Another is

that many of the higher cognitive regions in question have expanded dramatically in humans relative to the intensively and invasively studied macaque monkey (Van Essen and Dierker, 2007). These regions also have dramatically differing patterns of structural connectivity (Rilling et al., 2008), and thus are likely very different from putatively homologous regions in monkeys. Because the topographic organization of early somatosensory-motor cortex is well understood, we were able to separate which gradients defined topographically organized cortical areas (4, 3a, 3b, 1, and 2) from topographic subregions (F, E, UL, T, LL) as described in Supplementary Neuroanatomical Results #6. However, in higher cognitive regions, we don't have the benefit of such prior knowledge. Thus, future versions of the human multi-modal parcellation may be revised to classify some of the subdivisions reported here as subareas rather than areas as new information becomes available and the topographic organization of human cerebral cortex becomes better understood.

Additional topics of interest include analyses of the patterns of interhemispheric symmetry and asymmetry, and specific aspects of functional specialization (e.g., degree of segregation vs partial overlap for regions activated by faces, body parts, tools, and places). Some of these are covered in the Supplementary Neuroanatomical Results. Others can be examined in detail by downloading and analyzing the datasets associated with this study (see below #2.10).

2.9 Analysis strategies and cross study comparisons.

We have made significant efforts to enable other investigators to compare their data as precisely as possible with our parcellation though extensive releases of software tools that enable dramatically improved spatial localization: the CIFTI grayordinates neuroimaging analysis framework (Glasser et al., 2013), areal-feature-based surface registration with MSM (Robinson et al., 2014), group average registration drift removal during template generation (Abdollahi et al., 2014), and an extensive datasharing effort described below.

In general, neuroimaging studies that are mainly interested in what brain areas are activated/connected/different in some way will likely benefit from parcellated analyses due to their increased statistical sensitivity and power. Additionally, the trained classifier will hopefully enable identification of these cortical areas in individuals from future studies imaged with high quality "HCP-style" data acquisition and analysis strategies, such as the forthcoming Lifespan Connectome or Connectomes Related to Human Disease projects, which meet the minimal requirements of the HCP Preprocessing Pipelines, the MSMAll registration pipeline, and the individual subject areal classifier (i.e. high spatial and temporal resolution T1w, T2w, fMRI, and spin echo b0 fieldmap (Glasser et al., 2013; 2016)).

2.10 Sharing data via the BALSA database.

The ConnectomeDB database (Hodge et al., 2015; Marcus et al., 2013); https://db.humanconnectome.org) provides a user-friendly source for accessing unprocessed, minimally preprocessed, and subject-wise extensively analyzed HCP datasets. However, ConnectomeDB is not designed for sharing group average data or results from

neuroimaging studies such as this study. For this purpose, we designed and recently implemented the BALSA (Brain Analysis Library of Spatial maps and Atlases) database (Van Essen et al., 2016) (http://balsa.wustl.edu). BALSA is organized around scene files that provide all of the information needed to upload, download, and visualize in Connectome Workbench the neuroanatomical illustrations associated with this study. In essence, each scene in a scene file includes detailed information about the files used to generate the display of each of the figure panels. This includes the specific geometric configurations, overlays of different data types, labels and annotations used in each figure panel (generally, a separate 'tab' in the 'tile tabs' display enabled in wb_view, the Connectome Workbench visualization software platform). The process of uploading a scene file to BALSA imports all of the data files needed to regenerate its constituent scenes and includes the directory structures needed for successful scene visualization upon downloading. In addition to providing the scenes for each figure in this study, there will be additional reference data related to this study available in BALSA in the future.

Users accessing BALSA can navigate to the available datasets associated with the current study and inspect previews of each scene in each of the available scene files (one for each of the Main Text (https://balsa.wustl.edu/sceneFile/show/lLMz), Supplementary Results and Discussion (https://balsa.wustl.edu/sceneFile/show/X59l), Supplementary Methods (https://balsa.wustl.edu/sceneFile/show/PrGD), and Supplementary Neuroanatomical Results (https://balsa.wustl.edu/sceneFile/show/D4zL)). Also, we have provided a Study Dataset (https://balsa.wustl.edu/sceneFile/show/L731) that includes the group average data and gradients used to generate the parcellation, the original semi-automated parcellation, the 210P and 210V probabilistic areas, and the 210P and 210V group MPMs. Once analysis is completed on the full ~1100 subject HCP dataset, a Reference Dataset will be provided on the BALSA database. Users can download the data after obtaining a BALSA user account and agreeing electronically to HCP Open Access Data Use Terms.

References

Abdollahi, R.O., Kolster, H., Glasser, M.F., Robinson, E.C., Coalson, T.S., Dierker, D., Jenkinson, M., Van Essen, D.C., Orban, G.A., 2014. Correspondences between retinotopic areas and myelin maps in human visual cortex. Neuroimage 99, 509-524.

Behrens, T.E., Johansen-Berg, H., 2005. Relating connectional architecture to grey matter function using diffusion imaging. Philos Trans R Soc Lond B Biol Sci 360, 903-911.

Buckner, R.L., Krienen, F.M., Castellanos, A., Diaz, J.C., Yeo, B.T., 2011. The organization of the human cerebellum estimated by intrinsic functional connectivity. Journal of neurophysiology 106, 2322-2345.

Canales-Rodríguez, E.J., Daducci, A., Sotiropoulos, S.N., Caruyer, E., Aja-Fernández, S., Radua, J., Mendizabal, J.M.Y., Iturria-Medina, Y., Melie-García, L., Alemán-Gómez, Y., 2015. Spherical Deconvolution of Multichannel Diffusion MRI Data with Non-Gaussian Noise Models and Spatial Regularization. PloS one 10, e0138910.

Caspers, S., Eickhoff, S.B., Zilles, K., Amunts, K., 2013. Microstructural grey matter parcellation and its relevance for connectome analyses. Neuroimage 80, 18-26.

Cole, M.W., Bassett, D.S., Power, J.D., Braver, T.S., Petersen, S.E., 2014. Intrinsic and task-evoked network architectures of the human brain. Neuron 83, 238-251.

Fischl, B., Rajendran, N., Busa, E., Augustinack, J., Hinds, O., Yeo, B.T., Mohlberg, H., Amunts, K., Zilles, K., 2008. Cortical folding patterns and predicting cytoarchitecture. Cereb Cortex 18, 1973-1980.

Glasser, M.F., Goyal, M.S., Preuss, T.M., Raichle, M.E., Van Essen, D.C., 2014. Trends and properties of human cerebral cortex: correlations with cortical myelin content. Neuroimage 93 Pt 2, 165-175.

Glasser, M.F., Smith, S.M., Marcus, D.S., Andersson, J. Auerbach, E.J., Behrens, T.E.J., Coalson, T.S., Harms, M.P., Jenkinson, M. Moeller, S., Robinson, E.C., Sotiropoulos, S.N., Xu, J, Yacoub, E., Ugurbil, K., and Van Essen, D.C., 2016. The Human Connectome Project's neuroimaging approach. Nature Neuroscience (in press).

Glasser, M.F., Sotiropoulos, S.N., Wilson, J.A., Coalson, T.S., Fischl, B., Andersson, J.L., Xu, J., Jbabdi, S., Webster, M., Polimeni, J.R., Van Essen, D.C., Jenkinson, M., Consortium, W.U.-M.H., 2013. The minimal preprocessing pipelines for the Human Connectome Project. Neuroimage 80, 105-124.

Glasser, M.F., Van Essen, D.C., 2011. Mapping human cortical areas in vivo based on myelin content as revealed by T1- and T2-weighted MRI. J Neurosci 31, 11597-11616.

Golestani, A.M., Chang, C., Kwinta, J.B., Khatamian, Y.B., Jean Chen, J., 2015. Mapping the end-tidal CO2 response function in the resting-state BOLD fMRI signal: spatial specificity, test-retest reliability and effect of fMRI sampling rate. Neuroimage 104, 266-277.

Gordon, E.M., Laumann, T.O., Adeyemo, B., Huckins, J.F., Kelley, W.M., Petersen, S.E., 2014. Generation and Evaluation of a Cortical Area Parcellation from Resting-State Correlations. Cereb Cortex.

Gravel, N., Harvey, B., Nordhjem, B., Haak, K.V., Dumoulin, S.O., Renken, R., Ćurčić-Blake, B., Cornelissen, F.W., 2014. Cortical connective field estimates from resting state fMRI activity. Frontiers in neuroscience 8.

Griffanti, L., Salimi-Khorshidi, G., Beckmann, C.F., Auerbach, E.J., Douaud, G., Sexton, C.E., Zsoldos, E., Ebmeier, K.P., Filippini, N., Mackay, C.E., 2014. ICA-based artefact removal and accelerated fMRI acquisition for improved resting state network imaging. Neuroimage 95, 232-247.

Heinzle, J., Kahnt, T., Haynes, J.D., 2011. Topographically specific functional connectivity between visual field maps in the human brain. Neuroimage 56, 1426-1436.

Hodge, M.R., Horton, W., Brown, T., Herrick, R., Olsen, T., Hileman, M.E., McKay, M., Archie, K.A., Cler, E., Harms, M.P., 2015. ConnectomeDB—sharing human brain connectivity data. Neuroimage.

Jbabdi, S., Behrens, T.E., 2013. Long‐range connectomics. Annals of the New York Academy of Sciences 1305, 83-93.

Marcus, D.S., Harms, M.P., Snyder, A.Z., Jenkinson, M., Wilson, J.A., Glasser, M.F., Barch, D.M., Archie, K.A., Burgess, G.C., Ramaratnam, M., Hodge, M., Horton, W., Herrick, R., Olsen, T., McKay, M., House, M., Hileman, M., Reid, E., Harwell, J., Coalson, T., Schindler, J., Elam, J.S., Curtiss, S.W., Van Essen, D.C., Consortium, W.U.-M.H., 2013. Human Connectome Project informatics: quality control, database services, and data visualization. Neuroimage 80, 202-219.

Meier, J.D., Aflalo, T.N., Kastner, S., Graziano, M.S., 2008. Complex organization of human primary motor cortex: a high-resolution fMRI study. J Neurophysiol 100, 1800-1812.

Ongur, D., Ferry, A.T., Price, J.L., 2003. Architectonic subdivision of the human orbital and medial prefrontal cortex. J Comp Neurol 460, 425-449.
Reveley, C., Seth, A.K., Pierpaoli, C., Silva, A.C., Yu, D., Saunders, R.C., Leopold, D.A., Frank, Q.Y., 2015. Superficial white matter fiber systems impede detection of long-range cortical connections in diffusion MR tractography. Proceedings of the National Academy of Sciences 112, E2820-E2828.
Rilling, J.K., Glasser, M.F., Preuss, T.M., Ma, X., Zhao, T., Hu, X., Behrens, T.E., 2008. The evolution of the arcuate fasciculus revealed with comparative DTI. Nat Neurosci 11, 426-428.
Robinson, E.C., Jbabdi, S., Glasser, M.F., Andersson, J., Burgess, G.C., Harms, M.P., Smith, S.M., Van Essen, D.C., Jenkinson, M., 2014. MSM: a new flexible framework for Multimodal Surface Matching. Neuroimage 100, 414-426.
Salimi-Khorshidi, G., Douaud, G., Beckmann, C.F., Glasser, M.F., Griffanti, L., Smith, S.M., 2014. Automatic denoising of functional MRI data: combining independent component analysis and hierarchical fusion of classifiers. Neuroimage 90, 449-468.
Shen, X., Tokoglu, F., Papademetris, X., Constable, R.T., 2013. Groupwise whole-brain parcellation from resting-state fMRI data for network node identification. Neuroimage 82, 403-415.
Van Essen, D.C., 2002. Surface‐Based Atlases of Cerebellar Cortex in the Human, Macaque, and Mouse. Annals of the New York Academy of Sciences 978, 468-479.
Van Essen, D.C., Dierker, D.L., 2007. Surface-based and probabilistic atlases of primate cerebral cortex. Neuron 56, 209-225.
Van Essen, D.C., Jbabdi, S., Sotiropoulos, S.N., Chen, C., Dikranian, K., Coalson, T., Harwell, J., Behrens, T.E.J., Glasser, M.F., 2014. Mapping Connections in Humans and Non-Human Primates. 337-358.
Van Essen, D.C., Smith, J., Glasser, M.F., Elam, J., Donahue, C.J., Dierker, D.L., Reid, E.K., Coalson, T., Harwell, J., 2016. The Brain Analysis Library of Spatial maps and Atlases (BALSA) Database. Neuroimage.
Wandell, B.A., Winawer, J., 2015. Computational neuroimaging and population receptive fields. Trends in cognitive sciences.
Wang, J., Qiu, M., Constable, R.T., 2005. In vivo method for correcting transmit/receive nonuniformities with phased array coils. Magn Reson Med 53, 666-674.
Yeo, B.T., Krienen, F.M., Sepulcre, J., Sabuncu, M.R., Lashkari, D., Hollinshead, M., Roffman, J.L., Smoller, J.W., Zollei, L., Polimeni, J.R., Fischl, B., Liu, H., Buckner, R.L., 2011. The organization of the human cerebral cortex estimated by intrinsic functional connectivity. J Neurophysiol 106, 1125-1165.
Zilles, K., Bacha-Trams, M., Palomero-Gallagher, N., Amunts, K., Friederici, A.D., 2015. Common molecular basis of the sentence comprehension network revealed by neurotransmitter receptor fingerprints. Cortex 63, 79-89.